

**A fiber-free approach  
to the inelastic analysis  
of reinforced concrete structures**

*Ph.D. Dissertation*

***Francesco Marmo***

Corso di Dottorato di Ricerca in Ingegneria delle Costruzioni, XX ciclo

Dipartimento di Ingegneria Strutturale  
Università di Napoli "Federico II"  
Via Claudio, 21 - 80125 Napoli  
e-mail: f.marmo@unina.it

November, 2007

Tutor:  
Prof. L. Rosati

Coordinatore del corso:  
Prof. F. Mazzolani



# Acknowledgements

The present research work will not have been possible without the warm, dedicated and inspiring guidance of my advisor Professor Luciano Rosati, which my acknowledgements for his interest and care goes to.

I am also indebted to many other people for their support and encouragement. I would like to express here my gratitude to Prof. Giulio Alfano, Prof. Nunziante Valoroso and Dr. Roberto Serpieri for their help and advices, to Prof. Robert L. Taylor and Filip C. Filippou for their stimulating influence and to Dr. Joao Pina and Dr. Paolo Martinelli for the useful discussions.

Finally, I am grateful to my family and Valeria, which always supported me with their love.

Napoli, November 2007

Francesco Marmo



# Contents

<b>1</b>	<b>Introduction</b>	<b>7</b>
1.1	ULS analysis of RC cross sections . . . . .	8
1.2	Nonlinear analysis of RC frame structures . . . . .	10
<b>2</b>	<b>Ultimate Limit State analysis of RC sections subject to axial force and biaxial bending</b>	<b>13</b>
2.1	Assumptions and material properties . . . . .	14
2.2	Formulation of the problem . . . . .	15
2.3	Solution algorithm . . . . .	19
2.3.1	Solution scheme for the evaluation of $\lambda^*$ : Procedure A	19
2.3.2	Solution scheme for the evaluation of $\mathbf{u}(\mathbf{f})$ : Procedure B	24
2.3.3	Finding $\mathbf{u}(\mathbf{f})$ by solving a minimization problem . . .	28
2.3.4	Line search . . . . .	31
2.3.5	Global convergence of the solution algorithm . . . . .	33
2.4	Evaluation of the resultant force vector . . . . .	34
2.4.1	Integration formulas for the evaluation of $\mathbf{f}_r^{(k)}$ . . . . .	36
2.5	Evaluation of the matrix $\mathbf{H}^{(k)}$ . . . . .	41
2.5.1	Integration formulas for the evaluation of the tangent matrix $\mathbf{dR}^{(k)}$ . . . . .	42
2.5.2	Integration formulas for the evaluation of the matrix $\mathbf{H}^{(k)}$ . . . . .	52
2.6	Integration formulas for the evaluation of $\phi$ . . . . .	53
2.7	Numerical results . . . . .	55
<b>3</b>	<b>Nonlinear analysis of RC frame structures</b>	<b>73</b>
3.1	Two beam finite elements with displacement based formulations	76
3.1.1	Bending formulation . . . . .	76
3.1.2	Bending-shear formulation . . . . .	81
3.2	A beam finite element with force based formulation . . . . .	85

3.3	Tangent matrix and internal forces of the element cross sections	90
3.3.1	The fiber method . . . . .	92
3.3.2	Gradient of the section strain field . . . . .	94
<b>4</b>	<b>Integration formulas for polygonal sections</b>	<b>95</b>
4.1	Integration formulas for $f^{(k)}(\varepsilon)$ . . . . .	95
4.1.1	The case $\mathbf{g} = 0$ . . . . .	96
4.1.2	Some useful formulas . . . . .	96
4.1.3	Evaluation of the integral $N[f^{(k)}(\varepsilon)]$ . . . . .	98
4.1.4	Evaluation of the integral $\mathbf{m}^\perp[f^{(k)}(\varepsilon)]$ . . . . .	100
4.1.5	Evaluation of the integral $\mathbf{B}[f^{(k)}(\varepsilon)]$ . . . . .	101
4.2	Derivatives of $N[f^{(k)}(\varepsilon)]$ , $\mathbf{m}^\perp[f^{(k)}(\varepsilon)]$ and $\mathbf{B}[f^{(k)}(\varepsilon)]$ with respect to $\varepsilon$ and $\mathbf{g}$ . . . . .	104
4.2.1	The case $\mathbf{g} = 0$ . . . . .	105
4.2.2	Derivatives of $N[f^{(k)}(\varepsilon)]$ . . . . .	107
4.2.3	Derivatives of $\mathbf{m}^\perp[f^{(k)}(\varepsilon)]$ . . . . .	109
4.2.4	Derivatives of $\mathbf{B}[f^{(k)}(\varepsilon)]$ . . . . .	112
<b>5</b>	<b>Inelastic stress-strain laws</b>	<b>117</b>
5.1	Partition of the section . . . . .	120
5.2	Integration of inelastic stress-strain laws and relevant derivatives . . . . .	124
5.3	Inelastic bilinear stress-strain law with no tensile strength . . . . .	126
5.3.1	Determination of the functions $h(\varepsilon_m)$ , $k(\varepsilon_m)$ and $l(\varepsilon)$ . . . . .	128
5.4	Inelastic stress strain law with Mander's envelope curve . . . . .	133
5.4.1	Determination of the functions $h(\varepsilon_m)$ , $k(\varepsilon_m)$ and $l(\varepsilon)$ . . . . .	136
5.4.2	Considerations upon the partition of the section . . . . .	137
5.4.3	Spline interpolation of $h(\varepsilon_m)$ , $k(\varepsilon_m)$ and $l(\varepsilon)$ . . . . .	138
<b>6</b>	<b>Numerical results</b>	<b>143</b>
6.1	Integration of bilinear stress-strain laws . . . . .	143
6.2	Integration of the stress-strain law with Mander's envelope curve . . . . .	150
6.2.1	Interpolation of $l(\varepsilon)$ , $h(\varepsilon_m)$ , $k(\varepsilon_m)$ and $\varepsilon_p(\varepsilon_m)$ . . . . .	150
6.2.2	Section analysis . . . . .	154

# Chapter 1

## Introduction

The main objective of this thesis is to develop analytical formulas capable of capturing the non-linear response of arbitrarily shaped reinforced concrete (RC) cross sections subject to biaxial bending and axial force.

Namely, integration of non-linear elastic and elasto-plastic normal stresses acting on a section is carried out analitically without making recourse to the so-called fiber approach.

In this respect two separate formulations are presented. The first one is specifically devoted to the ultimate limit state analysis of RC sections by means of a tangent approach enhanced with line searches which is proved to be unconditionally convergent. The internal forces and the tangent matrix of the section, which are associated with the non-linear elastic stress-strain law typically specified by the international codes of practice [39], are computed exactly as function of the position vectors of the vertices of the section, assumed to be polygonal and of general shape.

The second formulation, which embodies the first one as special case, has been developed for the elasto-plastic constitutive laws typically adopted in the non-linear static and dynamic analysis of RC frames.

It is based on the use of special formulas which allow one to compute exactly the stress resultants of normal stresses acting on a section and the relevant derivatives provided that the given expression of the constitutive law is amenable to be analytically integrated four times as a maximum.

This is certainly true for the simplest constitutive laws such as the bilinear ones while more complex stress-strain laws, such as the popular one due to Mander et al. [61], can have particularly complex expression and/or be defined by values of the constitutive parameters which make them fall within special classes of real valued functions which are known not to be integrable

exactly [55].

In the last circumstance the constitutive law is first interpolated by means of splines so that the analytical formulas referred to above can be applied as well. Thus, exact values of the stress resultants and their derivatives are not obtained for the original constitutive law but for its interpolation.

Although not explicitly addressed in the thesis, the procedure can be extended to experimentally determined constitutive laws which only discrete pairs of stress-strain values are available for.

Apart from the exactness of the results entailed by the proposed approach, which has been termed fiber-free for obvious reasons, it is worth noting that considerable savings are obtained at the computational level since the history variables which need to be stored during a non-linear sectional analysis amount to some dozens since they are associated uniquely with the time-dependent partition of the section as function of the past history of deformation.

Conversely, several thousands of history variables need to be stored in the fiber approach to achieve a degree of accuracy at least comparable with that permitted by the fiber-free approach. Moreover this last one does not need any modification for sections of arbitrary shape while the traditional fiber approach is typically conceived for sections composed of rectangles.

Finally, some structural examples have been reported in order to illustrate the differences in the response predicted by the fiber-free and fiber approach.

## 1.1 ULS analysis of RC cross sections

Within the framework of nonlinear analysis of RC structures a prominent place is represented by RC sections of arbitrary shape, either single- or multi-cell, subject to axial force and biaxial bending since their ultimate limit state analysis routinely occurs in a huge variety of practical cases such as abutments, bridge piers, columns or core wall systems.

Furthermore, the nonlinear finite element analysis of reinforced concrete structures, often based on a tangent approach, requires the calculation of the stiffness matrix of the cross section and the evaluation of the internal forces obtained by integrating nonlinear stress fields over the section.

Several contributions have appeared in the past on the two issues referred to above. With specific reference to the ultimate limit state analysis of RC sections we mention, without any claim of completeness, the research by Brondum [15, 16] and Yen [105] who adopted a method based upon a

rectangular stress block. More refined approaches have been proposed in [19, 26, 35, 52, 56, 60, 84, 87].

Recently, Fafitis [40] developed a method for the computation of the interaction surface of reinforced concrete sections subject to axial force and biaxial bending based upon the Green's theorem. The method, which is based on special assumptions on the stress distribution in the cross section, has been subsequently employed in [20].

A different approach for computing the stiffness matrix and the internal forces of the section have been presented in [11, 99]. Particularly original is the approach presented in [11] since the authors developed a numerical algorithm based upon the decomposition of the section in quadrilaterals in order to generalize the classical cells (or fibers) and layers methods currently employed in fiber-based finite element nonlinear analysis of RC frames [90, 91, 92].

Clearly, the technique which adopts the decomposition of the cross section in a dense grid of cells is extremely expensive from the computational point of view due to the large amount of information needed to characterize the nonlinear behaviour of the section, through its tangent stiffness matrix, and to evaluate the internal forces.

In chapter 2 we illustrate a solution strategy of tangent type for evaluating the ultimate limit state of RC sections of arbitrary shape and degree of connection in which the above mentioned drawback are completely ruled out.

The proposed strategy adopts two nested iterative schemes: the first one updates the current value of the tentative ultimate load in the form  $\mathbf{f}_i = \mathbf{f}_e + (\lambda_i - 1)\mathbf{f}_1$  by searching for a positive scalar  $\lambda_i$  which amplifies along a specified load direction  $\mathbf{f}_1$  the initial set  $\mathbf{f}_e$  of the applied forces, typically the values obtained at a given section by the analysis of the structural model which the section belongs to.

Under the typically satisfied hypothesis that the admissible domain is convex and assuming  $\mathbf{f}_e$  internal to such domain, the existence and uniqueness of the load multiplier  $\lambda^*$  corresponding to the attainment of the ultimate limit state is easily verified. It is also proved that the proposed algorithm is globally convergent to this unique solution.

The second iterative procedure represents the main computational burden of the proposed solution strategy since it amounts to evaluating the parameters of the unknown strain field associated with  $\mathbf{f}_i$ . This task is accomplished by means of a modified Newton method, occasionally enhanced with line searches, so that the evaluation of the tangent stiffness matrix of the cross section and of the internal forces associated with the nonlinear

stress field is required.

Global convergence of the second iterative procedure is ensured by proving its equivalence to the minimization of a convex potential which is bounded below and adopting a suitable modification of the exact Hessian of the potential. The rate of convergence of the procedure is quite satisfactory since it has been found to be quadratic in most of the performed numerical tests.

It is worth noting that the second procedure of the proposed solution strategy involves two of the basic ingredients of any nonlinear finite element analysis of RC structures, that is the evaluation of the tangent stiffness matrix and of the internal forces of a given element to be later assembled at the structural level. Therefore the proposed algorithm can also represent a useful contribution to the nonlinear finite element analysis of RC structures.

An additional nice feature of the proposed solution strategy, analogous to an early proposal on the same subject [35], is to provide directly the ultimate load starting from an initial value  $\mathbf{f}_e$ . The ultimate load is obtained by increasing  $\mathbf{f}_e$  along a defined loading direction  $\mathbf{f}_l$  without the need of knowing or constructing explicitly the whole interaction surface. Clearly, this represents a particularly useful property for efficiently post-processing the values of the internal forces obtained from the analysis of the structural model since we directly estimate whether they are safe by checking that the ultimate load  $\mathbf{f}^* = \mathbf{f}_e + (\lambda^* - 1)\mathbf{f}_l$  is associated with a value of  $\lambda^* > 1$ ; thus  $\lambda^*$  provides a sort of safety factor against the ultimate state.

## 1.2 Nonlinear analysis of RC frame structures

Current seismic design recommendations assume that structures respond elastically only to small magnitude earthquakes but are expected to experience different degrees of damage during moderate and strong ground motions. Thus, in regions of high seismic risk, structures are required to respond inelastically to the maximum earthquake expected at the site during their usable life.

To date several models for the nonlinear response analysis of reinforced concrete structures have been developed [80].

In particular, the present thesis concentrates on RC buildings and, within this class of structural models, on the beam-column discretization. Actually, it still represents the best compromise between simplicity and accuracy in nonlinear seismic modelling since a significant insight into the response of each members and of the entire structure is achieved at the price of a reasonable computational effort, presently sustainable by every design office.

In the beam-column approach to the analysis of RC buildings, the structure is modelled as an assembly of interconnected elements whose nonlinear constitutive behaviour is either introduced at the element level in an average sense or at the section level. The former approach is usually referred to as element formulation with lumped nonlinearity while the latter leads to member models with distributed nonlinearity.

Referring the reader to chapter 3 for an historical perspective of the lumped approach, the thesis focuses on the fiber beam elements which have been developed in the last twenty years.

The first elements with distributed non linearity were formulated with the classical stiffness method using cubic Hermitian polynomials to approximate the deformations along the element [45, 63]. The formulation has been extended in [6] to include the effect of shear by means of multiaxial constitutive laws based on the endochronic theory.

However, serious inaccuracy problems affect stiffness-based elements due to their inability to describe the behaviour of the member near its ultimate resistance and after the onset of strain softening. The assumption of a cubic interpolation for the displacements, which resulting in a linear curvature distribution along the element, leads to satisfactory results under linear or nearly linear response. However, when the reinforced concrete member undergoes significant yielding at the ends, the curvature distribution becomes highly non-linear and a very fine discretization is required.

For this reason both computational savings and improved representation of internal deformations can be achieved by the combined approximation of the section deformations, which are the basic unknowns of the problem, and the section flexibilities. For this reason both variables have been interpolated in [69] and the axial force-bending moment interaction included. In this way fewer sections need to be monitored and, hence, the number of variables that need to be computed and stored is smaller than in stiffness models of comparable level of discretization.

More recent efforts aiming at developing robust and reliable reinforced-concrete frame elements have focused, on one side, on flexibility-based formulations, to achieve a more accurate description of the force distribution within the element and, on the other one, on the subdivision of elements into longitudinal fibers.

This second aspect engenders two main advantages: first, the reinforced concrete section behaviour is derived from the uniaxial stress-strain behaviour of the fibers so that three-dimensional effects, such as concrete confinement by transverse steel, can be incorporated into the uniaxial stress-strain relation; second, the interaction between bending moment and axial

force can be described accurately.

The milestone in the flexibility-based approach is represented by the rightly celebrated papers by Spacone, Taucer and Filippou [91, 92].

Subsequently several additional formulations have appeared [90, 72, 77, 98]. They have been recently extended in [2, 17] to account for the interaction of normal and shear stresses. Nonetheless displacement based formulations are still object of active research [48, 49].

For this reason two displacement based formulations are described in the thesis mainly to show how the section analysis presented in chapters 3 e 4 can be used in a non-linear finite element analysis of the structure. With the aim of pointing out the general application of the proposed fiber-free approach, a force-based formulation is also described since the same integration method is required indifferently in displacement-based, force-based and mixed elements.

## Chapter 2

# Ultimate Limit State analysis of RC sections subject to axial force and biaxial bending

In this chapter a numerical procedure, based upon a tangent approach, for evaluating the ultimate limit state (ULS) of reinforced concrete (RC) sections subject to axial force and biaxial bending is presented. The RC sections are assumed to be of arbitrary polygonal shape and degree of connection; furthermore, it is possible to keep fixed a given amount of the total load and to find the ULS associated only with the remaining part which can be increased by means of a load multiplier. The solution procedure adopts two nested iterative schemes which, in turn, update the current value of the tentative ultimate load and the associated strain parameters. In this second scheme an effective integration procedure is used for evaluating in closed form, as explicit functions of the position vectors of the vertices of the section, the domain integrals appearing in the definition of the tangent matrix and of the stress resultants. Under mild hypotheses, which are practically satisfied for all cases of engineering interest, the existence and uniqueness of the ULS load multiplier is ensured and the global convergence of the proposed solution algorithm to such value is proved. An extensive set of numerical tests, carried out for rectangular, L-shaped and multicell sections shows the effectiveness of the proposed solution procedure.

## 2.1 Assumptions and material properties

The ultimate limit state (ULS) analysis of RC sections subject to axial load and biaxial bending is carried out by adopting the assumptions specified in [33, 39]; for the reader's ease, they are briefly recalled below:

a) beam sections remain plane after deformation and perfect bond between steel bars and concrete is assumed. Hence the strain in the concrete and in the steel rebars, in the direction of the beam axis, is provided by the same linear function which will be denoted by  $\varepsilon$ ;

b) the stress state is uniaxial in the direction of the beam axis. Hence the stress and strain components in this direction will be simply referred to as stress and strain;

c) the tensile strength of concrete is neglected;

d) the constitutive law of concrete is provided by:

$$\sigma_c(\varepsilon) = \begin{cases} 0 & \text{if } 0 < \varepsilon \\ \alpha \varepsilon + \beta \varepsilon^2 & \text{if } \varepsilon_{cp} < \varepsilon \leq 0 \\ \sigma_{cu} & \text{if } \varepsilon_{cu} < \varepsilon \leq \varepsilon_{cp} \end{cases} \quad (2.1)$$

where  $\sigma_c$  denotes the stress in the concrete,  $\alpha = -1000\sigma_{cu}$ ,  $\beta = 250\alpha$ , the ultimate stress  $\sigma_{cu} = -0.85f_{ck}/1.6$  is expressed as function of the characteristic compression strength  $f_{ck}$  of the concrete while  $\varepsilon_{cp} = -0.002$  and  $\varepsilon_{cu} = -0.0035$ . The constitutive law (2.1) is reported diagrammatically in figure 2.1(a);

e) the following elastic-perfectly plastic constitutive law is assumed for the reinforcing bars, see e.g. figure 2.1(b):

$$\sigma_s(\varepsilon) = \begin{cases} -\sigma_{sy} & \text{if } -\varepsilon_{su} < \varepsilon \leq -\varepsilon_{sy} \\ E_s \varepsilon & \text{if } -\varepsilon_{sy} < \varepsilon \leq \varepsilon_{sy} \\ \sigma_{sy} & \text{if } \varepsilon_{sy} < \varepsilon \leq \varepsilon_{su} \end{cases} \quad (2.2)$$

where  $\sigma_s$  denotes the steel stress,  $E_s$  the Young modulus,  $\sigma_{sy}$  and  $\varepsilon_{sy} = \sigma_{sy}/E_s$  represent in turn the yield stress and the yield strain and  $\varepsilon_{su}$  is the ultimate strain. It is assumed  $\varepsilon_{su} = 0.01$  while, denoting by  $f_{yk}$  the characteristic yield stress,  $\sigma_{sy} = f_{yk}/1.15$ .

The ULS of the section is established to be attained when the maximum compressive strain in the concrete is equal to  $\varepsilon_{cu}$  and/or the maximum steel tensile strain is equal to  $\varepsilon_{su}$ .

Furthermore, in the case of a fully compressed section and denoting by  $h$  the section depth along the direction orthogonal to the neutral axis, it is

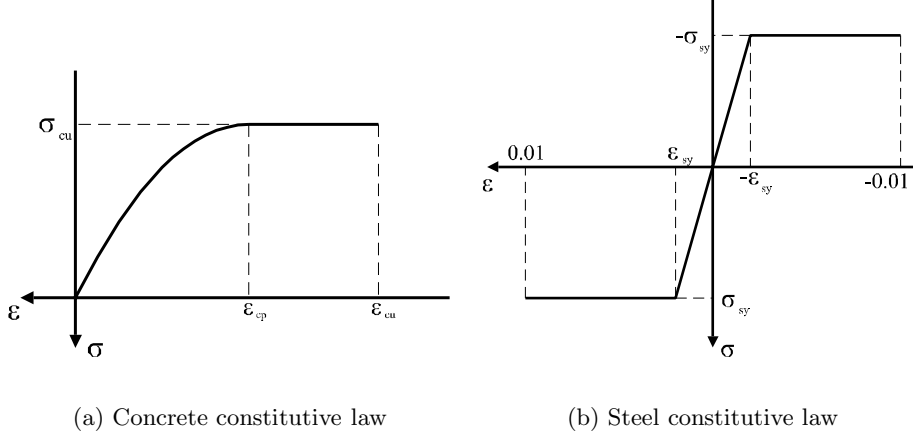


Figure 2.1: Constitutive laws of materials

assumed that for the concrete fibers lying at a distance equal to  $\frac{3}{7}h$  from the most compressed vertex strain attains values which do not exceed the value  $\varepsilon_{cp}$ . In this circumstance we shall denote the strain at the most compressed vertex as  $\varepsilon_c^-$  so that the minimum strain attainable in the concrete is equal to  $\varepsilon_{cl}$  where  $\varepsilon_{cl} = \varepsilon_c^-$  for a fully compressed section or  $\varepsilon_{cl} = \varepsilon_{cu}$  otherwise.

## 2.2 Formulation of the problem

Let us consider a beam section having a completely arbitrary polygonal shape, either single- or multi-cell. Introducing a cartesian reference frame, see figure 2.2, having an arbitrary point  $O$  as origin, each point of the section is identified by a two-dimensional position vector  $\mathbf{r} = \{x, y\}$ . The vertices of the section boundary are numbered in consecutive order by circulating along the boundary in a counter-clockwise sense. We shall further denote by  $\mathbf{k}$  the unit vector directed along the  $z$  axis.

The domain occupied by the section is denoted by  $\Omega_c$  and it is assumed that the RC section embodies a non empty set  $I_s = \{(\mathbf{r}_{bj}, A_{bj}), j = 1, \dots, n_b\}$  collecting the steel reinforcements of the section. They are composed by  $n_b$  bars, the  $j$ -th of which has area  $A_{bj}$  and is placed at  $\mathbf{r}_{bj}$ . As usual in the flexural analysis of RC sections the reduction of the concrete section due to the presence of reinforcements is neglected since these last ones are assumed to be of zero diameter. For the same reason each steel bar contributes to the geometric properties of the RC section as a lumped area.

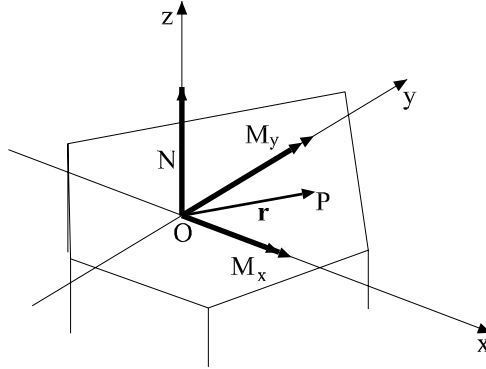


Figure 2.2: Cartesian reference frame and forces over the section

On account of the hypotheses detailed in the previous section the function  $\varepsilon$  which associates with each point  $\mathbf{r}$  of the section the corresponding strain is linear:

$$\varepsilon(\mathbf{r}) = \mathbf{g} \cdot \mathbf{r} + \varepsilon_o \quad (2.3)$$

where  $\mathbf{g} = \{g_x, g_y\}$  is the flexural curvature of the cross section and  $\varepsilon_o$  is the strain at the origin of the reference frame. For later convenience such strain parameters are assembled in the strain vector  $\mathbf{u} = \{\varepsilon_o, g_x, g_y\}$ .

Defining the three-dimensional vector  $\boldsymbol{\rho} = \{\mathbf{r}, 0\}$ , the stress resultants are:

$$N_r = \int_{\Omega_c} \sigma_c[\varepsilon(\mathbf{r})] d\Omega + \sum_{j=1}^{n_b} \sigma_s[\varepsilon(\mathbf{r}_{bj})] A_{bj} \quad (2.4)$$

$$\mathbf{M}_r = \int_{\Omega_c} \boldsymbol{\rho} \times \{\sigma_c[\varepsilon(\mathbf{r})] \mathbf{k}\} d\Omega + \sum_{j=1}^{n_b} \boldsymbol{\rho} \times \{\sigma_s[\varepsilon(\mathbf{r}_{bj})] \mathbf{k}\} A_{bj} \quad (2.5)$$

where  $N_r$  is the internal axial force and the vector  $\mathbf{M}_r^T = \{(\mathbf{M}_r)_x, (\mathbf{M}_r)_y, 0\}$  is the internal bending moment.

For the ensuing developments it is more convenient to express the previous relation in a simpler form by introducing the two-dimensional vector  $([\mathbf{M}_r]^\perp)^T = \{-(\mathbf{M}_r)_y, (\mathbf{M}_r)_x\}$  obtained by picking the two non-zero entries of the vector  $\mathbf{k} \times \mathbf{M}_r$ :

$$[\mathbf{M}_r]^\perp = \int_{\Omega_c} \sigma_c[\varepsilon(\mathbf{r})] \mathbf{r} d\Omega + \sum_{j=1}^{n_b} \sigma_s[\varepsilon(\mathbf{r}_{bj})] A_{bj} \mathbf{r}_{bj} \quad (2.6)$$

In the sequel the stress resultants will be collectively referred to as  $\mathbf{f}_r^T = \{N_r, -(\mathbf{M}_r)_y, (\mathbf{M}_r)_x\}$ . Clearly, on the basis of the hypothesis made on the concrete behaviour in tension and of the nonlinear behaviour of materials, the vector  $\mathbf{f}_r$  is a non-linear function of  $\mathbf{u}$ .

The set of values of  $\mathbf{f}_r$  associated with a strain field  $\varepsilon_c \geq \varepsilon_{cl}$  in the concrete and  $\varepsilon_s \leq \varepsilon_{su}$  for the steel bars, defines the admissible domain. Its boundary represents the interaction surface.

We shall also indicate by  $\mathbf{f}_e$  an external force vector, i.e. the vector  $\mathbf{f}_e^T = \{N_e, -(\mathbf{M}_e)_y, (\mathbf{M}_e)_x\}$  collecting the known values of axial force and biaxial bending moments which have to be checked against the ultimate limit state, typically the values resulting from the analysis of the structural model which the given section belongs to.

Similarly to [35] we don't explicitly evaluate the interaction surface in order to check whether the external forces collected in the vector  $\mathbf{f}_e$  lie inside the admissible domain since this task is not only expensive to achieve but completely unnecessary. Rather, we verify that the strain field  $\varepsilon(\mathbf{r})$  induced by  $\mathbf{f}_e$  fulfills the above defined limitations.

Furthermore, we suppose that the external force vector  $\mathbf{f}_e$  can be decomposed as follows:

$$\mathbf{f}_e = \mathbf{f}_d + \mathbf{f}_l \quad (2.7)$$

where  $\mathbf{f}_d$  is associated with the dead load and  $\mathbf{f}_l$  embodies the external forces induced in the section by the live load acting on the structure which the section belongs to. Thus, introducing the vector

$$\mathbf{f}(\lambda) = \mathbf{f}_d + \lambda \mathbf{f}_l = \mathbf{f}_e + (\lambda - 1) \mathbf{f}_l \quad (2.8)$$

the value  $\lambda^* > 0$  whereby  $\mathbf{f}(\lambda^*)$  belongs to the interaction surface gives us a measure of how much the external force vector  $\mathbf{f}_e$  is distant from the interaction surface along the direction of  $\mathbf{f}_l$ . Actually, a value  $\lambda > 1$  implies that the external force vector  $\mathbf{f}_e$  can be further increased, along the direction defined by  $\mathbf{f}_l$ , till when the ULS of the section is achieved.

On account of the above specifications we formulate the ULS problem of RC sections as follows.

### Ultimate limit state (ULS) problem of RC sections

Given an external load vector  $\mathbf{f}$ , sum of a constant part  $\mathbf{f}_d$  and a non-constant part  $\lambda \mathbf{f}_l$ , find the minimum positive value  $\lambda^*$  of the load amplifier so as to fulfill at least one of the following conditions:

$$\min_{\mathbf{r} \in \Omega_c} \{\mathbf{g}^* \cdot \mathbf{r} + \varepsilon_o^*\} = \varepsilon_{cl} \quad (2.9)$$

$$\max_{j=1,\dots,n_b} \{\mathbf{g}^* \cdot \mathbf{r}_{bj} + \varepsilon_o^*\} = \varepsilon_{su} \quad (2.10)$$

where  $\mathbf{g}^*$  and  $\varepsilon_o^*$  are the components of the strain parameters vector  $\mathbf{u}^*$  such that the nonlinear equilibrium equations

$$\mathbf{f}^* = \mathbf{f}_d + \lambda^* \mathbf{f}_l = \mathbf{f}_r(\mathbf{u}^*) \quad (2.11)$$

are fulfilled for the section.

In the sequel the admissible domain will be assumed to be convex and bounded. To the best of the authors knowledge this result has not yet been proved though it has been found to be always fulfilled, both for the few sections presented in the sequel and the other ones not documented here. In this respect, is worth noting that all classical results of ultimate limit strength analysis based on plasticity theory cannot be applied in this context. This is because, in accordance with most of the codes of practice, and in particular with the EC2 [39], the ultimate limit state analysis of RC sections is based on limitations to the strains, together with the specification of a nonlinear constitutive relationship for the materials. Instead, ultimate limit strength analysis based on classical plasticity theory is based on the hypothesis of infinite ductility of the material.

In order to make the ULS problem well defined it is further assumed that  $\mathbf{f}_d$  lies within the admissible domain in the sense previously defined.

Hence, because of the assumed convexity and boundedness of the admissible domain the following results clearly holds (see also figure 2.3):

**Proposition 2.2.1** *The solution to the ULS problem defined above exists and is unique.* ■

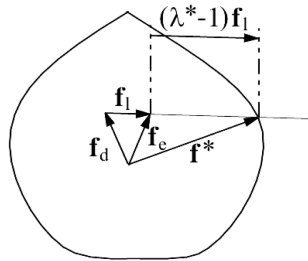


Figure 2.3: Uniqueness of the solution  $\lambda^*$

## 2.3 Solution algorithm

The peculiar form of the system (2.11) naturally suggests two alternative solution strategies: the first one, exploited in [35], iteratively looks for a strain vector  $\mathbf{u}_i$  fulfilling at least one of the constraints (2.9) - (2.10) and generating a stress field over the section such that the resultant can actually be decomposed as the sum of the fixed vector  $\mathbf{f}_d$  and of the variable one  $\lambda_i \mathbf{f}_1$ , where  $\lambda_i$  is evaluated as function of  $\mathbf{u}_i$ .

The second solution strategy, which is the one we are going to illustrate in the subsequent sections, first evaluates a tentative value of the variable load amplifier  $\lambda_i$  and only subsequently provides the strain vector  $\mathbf{u}_i$  associated with the updated value of the ultimate load  $\mathbf{f}_i = \mathbf{f}_d + \lambda_i \mathbf{f}_1$ .

Thus, at each iteration of this last solution strategy, two nested iterative schemes have to be carried out: the first one, which is indicated as *procedure A* and is by far simpler, amounts to estimating the current value  $\lambda_i$  as function of the quantities evaluated at the previous iterations.

The second iterative scheme, which will be referred to as *procedure B*, represents the main computational burden of the whole algorithm since it evaluates the strain parameters  $\mathbf{u}_i$  associated with  $\mathbf{f}_i$  by means of a modified Newton method enhanced with line searches.

Thus, at the  $i$ -th iteration of the solution algorithm, we first estimate a tentative value  $\lambda_i$  of the load amplifier  $\lambda^*$  and then the strain parameters  $\mathbf{u}_i$  associated with the load  $\mathbf{f}_i = \mathbf{f}_d + \lambda_i \mathbf{f}_1$ . The problem of evaluating the strain vector  $\mathbf{u}$  corresponding to a load  $\mathbf{f}$  will be often invoked in the sequel and denoted as *the nonlinear problem*  $\mathbf{u}(\mathbf{f})$ .

The whole solution algorithm is synthetically described in figures 2.4 and 2.7.

### 2.3.1 Solution scheme for the evaluation of $\lambda^*$ : Procedure A

The rationale of this phase of the solution algorithm is to associate with each estimate  $\lambda_i$  of the variable load amplifier an error  $e_i$  which measures the amount by which the current value  $\mathbf{u}_i$  of the strain parameters is far from the attainment of the ultimate limit state.

The error  $e_i$  is defined as follows:

$$e_i = \min \left\{ \frac{\varepsilon_{cl} - \varepsilon_{i,\min}^c}{\varepsilon_{cl}}; \frac{\varepsilon_{su} - \varepsilon_{i,\max}^s}{\varepsilon_{su}} \right\} \quad (2.12)$$

where

$$\varepsilon_{i,\min}^c = \min_{\mathbf{r} \in \Omega_c} \left\{ \varepsilon_o^{(i)} + \mathbf{g}^{(i)} \cdot \mathbf{r} \right\} \quad \varepsilon_{i,\max}^s = \max_{j=1,\dots,n_b} \left\{ \varepsilon_o^{(i)} + \mathbf{g}^{(i)} \cdot \mathbf{r}_{bj} \right\} \quad (2.13)$$

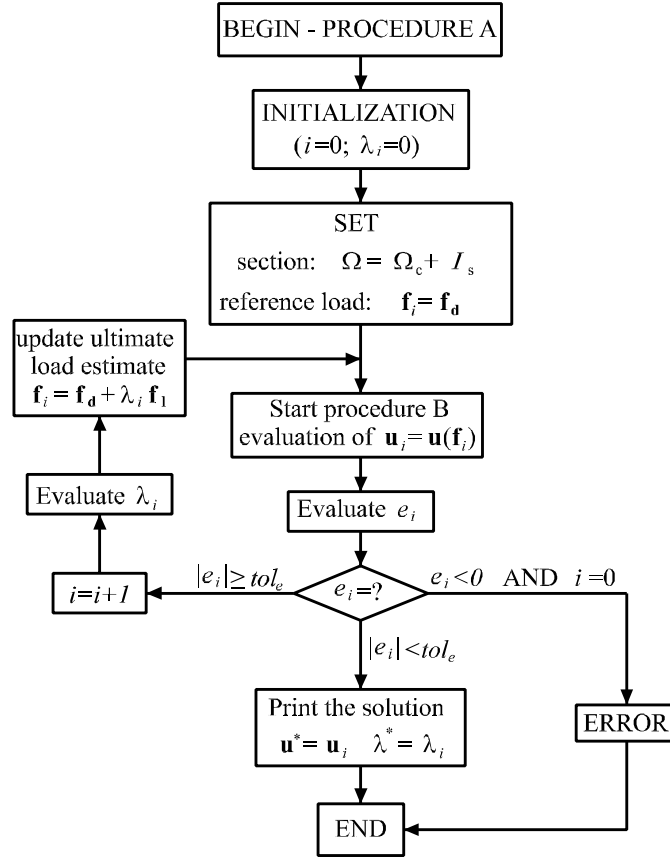


Figure 2.4: Solution scheme for the evaluation of  $\lambda^*$

and  $\varepsilon_o^{(i)}$  and  $\mathbf{g}^{(i)}$  are the entries of the vector  $\mathbf{u}_i$ . Accordingly, the error  $e_i$  can be considered as a composite function of  $\mathbf{u}_i$  and  $\lambda_i$ .

Clearly, a null value of  $e_i$  is indicative of the attainment of an ultimate state for the section while a positive (negative) value of  $e_i$  is associated with a current estimate of the ultimate load  $\mathbf{f}_i = \mathbf{f}_d + \lambda_i \mathbf{f}_1$  which lies inside (outside) the admissible domain. Convergence is attained if

$$|e_i| < tol_e \tag{2.14}$$

where, in our calculations, it has been assumed  $tol_e = 10^{-5}$ .

The solution algorithm starts ( $i = 0$ ) by setting  $\lambda_0 = 0$  so that only the fixed part  $\mathbf{f}_d$  of the load is initially supposed to act on the section.

In this way one can immediately check wheter or not the ultimate limit

state problem is well posed in the sense that the fixed part of the load  $\mathbf{f}_d$  lies inside or outside the admissible domain. In the former case, which is typically the case of interest, the strain parameters  $\mathbf{u}_0$  associated with  $\mathbf{f}_d$  are such that the strain  $\varepsilon_c$  in the most compressed vertex of the concrete section is greater than  $\varepsilon_{cl}$  and the strain  $\varepsilon_s$ , defined as the maximum tensile stress in all steel bars, is lower than  $\varepsilon_{su}$ . Therefore, the error  $e_0$  associated with  $\mathbf{u}_0$ , to be evaluated by means of formula (2.12), is certainly positive.

At subsequent iterations ( $i \geq 2$ ) the current estimate  $\lambda_i$  is evaluated, as a rule, as function of two pairs  $(\lambda_a, e_a) - (\lambda_b, e_b)$  computed at iterations  $a$  and  $b$  of the solution algorithm previous than the current one by means of the following formula:

$$\lambda_i = \frac{e_a \lambda_b - e_b \lambda_a}{e_a - e_b} \quad i \geq 2 \quad (2.15)$$

Specifically, if at least one of the errors  $e_j$  ( $j < i$ ) is negative, the previous formula is applied to the pairs  $(\lambda_n, e_n)$  and  $(\lambda_p, e_p)$  where  $\lambda_n$  is the minimum value among all values whose associated errors  $e_n$  are negative and  $\lambda_p$  is the maximum value which positive errors  $e_p$  correspond to. Clearly, the resulting expression does not depend on the order adopted to associate the pairs  $(\lambda_n, e_n) - (\lambda_p, e_p)$  with the pairs  $(\lambda_a, e_a) - (\lambda_b, e_b)$ . Thus, in this case formula (2.15) results in the following linear interpolation:

$$\lambda_i = \frac{e_p \lambda_n - e_n \lambda_p}{e_p - e_n} \quad i \geq 2 \quad (2.16)$$

Being  $\lambda_n$  and  $\lambda_p$  positive by definition, the previous formula always provides positive values for  $\lambda_i$ .

The same circumstance occurs if the errors  $e_j$ , evaluated at the iterations  $j$  previous than the current one, are positive but the last two pairs of errors  $(\lambda_{i-2}, e_{i-2}) - (\lambda_{i-1}, e_{i-1})$  define a decreasing linear function in the plane  $(\lambda, e)$ . In this case formula (2.15) results in the following linear extrapolation:

$$\lambda_i = \frac{e_{i-2} \lambda_{i-1} - e_{i-1} \lambda_{i-2}}{e_{i-2} - e_{i-1}} \quad i \geq 2 \quad (2.17)$$

which supplies a positive value for  $\lambda_i$  since, by hypothesis,  $e_{i-2} > e_{i-1}$  and  $\lambda_{i-2} < \lambda_{i-1}$ .

Finally, when the errors  $e_j$  are positive but the pairs  $(\lambda_{i-2}, e_{i-2})$  and  $(\lambda_{i-1}, e_{i-1})$  define a non-decreasing linear function, we update  $\lambda_i$  in the form:

$$\lambda_i = 2(\lambda_{i-1} - \lambda_{i-2}) + \lambda_{i-1} \quad i \geq 2 \quad (2.18)$$

that is by adding to the last value  $\lambda_{i-1}$  twice the interval between the two last estimates of  $\lambda$ .

In fact, because of the existence and uniqueness of the solution to the ULS problem and the fact that  $e_0 = e(0) > 0$ , we are sure that, for a sufficiently large value of  $\lambda_i$ ,  $e$  will become negative. Notice that, there is no theoretical reason for adopting 2 as amplification of the interval  $\lambda_{i-1} - \lambda_{i-2}$  if not the objective of achieving as soon as possible values of  $\lambda_i$  which make  $e_i$  negative. In this way we can more rapidly individuate the value  $\lambda^*$  which makes the error  $e$  vanish and hence characterize the ultimate limit state of the section.

It is worth notice that the use of formula (2.18) is typically invoked at the very beginning of the solution algorithm whenever we are, depending on the adopted values of  $\mathbf{f}_d$  and  $\mathbf{f}_l$ , particularly far from the solution.

In fact, suppose that  $\mathbf{f}_d$  has been chosen very close to the (unknown) interaction surface, hence the error  $e_0$  is very small, and that we are moving along a direction  $\mathbf{f}_l$  which makes the ultimate load  $\mathbf{f}^*$  be attained for a value of  $\lambda^*$  by far greater than the one associated with  $-\mathbf{f}_l$ . In this case the numerical experiments have shown that the function  $e(\lambda)$  corresponding to the adopted choice of  $\mathbf{f}_l$  is increasing in the vicinity of  $\lambda_0 = 0$  so that formula (2.18) must be necessarily resorted to (see figure 2.5).

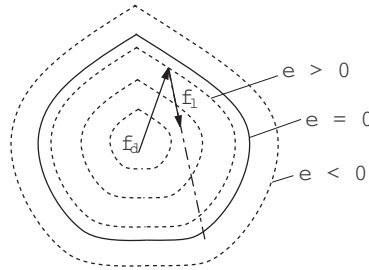


Figure 2.5: Typical case when formula (2.18) is used; the dashed lines are the level sets of  $e(\lambda)$

Let us now detail how the numerical algorithm for the evaluation of  $\lambda^*$  proceeds after that the pair  $(0, e_0)$  has been determined. Actually, it is apparent that, in order to employ formulas (2.16), (2.17) and (2.18), at least two values of the pair  $(\lambda, e)$  are needed.

The second pair  $(\lambda_1, e_1)$ , to be used at the beginning of the algorithm is

estimated as follows. Let us linearize the function  $\mathbf{u} = \mathbf{u}(\mathbf{f})$  at  $\mathbf{f} = \mathbf{f}_d$ :

$$\mathbf{u}(\mathbf{f}_d + \lambda \mathbf{f}_1) \simeq \mathbf{u}(\mathbf{f}_d) + \left( \frac{\partial \mathbf{u}}{\partial \mathbf{f}_r} \right)_{\mathbf{f}_d} \lambda \mathbf{f}_1 = \mathbf{u}_0 + \left( \frac{\partial \mathbf{f}_r}{\partial \mathbf{u}} \right)_{\mathbf{u}_0}^{-1} \lambda \mathbf{f}_1 \quad (2.19)$$

where  $(\partial \mathbf{f}_r / \partial \mathbf{u})_{\mathbf{u}_0}$  is the tangent operator evaluated at solution of the iterative scheme, to be detailed in the next subsection, which provides the strain vector  $\mathbf{u}_0$  associated with  $\mathbf{f}_d$ .

Since  $\mathbf{u}_0$  is not a limit state, the strain limits  $\varepsilon_{cl}$  and  $\varepsilon_{su}$  are not attained at any point of the section; accordingly, we evaluate the positive scalar  $\lambda_1$  by scaling the fixed quantity  $(\partial \mathbf{f}_r / \partial \mathbf{u})_{\mathbf{u}_0}^{-1} \mathbf{f}_1$  added to  $\mathbf{u}_0$  so as to make the strain limits attained at least at one point of the section.

In particular, being the strain  $\varepsilon_j$  at the generic vertex of the concrete section or at the generic steel bar a linear function of  $\lambda$ :

$$\varepsilon_j = \mathbf{u} \cdot \begin{pmatrix} 1 \\ x_j \\ y_j \end{pmatrix} = \mathbf{u}_0 \cdot \begin{pmatrix} 1 \\ x_j \\ y_j \end{pmatrix} + \lambda \left( \frac{\partial \mathbf{f}_r}{\partial \mathbf{u}} \right)_{\mathbf{u}_0}^{-1} \mathbf{f}_1 \cdot \begin{pmatrix} 1 \\ x_j \\ y_j \end{pmatrix} = a_j + \lambda b_j \quad (2.20)$$

it is an easy matter to compute the value  $\lambda_j^c$  necessary to enforce the ultimate strain  $\varepsilon_{cl}$  at the  $j$ -th vertex of the concrete section:

$$\lambda_j^c = \frac{\varepsilon_{cl} - a_j}{b_j} \quad (2.21)$$

or, analogously, the value

$$\lambda_k^s = \frac{\varepsilon_{su} - a_k}{b_k} \quad (2.22)$$

associated with the attainment of  $\varepsilon_{su}$  at the  $k$ -th bar.

Accordingly, the required value of  $\lambda_1$  is given by

$$\lambda_1 = \min_{\lambda > 0} \{ \lambda_j^c, \lambda_k^s \} \quad j \in V_{\Omega_c}; \quad k \in \{1, \dots, n_b\} \quad (2.23)$$

where  $V_{\Omega_c}$  denotes the set collecting the vertices of the concrete section.

Starting from the value  $\lambda_1$  we can solve the nonlinear problem  $\mathbf{u}(\mathbf{f}_d + \lambda_1 \mathbf{f}_1)$ , that provides the actual strain parameters  $\mathbf{u}_1$  associated with the load  $\mathbf{f}_d + \lambda_1 \mathbf{f}_1$ , and evaluate the relevant error  $e_1$  by means of (2.12).

We now dispose of two pairs  $(0, e_0)$  and  $(\lambda_1, e_1)$  which allow us to get the load amplifier at the second iteration of the solution algorithm; namely, if  $e_1 < e_0$  we get from (2.16) or (2.17):

$$\lambda_2 = \frac{e_0 \lambda_1}{e_0 - e_1} \quad (2.24)$$

while, in the opposite case, the value:

$$\lambda_2 = 3\lambda_1 \quad (2.25)$$

is obtained from formula (2.18).

For the reader's convenience the essential steps of the algorithm are summarized in figure 2.4.

### 2.3.2 Solution scheme for the evaluation of $\mathbf{u}(\mathbf{f})$ : Procedure B

As repeatedly pointed out in the previous subsection the proposed solution algorithm requires the evaluation of the strain parameters  $\mathbf{u}$  associated with a given value  $\mathbf{f} = \mathbf{f}_d + \lambda \mathbf{f}_l$  of the axial force and bending moments acting on the section.

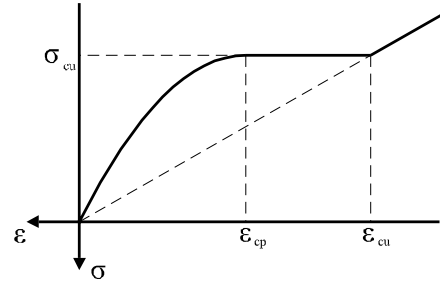
In this respect we remark that, in this phase of the solution algorithm, we are not looking for a limit state of the section but simply evaluating the strain field in the section corresponding to a given load value. Actually, the load  $\mathbf{f}_i = \mathbf{f}_d + \lambda_i \mathbf{f}_l$  associated with  $i$ -th estimate of  $\lambda$  may lie outside the admissible domain so that stress on the section relative to  $\mathbf{u}(\mathbf{f}_i)$  may attain values beyond the ultimate values reported in (2.1) and (2.2).

Therefore, in order to compute the resultant vector  $\mathbf{f}_r$  associated with such a stress field, we need to define the constitutive laws (2.1) and (2.2) for strain values external to the intervals considered therein. For this reason the nonlinear constitutive laws of the materials have been extended beyond the ultimate values, as illustrated in figure 2.6(a) and figure 2.6(b), by means of the following relationship for concrete:

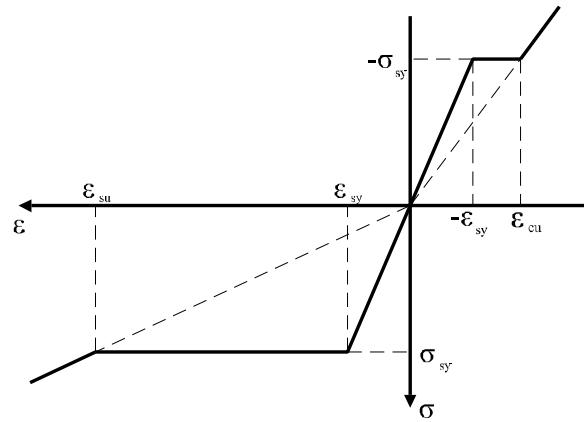
$$\sigma_c^r(\varepsilon) = \begin{cases} 0 & \text{if } 0 < \varepsilon \\ \alpha \varepsilon + \beta \varepsilon^2 & \text{if } \varepsilon_{cp} < \varepsilon \leq 0 \\ \sigma_{cu} & \text{if } \varepsilon_{cu} < \varepsilon \leq \varepsilon_{cp} \\ E_c^{sec} \varepsilon = \frac{\sigma_{cu}}{\varepsilon_{cu}} \varepsilon & \text{if } \varepsilon < \varepsilon_{cu} \end{cases} \quad (2.26)$$

and the additional one for steel

$$\sigma_s^r(\varepsilon) = \begin{cases} E_{sc}^{sec} \varepsilon = -\frac{\sigma_{sy}}{\varepsilon_{cu}} \varepsilon & \text{if } \varepsilon \leq \varepsilon_{cu} \\ -\sigma_{sy} & \text{if } \varepsilon_{cu} < \varepsilon \leq -\varepsilon_{sy} \\ E_s \varepsilon & \text{if } -\varepsilon_{sy} < \varepsilon \leq \varepsilon_{sy} \\ \sigma_{sy} & \text{if } \varepsilon_{sy} < \varepsilon \leq \varepsilon_{su} \\ E_{st}^{sec} \varepsilon = \frac{\sigma_{sy}}{\varepsilon_{su}} \varepsilon & \text{if } \varepsilon_{su} < \varepsilon \end{cases} \quad (2.27)$$



(a) Concrete constitutive law for the evaluation of the resultant load



(b) Steel constitutive law for the evaluation of the resultant load

Figure 2.6: Constitutive laws of materials for the evaluation of the resultant load

It is apparent that  $\sigma_c^r$  coincides with the function  $\sigma_c$  defined by (2.1) for  $\varepsilon_{cu} \leq \varepsilon$  and  $\sigma_s^r$  coincides with the function  $\sigma_s$  in the range  $\varepsilon_{cu} \leq \varepsilon \leq \varepsilon_{su}$ .

Furthermore, outside the previously defined strain intervals,  $\sigma_c^r$  and  $\sigma_s^r$  have been expressed, respectively, in terms of the secant modulus  $E_c^{sec}$  of concrete and of the secant moduli  $E_{sc}^{sec}$  and  $E_{st}^{sec}$  of steel. Clearly, apart from the algorithmic considerations detailed below, the choice of the constitutive laws outside the strain limits defined in (2.1) and (2.2) does not affect the

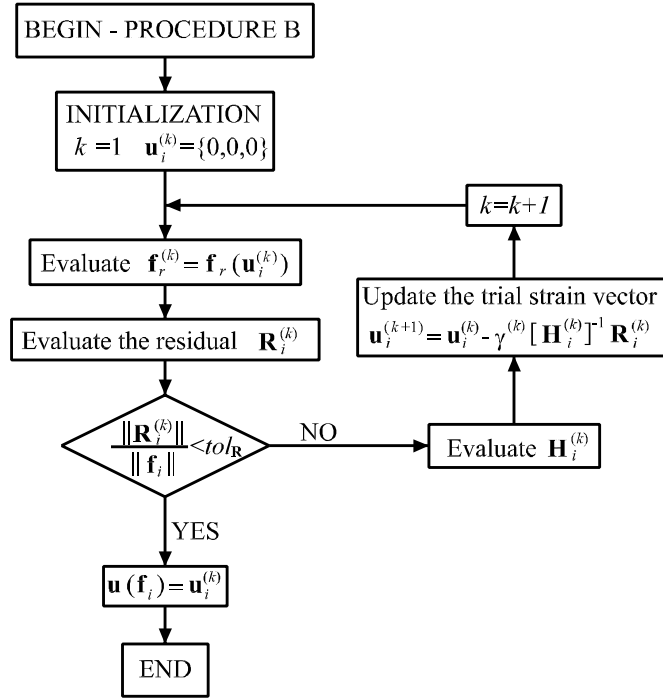


Figure 2.7: Solution scheme for the evaluation of  $\mathbf{u}(\mathbf{f}_i)$

final result since, within the numerical tolerance  $tol_e$ , the constraints  $\varepsilon_{cu} \leq \varepsilon^* \leq \varepsilon_{su}$  have to be fulfilled by the strain field  $\varepsilon^*$  associated with the solution  $\mathbf{u}^*$ .

To avoid proliferation of symbolism the stress resultants associated with the fields  $\sigma_c^r$  and  $\sigma_s^r$  will be collected in the vector  $\mathbf{f}_r$ , thus extending the original definition introduced after formulas (2.4) and (2.5).

Notice that any increasing function is adequate to extend  $\sigma_c^r$  below  $\varepsilon_{cu}$  and  $\sigma_s^r$  outside the range  $[\varepsilon_{cu}, \varepsilon_{su}]$  since, otherwise, the resultant vector  $\mathbf{f}_r$  could not be able to equilibrate an arbitrary value of the applied load  $\mathbf{f}$ ; thus, the most natural choice for extending the definition of the constitutive laws, which amounts to keeping constant the stresses for values of strain exceeding  $\varepsilon_{cu}$  and  $\varepsilon_{su}$ , would not meet our purposes.

Let us now illustrate the details of the modified Newton algorithm enhanced with line searches which has been adopted to solve the nonlinear problem  $\mathbf{u}(\mathbf{f}_i)$ .

Suppose that a given load  $\mathbf{f}_i^T = \mathbf{f}_d^T + \lambda_i \mathbf{f}_1^T = \{N_i, -(\mathbf{M}_i)_y, (\mathbf{M}_i)_x\}$  is

assigned at the  $i$ -th iteration of the solution algorithm and denote by  $\mathbf{u}_i^{(k)}$  the estimate of the relevant strain parameters  $\mathbf{u}_i$  at the  $k$ -th iteration of the modified Newton algorithm described in the sequel.

To avoid cumbersome symbolism the quantity  $\mathbf{u}_i^{(k)}$  will be simplified to  $\mathbf{u}^{(k)}$  while the vector  $\mathbf{f}_r^{(k)} = \{N_r^{(k)}, -(\mathbf{M}_r^{(k)})_y, (\mathbf{M}_r^{(k)})_x\}$  will denote the resultant of the stress field generated by  $\mathbf{u}^{(k)}$ . Analogously we shall set  $\mathbf{f} = \mathbf{f}_i$ . In other words, from now on, we shall describe in detail the procedure in figure 2.7 by assuming tacitly that it is started at the  $i$ -th iteration of procedure A illustrated in figure 2.4 and discussed in the previous section.

According to the Newton method we introduce the residual vector

$$\mathbf{R}^{(k)} = \mathbf{R}(\mathbf{u}^{(k)}) = \mathbf{f}_r^{(k)} - \mathbf{f} = \begin{bmatrix} N_r^{(k)} - N \\ [\mathbf{M}_r^{(k)}]^\perp - [\mathbf{M}]^\perp \end{bmatrix} \quad (2.28)$$

and its derivative with respect to the strain vector evaluated at  $\mathbf{u}^{(k)}$ :

$$\mathbf{dR}^{(k)} = \left( \frac{\partial \mathbf{R}}{\partial \mathbf{u}} \right)_{\mathbf{u}^{(k)}} = \frac{\partial \mathbf{f}_r}{\partial \mathbf{u}} \Big|_{\mathbf{u}^{(k)}} = \begin{bmatrix} \frac{\partial N_r}{\partial \varepsilon_o} \Big|_{\mathbf{u}^{(k)}} & \left[ \frac{\partial N_r}{\partial \mathbf{g}} \right]_{\mathbf{u}^{(k)}}^T \\ \frac{\partial [\mathbf{M}_r]^\perp}{\partial \varepsilon_o} \Big|_{\mathbf{u}^{(k)}} & \frac{\partial [\mathbf{M}_r]^\perp}{\partial \mathbf{g}} \Big|_{\mathbf{u}^{(k)}} \end{bmatrix} \quad (2.29)$$

The strain vector  $\mathbf{u}^{(k)}$  is updated in the form

$$\mathbf{u}^{(k+1)} = \mathbf{u}^{(k)} - \gamma^{(k)} [\mathbf{H}^{(k)}]^{-1} \mathbf{R}^{(k)} = \mathbf{u}^{(k)} + \gamma^{(k)} \mathbf{d}^{(k)} \quad (2.30)$$

where  $\mathbf{d}^{(k)} = -[\mathbf{H}^{(k)}]^{-1} \mathbf{R}^{(k)}$  and  $\gamma^{(k)}$  is a positive line search parameter.

The matrix  $\mathbf{H}^{(k)}$  represents a positive-definite matrix which is obtained by suitably modifying  $\mathbf{dR}^{(k)}$ , as detailed in section 2.5, in such a way that the algorithm is globally convergent and, in most of the cases, still possess quadratic rate of convergence.

Actually, the very special form of the constitutive laws (2.26) and (2.27) can lead to ill conditioning or even singularity of the tangent matrix  $\mathbf{dR}^{(k)}$ . This may happen, for instance, when large positive values of the axial force, near the ultimate load in pure traction, are applied to the section. In this case the compressed portion of the concrete section is void and all of the steel bars are yielded.

A similar circumstance occurs when the concrete section is uniformly compressed and the strain value ranges between  $\varepsilon_{cu}$  and  $\varepsilon_{cp}$ .

Thus, as suggested in [59], it is necessary to modify the tangent matrix  $\mathbf{dR}^{(k)}$  in order to guarantee convergence of the Newton method. As shown

in section 2.5 such a modification is naturally suggested by physical considerations and represents a viable alternative to additional techniques such as the Levenberg-Marquardt approach.

Convergence of the Newton method is attained if

$$\frac{\|\mathbf{R}^{(k)}\|}{\|\mathbf{f}\|} < tol_{\mathbf{R}}; \quad (2.31)$$

specifically, in the numerical examples reported in the sequel, it has been assumed  $tol_{\mathbf{R}} = 10^{-5}$ .

### 2.3.3 Finding $\mathbf{u}(\mathbf{f})$ by solving a minimization problem

In order to prove the global convergence of the proposed algorithm the following result is important:

**Proposition 2.3.1** *The function  $\mathbf{f}_r$  is integrable and admits the following convex,  $C^1$  potential:*

$$\phi(\mathbf{u}) = \int_{\Omega_c} \int_0^{\varepsilon(\mathbf{r}, \mathbf{u})} \sigma_c^r(\tilde{\varepsilon}) \, d\tilde{\varepsilon} + \sum_{j=1}^{n_b} A_{bj} \int_0^{\varepsilon(\mathbf{r}_{bj}, \mathbf{u})} \sigma_s^r(\tilde{\varepsilon}) \, d\tilde{\varepsilon} \quad (2.32)$$

*Proof:* Let  $\Gamma(\mathbf{u}_o, \mathbf{u})$  be a generic regular curve in  $\mathfrak{R}^3$  which connects the two points  $\mathbf{u}_o$  and  $\mathbf{u}$ , having a parametric description in terms of an arc length  $\tilde{s}$  given by  $\tilde{\mathbf{u}} = \tilde{\mathbf{u}}(\tilde{s})$ , with  $\tilde{\mathbf{u}}(s_o) = \mathbf{u}_o$  and  $\tilde{\mathbf{u}}(s) = \mathbf{u}$ . In absence of steel bars, the work  $L_{\Gamma}^c$  performed by  $\mathbf{f}_r(\mathbf{u})$  along  $\Gamma$  is given by:

$$\begin{aligned} L_{\Gamma}^c &= \int_{s_o}^s \left\{ \int_{\Omega_c} \begin{bmatrix} \sigma_c^r[\varepsilon(\mathbf{r}, \tilde{\mathbf{u}}(\tilde{s}))] \\ \sigma_c^r[\varepsilon(\mathbf{r}, \tilde{\mathbf{u}}(\tilde{s}))] \mathbf{r} \end{bmatrix} \cdot \tilde{\mathbf{u}}'(\tilde{s}) \, d\Omega \right\} d\tilde{s} = \\ &= \int_{s_o}^s \left[ \int_{\Omega_c} F(\mathbf{r}, \tilde{s}) \, d\Omega \right] d\tilde{s} \end{aligned} \quad (2.33)$$

Being  $F$  a compound function of continuous functions, it is continuous, too. Furthermore, since  $\Omega \times [s_o, s]$  is a compact set of  $\mathfrak{R}^3$ , the last integral exists and is finite, thus Fubini's theorem allows us to change the order of integration and obtain:

$$L_{\Gamma}^c = \int_{\Omega_c} \left[ \int_{\Gamma(\mathbf{u}_o, \mathbf{u})} \sigma_c^r[\varepsilon(\mathbf{r}, \tilde{\mathbf{u}})] (d\tilde{\varepsilon}_o + d\tilde{\mathbf{g}} \cdot \mathbf{r}) \right] d\Omega \quad (2.34)$$

Since  $\varepsilon(\mathbf{r}, \tilde{\mathbf{u}}) = \tilde{\varepsilon}_o + \tilde{\mathbf{g}} \cdot \mathbf{r}$ , we can write  $d\varepsilon(\mathbf{r}, \tilde{\mathbf{u}}) = d\tilde{\varepsilon}_o + d\tilde{\mathbf{g}} \cdot \mathbf{r}$  and then, changing variable of integration we obtain:

$$L_\Gamma^c = \int_{\Omega_c} \left[ \int_{\varepsilon(\mathbf{r}, \mathbf{u}_o)}^{\varepsilon(\mathbf{r}, \mathbf{u})} \sigma_c^r(\tilde{\varepsilon}) d\tilde{\varepsilon} \right] d\Omega \quad (2.35)$$

in which the dependance on the curve  $\Gamma$  has disappeared.

Analogous developments for the steel bars allow us to conclude that, for a given initial point  $\mathbf{u}_o$ ,  $L_\Gamma$  is a function only of  $\mathbf{u}$ , that is the potential  $\phi$  of the function  $\mathbf{f}_r$ . Assuming  $\mathbf{u}_o = \mathbf{0}$  it results:

$$\phi(\mathbf{u}) = \int_{\Omega_c} \left[ \int_0^{\tilde{\varepsilon}(\mathbf{r}, \mathbf{u})} \sigma_c^r(\varepsilon) d\varepsilon \right] d\Omega + \sum_{j=1}^{n_b} A_{bj} \int_0^{\varepsilon(\mathbf{r}_{bj}, \mathbf{u})} \sigma_s^r(\tilde{\varepsilon}) d\tilde{\varepsilon} \quad (2.36)$$

To prove that the  $\phi$  is convex, it is equivalent to demonstrate that its derivatives, that is  $\mathbf{f}_r$ , is monotonically increasing. This follows from:

$$\begin{aligned} & [\mathbf{f}_r(\mathbf{u}_2) - \mathbf{f}_r(\mathbf{u}_1)] \cdot (\mathbf{u}_2 - \mathbf{u}_1) = \\ & = \left[ \begin{array}{c} N_r(\varepsilon_{o2}, \mathbf{g}_2) - N_r(\varepsilon_{o1}, \mathbf{g}_1) \\ [\mathbf{M}_r]^\perp(\varepsilon_{o2}, \mathbf{g}_2) - [\mathbf{M}_r]^\perp(\varepsilon_{o1}, \mathbf{g}_1) \end{array} \right] \cdot \left[ \begin{array}{c} \varepsilon_{o2} - \varepsilon_{o1} \\ \mathbf{g}_2 - \mathbf{g}_1 \end{array} \right] = \\ & = \int_{\Omega_c} \{ \sigma_c^r[\varepsilon(\mathbf{r}, \mathbf{u}_2)] - \sigma_c^r[\varepsilon(\mathbf{r}, \mathbf{u}_1)] \} [\varepsilon(\mathbf{r}, \mathbf{u}_2) - \varepsilon(\mathbf{r}, \mathbf{u}_1)] d\Omega + \\ & + \sum_{j=1}^{n_b} \{ \{ \sigma_s^r[\varepsilon(\mathbf{r}_{bj}, \mathbf{u}_2)] - \sigma_s^r[\varepsilon(\mathbf{r}_{bj}, \mathbf{u}_1)] \} A_{bj} [\varepsilon(\mathbf{r}_{bj}, \mathbf{u}_2) + \\ & - \varepsilon(\mathbf{r}_{bj}, \mathbf{u}_1)] \} \geq 0 \end{aligned} \quad (2.37)$$

Since the stress-strain laws are monotonically increasing both for concrete and for steel, the last inequality holds because the two terms on its left-hand side are integral or sums of non-negative terms.  $\blacksquare$

The closed form expression of  $\phi$  as a function of the coordinates of the vertices and of the bars is given in section 2.6.

Hence, the problem of evaluating the strain parameters  $\mathbf{u}$  corresponding to a given applied load  $\mathbf{f}$  is equivalent to that of minimizing a convex function  $\psi$ , which is defined as follows:

$$\psi(\mathbf{u}) = \phi(\mathbf{u}) - \mathbf{f} \cdot \mathbf{u} \quad (2.38)$$

Clearly, it results  $\mathbf{R}^{(k)} = \nabla\psi(\mathbf{u}^{(k)})$ , so that the updating formula (2.30) can be rewritten as follows:

$$\mathbf{u}^{(k+1)} = \mathbf{u}^{(k)} - \gamma^{(k)} \mathbf{H}^{(k)} \nabla\psi(\mathbf{u}^{(k)}) \quad (2.39)$$

Hence, since  $\mathbf{H}^{(k)}$  is positive definite the updating formula provides a descent algorithm.

From the expression of  $\phi$ , provided in appendix E, it is easy to verify that for any section which has at least one steel bar in its interior, i.e. always in practice, some quadratic or cubic terms in the potential grows indefinitely when  $\mathbf{u} = \delta(\varepsilon_o, \mathbf{g})$  and  $\delta \rightarrow +\infty$ . This also means that  $\lim_{\delta \rightarrow +\infty} \psi(\delta \mathbf{u}) = +\infty$  for any  $\mathbf{u}$ , so that the recession cone of  $\psi$  is the null vector. Then, by applying theorem 1 (ii) of [51], or equivalently theorem 27.1 of [83], the following existence result is obtained:

**Proposition 2.3.2** *A solution  $\mathbf{u}^*$  to the problem  $\mathbf{u}(\mathbf{f})$  always exists, with  $\psi(\mathbf{u})$  attaining a finite global minimum at  $\mathbf{u}^*$ . Convexity of the function  $\psi$  also ensures the existence of the solution to the line search problem. ■*

The solution is not necessarily unique in terms of the strain-parameter vector  $\mathbf{u}$ . In fact, there exist possible states of deformation for the section whereby, in each point of the concrete part and in each steel bar, stress and strain define a point within a flat part of the corresponding stress-strain curves. For example this is the case when the whole section is in tension, with a zero stress in the concrete and all the steel bars yielded but with a strain below 0.01, or when the whole section is in compression, with a strain in the concrete  $\varepsilon_c$  verifying  $\varepsilon_{cu} < \varepsilon_c < \varepsilon_{cp}$ , and all the steel bars yielded in compression. If one of these states, say  $\mathbf{u}$ , corresponds to the solution of the problem  $\mathbf{u}(\mathbf{f})$  for a given applied load  $\mathbf{f}$ , it is then clear that a small enough variation  $\delta\mathbf{u}$  of  $\mathbf{u}$  will not change the internal force vector  $\mathbf{f}_r$ , so that  $\mathbf{u} + \delta\mathbf{u}$  will also be a solution. On the contrary, the solution is obviously unique in terms of internal force  $\mathbf{f}_r$ .

Furthermore, by making use of corollary 8.7.1 of [83], we can also state the following result:

**Proposition 2.3.3** *Given  $\delta \in \mathbf{R}$  the level set  $\{\mathbf{u} : \psi(\mathbf{u}) \leq \delta\}$ , if not empty, is always compact. ■*

which will be used in the next section.

### 2.3.4 Line search

The line search parameter  $\gamma^{(k)}$  is estimated as the final value of the iterative estimates  $\gamma_l^{(k)}$  evaluated in such a way that the residual [30]:

$$r_l^{(k)} = r^{(k)}(\gamma_l^{(k)}) = \frac{\mathbf{R}(\mathbf{u}^{(k)} + \gamma_l^{(k)} \mathbf{d}^{(k)}) \cdot \mathbf{d}^{(k)}}{\mathbf{R}(\mathbf{u}^{(k)}) \cdot \mathbf{d}^{(k)}} \quad (2.40)$$

fulfills the stopping criterion:

$$r^{(k)}(\gamma^{(k)}) \leq 0.9 \quad (2.41)$$

Further, in order to ensure that the function  $\psi$  actually decreases, another requirement on  $\gamma^{(k)}$  is [42]:

$$\frac{\psi(\mathbf{u}^{(k)}) - \psi(\mathbf{u}^{(k)} + \gamma^{(k)} \mathbf{d}^{(k)})}{\gamma^{(k)} \mathbf{R}(\mathbf{u}^{(k)}) \cdot \mathbf{d}^{(k)}} \leq -0.1 \quad (2.42)$$

**Lemma:** The scalar function  $r^{(k)}$  defined by (2.40) is a non-increasing function of  $\gamma_l^{(k)}$ .

*Proof:* Being the resultant force  $\mathbf{f}_r$  a non-decreasing function of the strain vector  $\mathbf{u}$ :

$$[\mathbf{f}_r(\mathbf{u}_2) - \mathbf{f}_r(\mathbf{u}_1)] \cdot (\mathbf{u}_2 - \mathbf{u}_1) \geq 0 \quad \forall \mathbf{u}_1, \mathbf{u}_2 \quad (2.43)$$

since  $\mathbf{f}_r$  is the gradient of  $\phi$ , see e.g. [83].

The same property is fulfilled by  $\mathbf{R} = \mathbf{f}_r - \mathbf{f}$ . In particular, at the  $k$ -th iteration of the procedure B reported in fig. 2.7 and for any  $\gamma_a^{(k)}$  and  $\gamma_b^{(k)}$ :

$$\begin{aligned} & [\mathbf{R}(\mathbf{u}^{(k)} + \gamma_a^{(k)} \mathbf{d}^{(k)}) - \mathbf{R}(\mathbf{u}^{(k)} + \gamma_b^{(k)} \mathbf{d}^{(k)})] \cdot (\mathbf{u}^{(k)} + \gamma_a^{(k)} \mathbf{d}^{(k)} + \\ & - \mathbf{u}^{(k)} - \gamma_b^{(k)} \mathbf{d}^{(k)}) \geq 0 \end{aligned} \quad (2.44)$$

from which one infers:

$$[\mathbf{R}(\mathbf{u}^{(k)} + \gamma_a^{(k)} \mathbf{d}^{(k)}) \cdot \mathbf{d}^{(k)} - \mathbf{R}(\mathbf{u}^{(k)} + \gamma_b^{(k)} \mathbf{d}^{(k)}) \cdot \mathbf{d}^{(k)}] (\gamma_a^{(k)} - \gamma_b^{(k)}) \geq 0 \quad (2.45)$$

Thus,  $\mathbf{R}(\mathbf{u}^{(k)} + \gamma^{(k)} \mathbf{d}^{(k)}) \cdot \mathbf{d}^{(k)}$  is a non-decreasing function of  $\gamma^{(k)}$ .

On the other hand the definition of  $\mathbf{d}^{(k)}$  yields:

$$\mathbf{R}(\mathbf{u}^{(k)}) \cdot \mathbf{d}^{(k)} = -\mathbf{R}(\mathbf{u}^{(k)}) \cdot \{[\mathbf{H}^{(k)}]^{-1} \mathbf{R}(\mathbf{u}^{(k)})\} < 0 \quad (2.46)$$

Hence, due to the positive-definiteness of  $\mathbf{H}^{(k)}$  and to the fact that the residual  $\mathbf{R}(\mathbf{u}^{(k)})$  is always different from zero when  $\mathbf{u}^{(k)}$  is not a solution vector, the scalar function  $r^{(k)}$  defined by formula (2.40) is a non-increasing function of  $\gamma^{(k)}$  and the lemma is proved.  $\blacksquare$

The line search parameter  $\gamma^{(k)}$  is estimated as functions of two pairs  $(\gamma_a^{(k)}, r_a^{(k)})$  and  $(\gamma_b^{(k)}, r_b^{(k)})$  computed at iterations  $a$  and  $b$  previous than the current one  $l$ , by the linear interpolation formula:

$$\gamma_l^{(k)} = \frac{r_a^{(k)}\gamma_b^{(k)} - r_b^{(k)}\gamma_a^{(k)}}{r_a^{(k)} - r_b^{(k)}} \quad l \geq 2 \quad (2.47)$$

which is identical to the one adopted in the previous section for updating  $\lambda_i$ .

Specifically, if at least one of the residual  $r_j^{(k)}$  ( $j < l$ ) is negative, the previous formula is applied to the pairs  $(\gamma_n^{(k)}, r_n^{(k)}) - (\gamma_p^{(k)}, r_p^{(k)})$ , irrespective of the order of association, where  $\gamma_n^{(k)}$  is the minimum among all values whose associated residuals  $r_n^{(k)}$  are negative and  $\gamma_p^{(k)}$  is the maximum value which positive residuals  $r_p^{(k)}$  correspond to. We thus write

$$\gamma_l^{(k)} = \frac{r_p^{(k)}\gamma_n^{(k)} - r_n^{(k)}\gamma_p^{(k)}}{r_p^{(k)} - r_n^{(k)}} \quad l \geq 2 \quad (2.48)$$

In order to handle the situations in which the iterations previous than the current one are characterized only by positive residuals we specialize formula (2.47) as follows:

$$\gamma_l^{(k)} = \frac{r_{l-2}^{(k)}\gamma_{l-1}^{(k)} - r_{l-1}^{(k)}\gamma_{l-2}^{(k)}}{r_{l-2}^{(k)} - r_{l-1}^{(k)}} \quad l \geq 2; \quad (2.49)$$

it certainly provides positive values for  $\gamma_l^{(k)}$  when  $r_{l-2}^{(k)} \neq r_{l-1}^{(k)}$  since the function  $r^{(k)}$  is non-increasing. Finally, whenever should it be

$$\left| \frac{r_{l-2}^{(k)} - r_{l-1}^{(k)}}{r_{l-2}^{(k)}} \right| < 10^{-5} \quad (2.50)$$

it is adopted the formula:

$$\gamma_l^{(k)} = 2(\gamma_{l-1}^{(k)} - \gamma_{l-2}^{(k)}) + \gamma_{l-1}^{(k)} \quad l \geq 2 \quad (2.51)$$

Similarly to the updating formulas for  $\lambda_i$ , the numerical procedure detailed above can be initiated only if two pairs  $(\gamma_l^{(k)}, r_l^{(k)})$  are available. They are simply provided by the values  $(0, 1)$  and  $(1, r^{(k)}(1))$  so that formula (2.48) or (2.49) supplies

$$\gamma_2^{(k)} = \frac{1}{1 - r^{(k)}(1)} \quad (2.52)$$

if  $r^{(k)}(1) < 1$  while formula (2.49) specializes to:

$$\gamma_2^{(k)} = 3\gamma_1^{(k)} \quad (2.53)$$

if  $|1 - r^{(k)}(1)| < 10^{-5}$ .

### 2.3.5 Global convergence of the solution algorithm

In order to prove the global convergence of the entire solution algorithm, we first prove that procedure B always converges. To this end we invoke the global convergence theorem (2.4.1) proved in [42] when formula (2.4.7) replaces (2.4.3). Actually, the theorem still holds in this case as proved at page 22 of reference [42].

This is here specialized to the present context for the reader's convenience:

**Proposition 2.3.4** *For a descent method with partial line search, in which criteria (2.4.1) and (2.4.2) are used and the following ‘angle condition’*

$$-\frac{\mathbf{f}_r^{(k)} \cdot \mathbf{d}^{(k)}}{\|\mathbf{f}_r^{(k)}\| \|\mathbf{d}^{(k)}\|} \geq \mu > 0 \quad (2.54)$$

*is satisfied for some fixed  $\mu$ , and if  $\nabla\psi$  exists and is uniformly continuous on the level set  $\{\mathbf{u} : \psi(\mathbf{u}) < \psi(\mathbf{u}^{(1)})\}$ , then either  $\mathbf{f}_r^{(k)} = \mathbf{0}$  for some  $k$ , or  $\psi^{(k)} \rightarrow -\infty$ , or  $\mathbf{f}_r^{(k)} \rightarrow \mathbf{0}$ . ■*

The angle criterion is certainly satisfied when the condition number of  $\mathbf{H}^{(k)}$ , i.e. the ratio between the maximum and the minimum eigenvalue of  $\mathbf{H}^{(k)}$ , is bounded above (see [42], pag. 23) as is detailed in section 2.5.2, which describes how  $\mathbf{H}^{(k)}$  is obtained modifying the exact hessian matrix. In our case  $\mathbf{H}^{(k)}$  is assembled as a sum of two terms. One, which is contributed by the concrete part, is positive semidefinite and has a maximum eigenvalue bounded above by the eigenvalue of the matrix obtained using the initial stiffness of the concrete stress-strain curve. The second term, which is contributed by the steel bars, is also positive definite. Its minimum eigenvalue is bounded both below, by the eigenvalue of the matrix obtained using the minimum stiffness used when the bar is yielded, and above, by the eigenvalue of the matrix obtained using always the elastic stiffness for all the bars. Hence, the condition number of the sum of the two terms is certainly bounded above and the angle criterion is then satisfied.

Furthermore, because of proposition 2.3.3, the level set  $\{\mathbf{u} : \psi(\mathbf{u}) \leq \delta\}$  is compact. Hence, by the Heine-Cantor theorem  $\nabla\psi$  is uniformly continuous on it, so that it is also uniformly continuous on  $\{\mathbf{u} : \psi(\mathbf{u}) < \psi(\mathbf{u}^{(1)})\}$ . Furthermore, because of proposition 2.3.2, we can rule out the case that  $\psi^{(k)} \rightarrow -\infty$ , so that only the two remaining cases are possible, both of them implying convergence of procedure B.

On the other hand, we have seen that procedure A starts with a positive value of the error  $e$ , and that for the assumed case of a convex admissible domain there is only one value  $\lambda^*$  of the load multiplier, corresponding to the ULS sought, that makes the error  $e$  vanish. For greater values of  $\lambda$  the error is always negative. The extrapolation/interpolation procedure used for procedure A is then convergent to the solution  $\lambda^*$ . Also in terms of ULS the solution is not unique in terms of the strain parameters vector  $\mathbf{u}$ .

In conclusion, the following global convergence result can be stated:

**Proposition 2.3.5** *If the admissible domain is convex and bounded, the solution  $\lambda^*$  to the ULS problem exists and is unique, and the algorithm described in Sections 4.1 and 4.2 converges to it for any assigned values of  $\mathbf{f}_d$  and  $\mathbf{f}_i$ , provided that  $\mathbf{f}_d$  is internal to the admissible domain. ■*

## 2.4 Evaluation of the resultant force vector

The main computational burden of the modified Newton algorithm described in the previous section for the evaluation of the strain vector associated with a given load  $\mathbf{f}_i$  is represented by the evaluation of the residual  $\mathbf{R}^{(k)}$  and the matrix  $\mathbf{H}^{(k)}$ . Postponing to the next section a detailed account of the latter issue we here address the computation of the residual  $\mathbf{R}^{(k)}$ , see formula (2.28).

In particular, being  $\mathbf{f}_i$  fixed, we actually need to compute only  $(\mathbf{f}_r^{(k)})^T = \{N_r^{(k)}, -(\mathbf{M}_r^{(k)})_y, (\mathbf{M}_r^{(k)})_x\}$  that is the axial force and the biaxial moments in equilibrium with the stress field  $\sigma^{(k)}$  associated with the strain field  $\varepsilon^{(k)}$ , resulting from  $\mathbf{u}^{(k)}$ , via the constitutive laws (2.26) and (2.27).

According to (2.4) and (2.6) the internal resultants of the stress field on the section can be written as:

$$N_r^{(k)} = \int_{\Omega_c} \sigma_c^r[\varepsilon^{(k)}(\mathbf{r})]d\Omega + \sum_{j=1}^{n_b} \sigma_s^r[\varepsilon^{(k)}(\mathbf{r}_{bj})]A_{bj} \quad (2.55)$$

$$[\mathbf{M}_r^{(k)}]^\perp = \int_{\Omega_c} \sigma_c^r[\varepsilon^{(k)}(\mathbf{r})] \mathbf{r} d\Omega + \sum_{j=1}^{n_b} \sigma_s^r[\varepsilon^{(k)}(\mathbf{r}_{bj})] A_{bj} \mathbf{r}_{bj} \quad (2.56)$$

where  $\varepsilon^{(k)}(\mathbf{r}) = \varepsilon_o^{(k)} + \mathbf{g}^{(k)} \cdot \mathbf{r}$  is the strain at the generic point associated with the parameters of the strain vector  $(\mathbf{u}^{(k)})^T = \{\varepsilon_o^{(k)}, g_x^{(k)}, g_y^{(k)}\}$ .

The integrals in the previous formulas are evaluated by subdividing the domain of integration in several subdomains depending on the strain ranges appearing in the definition of the function  $\sigma_c^r$  and  $\sigma_s^r$ , see e.g. (2.26) and (2.27). Thus, the domain  $\Omega_c$  of the cross section is assumed to be the union of four subdomains (e.g. see figure 2.8):

$$\Omega_c = \begin{cases} \Omega_{c0}^{(k)} : \{\mathbf{r} \in \Omega_c : 0 \leq \varepsilon^{(k)}(\mathbf{r})\} \\ \Omega_{c1}^{(k)} : \{\mathbf{r} \in \Omega_c : \varepsilon_{cp} \leq \varepsilon^{(k)}(\mathbf{r}) \leq 0\} \\ \Omega_{c2}^{(k)} : \{\mathbf{r} \in \Omega_c : \varepsilon_{cu} \leq \varepsilon^{(k)}(\mathbf{r}) \leq \varepsilon_{cp}\} \\ \Omega_{c3}^{(k)} : \{\mathbf{r} \in \Omega_c : \varepsilon^{(k)}(\mathbf{r}) \leq \varepsilon_{cu}\} \end{cases} \quad (2.57)$$

Similarly the set of bars  $I_s$  is subdivided in five non-overlapping subsets:

$$I_s = \begin{cases} I_{s1}^{(k)} : \{(\mathbf{r}_{bj}, A_{bj}) \in I_s : \varepsilon^{(k)}(\mathbf{r}_{bj}) < \varepsilon_{cu}\} \\ I_{s2}^{(k)} : \{(\mathbf{r}_{bj}, A_{bj}) \in I_s : \varepsilon_{cu} \leq \varepsilon^{(k)}(\mathbf{r}_{bj}) < -\varepsilon_{sy}\} \\ I_{s3}^{(k)} : \{(\mathbf{r}_{bj}, A_{bj}) \in I_s : -\varepsilon_{sy} \leq \varepsilon^{(k)}(\mathbf{r}_{bj}) < \varepsilon_{sy}\} \\ I_{s4}^{(k)} : \{(\mathbf{r}_{bj}, A_{bj}) \in I_s : \varepsilon_{sy} \leq \varepsilon^{(k)}(\mathbf{r}_{bj}) < \varepsilon_{su}\} \\ I_{s5}^{(k)} : \{(\mathbf{r}_{bj}, A_{bj}) \in I_s : \varepsilon_{su} \leq \varepsilon^{(k)}(\mathbf{r}_{bj})\} \end{cases} \quad (2.58)$$

where the apex  $(\cdot)^{(k)}$  emphasizes that the subdomains iteratively change during the solution of the nonlinear problem  $\mathbf{u}(\mathbf{f})$ .

We further remark that  $\Omega_{c0}^{(k)}$ , although inessential in our calculations, has been explicitly considered in (2.57) in order to easily extend our treatment to the cases in which concrete tensile resistance needs to be taken into account, e.g. for the serviceability limit state analyses, or for the nonlinear finite-element analysis of RC frames. Clearly, to this end the constitutive assumptions listed in section 2.1 will have to be modified and, in particular, assumption c) will have to be removed.

In conclusion we express the internal axial force in equilibrium with the  $k$ -th estimate of the strain vector  $\mathbf{u}^{(k)}$  as follows:

$$N_r^{(k)} = \sum_{q=1}^3 N_{cq}^{(k)} + \sum_{q=1}^5 N_{sq}^{(k)} \quad (2.59)$$

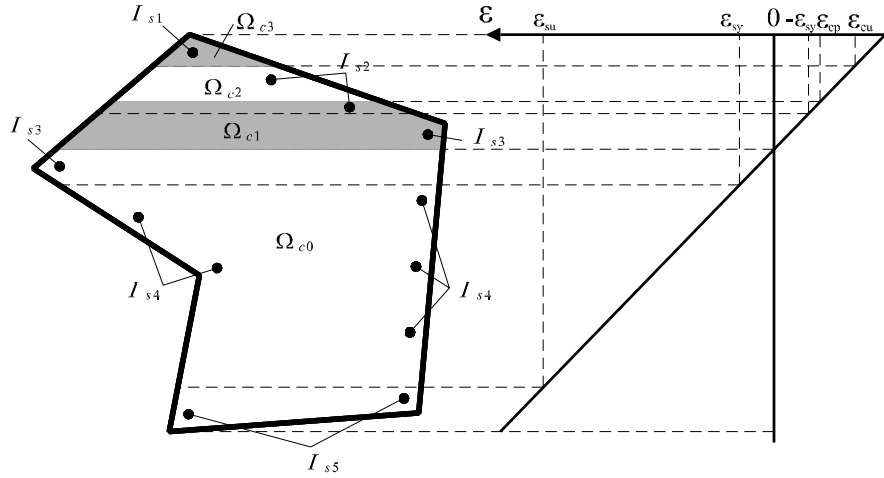


Figure 2.8: Partition of the section

and the bending moment in the form

$$[\mathbf{M}_r^{(k)}]^\perp = \sum_{q=1}^3 [\mathbf{M}_{cq}^{(k)}]^\perp + \sum_{q=1}^5 [\mathbf{M}_{sq}^{(k)}]^\perp \quad (2.60)$$

The explicit expression of each addend is reported in section 2.4.1.

As a final remark we emphasize that the integrals over  $\Omega_{c1}^{(k)}$ ,  $\Omega_{c2}^{(k)}$  and  $\Omega_{c3}^{(k)}$  appearing in the definition of  $N_{cq}^{(k)}$  and  $[\mathbf{M}_{cq}^{(k)}]^\perp$ ,  $q = 1, 2, 3$ , are evaluated in closed form as explicit function of the position vectors of the vertices of each subdomain  $\Omega_{cq}^{(k)}$ , as shown in section 2.4.1.

### 2.4.1 Integration formulas for the evaluation of $\mathbf{f}_r^{(k)}$

Recalling the definition (2.57)-(2.58) and that  $\varepsilon_o^{(k)}$  and  $\mathbf{g}^{(k)}$  are the components of  $\mathbf{u}^{(k)}$ , the explicit expression of the terms which contribute to the

sums in (2.59) and (2.60) are:

$$\begin{aligned}
N_{c1}^{(k)} &= \int_{\Omega_{c1}^{(k)}} \sigma_c^r d\Omega = (\alpha \varepsilon_o^{(k)} + \beta (\varepsilon_o^{(k)})^2) A_{c1}^{(k)} + \\
&\quad + (\alpha + 2\beta \varepsilon_o^{(k)}) \mathbf{s}_{c1}^{(k)} \cdot \mathbf{g}^{(k)} + \beta \mathbf{J}_{c1}^{(k)} \mathbf{g}^{(k)} \cdot \mathbf{g}^{(k)} \\
N_{c2}^{(k)} &= \int_{\Omega_{c2}^{(k)}} \sigma_c^r d\Omega = A_{c2}^{(k)} \sigma_{cu}
\end{aligned} \tag{2.61}$$

$$N_{c3}^{(k)} = \int_{\Omega_{c3}^{(k)}} \sigma_c^r d\Omega = E_c^{sec} A_{c3}^{(k)} \varepsilon_o^{(k)} + E_c^{sec} \mathbf{s}_{c3}^{(k)} \cdot \mathbf{g}^{(k)}$$

where  $A_{cq}^{(k)}$ ,  $\mathbf{s}_{cq}^{(k)}$  and  $\mathbf{J}_{cq}^{(k)}$  denote the first three area moments of each concrete subdomains  $\Omega_{cq}^{(k)}$ .

Since each subdomain is polygonal, the three moments above can be evaluated as functions of the position vectors of the relevant vertices  $\mathbf{r}_{qj}^{(k)}$  by means of the general formula reported in [35]:

$$A_{cq}^{(k)} = \int_{\Omega_{cq}^{(k)}} d\Omega = \frac{1}{2} \sum_{j=1}^{n_{cq}^{(k)}} c_{qj}^{(k)} \tag{2.62}$$

$$\mathbf{s}_{cq}^{(k)} = \int_{\Omega_{cq}^{(k)}} \mathbf{r} d\Omega = \frac{1}{6} \sum_{j=1}^{n_{cq}^{(k)}} c_{qj}^{(k)} (\mathbf{r}_{qj}^{(k)} \mathbf{r}_{q(j+1)}^{(k)}) \tag{2.63}$$

$$\begin{aligned}
\mathbf{J}_{cq}^{(k)} &= \int_{\Omega_{cq}^{(k)}} (\mathbf{r} \otimes \mathbf{r}) d\Omega = \frac{1}{12} \sum_{j=1}^{n_{cq}^{(k)}} c_{qj}^{(k)} [\mathbf{r}_{qj}^{(k)} \otimes \mathbf{r}_{qj}^{(k)} + \\
&\quad + \text{sym}(\mathbf{r}_{qj}^{(k)} \otimes \mathbf{r}_{q(j+1)}^{(k)}) + \mathbf{r}_{q(j+1)}^{(k)} \otimes \mathbf{r}_{q(j+1)}^{(k)}]
\end{aligned} \tag{2.64}$$

where  $n_{cq}^{(k)}$  is the number of vertices of  $\Omega_{cq}^{(k)}$  and

$$c_{qj}^{(k)} = \mathbf{r}_{qj}^{(k)} \cdot [\mathbf{r}_{q(j+1)}^{(k)}]^\perp = \begin{pmatrix} x_{qj}^{(k)} \\ y_{qj}^{(k)} \end{pmatrix} \cdot \begin{pmatrix} y_{q(j+1)}^{(k)} \\ -x_{q(j+1)}^{(k)} \end{pmatrix} \tag{2.65}$$

provided that the vertices of the boundary of each subdomain  $\Omega_{cq}^{(k)}$  have been numbered in consecutive order by circulating in counter-clockwise sense.

Furthermore, the contributions to the expression of  $N_r^{(k)}$  in (2.59) due to steel are provided by

$$\begin{aligned}
 N_{s1}^{(k)} &= \sum_{j \in I_{s1}^{(k)}} \sigma_s^r(\varepsilon(\mathbf{r}_{bj})) A_{bj} = E_{sc}^{sec} A_{s1}^{(k)} \varepsilon_o^{(k)} + E_{sc}^{sec} \mathbf{s}_{s1}^{(k)} \cdot \mathbf{g}^{(k)} \\
 N_{s2}^{(k)} &= \sum_{j \in I_{s2}^{(k)}} \sigma_s^r(\varepsilon(\mathbf{r}_{bj})) A_{bj} = -\sigma_{sy} A_{s2}^{(k)} \\
 N_{s3}^{(k)} &= \sum_{j \in I_{s3}^{(k)}} \sigma_s^r(\varepsilon(\mathbf{r}_{bj})) A_{bj} = E_s A_{s3}^{(k)} \varepsilon_o^{(k)} + E_s \mathbf{s}_{s3}^{(k)} \cdot \mathbf{g}^{(k)} \\
 N_{s4}^{(k)} &= \sum_{j \in I_{s4}^{(k)}} \sigma_s^r(\varepsilon(\mathbf{r}_{bj})) A_{bj} a = \sigma_{sy} A_{s4}^{(k)} \\
 N_{s5}^{(k)} &= \sum_{j \in I_{s5}^{(k)}} \sigma_s^r(\varepsilon(\mathbf{r}_{bj})) A_{bj} = E_{st}^{sec} A_{s5}^{(k)} \varepsilon_o^{(k)} + E_{st}^{sec} \mathbf{s}_{s5}^{(k)} \cdot \mathbf{g}^{(k)}
 \end{aligned} \tag{2.66}$$

where  $A_{sq}^{(k)}$  denotes the total area of bars included in the  $q$ -th steel subset  $I_{sq}^{(k)}$  of the reinforcements set  $I_s$  and  $\mathbf{s}_{sq}^{(k)}$  the relevant first moment of inertia.

Accordingly

$$A_{sq}^{(k)} = \sum_{j \in I_{sq}^{(k)}} A_{bj} \quad \mathbf{s}_{sq}^{(k)} = \sum_{j \in I_{sq}^{(k)}} A_{bj} \mathbf{r}_{bj} \tag{2.67}$$

For what concerns the bending moment the sums in (2.60) associated with the concrete subdomains are given by

$$\begin{aligned}
[\mathbf{M}_{c1}^{(k)}]^\perp &= \int_{\Omega_{c1}^{(k)}} \sigma_c^r \mathbf{r} \, d\Omega = [\alpha \varepsilon_o^{(k)} + \beta (\varepsilon_o^{(k)})^2] \mathbf{s}_{c1}^{(k)} + \\
&\quad + (\alpha + 2\beta \varepsilon_o^{(k)}) \mathbf{J}_{c1}^{(k)} \mathbf{g}^{(k)} + \beta \bar{\mathbf{J}}_{c1}^{(k)} (\mathbf{g}^{(k)} \otimes \mathbf{g}^{(k)}) \\
[\mathbf{M}_{c2}^{(k)}]^\perp &= \int_{\Omega_{c2}^{(k)}} \sigma_c^r \mathbf{r} \, d\Omega = \sigma_{cu} \mathbf{s}_{c2}^{(k)} \\
[\mathbf{M}_{c3}^{(k)}]^\perp &= \int_{\Omega_{c3}^{(k)}} \sigma_c^r \mathbf{r} \, d\Omega = E_c^{sec} \varepsilon_o^{(k)} \mathbf{s}_{c3}^{(k)} + E_c^{sec} \mathbf{J}_{c3}^{(k)} \mathbf{g}^{(k)}
\end{aligned} \tag{2.68}$$

while those associated with steel are

$$\begin{aligned}
[\mathbf{M}_{s1}^{(k)}]^\perp &= \sum_{j \in I_{s1}^{(k)}} \sigma_s^r(\varepsilon(\mathbf{r}_{bj})) A_{bj} \mathbf{r}_{bj} = E_{sc}^{sec} \varepsilon_o^{(k)} \mathbf{s}_{s1}^{(k)} + E_{sc}^{sec} \mathbf{J}_{s1}^{(k)} \mathbf{g}^{(k)} \\
[\mathbf{M}_{s2}^{(k)}]^\perp &= \sum_{j \in I_{s2}^{(k)}} \sigma_s^r(\varepsilon(\mathbf{r}_{bj})) A_{bj} \mathbf{r}_{bj} = -\sigma_{sy} \mathbf{s}_{s2}^{(k)} \\
[\mathbf{M}_{s3}^{(k)}]^\perp &= \sum_{j \in I_{s3}^{(k)}} \sigma_s^r(\varepsilon(\mathbf{r}_{bj})) A_{bj} \mathbf{r}_{bj} = E_s \varepsilon_o^{(k)} \mathbf{s}_{s3}^{(k)} + E_s \mathbf{J}_{s3}^{(k)} \mathbf{g}^{(k)} \\
[\mathbf{M}_{s4}^{(k)}]^\perp &= \sum_{j \in I_{s4}^{(k)}} \sigma_s^r(\varepsilon(\mathbf{r}_{bj})) A_{bj} \mathbf{r}_{bj} = \sigma_{sy} \mathbf{s}_{s4}^{(k)} \\
[\mathbf{M}_{s5}^{(k)}]^\perp &= \sum_{j \in I_{s5}^{(k)}} \sigma_s^r(\varepsilon(\mathbf{r}_{bj})) A_{bj} \mathbf{r}_{bj} = E_{st}^{sec} \varepsilon_o^{(k)} \mathbf{s}_{s5}^{(k)} + E_{st}^{sec} \mathbf{J}_{s5}^{(k)} \mathbf{g}^{(k)}
\end{aligned} \tag{2.69}$$

The third order tensor  $\bar{\mathbf{J}}_{cq}^{(k)}$  appearing in (2.68) is evaluated by means of the same general formula reported in [35]:

$$\begin{aligned}
 \bar{\mathbf{J}}_{cq}^{(k)} &= \int_{\Omega_{cq}^{(k)}} (\mathbf{r} \otimes \mathbf{r} \otimes \mathbf{r}) \, d\Omega = \frac{1}{20} \sum_{j=1}^{n_{cq}^{(k)}} c_{qj}^{(k)} [\mathbf{r}_{qj}^{(k)} \otimes \mathbf{r}_{qj}^{(k)} \otimes \mathbf{r}_{qj}^{(k)} + \\
 &+ \frac{1}{3} (\mathbf{r}_{q(j+1)}^{(k)} \otimes \mathbf{r}_{qj}^{(k)} \otimes \mathbf{r}_{qj}^{(k)} + \mathbf{r}_{q(j+1)}^{(k)} \otimes \mathbf{r}_{q(j+1)}^{(k)} \otimes \mathbf{r}_{qj}^{(k)} + \\
 &+ \mathbf{r}_{q(j+1)}^{(k)} \otimes \mathbf{r}_{qj}^{(k)} \otimes \mathbf{r}_{q(j+1)}^{(k)} + \mathbf{r}_{qj}^{(k)} \otimes \mathbf{r}_{q(j+1)}^{(k)} \otimes \mathbf{r}_{qj}^{(k)} + \\
 &+ \mathbf{r}_{qj}^{(k)} \otimes \mathbf{r}_{q(j+1)}^{(k)} \otimes \mathbf{r}_{q(j+1)}^{(k)} + \mathbf{r}_{qj}^{(k)} \otimes \mathbf{r}_{qj}^{(k)} \otimes \mathbf{r}_{q(j+1)}^{(k)}) + \\
 &+ \mathbf{r}_{q(j+1)}^{(k)} \otimes \mathbf{r}_{q(j+1)}^{(k)} \otimes \mathbf{r}_{q(j+1)}^{(k)}]
 \end{aligned} \tag{2.70}$$

where  $n_{cq}^{(k)}$  is the number of vertices of  $\Omega_{cq}^{(k)}$  and

$$c_{qj}^{(k)} = \mathbf{r}_{qj}^{(k)} \cdot [\mathbf{r}_{q(j+1)}^{(k)}]^\perp = \begin{pmatrix} x_{qj}^{(k)} \\ y_{qj}^{(k)} \end{pmatrix} \cdot \begin{pmatrix} y_{q(j+1)}^{(k)} \\ -x_{q(j+1)}^{(k)} \end{pmatrix} \tag{2.71}$$

provided that the vertices of the boundary of each subdomain  $\Omega_{cq}^{(k)}$  have been numbered in consecutive order by circulating in counter-clockwise sense.

Composition of  $\bar{\mathbf{J}}_{cq}^{(k)}$  with the second-order tensor  $\mathbf{g}^{(k)} \otimes \mathbf{g}^{(k)}$ , see e.g. (2.68)<sub>1</sub>, is performed as follows:

$$[\bar{\mathbf{J}}_{cq}^{(k)} (\mathbf{g}^{(k)} \otimes \mathbf{g}^{(k)})]_i = [\bar{\mathbf{J}}_{cq}^{(k)}]_{ijk} [\mathbf{g}^{(k)} \otimes \mathbf{g}^{(k)}]_{jk} \tag{2.72}$$

Finally, the second area moment of the q-th steel subdomain is

$$\mathbf{J}_{sq}^{(k)} = \sum_{j \in I_{sq}^{(k)}} A_{bj} \mathbf{r}_{bj} \otimes \mathbf{r}_{bj} \tag{2.73}$$

where the significance of the adopted symbols is analogous to that employed in (2.67).

## 2.5 Evaluation of the matrix $\mathbf{H}^{(k)}$

The second task to accomplish for the actual implementation of the procedure B is the evaluation of the matrix  $\mathbf{H}^{(k)}$ . To this end, we start evaluating the tangent matrix  $\mathbf{dR}^{(k)}$ , reported in equation (2.29), which is the Hessian of both functions  $\phi$  and  $\psi$ .

Similarly to  $\mathbf{f}_r^{(k)}$  we shall provide a set of formulas which allow us to evaluate  $\mathbf{dR}^{(k)}$  as sum of separate contributions represented by terms which are expressed solely as function of the vertices of the section and of the constitutive parameters of the materials.

Adopting the same procedure illustrated for  $\mathbf{f}_r^{(k)}$  we subdivide the concrete cross section in four subdomains  $\Omega_{cq}^{(k)}$  for computing the integrals associated with concrete and five subsets  $I_{sq}^{(k)}$  for steel.

The entries of the matrix (2.29) have been evaluated as follows

$$\left. \frac{\partial N_r}{\partial \varepsilon_o} \right|_{\mathbf{u}^{(k)}} = \sum_{q=1}^3 \left. \frac{\partial N_{cq}}{\partial \varepsilon_o} \right|_{\mathbf{u}^{(k)}} + \sum_{q=1}^5 \left. \frac{\partial N_{sq}}{\partial \varepsilon_o} \right|_{\mathbf{u}^{(k)}} \quad (2.74)$$

$$\left. \frac{\partial N_r}{\partial \mathbf{g}} \right|_{\mathbf{u}^{(k)}} = \sum_{q=1}^3 \left. \frac{\partial N_{cq}}{\partial \mathbf{g}} \right|_{\mathbf{u}^{(k)}} + \sum_{q=1}^5 \left. \frac{\partial N_{sq}}{\partial \mathbf{g}} \right|_{\mathbf{u}^{(k)}} \quad (2.75)$$

for what concerns the derivatives of the axial force  $N_r$  and

$$\left. \frac{\partial [\mathbf{M}_r]^\perp}{\partial \varepsilon_o} \right|_{\mathbf{u}^{(k)}} = \sum_{q=1}^3 \left. \frac{\partial [\mathbf{M}_{cq}]^\perp}{\partial \varepsilon_o} \right|_{\mathbf{u}^{(k)}} + \sum_{q=1}^5 \left. \frac{\partial [\mathbf{M}_{sq}]^\perp}{\partial \varepsilon_o} \right|_{\mathbf{u}^{(k)}} \quad (2.76)$$

$$\left. \frac{\partial [\mathbf{M}_r]^\perp}{\partial \mathbf{g}} \right|_{\mathbf{u}^{(k)}} = \sum_{q=1}^3 \left. \frac{\partial [\mathbf{M}_{cq}]^\perp}{\partial \mathbf{g}} \right|_{\mathbf{u}^{(k)}} + \sum_{q=1}^5 \left. \frac{\partial [\mathbf{M}_{sq}]^\perp}{\partial \mathbf{g}} \right|_{\mathbf{u}^{(k)}} \quad (2.77)$$

for the derivatives of  $[\mathbf{M}_r]^\perp$ . The explicit expression of each addend in the sums above is reported in section 2.5.1.

However, it has been emphasized in section 2.3 that the tangent matrix  $\mathbf{dR}^{(k)}$  may be ill conditioned or singular in special situations which can occur during the iterations of the Newton method when large compressive or tensile axial forces are near the ultimate values corresponding to pure axial strain applied to the section.

For this reason the matrix  $\mathbf{H}^{(k)}$  used in the update formula (2.30) is obtained by suitably modifying  $\mathbf{dR}^{(k)}$ , in order to get positive definiteness and good conditioning. To this end, the entries of  $\mathbf{H}^{(k)}$  are evaluated as in

the formulas (2.74)-(2.77) above except for the derivatives of the quantities  $N_{s2}$ ,  $N_{s4}$ ,  $[\mathbf{M}_{s2}]^\perp$  and  $[\mathbf{M}_{s4}]^\perp$  associated in turn with the horizontal plateau of the steel constitutive law.

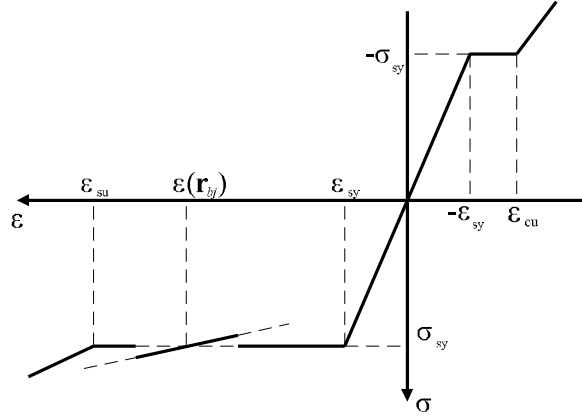


Figure 2.9: Steel constitutive law for the evaluation of  $\mathbf{H}^{(k)}$

Accordingly, a fictitious hardening constitutive law (see figure 2.9), whose constant slope has been numerically evaluated in order to improve the convergence rate of procedure B, has been assigned to the steel bars belonging to the sets  $I_{s2}^{(k)}$  and  $I_{s4}^{(k)}$ . Obviously, in order to correctly evaluate the resultant vector  $\mathbf{f}_r^{(k)}$ , the stress pertaining to each bar in the sets  $I_{s2}^{(k)}$  and  $I_{s4}^{(k)}$  has been left constant and equal to  $-\sigma_{sy}$  and  $\sigma_{sy}$  respectively. For the details the reader is referred to section 2.5.2.

### 2.5.1 Integration formulas for the evaluation of the tangent matrix $d\mathbf{R}^{(k)}$

Aim of this section is to detail the computation of the derivatives appearing in the expressions (2.74)-(2.77) for each one of the subdomains defined in (2.57)-(2.58). In this respect we remark that the sets  $I_{sq}^{(k)}$  are collections of lumped areas, so that the area moments of the steel bars belonging to the generic set  $I_{sq}^{(k)}$  are discontinuously dependent on  $\varepsilon_o^{(k)}$  and  $\mathbf{g}^{(k)}$ , i.e. they are piecewise constant. Accordingly, the derivatives of the area moments of the steel bars are zero and will be omitted in the sequel.

The addends of the sums in (2.74) are given by

$$\begin{aligned}
\frac{\partial N_{c1}}{\partial \varepsilon_o} \Big|_{\mathbf{u}^{(k)}} &= (\alpha + 2\beta \varepsilon_o^{(k)}) A_{c1}^{(k)} + [\alpha \varepsilon_o^{(k)} + \beta (\varepsilon_o^{(k)})^2] \frac{\partial A_{c1}}{\partial \varepsilon_o} \Big|_{\mathbf{u}^{(k)}} + \\
&\quad + 2\beta \mathbf{s}_{c1}^{(k)} \cdot \mathbf{g}^{(k)} + (\alpha + 2\beta \varepsilon_o^{(k)}) \frac{\partial \mathbf{s}_{c1}}{\partial \varepsilon_o} \Big|_{\mathbf{u}^{(k)}} \cdot \mathbf{g}^{(k)} + \\
&\quad + \beta \frac{\partial \mathbf{J}_{c1}}{\partial \varepsilon_o} \Big|_{\mathbf{u}^{(k)}} \mathbf{g}^{(k)} \cdot \mathbf{g}^{(k)}
\end{aligned} \tag{2.78}$$

$$\frac{\partial N_{c2}}{\partial \varepsilon_o} \Big|_{\mathbf{u}^{(k)}} = \frac{\partial A_{c2}}{\partial \varepsilon_o} \Big|_{\mathbf{u}^{(k)}} \sigma_{cu}$$

$$\frac{\partial N_{c3}}{\partial \varepsilon_o} \Big|_{\mathbf{u}^{(k)}} = E_c^{sec} A_{c3}^{(k)} + E_c^{sec} \varepsilon_o^{(k)} \frac{\partial A_{c3}}{\partial \varepsilon_o} \Big|_{\mathbf{u}^{(k)}} + E_c^{sec} \frac{\partial \mathbf{s}_{c3}}{\partial \varepsilon_o} \Big|_{\mathbf{u}^{(k)}} \mathbf{g}^{(k)}$$

for concrete and

$$\begin{aligned}
\frac{\partial N_{s1}}{\partial \varepsilon_o} \Big|_{\mathbf{u}^{(k)}} &= E_{sc}^{sec} A_{s1}^{(k)}; & \frac{\partial N_{s2}}{\partial \varepsilon_o} \Big|_{\mathbf{u}^{(k)}} &= 0 \\
\frac{\partial N_{s3}}{\partial \varepsilon_o} \Big|_{\mathbf{u}^{(k)}} &= E_s A_{s3}^{(k)}; & \frac{\partial N_{s4}}{\partial \varepsilon_o} \Big|_{\mathbf{u}^{(k)}} &= 0 \\
\frac{\partial N_{s5}}{\partial \varepsilon_o} \Big|_{\mathbf{u}^{(k)}} &= E_{st}^{sec} A_{s5}^{(k)}
\end{aligned} \tag{2.79}$$

for steel bars.

Similarly, the derivatives in (2.75) of the axial force with respect to  $\mathbf{g}$

evaluated at  $\mathbf{u}^{(k)}$  are given by

$$\begin{aligned} \frac{\partial N_{c1}}{\partial \mathbf{g}} \Big|_{\mathbf{u}^{(k)}} &= (\alpha \varepsilon_o^{(k)} + \beta (\varepsilon_o^{(k)})^2) \frac{\partial A_{c1}}{\partial \mathbf{g}} \Big|_{\mathbf{u}^{(k)}} + (\alpha + 2\beta \varepsilon_o^{(k)}) \mathbf{s}_{c1}^{(k)} + \\ &+ (\alpha + 2\beta \varepsilon_o^{(k)}) \left[ \frac{\partial \mathbf{s}_{c1}}{\partial \mathbf{g}} \Big|_{\mathbf{u}^{(k)}} \right]^T \mathbf{g}^{(k)} + 2\beta \mathbf{J}_{c1}^{(k)} \mathbf{g}^{(k)} + \\ &+ \beta \frac{\partial \mathbf{J}_{c1}}{\partial \mathbf{g}} \Big|_{\mathbf{u}^{(k)}} (\mathbf{g}^{(k)} \otimes \mathbf{g}^{(k)}) \end{aligned} \quad (2.80)$$

$$\frac{\partial N_{c2}}{\partial \mathbf{g}} \Big|_{\mathbf{u}^{(k)}} = \frac{\partial A_{c2}}{\partial \mathbf{g}} \Big|_{\mathbf{u}^{(k)}} \sigma_{cu}$$

$$\frac{\partial N_{c3}}{\partial \mathbf{g}} \Big|_{\mathbf{u}^{(k)}} = E_c^{sec} \varepsilon_o^{(k)} \frac{\partial A_{c3}}{\partial \mathbf{g}} \Big|_{\mathbf{u}^{(k)}} + E_c^{sec} \mathbf{s}_{c3}^{(k)} + E_c^{sec} \left[ \frac{\partial \mathbf{s}_{c3}}{\partial \mathbf{g}} \Big|_{\mathbf{u}^{(k)}} \right]^T \mathbf{g}^{(k)}$$

for concrete and

$$\begin{aligned} \frac{\partial N_{s1}}{\partial \mathbf{g}} \Big|_{\mathbf{u}^{(k)}} &= E_{sc}^{sec} \mathbf{s}_{s1}^{(k)}; & \frac{\partial N_{s2}}{\partial \mathbf{g}} \Big|_{\mathbf{u}^{(k)}} &= \mathbf{0} \\ \frac{\partial N_{s3}}{\partial \mathbf{g}} \Big|_{\mathbf{u}^{(k)}} &= E_s \mathbf{s}_{s3}^{(k)}; & \frac{\partial N_{s4}}{\partial \mathbf{g}} \Big|_{\mathbf{u}^{(k)}} &= \mathbf{0} \\ \frac{\partial N_{s5}}{\partial \mathbf{g}} \Big|_{\mathbf{u}^{(k)}} &= E_{st}^{sec} \mathbf{s}_{s5}^{(k)} \end{aligned} \quad (2.81)$$

for steel bars. Notice that the composition of the third-order tensor  $[\partial \mathbf{J}_{c1} / \partial \mathbf{g}]_{\mathbf{u}^{(k)}}$  with  $(\mathbf{g}^{(k)} \otimes \mathbf{g}^{(k)})$  is performed as in (2.72):

$$\begin{aligned} \left[ \frac{\partial \mathbf{J}_{c1}}{\partial \mathbf{g}} \Big|_{\mathbf{u}^{(k)}} (\mathbf{g}^{(k)} \otimes \mathbf{g}^{(k)}) \right]_i &= \left[ \frac{\partial \mathbf{J}_{c1}}{\partial \mathbf{g}} \Big|_{\mathbf{u}^{(k)}} \right]_{jli} [\mathbf{g}^{(k)}]_j [\mathbf{g}^{(k)}]_l = \\ &= \frac{\partial [\mathbf{J}_{c1}]_{jl}}{\partial \mathbf{g}_i} \Big|_{\mathbf{u}^{(k)}} [\mathbf{g}^{(k)}]_j [\mathbf{g}^{(k)}]_l \end{aligned} \quad (2.82)$$

The derivatives at  $\mathbf{u}^{(k)}$  of the three area moments  $A_{cq}$ ,  $\mathbf{s}_{cq}$  and  $\mathbf{J}_{cq}$  of the generic concrete subdomain  $\Omega_{cq}^{(k)}$  with respect to the strain parameters  $\varepsilon_o$  and  $\mathbf{g}$  can be evaluated by invoking (2.62), (2.63) and (2.64) and recalling that each subdomain is polygonal. Actually, each subdomain  $\Omega_{cq}^{(k)}$  changes with the strain parameters and the same happens for the area moments.

- derivatives of area:

$$\begin{aligned} \frac{\partial A_{cq}}{\partial \varepsilon_o} \Big|_{\mathbf{u}^{(k)}} &= \frac{1}{2} \sum_{j=1}^{n_{cq}^{(k)}} \left( \frac{\partial \mathbf{r}_{qj}}{\partial \varepsilon_o} \Big|_{\mathbf{u}^{(k)}} \cdot [\mathbf{r}_{q(j+1)}^{(k)}]^\perp + \right. \\ &\quad \left. + \mathbf{r}_{qj}^{(k)} \cdot \frac{\partial [\mathbf{r}_{q(j+1)}]^\perp}{\partial \varepsilon_o} \Big|_{\mathbf{u}^{(k)}} \right) = \frac{1}{2} \sum_{j=1}^{n_{cq}^{(k)}} p_{qj}^{(k)} \end{aligned} \quad (2.83)$$

$$\begin{aligned} \frac{\partial A_{cq}}{\partial \mathbf{g}} \Big|_{\mathbf{u}^{(k)}} &= \frac{1}{2} \sum_{j=1}^{n_{cq}^{(k)}} \left( \left[ \frac{\partial \mathbf{r}_{qj}}{\partial \mathbf{g}} \right]_{\mathbf{u}^{(k)}}^T [\mathbf{r}_{q(j+1)}^{(k)}]^\perp + \right. \\ &\quad \left. + \left[ \frac{\partial [\mathbf{r}_{q(j+1)}]^\perp}{\partial \mathbf{g}} \right]_{\mathbf{u}^{(k)}}^T \mathbf{r}_{qj}^{(k)} \right) = \frac{1}{2} \sum_{j=1}^{n_{cq}^{(k)}} \mathbf{q}_{qj}^{(k)} \end{aligned}$$

- derivatives of first area moment:

$$\begin{aligned} \frac{\partial \mathbf{s}_{cq}}{\partial \varepsilon_o} \Big|_{\mathbf{u}^{(k)}} &= \frac{1}{6} \sum_{j=1}^{n_{cq}^{(k)}} \left[ p_{qj}^{(k)} \left( \mathbf{r}_{qj}^{(k)} + \mathbf{r}_{q(j+1)}^{(k)} \right) + \right. \\ &\quad \left. + c_{qj}^{(k)} \left( \frac{\partial \mathbf{r}_{qj}}{\partial \varepsilon_o} \Big|_{\mathbf{u}^{(k)}} + \frac{\partial \mathbf{r}_{q(j+1)}}{\partial \varepsilon_o} \Big|_{\mathbf{u}^{(k)}} \right) \right] \end{aligned} \quad (2.84)$$

$$\begin{aligned} \frac{\partial \mathbf{s}_{cq}}{\partial \mathbf{g}} \Big|_{\mathbf{u}^{(k)}} &= \frac{1}{6} \sum_{j=1}^{n_{cq}^{(k)}} \left[ \left( \mathbf{r}_{qj}^{(k)} + \mathbf{r}_{q(j+1)}^{(k)} \right) \otimes \mathbf{q}_{qj}^{(k)} + \right. \\ &\quad \left. + c_{qj}^{(k)} \left( \frac{\partial \mathbf{r}_{qj}}{\partial \mathbf{g}} \Big|_{\mathbf{u}^{(k)}} + \frac{\partial \mathbf{r}_{q(j+1)}}{\partial \mathbf{g}} \Big|_{\mathbf{u}^{(k)}} \right) \right] \end{aligned}$$

- derivatives of second area moment:

$$\begin{aligned}
 \frac{\partial \mathbf{J}_{cq}}{\partial \varepsilon_o} \Big|_{\mathbf{u}^{(k)}} &= \frac{1}{12} \sum_{j=1}^{n_{cq}^{(k)}} \left\{ p_{qj}^{(k)} \left[ \mathbf{r}_{qj}^{(k)} \otimes \mathbf{r}_{qj}^{(k)} + \text{sym} \left( \mathbf{r}_{q(j+1)}^{(k)} \otimes \mathbf{r}_{qj}^{(k)} \right) + \right. \right. \\
 &\quad \left. \left. + \mathbf{r}_{q(j+1)}^{(k)} \otimes \mathbf{r}_{q(j+1)}^{(k)} \right] + \right. \\
 &\quad \left. + c_{qj}^{(k)} \left[ \frac{\partial \mathbf{r}_{qj}}{\partial \varepsilon_o} \Big|_{\mathbf{u}^{(k)}} \otimes \mathbf{r}_{qj}^{(k)} + \text{sym} \left( \frac{\partial \mathbf{r}_{q(j+1)}}{\partial \varepsilon_o} \Big|_{\mathbf{u}^{(k)}} \otimes \mathbf{r}_{qj}^{(k)} \right) + \right. \\
 &\quad \left. + \frac{\partial \mathbf{r}_{q(j+1)}}{\partial \varepsilon_o} \Big|_{\mathbf{u}^{(k)}} \otimes \mathbf{r}_{q(j+1)}^{(k)} + \mathbf{r}_{qj}^{(k)} \otimes \frac{\partial \mathbf{r}_{qj}}{\partial \varepsilon_o} \Big|_{\mathbf{u}^{(k)}} + \right. \\
 &\quad \left. \left. + \text{sym} \left( \mathbf{r}_{q(j+1)}^{(k)} \otimes \frac{\partial \mathbf{r}_{qj}}{\partial \varepsilon_o} \Big|_{\mathbf{u}^{(k)}} \right) + \mathbf{r}_{q(j+1)}^{(k)} \otimes \frac{\partial \mathbf{r}_{q(j+1)}}{\partial \varepsilon_o} \Big|_{\mathbf{u}^{(k)}} \right] \right\} \quad (2.85)
 \end{aligned}$$

$$\begin{aligned}
 \frac{\partial \mathbf{J}_{cq}}{\partial \mathbf{g}} \Big|_{\mathbf{u}^{(k)}} &= \frac{1}{12} \sum_{j=1}^{n_{cq}^{(k)}} \left\{ \left[ \mathbf{r}_{qj}^{(k)} \otimes \mathbf{r}_{qj}^{(k)} + \text{sym} \left( \mathbf{r}_{q(j+1)}^{(k)} \otimes \mathbf{r}_{qj}^{(k)} \right) + \right. \right. \\
 &\quad \left. \left. + \mathbf{r}_{q(j+1)}^{(k)} \otimes \mathbf{r}_{q(j+1)}^{(k)} \right] \otimes \mathbf{q}_{qj}^{(k)} + \right. \\
 &\quad \left. + c_{qj}^{(k)} \left[ \frac{\partial \mathbf{r}_{qj}}{\partial \mathbf{g}} \Big|_{\mathbf{u}^{(k)}} \otimes \mathbf{r}_{qj}^{(k)} + \text{sym} \left( \frac{\partial \mathbf{r}_{q(j+1)}}{\partial \mathbf{g}} \Big|_{\mathbf{u}^{(k)}} \otimes \mathbf{r}_{qj}^{(k)} \right) + \right. \\
 &\quad \left. + \frac{\partial \mathbf{r}_{q(j+1)}}{\partial \mathbf{g}} \Big|_{\mathbf{u}^{(k)}} \otimes \mathbf{r}_{q(j+1)}^{(k)} + \mathbf{r}_{qj}^{(k)} \otimes \frac{\partial \mathbf{r}_{qj}}{\partial \mathbf{g}} \Big|_{\mathbf{u}^{(k)}} + \right. \\
 &\quad \left. \left. + \text{sym} \left( \mathbf{r}_{q(j+1)}^{(k)} \otimes \frac{\partial \mathbf{r}_{qj}}{\partial \mathbf{g}} \Big|_{\mathbf{u}^{(k)}} \right) + \mathbf{r}_{q(j+1)}^{(k)} \otimes \frac{\partial \mathbf{r}_{q(j+1)}}{\partial \mathbf{g}} \Big|_{\mathbf{u}^{(k)}} \right] \right\}
 \end{aligned}$$

The previous formulas emphasize that the required derivatives of the area moments depend upon the change, with respect to  $\varepsilon_o$  and  $\mathbf{g}$ , of the position vectors which define each subdomain  $\Omega_{cq}^{(k)}$ . Such vectors can be grouped in two mutually disjoint subsets. The first one contains the position vectors which define the boundary of  $\Omega_c$ ; accordingly their coordinates are fixed and the relevant derivatives with respect to  $\varepsilon_o$  and  $\mathbf{g}$  are trivially zero.

Therefore, we shall concentrate on the second set, denoted in the sequel by  $\Gamma_{cq}^{(k)}$ , which collects the position vectors  $\mathbf{r}_{qj}^{(k)}$  belonging to the generic

edge of the boundary of  $\Omega_c$  with the exception of the relevant end points. In other words the position vectors included in  $\Gamma_{cq}^{(k)}$  are those which define vertices belonging to two adjacent subdomains  $\Omega_{c,j}^{(k)}$  and  $\Omega_{c,j+1}^{(k)}$  but different from the vertices defining the boundary of  $\Omega_c$ .

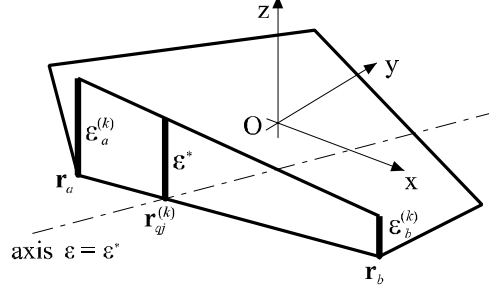


Figure 2.10: Evaluation of the position vector  $\mathbf{r}_{qj}^{(k)}$

The derivative at  $\mathbf{u}^{(k)}$  of each  $\mathbf{r}_{qj} \in \Gamma_{cq}^{(k)}$  with respect to  $\varepsilon_o$  and  $\mathbf{g}$  can be derived as follows. Let  $\mathbf{r}_a$  and  $\mathbf{r}_b$  be the end vertices of the edge of the section boundary which  $\mathbf{r}_{qj}^{(k)}$  belongs to (see figure 2.10). Thus  $\mathbf{r}_{qj}^{(k)}$  can be expressed in parametric form as

$$\mathbf{r}_{qj}^{(k)} = \mathbf{r}_a + \vartheta_{qj}^{(k)} (\mathbf{r}_b - \mathbf{r}_a) \quad (2.86)$$

Since  $\mathbf{r}_{qj}^{(k)} \in \Gamma_{cq}^{(k)}$  we can set  $\varepsilon(\mathbf{r}_{qj}^{(k)}) = \varepsilon^*$  where  $\varepsilon^* = 0$  if  $\mathbf{r}_{qj}^{(k)}$  belongs to the neutral axis i.e.  $\mathbf{r}_{qj}^{(k)} \in \Omega_{c0}^{(k)} \cap \Omega_{c1}^{(k)}$ ,  $\varepsilon^* = \varepsilon_{cp}$  if  $\mathbf{r}_{qj}^{(k)} \in \Omega_{c1}^{(k)} \cap \Omega_{c2}^{(k)}$ , and  $\varepsilon^* = \varepsilon_{cu}$  if  $\mathbf{r}_{qj}^{(k)} \in \Omega_{c2}^{(k)} \cap \Omega_{c3}^{(k)}$ . Thus the parameter  $\vartheta_{qj}^{(k)}$  in (2.86) can be evaluated explicitly as

$$\vartheta_{qj}^{(k)} = \frac{\varepsilon^* - \varepsilon_a^{(k)}}{\varepsilon_b^{(k)} - \varepsilon_a^{(k)}} \quad (2.87)$$

where

$$\varepsilon_a^{(k)} = \varepsilon_o^{(k)} + \mathbf{g}^{(k)} \cdot \mathbf{r}_a \quad \varepsilon_b^{(k)} = \varepsilon_o^{(k)} + \mathbf{g}^{(k)} \cdot \mathbf{r}_b \quad (2.88)$$

Notice that the case  $\varepsilon_a^{(k)} = \varepsilon_b^{(k)}$  can be excluded since, otherwise, the edge defined by the end vertices  $\mathbf{r}_a$  and  $\mathbf{r}_b$  would be parallel to or belong to a generic axis of constant strain subdividing two adjacent subdomains  $\Omega_{c,j}$  and  $\Omega_{c,j+1}$ ; in both cases no point of the edge belongs to  $\Gamma_{cq}^{(k)}$ .

In conclusion, on the basis of the previous three formulas we can write

$$\left. \frac{\partial \mathbf{r}_{qj}}{\partial \varepsilon_o} \right|_{\mathbf{u}^{(k)}} = \left. \frac{\partial \vartheta_{qj}}{\partial \varepsilon_o} \right|_{\mathbf{u}^{(k)}} (\mathbf{r}_b - \mathbf{r}_a) \quad \left. \frac{\partial \mathbf{r}_{qj}}{\partial \mathbf{g}} \right|_{\mathbf{u}^{(k)}} = (\mathbf{r}_b - \mathbf{r}_a) \otimes \left. \frac{\partial \vartheta_{qj}}{\partial \mathbf{g}} \right|_{\mathbf{u}^{(k)}} \quad (2.89)$$

where

$$\begin{aligned} \left. \frac{\partial \vartheta_{qj}}{\partial \varepsilon_o} \right|_{\mathbf{u}^{(k)}} &= -\frac{1}{\varepsilon_b^{(k)} - \varepsilon_a^{(k)}} \\ \left. \frac{\partial \vartheta_{qj}}{\partial \mathbf{g}} \right|_{\mathbf{u}^{(k)}} &= \frac{\mathbf{r}_a(\varepsilon^* - \varepsilon_b^{(k)}) - \mathbf{r}_b(\varepsilon^* - \varepsilon_a^{(k)})}{(\varepsilon_b^{(k)} - \varepsilon_a^{(k)})^2} \end{aligned} \quad (2.90)$$

Let us now consider the derivatives appearing in (2.76). Invoking (2.68) and (2.69) one gets:

$$\begin{aligned} \left. \frac{\partial [\mathbf{M}_{c1}]^\perp}{\partial \varepsilon_o} \right|_{\mathbf{u}^{(k)}} &= (\alpha + 2\beta\varepsilon_o^{(k)}) \mathbf{s}_{c1}^{(k)} + (\alpha\varepsilon_o + \beta(\varepsilon_o^{(k)})^2) \left. \frac{\partial \mathbf{s}_{c1}}{\partial \varepsilon_o} \right|_{\mathbf{u}^{(k)}} + \\ &\quad + 2\beta \mathbf{J}_{c1}^{(k)} \mathbf{g}^{(k)} + (\alpha + 2\beta\varepsilon_o^{(k)}) \left. \frac{\partial \mathbf{J}_{c1}}{\partial \varepsilon_o} \right|_{\mathbf{u}^{(k)}} \mathbf{g}^{(k)} + \\ &\quad + \beta \left. \frac{\partial \bar{\mathbf{J}}_{c1}}{\partial \varepsilon_o} \right|_{\mathbf{u}^{(k)}} (\mathbf{g}^{(k)} \otimes \mathbf{g}^{(k)}) \end{aligned} \quad (2.91)$$

$$\left. \frac{\partial [\mathbf{M}_{c2}]^\perp}{\partial \varepsilon_o} \right|_{\mathbf{u}^{(k)}} = \sigma_{cu} \left. \frac{\partial \mathbf{s}_{c2}}{\partial \varepsilon_o} \right|_{\mathbf{u}^{(k)}}$$

$$\left. \frac{\partial [\mathbf{M}_{c3}]^\perp}{\partial \varepsilon_o} \right|_{\mathbf{u}^{(k)}} = E_c^{sec} \mathbf{s}_{c3}^{(k)} + E_c^{sec} \varepsilon_o^{(k)} \left. \frac{\partial \mathbf{s}_{c3}}{\partial \varepsilon_o} \right|_{\mathbf{u}^{(k)}} + E_c^{sec} \left. \frac{\partial \mathbf{J}_{c3}}{\partial \varepsilon_o} \right|_{\mathbf{u}^{(k)}} \mathbf{g}^{(k)}$$

for concrete and

$$\begin{aligned} \left. \frac{\partial [\mathbf{M}_{s1}]^\perp}{\partial \varepsilon_o} \right|_{\mathbf{u}^{(k)}} &= E_{sc}^{sec} \mathbf{s}_{s1}^{(k)}; & \left. \frac{\partial [\mathbf{M}_{s2}]^\perp}{\partial \varepsilon_o} \right|_{\mathbf{u}^{(k)}} &= \mathbf{0} \\ \left. \frac{\partial [\mathbf{M}_{s3}]^\perp}{\partial \varepsilon_o} \right|_{\mathbf{u}^{(k)}} &= E_s \mathbf{s}_{s3}^{(k)}; & \left. \frac{\partial [\mathbf{M}_{s4}]^\perp}{\partial \varepsilon_o} \right|_{\mathbf{u}^{(k)}} &= \mathbf{0} \\ \left. \frac{\partial [\mathbf{M}_{s5}]^\perp}{\partial \varepsilon_o} \right|_{\mathbf{u}^{(k)}} &= E_{st}^{sec} \mathbf{s}_{s5}^{(k)} \end{aligned} \quad (2.92)$$

for steel bars.

Finally, the derivatives in (2.77) at  $\mathbf{u}^{(k)}$  of  $[\mathbf{M}_{cq}]^\perp$  and  $[\mathbf{M}_{sq}]^\perp$  with respect to  $\mathbf{g}$  are given by

$$\begin{aligned} \left. \frac{\partial[\mathbf{M}_{c1}]^\perp}{\partial \mathbf{g}} \right|_{\mathbf{u}^{(k)}} &= (\alpha \varepsilon_o^{(k)} + \beta (\varepsilon_o^{(k)})^2) \left. \frac{\partial \mathbf{s}_{c1}}{\partial \mathbf{g}} \right|_{\mathbf{u}^{(k)}} + (\alpha + 2\beta \varepsilon_o^{(k)}) \mathbf{J}_{c1}^{(k)} + \\ &+ (\alpha + 2\beta \varepsilon_o^{(k)}) \left. \frac{\partial \mathbf{J}_{c1}}{\partial \mathbf{g}} \right|_{\mathbf{u}^{(k)}} \mathbf{g}^{(k)} + 2\beta \bar{\mathbf{J}}_{c1}^{(k)} \mathbf{g}^{(k)} + \\ &+ \beta \left. \frac{\partial \bar{\mathbf{J}}_{c1}}{\partial \mathbf{g}} \right|_{\mathbf{u}^{(k)}} (\mathbf{g}^{(k)} \otimes \mathbf{g}^{(k)}) \end{aligned} \quad (2.93)$$

$$\left. \frac{\partial[\mathbf{M}_{c2}]^\perp}{\partial \mathbf{g}} \right|_{\mathbf{u}^{(k)}} = \sigma_{cu} \left. \frac{\partial \mathbf{s}_{c2}}{\partial \mathbf{g}} \right|_{\mathbf{u}^{(k)}}$$

$$\left. \frac{\partial[\mathbf{M}_{c3}]^\perp}{\partial \mathbf{g}} \right|_{\mathbf{u}^{(k)}} = E_c^{sec} \varepsilon_o^{(k)} \left. \frac{\partial \mathbf{s}_{c3}}{\partial \mathbf{g}} \right|_{\mathbf{u}^{(k)}} + E_c^{sec} \mathbf{J}_{c3}^{(k)} + E_c^{sec} \left. \frac{\partial \mathbf{J}_{c3}}{\partial \mathbf{g}} \right|_{\mathbf{u}^{(k)}} \mathbf{g}^{(k)}$$

for concrete and

$$\begin{aligned} \left. \frac{\partial[\mathbf{M}_{s1}]^\perp}{\partial \mathbf{g}} \right|_{\mathbf{u}^{(k)}} &= E_{sc}^{sec} \mathbf{J}_{s1}^{(k)}; & \left. \frac{\partial[\mathbf{M}_{s2}]^\perp}{\partial \mathbf{g}} \right|_{\mathbf{u}^{(k)}} &= \mathbf{0} \\ \left. \frac{\partial[\mathbf{M}_{s3}]^\perp}{\partial \mathbf{g}} \right|_{\mathbf{u}^{(k)}} &= E_s \mathbf{J}_{s3}^{(k)}; & \left. \frac{\partial[\mathbf{M}_{s4}]^\perp}{\partial \mathbf{g}} \right|_{\mathbf{u}^{(k)}} &= \mathbf{0} \\ \left. \frac{\partial[\mathbf{M}_{s5}]^\perp}{\partial \mathbf{g}} \right|_{\mathbf{u}^{(k)}} &= E_{st}^{sec} \mathbf{J}_{s1}^{(k)} \end{aligned} \quad (2.94)$$

for steel bars.

With reference to (2.93) we remark that

$$\left[ \left. \frac{\partial \mathbf{J}_{cq}}{\partial \mathbf{g}} \right|_{\mathbf{u}^{(k)}} \mathbf{g}^{(k)} \right]_{ij} = \left[ \left. \frac{\partial \mathbf{J}_{cq}}{\partial \mathbf{g}} \right|_{\mathbf{u}^{(k)}} \right]_{ilj} [\mathbf{g}^{(k)}]_l = \left. \frac{\partial [\mathbf{J}_{cq}]_{il}}{\partial \mathbf{g}_j} \right|_{\mathbf{u}^{(k)}} [\mathbf{g}^{(k)}]_l \quad (2.95)$$

$$\begin{aligned} \left[ \left. \frac{\partial \bar{\mathbf{J}}_{cq}}{\partial \mathbf{g}} \right|_{\mathbf{u}^{(k)}} \mathbf{g}^{(k)} \otimes \mathbf{g}^{(k)} \right]_{ij} &= \left[ \left. \frac{\partial \bar{\mathbf{J}}_{cq}}{\partial \mathbf{g}} \right|_{\mathbf{u}^{(k)}} \right]_{ilmj} [\mathbf{g}]_l [\mathbf{g}]_m = \\ &= \left. \frac{\partial [\bar{\mathbf{J}}_{cq}]_{ilm}}{\partial \mathbf{g}_j} \right|_{\mathbf{u}^{(k)}} [\mathbf{g}]_l [\mathbf{g}]_m \end{aligned} \quad (2.96)$$

The third and fourth order tensor reported above can be computed as follows

$$\begin{aligned}
 \left. \frac{\partial \bar{\mathbf{J}}_{cq}}{\partial \varepsilon_o} \right|_{\mathbf{u}^{(k)}} &= \frac{1}{20} \sum_{j=1}^{n_{cq}^{(k)}} \left\{ p_{qj}^{(k)} \left[ \mathbf{r}_{qj}^{(k)} \otimes \mathbf{r}_{qj}^{(k)} \otimes \mathbf{r}_{qj}^{(k)} + \frac{1}{3} \left( \mathbf{r}_{q(j+1)}^{(k)} \otimes \mathbf{r}_{qj}^{(k)} \otimes \mathbf{r}_{qj}^{(k)} + \right. \right. \\
 &\quad \left. \left. + \mathbf{r}_{q(j+1)}^{(k)} \otimes \mathbf{r}_{q(j+1)}^{(k)} \otimes \mathbf{r}_{qj}^{(k)} + \mathbf{r}_{q(j+1)}^{(k)} \otimes \mathbf{r}_{qj}^{(k)} \otimes \mathbf{r}_{q(j+1)}^{(k)} + \right. \right. \\
 &\quad \left. \left. + \mathbf{r}_{qj}^{(k)} \otimes \mathbf{r}_{q(j+1)}^{(k)} \otimes \mathbf{r}_{qj}^{(k)} + \mathbf{r}_{qj}^{(k)} \otimes \mathbf{r}_{q(j+1)}^{(k)} \otimes \mathbf{r}_{q(j+1)}^{(k)} + \right. \right. \\
 &\quad \left. \left. \mathbf{r}_{qj}^{(k)} \otimes \mathbf{r}_{qj}^{(k)} \otimes \mathbf{r}_{q(j+1)}^{(k)} \right) + \mathbf{r}_{q(j+1)}^{(k)} \otimes \mathbf{r}_{q(j+1)}^{(k)} \otimes \mathbf{r}_{q(j+1)}^{(k)} \right] + \\
 &\quad \left. + c_{qj}^{(k)} \frac{\partial}{\partial \varepsilon_o} \left[ \mathbf{r}_{qj} \otimes \mathbf{r}_{qj} \otimes \mathbf{r}_{qj} + \frac{1}{3} \left( \mathbf{r}_{q(j+1)} \otimes \mathbf{r}_{qj} \otimes \mathbf{r}_{qj} + \right. \right. \right. \\
 &\quad \left. \left. + \mathbf{r}_{q(j+1)} \otimes \mathbf{r}_{q(j+1)} \otimes \mathbf{r}_{qj} + \mathbf{r}_{q(j+1)} \otimes \mathbf{r}_{qj} \otimes \mathbf{r}_{q(j+1)} + \right. \right. \\
 &\quad \left. \left. + \mathbf{r}_{qj} \otimes \mathbf{r}_{q(j+1)} \otimes \mathbf{r}_{qj} + \mathbf{r}_{qj} \otimes \mathbf{r}_{q(j+1)} \otimes \mathbf{r}_{q(j+1)} + \right. \right. \\
 &\quad \left. \left. \left. \mathbf{r}_{qj} \otimes \mathbf{r}_{qj} \otimes \mathbf{r}_{q(j+1)} \right) + \mathbf{r}_{q(j+1)} \otimes \mathbf{r}_{q(j+1)} \otimes \mathbf{r}_{q(j+1)} \right] \right\}_{\mathbf{u}^{(k)}} \quad (2.97)
 \end{aligned}$$

where  $\frac{\partial}{\partial \varepsilon_o} (\mathbf{a} \otimes \mathbf{b} \otimes \mathbf{c}) = \frac{\partial \mathbf{a}}{\partial \varepsilon_o} \otimes \mathbf{b} \otimes \mathbf{c} + \mathbf{a} \otimes \frac{\partial \mathbf{b}}{\partial \varepsilon_o} \otimes \mathbf{c} + \mathbf{a} \otimes \mathbf{b} \otimes \frac{\partial \mathbf{c}}{\partial \varepsilon_o}$ .

Finally:

$$\begin{aligned}
\left. \frac{\partial \bar{\mathbf{J}}_{cq}}{\partial \mathbf{g}} \right|_{\mathbf{u}^{(k)}} &= \frac{1}{20} \sum_{j=1}^{n_{cq}^{(k)}} \left\{ \left[ \mathbf{r}_{qj}^{(k)} \otimes \mathbf{r}_{qj}^{(k)} \otimes \mathbf{r}_{qj}^{(k)} + \frac{1}{3} \left( \mathbf{r}_{q(j+1)}^{(k)} \otimes \mathbf{r}_{qj}^{(k)} \otimes \mathbf{r}_{qj}^{(k)} + \right. \right. \\
&+ \mathbf{r}_{q(j+1)}^{(k)} \otimes \mathbf{r}_{q(j+1)}^{(k)} \otimes \mathbf{r}_{qj}^{(k)} + \mathbf{r}_{q(j+1)}^{(k)} \otimes \mathbf{r}_{qj}^{(k)} \otimes \mathbf{r}_{q(j+1)}^{(k)} + \\
&+ \mathbf{r}_{qj}^{(k)} \otimes \mathbf{r}_{q(j+1)}^{(k)} \otimes \mathbf{r}_{qj}^{(k)} + \mathbf{r}_{qj}^{(k)} \otimes \mathbf{r}_{q(j+1)}^{(k)} \otimes \mathbf{r}_{q(j+1)}^{(k)} + \\
&\left. \left. + \mathbf{r}_{qj}^{(k)} \otimes \mathbf{r}_{qj}^{(k)} \otimes \mathbf{r}_{q(j+1)}^{(k)} \right) + \mathbf{r}_{q(j+1)}^{(k)} \otimes \mathbf{r}_{q(j+1)}^{(k)} \otimes \mathbf{r}_{q(j+1)}^{(k)} \right] \otimes \mathbf{q}_{qj}^{(k)} + \\
&+ c_{qj}^{(k)} \frac{\partial}{\partial \mathbf{g}} \left[ \mathbf{r}_{qj} \otimes \mathbf{r}_{qj} \otimes \mathbf{r}_{qj} + \frac{1}{3} \left( \mathbf{r}_{q(j+1)} \otimes \mathbf{r}_{qj} \otimes \mathbf{r}_{qj} + \right. \right. \\
&+ \mathbf{r}_{q(j+1)} \otimes \mathbf{r}_{q(j+1)} \otimes \mathbf{r}_{qj} + \mathbf{r}_{q(j+1)} \otimes \mathbf{r}_{qj} \otimes \mathbf{r}_{q(j+1)} + \\
&+ \mathbf{r}_{qj} \otimes \mathbf{r}_{q(j+1)} \otimes \mathbf{r}_{qj} + \mathbf{r}_{qj} \otimes \mathbf{r}_{q(j+1)} \otimes \mathbf{r}_{q(j+1)} + \\
&\left. \left. + \mathbf{r}_{qj} \otimes \mathbf{r}_{qj} \otimes \mathbf{r}_{q(j+1)} \right) + \mathbf{r}_{q(j+1)} \otimes \mathbf{r}_{q(j+1)} \otimes \mathbf{r}_{q(j+1)} \right]_{\mathbf{u}^{(k)}} \right\} \quad (2.98)
\end{aligned}$$

where  $\frac{\partial}{\partial \mathbf{g}}(\mathbf{a} \otimes \mathbf{b} \otimes \mathbf{c}) = \frac{\partial \mathbf{a}}{\partial \mathbf{g}} \otimes \mathbf{b} \otimes \mathbf{c} + \mathbf{a} \otimes \frac{\partial \mathbf{b}}{\partial \mathbf{g}} \otimes \mathbf{c} + \mathbf{a} \otimes \mathbf{b} \otimes \frac{\partial \mathbf{c}}{\partial \mathbf{g}}$ .

As a final remark, we draw the reader's attention on the fact that the derivatives of  $N_{s2}$  and  $N_{s4}$ , see e.g. formulas (2.79) and (2.81), as well as the derivatives of  $[\mathbf{M}_{s2}]^\perp$  and  $[\mathbf{M}_{s4}]^\perp$ , formulas (2.92) and (2.94), with respect to  $\varepsilon_o$  and  $\mathbf{g}$  are zero.

Farther, if the strain is  $\varepsilon_{cu} \leq \varepsilon \leq \varepsilon_{cp}$  over the entire concrete section then  $\Omega_{c1}^{(k)}$ ,  $\Omega_{c3}^{(k)}$  and  $\Gamma_{cq}^{(k)}$ ,  $q = 1, 2, 3$ , are empty being  $\Omega_{c2}^{(k)} \equiv \Omega_c$ , thus the derivatives of the area moments of  $\Omega_{cq}^{(k)}$  as well as the derivatives of  $N_{cq}$  and  $[\mathbf{M}_{cq}]^\perp$ ,  $q = 1, 2, 3$ , with respect to  $\varepsilon_o$  and  $\mathbf{g}$  are zero.

This motivates the necessity of modifying the tangent matrix in order to avoid singularity.

### 2.5.2 Integration formulas for the evaluation of the matrix $\mathbf{H}^{(k)}$

Aim of this section is to define a proper modification for the tangent matrix in order to avoid its singularity. To this end, it is enough to replace the derivatives of the axial force and of the bending moment associated with the steel bars pertaining to the sets  $I_{s2}^{(k)}$  and  $I_{s4}^{(k)}$  with suitably defined values which result in a positive definite matrix  $\mathbf{H}^{(k)}$ . In this respect we define for each bar belonging to  $I_{s2}^{(k)}$  and  $I_{s4}^{(k)}$  a modified constitutive law  $\sigma_{bj}^{rm}$  having constant slope:

$$\frac{\partial \sigma_{bj}^{rm}(\varepsilon)}{\partial \varepsilon} = b \quad \varepsilon_{sy} \leq \varepsilon \leq \varepsilon_{su} \quad (2.99)$$

where the parameter  $b$  is defined by

$$b = \frac{\alpha \sigma_{sy} - \sigma_{sy}}{\varepsilon_{su} - \varepsilon_{sy}} \quad (2.100)$$

Numerical experiments have been carried out by making  $\alpha$  range in the interval  $[1.0001; 1.1]$ . They have shown that the better performances are obtained by setting  $\alpha = 1.01$ .

Integration of equation (2.99) leads to:

$$\sigma_{bj}^{rm}(\varepsilon) = a_{bj} + b\varepsilon \quad \varepsilon_{sy} \leq \varepsilon \leq \varepsilon_{su} \quad (2.101)$$

If we wanted to evaluate  $\mathbf{R}^{(k)}$  using eq. (2.101), we would need to evaluate the integration constant  $a_{bj}$  by using the condition  $\sigma_{bj}^{rm}[\varepsilon^{(k)}(\mathbf{r}_{bj})] = \sigma_{sy}$ . This would ensure that the resultant  $\mathbf{f}_r^{(k)}$ , and hence the residual  $\mathbf{R}^{(k)}$  in (2.28), is not affected by the modified constitutive law (2.101) whose only purpose is to ensure a positive-definite matrix  $\mathbf{H}^{(k)}$  in the modified Newton method. However, the residual  $\mathbf{R}^{(k)}$  is always evaluated using the constitutive laws (2.26) and (2.27) and it is worth noting that the values of the integration constant  $a_{bj}$  are inessential in the evaluation of  $\mathbf{H}^{(k)}$ .

To show this property we evaluate the stress resultants pertaining to the  $j$ -th bar belonging to  $I_{s2}^{(k)}$  and  $I_{s4}^{(k)}$ . On account of (2.101) the relevant expressions are provided by

$$\bar{N}_{bj}^{(k)} = \sigma_{bj}^{rm} A_{bj} = (a_{bj} + \varepsilon_o^{(k)} b) A_{bj} + b A_{bj} \mathbf{r}_{bj} \cdot \mathbf{g}^{(k)} \quad (2.102)$$

$$[\bar{\mathbf{M}}_{bj}^{(k)}]^\perp = \sigma_{bj}^{rm} A_{bj} \mathbf{r}_{bj} = (a_{bj} + \varepsilon_o^{(k)} b) A_{bj} \mathbf{r}_{bj} + b A_{bj} (\mathbf{r}_{bj} \otimes \mathbf{r}_{bj}) \mathbf{g}^{(k)} \quad (2.103)$$

Thus, the relevant derivatives with respect to the strain parameters become:

$$\begin{aligned} \left. \frac{\partial \bar{N}_{bj}}{\partial \varepsilon_o} \right|_{\mathbf{u}^{(k)}} &= bA_{bj}; & \left. \frac{\partial \bar{N}_{bj}}{\partial \mathbf{g}} \right|_{\mathbf{u}^{(k)}} &= bA_{bj} \mathbf{r}_{bj} \\ \left. \frac{\partial [\bar{\mathbf{M}}_{bj}]^\perp}{\partial \varepsilon_o} \right|_{\mathbf{u}^{(k)}} &= bA_{bj} \mathbf{r}_{bj}; & \left. \frac{\partial [\bar{\mathbf{M}}_{bj}]^\perp}{\partial \mathbf{g}} \right|_{\mathbf{u}^{(k)}} &= bA_{bj} \mathbf{r}_{bj} \otimes \mathbf{r}_{bj} \end{aligned} \quad (2.104)$$

Summing up the previous contributions for all bars we finally obtain

$$\begin{aligned} \left. \frac{\partial \bar{N}_{s2}}{\partial \varepsilon_o} \right|_{\mathbf{u}^{(k)}} &= bA_{s2}^{(k)}; & \left. \frac{\partial \bar{N}_{s2}}{\partial \mathbf{g}} \right|_{\mathbf{u}^{(k)}} &= b\mathbf{s}_{s2}^{(k)}; \\ \left. \frac{\partial [\bar{\mathbf{M}}_{s2}]^\perp}{\partial \varepsilon_o} \right|_{\mathbf{u}^{(k)}} &= b\mathbf{s}_{s2}^{(k)}; & \left. \frac{\partial [\bar{\mathbf{M}}_{s2}]^\perp}{\partial \mathbf{g}} \right|_{\mathbf{u}^{(k)}} &= b\mathbf{J}_{s2}^{(k)}; \end{aligned} \quad (2.105)$$

for the index set  $I_{s2}^{(k)}$  and

$$\begin{aligned} \left. \frac{\partial \bar{N}_{s4}}{\partial \varepsilon_o} \right|_{\mathbf{u}^{(k)}} &= bA_{s4}^{(k)}; & \left. \frac{\partial \bar{N}_{s4}}{\partial \mathbf{g}} \right|_{\mathbf{u}^{(k)}} &= b\mathbf{s}_{s4}^{(k)} \\ \left. \frac{\partial [\bar{\mathbf{M}}_{s4}]^\perp}{\partial \varepsilon_o} \right|_{\mathbf{u}^{(k)}} &= b\mathbf{s}_{s4}^{(k)}; & \left. \frac{\partial [\bar{\mathbf{M}}_{s4}]^\perp}{\partial \mathbf{g}} \right|_{\mathbf{u}^{(k)}} &= b\mathbf{J}_{s4}^{(k)} \end{aligned} \quad (2.106)$$

for the bars belonging to  $I_{s4}^{(k)}$ .

The above derivatives replace the analogous quantities appearing in formulas (2.74)-(2.77) so that the the so obtained matrix  $\mathbf{H}^{(k)}$  is always positive definite as well as symmetric.

## 2.6 Integration formulas for the evaluation of $\phi$

The expression of  $\phi$  as a closed form function of the coordinates of the vertices of the subdomains defined in (2.57) and of the bars pertaining to the subsets in (2.58) is as follows:

$$\phi(\mathbf{u}^{(k)}) = \sum_{q=1}^3 \phi_{cq}(\mathbf{u}^{(k)}) + \sum_{q=1}^5 \phi_{sq}(\mathbf{u}^{(k)}) \quad (2.107)$$

where

$$\begin{aligned} \phi_{c1}(\mathbf{u}^{(k)}) = & \left( \frac{\alpha}{2} (\varepsilon_o^{(k)})^2 + \frac{\beta}{3} (\varepsilon_o^{(k)})^3 \right) A_{c1}^{(k)} + \\ & + \left( \alpha \varepsilon_o^{(k)} + \beta (\varepsilon_o^{(k)})^2 \right) \mathbf{s}_{c1}^{(k)} \cdot \mathbf{g}^{(k)} + \end{aligned} \quad (2.108)$$

$$\begin{aligned} & + \left( \frac{\alpha}{2} + \beta (\varepsilon_o^{(k)}) \right) \mathbf{J}_{c1}^{(k)} \mathbf{g}^{(k)} \cdot \mathbf{g}^{(k)} + \frac{\beta}{3} \overline{\mathbf{J}}_{c1}^{(k)} \mathbf{g}^{(k)} \mathbf{g}^{(k)} \cdot \mathbf{g}^{(k)} \\ \phi_{c2}(\mathbf{u}^{(k)}) = & \left( \frac{\alpha}{2} \varepsilon_{cp}^2 + \frac{\beta}{3} \varepsilon_{cp}^3 \right) A_{c2}^{(k)} + \sigma_{co} (\varepsilon_o^{(k)} - \varepsilon_{cp}) A_{c2}^{(k)} + \\ & + \sigma_{co} \mathbf{s}_{c2}^{(k)} \cdot \mathbf{g}^{(k)} \end{aligned} \quad (2.109)$$

$$\begin{aligned} \phi_{c3}(\mathbf{u}^{(k)}) = & \left( \frac{\alpha}{2} \varepsilon_{cp}^2 + \frac{\beta}{3} \varepsilon_{cp}^3 \right) A_{c3}^{(k)} + \sigma_{co} (\varepsilon_{cu} - \varepsilon_{cp}) A_{c3}^{(k)} + \\ & + \frac{E_c^{sec}}{2} ((\varepsilon_o^{(k)})^2 - \varepsilon_{cu}^2) A_{c3}^{(k)} + \\ & + E_c^{sec} \varepsilon_o^{(k)} \mathbf{s}_{c3}^{(k)} \cdot \mathbf{g}^{(k)} + \frac{E_c^{sec}}{2} \mathbf{J}_{c3}^{(k)} \mathbf{g}^{(k)} \cdot \mathbf{g}^{(k)} \end{aligned} \quad (2.110)$$

for concrete, and

$$\begin{aligned} \phi_{s1}(\mathbf{u}^{(k)}) = & A_{s1}^{(k)} \left[ \frac{E_s}{2} \varepsilon_{sy}^2 - \sigma_{sy} (\varepsilon_{cu} + \varepsilon_{sy}) + \frac{E_{sc}^{sec}}{2} ((\varepsilon_o^{(k)})^2 - \varepsilon_{cu}^2) \right] + \\ & + E_{sc}^{sec} \varepsilon_o^{(k)} \mathbf{s}_{s1}^{(k)} \cdot \mathbf{g}^{(k)} + \frac{E_{sc}^{sec}}{2} \mathbf{J}_{s1}^{(k)} \mathbf{g}^{(k)} \cdot \mathbf{g}^{(k)} \end{aligned} \quad (2.111)$$

$$\phi_{s2}(\mathbf{u}^{(k)}) = A_{s2}^{(k)} \left[ \frac{E_s}{2} \varepsilon_{sy}^2 - \sigma_{sy} (\varepsilon_o^{(k)} + \varepsilon_{sy}) \right] - \sigma_{sy} \mathbf{s}_{s2}^{(k)} \cdot \mathbf{g}^{(k)} \quad (2.112)$$

$$\phi_{s3}(\mathbf{u}^{(k)}) = A_{s3}^{(k)} \frac{E_s}{2} (\varepsilon_o^{(k)})^2 + E_s \varepsilon_o^{(k)} \mathbf{s}_{s3}^{(k)} \cdot \mathbf{g}^{(k)} + \frac{E_s}{2} \mathbf{J}_{s3}^{(k)} \mathbf{g}^{(k)} \cdot \mathbf{g}^{(k)} \quad (2.113)$$

$$\phi_{s4}(\mathbf{u}^{(k)}) = A_{s4}^{(k)} \left[ \frac{E_s}{2} \varepsilon_{sy}^2 + \sigma_{sy} (\varepsilon_o^{(k)} - \varepsilon_{sy}) \right] + \sigma_{sy} \mathbf{s}_{s4}^{(k)} \cdot \mathbf{g}^{(k)} \quad (2.114)$$

$$\begin{aligned} \phi_{s5}(\mathbf{u}^{(k)}) = & A_{s5}^{(k)} \left[ \frac{E_s}{2} \varepsilon_{sy}^2 + \sigma_{sy} (\varepsilon_{su} - \varepsilon_{sy}) + \frac{E_{st}^{sec}}{2} ((\varepsilon_o^{(k)})^2 - \varepsilon_{su}^2) \right] + \\ & + E_{st}^{sec} \varepsilon_o^{(k)} \mathbf{s}_{s5}^{(k)} \cdot \mathbf{g}^{(k)} + \frac{E_{st}^{sec}}{2} \mathbf{J}_{s5}^{(k)} \mathbf{g}^{(k)} \cdot \mathbf{g}^{(k)} \end{aligned} \quad (2.115)$$

for the steel bars.

## 2.7 Numerical results

We present a comprehensive set of numerical examples which have been carried out with the aim of testing the proposed algorithm quite intensively.

Actually, although the algorithm has been conceived with the objective of finding the ultimate load associated with a fixed given load  $\mathbf{f}_d$  and a given load direction  $\mathbf{f}_1$ , it has been decided to construct the whole failure surface for several RC sections.

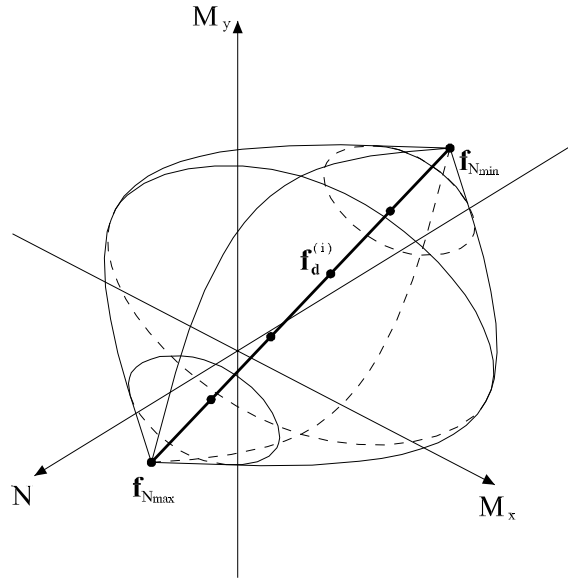


Figure 2.11: Assumption of the fixed load vector

In particular, see figure 2.11, each surface has been constructed in the space  $N, M_x, M_y$  by making the load  $\mathbf{f}_d$  move along the segment defined by end points  $\mathbf{f}_{N_{max}} - \mathbf{f}_{N_{min}}$  and assuming that, for each  $\mathbf{f}_d$ , the unit vector  $\mathbf{f}_1 = \{0, \cos \theta, \sin \theta\}$  uniformly spans the subspace  $M_x - M_y$ .

The vectors  $\mathbf{f}_{N_{max}}$  and  $\mathbf{f}_{N_{min}}$  are the resultant of the stress field corresponding to a uniform strain field  $\varepsilon_o$  over the section associated, respectively, with the values  $\varepsilon_o = \varepsilon_{sy}$  and  $\varepsilon_o = \varepsilon_{cp}$ .

All interaction surfaces have been constructed by considering 100 values of  $\mathbf{f}_d$  and, for each of them, 100 vectors  $\mathbf{f}_1$  so that the total number of analyses

carried out for each surface has an order of magnitude equal to  $10^4$ .

Several typology of RC sections have been analyzed with the aim of considering a representative set of the most typical shapes encountered in buildings, precast sheds and bridge piers. In this section we present numerical results obtained for rectangular, L-shaped, multicell, T-shaped and Y-shaped sections.

Geometric data and reinforcement pattern for each of them are reported in figures 2.12, 2.13(a), 2.15, 2.16 and 2.17 wherein  $R_{ck}$  is the characteristic compressive cubical strength of concrete. The value  $R_{ck} = 25N/mm^2$  has been used in all examples. In accordance with [33, 39], the corresponding value of  $f_{ck}$  is  $20.75N/mm^2$ .

The numerical performances of the solution algorithm are also supplied in table 2.1 which reports the minimum, maximum and average number of iterations necessary to achieve convergence in each of the separate iterative procedures namely:

- the iterative procedure used to evaluate  $\lambda^*$ ;
- the iterative procedure used to evaluate  $\mathbf{u}(\mathbf{f})$ ;
- the line-search (L-S) procedure.

	Rectangular			L-shaped			Multicell		
	Avg	Min	Max	Avg	Min	Max	Avg	Min	Max
$\lambda^*$	13.2	5	30	12.7	5	30	12.4	6	30
$\mathbf{u}(\mathbf{f}_i)$	6.72	2	26	6.65	2	392	6.94	1	57
L-S	0.121	0	59	0.138	0	26	0.105	0	27
	T-shaped			Y-shaped					
	Avg	Min	Max	Avg	Min	Max			
$\lambda^*$	13.1	5	30	12.6	5	30			
$\mathbf{u}(\mathbf{f}_i)$	6.68	2	96	6.78	2	78			
L-S	0.129	0	30	0.098	0	14			

Table 2.1: Number of iterations for the construction of the failure surfaces ( $100 \times 100$ ) of the rectangular, L-shaped, multicell, T-shaped and Y-shaped sections

In this respect we remind that the second iterative procedure is invoked at each single iteration of the first one and that, if necessary, the third iterative procedure is adopted within a single iteration of the second one. In particular the average number of L-S iterations reported in the table is by far less than 1; this confirms that the L-S procedure is actually resorted to only occasionally.

In order to show the convergence rates of the proposed algorithm we plot the average number of iterations needed by the two iterative procedures in order to achieve convergence as a function of the values assigned to  $tol_{\mathbf{e}}$  and  $tol_{\mathbf{R}}$ . Figure 2.14(b) numerically shows that procedure B is superlinearly convergent. Such result was expected because procedure B consists in a slight modification of the Newton method which is quadratically convergent. Conversely, procedure A is based upon a simpler iterative algorithm and, see figure 2.14(a), does not exhibit a rate of convergence as good as the one of procedure B.

Finally, we suggest to adopt the values  $tol_{\mathbf{e}} = 10^{-5}$  and  $tol_{\mathbf{R}} = 10^{-5}$  which were actually employed to construct the interaction surface above, since they represent a reasonable compromise between accuracy of the result and computational burden.

Furthermore, tables 2.4, 2.5, 2.6, 2.7 and 2.8 report, for each section, the points of the relevant failure surface determined assuming 12 values of  $\mathbf{f}_{\mathbf{d}}$  and, for each of them, 12 vectors  $\mathbf{f}_{\mathbf{l}}$ .

To provide further insights in the proposed numerical algorithm we report the sequence of load amplifiers  $\lambda_i$  and relevant errors  $e_i$  generated for two different sections. In the first case  $\mathbf{f}_{\mathbf{d}} = \mathbf{0}$ , while in the second case both  $\mathbf{f}_{\mathbf{d}}$  and  $\mathbf{f}_{\mathbf{l}}$  are non null. We further specify that, in the following, axial forces are expressed in Mega-Newton and bending moments in  $MNm$ .

The first case refers to the rectangular section of figure 2.12 in which the vector  $\mathbf{f}_{\mathbf{e}}^T = \{-0.65, -0.051, -0.082\}$ . Being  $\mathbf{f}_{\mathbf{l}} = \mathbf{f}_{\mathbf{e}}$  we are looking for the load amplifier  $\lambda > 0$  which proportionally increases  $\mathbf{f}_{\mathbf{e}}$  till reaching the ULS for the section. The ultimate load is  $(\mathbf{f}^*)^T = \{-0.7178, -0.0563, -0.0906\}$  and the load amplifier is  $\lambda^* = 1.104340$ ; the value of  $\lambda^*$  slightly greater than 1 means that the external load vector  $\mathbf{f}_{\mathbf{e}}$  lies very close to the interaction surface and within the admissible domain. The relevant results are reported in table 2.2.

Let us now considerate the multi-cell section of figure 2.15 and suppose that the external forces associated with dead load, e.g. self-weight and permanent loads, are kept fixed and equal to  $\mathbf{f}_{\mathbf{d}}^T = \{-1.50, 1.90, -3.60\}$ .

Assuming that the external forces due to live load are equal to  $\mathbf{f}_{\mathbf{l}}^T = \{-6.00, 3.40, 5.30\}$  we want to know the degree of safety of the load  $\mathbf{f}_{\mathbf{e}} = \mathbf{f}_{\mathbf{d}} + \mathbf{f}_{\mathbf{l}}$  when only the live load are increased, i.e. when we increase  $\mathbf{f}_{\mathbf{e}}$  along  $\mathbf{f}_{\mathbf{l}}$ . We obtain in this case the results reported in table 2.3, with  $\lambda^* = 2.104311$ .

$\lambda_i$	$e_i$
0.000000	+1.00E+00
2.479895	-2.97E+00
0.624736	+6.47E-01
0.956791	+3.38E-01
1.112499	-3.37E-02
1.098371	+2.36E-02
1.104184	+6.29E-04
1.104336	+1.54E-05
1.104340	+3.75E-07

Table 2.2: Iterations of Procedure B for the rectangular section subject to  $\mathbf{f}_d = \{0, 0, 0\}$  and  $\mathbf{f}_i = \{-0.65, -0.051, -0.082\}$

$\lambda_i$	$e_i$
0.000000	+7.98E-01
1.659495	+4.79E-01
4.146055	-2.88E+00
2.013478	+1.75E-01
2.135631	-8.39E-02
2.096068	+2.12E-02
2.104048	+6.94E-04
2.104307	+1.03E-05
2.104311	+1.50E-07

Table 2.3: Iterations of Procedure B for the multicell section subject to  $\mathbf{f}_d = \{-1.50, 1.90, -3.60\}$  and  $\mathbf{f}_i = \{-6.00, 3.40, 5.30\}$

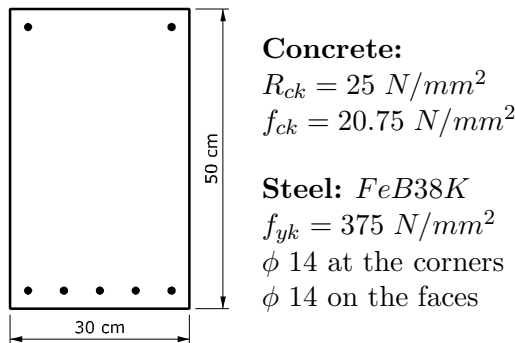


Figure 2.12: Rectangular section

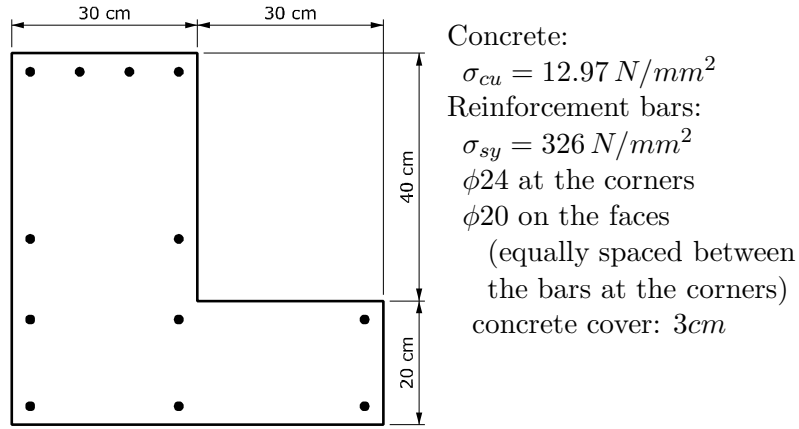
$N$ [MN]	$M_x$ [MNm]	$M_y$ [MNm]	$N$ [MN]	$M_x$ [MNm]	$M_y$ [MNm]
0.1701	-0.0134	-0.0225	-0.0111	0.0029	-0.0415
0.1701	0.0058	-0.0185	-0.0111	0.0363	-0.0331
0.1701	0.0068	0.0000	-0.0111	0.0462	0.0000
0.1701	0.0058	0.0185	-0.0111	0.0363	0.0331
0.1701	-0.0134	0.0225	-0.0111	0.0029	0.0415
0.1701	-0.0264	0.0227	-0.0111	-0.0211	0.0438
0.1701	-0.0395	0.0227	-0.0111	-0.0464	0.0438
0.1701	-0.0639	0.0217	-0.0111	-0.0862	0.0376
0.1701	-0.0714	0.0000	-0.0111	-0.1094	0.0000
0.1701	-0.0639	-0.0217	-0.0111	-0.0862	-0.0376
0.1701	-0.0395	-0.0227	-0.0111	-0.0464	-0.0438
0.1701	-0.0264	-0.0227	-0.0111	-0.0211	-0.0438
-0.1924	0.0162	-0.0555	-0.3736	0.0277	-0.0662
-0.1924	0.0582	-0.0427	-0.3736	0.0742	-0.0489
-0.1924	0.0846	0.0000	-0.3736	0.1213	0.0000
-0.1924	0.0582	0.0427	-0.3736	0.0742	0.0489
-0.1924	0.0162	0.0555	-0.3736	0.0277	0.0662
-0.1924	-0.0158	0.0608	-0.3736	-0.0105	0.0739
-0.1924	-0.0503	0.0598	-0.3736	-0.0510	0.0700
-0.1924	-0.0953	0.0459	-0.3736	-0.0992	0.0512
-0.1924	-0.1413	0.0000	-0.3736	-0.1621	0.0000
-0.1924	-0.0953	-0.0459	-0.3736	-0.0992	-0.0512
-0.1924	-0.0503	-0.0598	-0.3736	-0.0510	-0.0700
-0.1924	-0.0158	-0.0608	-0.3736	-0.0105	-0.0739
-0.5549	0.0372	-0.0736	-0.7361	0.0444	-0.0768
-0.5549	0.0868	-0.0531	-0.7361	0.0966	-0.0558
-0.5549	0.1495	0.0000	-0.7361	0.1669	0.0000
-0.5549	0.0868	0.0531	-0.7361	0.0966	0.0558
-0.5549	0.0372	0.0736	-0.7361	0.0444	0.0768
-0.5549	-0.0053	0.0825	-0.7361	0.0000	0.0856
-0.5549	-0.0482	0.0743	-0.7361	-0.0434	0.0751
-0.5549	-0.0986	0.0539	-0.7361	-0.0940	0.0543
-0.5549	-0.1728	0.0000	-0.7361	-0.1702	0.0000
-0.5549	-0.0986	-0.0539	-0.7361	-0.0940	-0.0543
-0.5549	-0.0482	-0.0743	-0.7361	-0.0434	-0.0751
-0.5549	-0.0053	-0.0825	-0.7361	0.0000	-0.0856

$N$ [MN]	$M_x$ [MNm]	$M_y$ [MNm]	$N$ [MN]	$M_x$ [MNm]	$M_y$ [MNm]
-0.9174	0.0500	-0.0774	-1.0986	0.0525	-0.0726
-0.9174	0.1029	-0.0564	-1.0986	0.1035	-0.0537
-0.9174	0.1741	0.0000	-1.0986	0.1669	0.0000
-0.9174	0.1029	0.0564	-1.0986	0.1035	0.0537
-0.9174	0.0500	0.0774	-1.0986	0.0525	0.0726
-0.9174	0.0053	0.0830	-1.0986	0.0105	0.0761
-0.9174	-0.0369	0.0731	-1.0986	-0.0285	0.0676
-0.9174	-0.0856	0.0524	-1.0986	-0.0737	0.0486
-0.9174	-0.1495	0.0000	-1.0986	-0.1268	0.0000
-0.9174	-0.0856	-0.0524	-1.0986	-0.0737	-0.0486
-0.9174	-0.0369	-0.0731	-1.0986	-0.0285	-0.0676
-0.9174	0.0053	-0.0830	-1.0986	0.0105	-0.0761
-1.2799	0.0530	-0.0645	-1.4611	0.0515	-0.0526
-1.2799	0.0994	-0.0482	-1.4611	0.0911	-0.0404
-1.2799	0.1502	0.0000	-1.4611	0.1280	0.0000
-1.2799	0.0994	0.0482	-1.4611	0.0911	0.0404
-1.2799	0.0530	0.0645	-1.4611	0.0515	0.0526
-1.2799	0.0158	0.0668	-1.4611	0.0211	0.0545
-1.2799	-0.0187	0.0598	-1.4611	-0.0074	0.0494
-1.2799	-0.0594	0.0434	-1.4611	-0.0422	0.0365
-1.2799	-0.1013	0.0000	-1.4611	-0.0719	0.0000
-1.2799	-0.0594	-0.0434	-1.4611	-0.0422	-0.0365
-1.2799	-0.0187	-0.0598	-1.4611	-0.0074	-0.0494
-1.2799	0.0158	-0.0668	-1.4611	0.0211	-0.0545
-1.6424	0.0479	-0.0373	-1.8236	0.0426	-0.0190
-1.6424	0.0784	-0.0301	-1.8236	0.0588	-0.0157
-1.6424	0.0988	0.0000	-1.8236	0.0654	0.0000
-1.6424	0.0784	0.0301	-1.8236	0.0588	0.0157
-1.6424	0.0479	0.0373	-1.8236	0.0426	0.0190
-1.6424	0.0264	0.0382	-1.8236	0.0316	0.0193
-1.6424	0.0058	0.0355	-1.8236	0.0209	0.0186
-1.6424	-0.0213	0.0275	-1.8236	0.0050	0.0154
-1.6424	-0.0379	0.0000	-1.8236	-0.0034	0.0000
-1.6424	-0.0213	-0.0275	-1.8236	0.0050	-0.0154
-1.6424	0.0058	-0.0355	-1.8236	0.0209	-0.0186
-1.6424	0.0264	-0.0382	-1.8236	0.0316	-0.0193

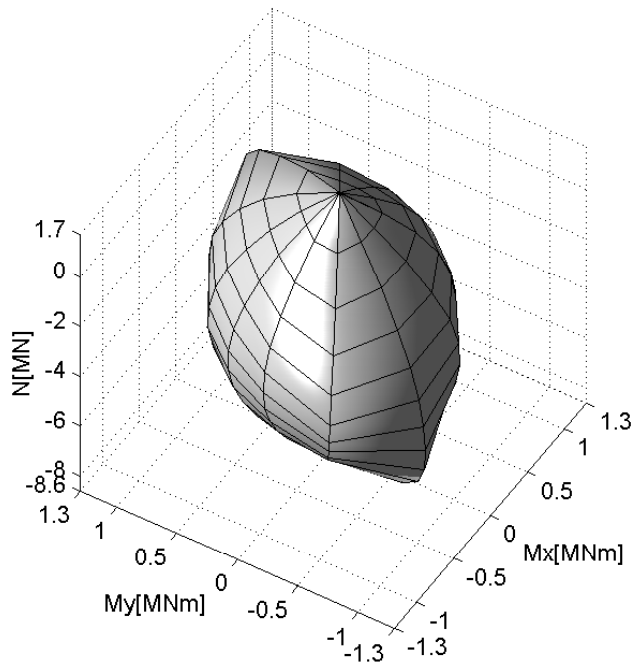
$$\{N, M_x, M_y\}_{\max} = \{0.3514, -0.0316, 0.0000\}$$

$$\{N, M_x, M_y\}_{\min} = \{-2.0049, 0.0316, 0.0000\}$$

Table 2.4: Failure surface points ( $12 \times 12$ ) of the rectangular section of figure 2.12

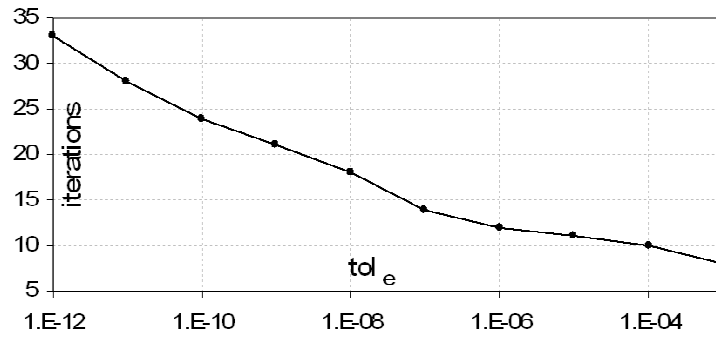


(a) L-shaped section

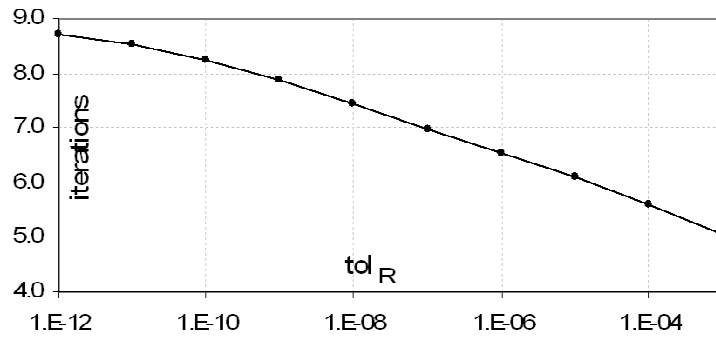


(b) Failure surface of the L-shaped section

Figure 2.13: L-shaped section: geometry and failure surface



(a) # iterations vs.  $tol_e$  (Procedure A)



(b) # iterations vs.  $tol_R$  (Procedure B)

Figure 2.14: Average number of iterations vs. tolerance for the L-shaped section

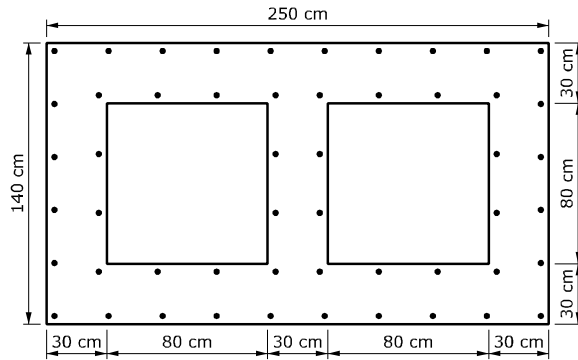
$N$ [MN]	$M_x$ [MNm]	$M_y$ [MNm]	$N$ [MN]	$M_x$ [MNm]	$M_y$ [MNm]
0.3513	0.0239	-0.0623	0.0469	0.0569	-0.1153
0.3513	0.0518	-0.0394	0.0469	0.1040	-0.0677
0.3513	0.0544	-0.0038	0.0469	0.1165	-0.0031
0.3513	0.0545	0.0333	0.0469	0.1168	0.0689
0.3513	0.0450	0.0912	0.0469	0.0916	0.1693
0.3513	-0.0098	0.0742	0.0469	-0.0079	0.1435
0.3513	-0.0425	0.0527	0.0469	-0.0684	0.1019
0.3513	-0.0713	0.0317	0.0469	-0.1113	0.0566
0.3513	-0.1047	-0.0038	0.0469	-0.1638	-0.0031
0.3513	-0.0986	-0.0551	0.0469	-0.1613	-0.0916
0.3513	-0.0438	-0.0626	0.0469	-0.0750	-0.1193
0.3513	-0.0098	-0.0626	0.0469	-0.0079	-0.1207
-0.2575	0.0768	-0.1455	-0.5619	0.0905	-0.1650
-0.2575	0.1373	-0.0850	-0.5619	0.1630	-0.0979
-0.2575	0.1681	-0.0023	-0.5619	0.2057	-0.0015
-0.2575	0.1709	0.0998	-0.5619	0.2145	0.1246
-0.2575	0.1225	0.2200	-0.5619	0.1351	0.2393
-0.2575	-0.0059	0.1916	-0.5619	-0.0039	0.2143
-0.2575	-0.0842	0.1333	-0.5619	-0.0964	0.1587
-0.2575	-0.1415	0.0760	-0.5619	-0.1645	0.0912
-0.2575	-0.2076	-0.0023	-0.5619	-0.2331	-0.0015
-0.2575	-0.2094	-0.1198	-0.5619	-0.2431	-0.1396
-0.2575	-0.1019	-0.1686	-0.5619	-0.1211	-0.2044
-0.2575	-0.0059	-0.1737	-0.5619	-0.0039	-0.2103
-0.8662	0.1000	-0.1773	-1.1706	0.1041	-0.1803
-0.8662	0.1768	-0.1040	-1.1706	0.1791	-0.1034
-0.8662	0.2298	-0.0008	-1.1706	0.2447	0.0000
-0.8662	0.2499	0.1447	-1.1706	0.2749	0.1587
-0.8662	0.1374	0.2406	-1.1706	0.1332	0.2308
-0.8662	-0.0020	0.2282	-1.1706	0.0000	0.2293
-0.8662	-0.1043	0.1765	-1.1706	-0.1051	0.1821
-0.8662	-0.1775	0.1006	-1.1706	-0.1819	0.1050
-0.8662	-0.2456	-0.0008	-1.1706	-0.2412	0.0000
-0.8662	-0.2663	-0.1534	-1.1706	-0.2700	-0.1559
-0.8662	-0.1341	-0.2296	-1.1706	-0.1400	-0.2426
-0.8662	-0.0020	-0.2274	-1.1706	0.0000	-0.2350

$N$ [MN]	$M_x$ [MNm]	$M_y$ [MNm]	$N$ [MN]	$M_x$ [MNm]	$M_y$ [MNm]
-1.4750	0.1010	-0.1708	-1.7794	0.0946	-0.1554
-1.4750	0.1762	-0.0998	-1.7794	0.1642	-0.0910
-1.4750	0.2497	0.0008	-1.7794	0.2412	0.0015
-1.4750	0.2783	0.1603	-1.7794	0.2574	0.1479
-1.4750	0.1265	0.2164	-1.7794	0.1164	0.1964
-1.4750	0.0020	0.2174	-1.7794	0.0039	0.1986
-1.4750	-0.1020	0.1808	-1.7794	-0.0938	0.1708
-1.4750	-0.1773	0.1042	-1.7794	-0.1651	0.0991
-1.4750	-0.2277	0.0008	-1.7794	-0.2053	0.0015
-1.4750	-0.2521	-0.1459	-1.7794	-0.2241	-0.1301
-1.4750	-0.1420	-0.2486	-1.7794	-0.1402	-0.2481
-1.4750	0.0020	-0.2344	-1.7794	0.0039	-0.2210
-2.0838	0.0850	-0.1347	-2.3881	0.0722	-0.1083
-2.0838	0.1459	-0.0786	-2.3881	0.1220	-0.0629
-2.0838	0.2184	0.0023	-2.3881	0.1851	0.0031
-2.0838	0.2247	0.1286	-2.3881	0.1844	0.1050
-2.0838	0.1026	0.1698	-2.3881	0.0844	0.1357
-2.0838	0.0059	0.1731	-2.3881	0.0079	0.1402
-2.0838	-0.0803	0.1516	-2.3881	-0.0632	0.1261
-2.0838	-0.1446	0.0892	-2.3881	-0.1168	0.0750
-2.0838	-0.1758	0.0023	-2.3881	-0.1380	0.0031
-2.0838	-0.1881	-0.1097	-2.3881	-0.1433	-0.0842
-2.0838	-0.1345	-0.2408	-2.3881	-0.1161	-0.2117
-2.0838	0.0059	-0.1942	-2.3881	0.0079	-0.1584
-2.6925	0.0557	-0.0757	-2.9969	0.0355	-0.0365
-2.6925	0.0918	-0.0435	-2.9969	0.0549	-0.0203
-2.6925	0.1401	0.0038	-2.9969	0.0815	0.0046
-2.6925	0.1355	0.0764	-2.9969	0.0756	0.0414
-2.6925	0.0620	0.0942	-2.9969	0.0381	0.0501
-2.6925	0.0098	0.0991	-2.9969	0.0118	0.0522
-2.6925	-0.0421	0.0938	-2.9969	-0.0157	0.0522
-2.6925	-0.0817	0.0567	-2.9969	-0.0382	0.0334
-2.6925	-0.0927	0.0038	-2.9969	-0.0410	0.0046
-2.6925	-0.0929	-0.0555	-2.9969	-0.0413	-0.0261
-2.6925	-0.0821	-0.1554	-2.9969	-0.0367	-0.0795
-2.6925	0.0098	-0.1131	-2.9969	0.0118	-0.0566

$$\{N, M_x, M_y\}_{\max} = \{0.6556, -0.0118, -0.0046\}$$

$$\{N, M_x, M_y\}_{\min} = \{-3.3013, 0.0118, 0.0046\}$$

Table 2.5: Failure surface points ( $12 \times 12$ ) of the L-shaped section of figure 2.13(a)

**Concrete:**

$$R_{ck} = 25 \text{ N/mm}^2$$

$$f_{ck} = 20.75 \text{ N/mm}^2$$

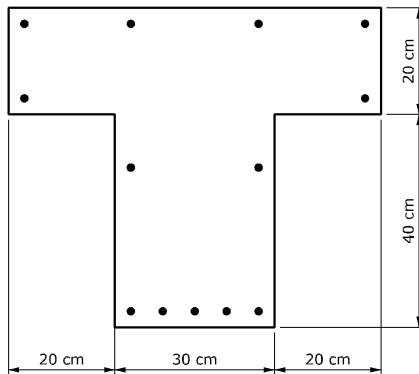
**Steel: FeB38K**

$$f_{yk} = 375 \text{ N/mm}^2$$

$$\phi 32 \text{ at the corners}$$

$$\phi 32 \text{ on the faces}$$

Figure 2.15: Multicell section

**Concrete:**

$$R_{ck} = 25 \text{ N/mm}^2$$

$$f_{ck} = 20.75 \text{ N/mm}^2$$

**Steel: FeB38K**

$$f_{yk} = 375 \text{ N/mm}^2$$

$$\phi 16 \text{ at the corners}$$

$$\phi 16 \text{ on the faces}$$

Figure 2.16: T-shaped section

**Ultimate Limit State analysis of RC sections subject to axial force and biaxial bending**

$N$ [MN]	$M_x$ [MNm]	$M_y$ [MNm]	$N$ [MN]	$M_x$ [MNm]	$M_y$ [MNm]
9.6567	2.1814	-3.7782	5.6762	3.9334	-6.8129
9.6567	2.5589	-1.4774	5.6762	4.8797	-2.8173
9.6567	2.6438	0.0000	5.6762	5.0050	0.0000
9.6567	2.5589	1.4774	5.6762	4.8797	2.8173
9.6567	2.1814	3.7782	5.6762	3.9334	6.8129
9.6567	0.0000	4.5735	5.6762	0.0000	8.8490
9.6567	-2.1814	3.7782	5.6762	-3.9334	6.8129
9.6567	-2.5589	1.4774	5.6762	-4.8797	2.8173
9.6567	-2.6438	0.0000	5.6762	-5.0050	0.0000
9.6567	-2.5589	-1.4774	5.6762	-4.8797	-2.8173
9.6567	-2.1814	-3.7782	5.6762	-3.9334	-6.8129
9.6567	0.0000	-4.5735	5.6762	0.0000	-8.8490
1.6957	5.1682	-8.9515	-2.2848	5.9269	-10.2656
1.6957	6.8784	-3.9712	-2.2848	8.3523	-4.8222
1.6957	7.2012	0.0000	-2.2848	9.0616	0.0000
1.6957	6.8784	3.9712	-2.2848	8.3523	4.8222
1.6957	5.1682	8.9515	-2.2848	5.9269	10.2656
1.6957	0.0000	12.6536	-2.2848	0.0000	15.2785
1.6957	-5.1682	8.9515	-2.2848	-5.9269	10.2656
1.6957	-6.8784	3.9712	-2.2848	-8.3523	4.8222
1.6957	-7.2012	0.0000	-2.2848	-9.0616	0.0000
1.6957	-6.8784	-3.9712	-2.2848	-8.3523	-4.8222
1.6957	-5.1682	-8.9515	-2.2848	-5.9269	-10.2656
1.6957	0.0000	-12.6536	-2.2848	0.0000	-15.2785
-6.2653	6.3460	-10.9916	-10.2458	6.4795	-11.2227
-6.2653	9.3005	-5.3696	-10.2458	9.6620	-5.5784
-6.2653	10.4881	0.0000	-10.2458	11.1203	0.0000
-6.2653	9.3005	5.3696	-10.2458	9.6620	5.5784
-6.2653	6.3460	10.9916	-10.2458	6.4795	11.2227
-6.2653	0.0000	16.5227	-10.2458	0.0000	16.8922
-6.2653	-6.3460	10.9916	-10.2458	-6.4795	11.2227
-6.2653	-9.3005	5.3696	-10.2458	-9.6620	5.5784
-6.2653	-10.4881	0.0000	-10.2458	-11.1203	0.0000
-6.2653	-9.3005	-5.3696	-10.2458	-9.6620	-5.5784
-6.2653	-6.3460	-10.9916	-10.2458	-6.4795	-11.2227
-6.2653	0.0000	-16.5227	-10.2458	0.0000	-16.8922

$N$ [MN]	$M_x$ [MNm]	$M_y$ [MNm]	$N$ [MN]	$M_x$ [MNm]	$M_y$ [MNm]
-14.2263	6.3306	-10.9649	-18.2068	5.9188	-10.2516
-14.2263	9.4080	-5.4317	-18.2068	8.6489	-4.9935
-14.2263	10.8522	0.0000	-18.2068	9.8212	0.0000
-14.2263	9.4080	5.4317	-18.2068	8.6489	4.9935
-14.2263	6.3306	10.9649	-18.2068	5.9188	10.2516
-14.2263	0.0000	16.6564	-18.2068	0.0000	15.5413
-14.2263	-6.3306	10.9649	-18.2068	-5.9188	10.2516
-14.2263	-9.4080	5.4317	-18.2068	-8.6489	4.9935
-14.2263	-10.8522	0.0000	-18.2068	-9.8212	0.0000
-14.2263	-9.4080	-5.4317	-18.2068	-8.6489	-4.9935
-14.2263	-6.3306	-10.9649	-18.2068	-5.9188	-10.2516
-14.2263	0.0000	-16.6564	-18.2068	0.0000	-15.5413
-22.1873	5.2693	-9.1268	-26.1678	4.4128	-7.6432
-22.1873	7.5233	-4.3436	-26.1678	6.0426	-3.4887
-22.1873	8.2538	0.0000	-26.1678	6.4791	0.0000
-22.1873	7.5233	4.3436	-26.1678	6.0426	3.4887
-22.1873	5.2693	9.1268	-26.1678	4.4128	7.6432
-22.1873	0.0000	13.5704	-26.1678	0.0000	11.1254
-22.1873	-5.2693	9.1268	-26.1678	-4.4128	7.6432
-22.1873	-7.5233	4.3436	-26.1678	-6.0426	3.4887
-22.1873	-8.2538	0.0000	-26.1678	-6.4791	0.0000
-22.1873	-7.5233	-4.3436	-26.1678	-6.0426	-3.4887
-22.1873	-5.2693	-9.1268	-26.1678	-4.4128	-7.6432
-22.1873	0.0000	-13.5704	-26.1678	0.0000	-11.1254
-30.1483	3.2638	-5.6530	-34.1288	1.7544	-3.0387
-30.1483	4.2420	-2.4491	-34.1288	2.1764	-1.2565
-30.1483	4.4113	0.0000	-34.1288	2.2424	0.0000
-30.1483	4.2420	2.4491	-34.1288	2.1764	1.2565
-30.1483	3.2638	5.6530	-34.1288	1.7544	3.0387
-30.1483	0.0000	7.8305	-34.1288	0.0000	3.9778
-30.1483	-3.2638	5.6530	-34.1288	-1.7544	3.0387
-30.1483	-4.2420	2.4491	-34.1288	-2.1764	1.2565
-30.1483	-4.4113	0.0000	-34.1288	-2.2424	0.0000
-30.1483	-4.2420	-2.4491	-34.1288	-2.1764	-1.2565
-30.1483	-3.2638	-5.6530	-34.1288	-1.7544	-3.0387
-30.1483	0.0000	-7.8305	-34.1288	0.0000	-3.9778

$$\{N, M_x, M_y\}_{\max} = \{13.6372, 0.0000, 0.0000\}$$

$$\{N, M_x, M_y\}_{\min} = \{-38.1093, 0.0000, 0.0000\}$$

Table 2.6: Failure surface points ( $12 \times 12$ ) of the multicell section of figure 2.15

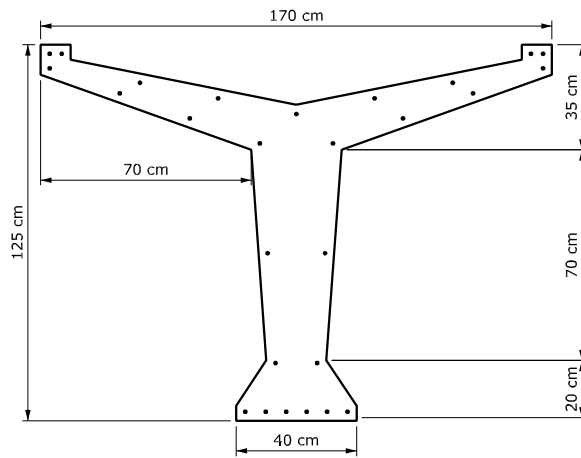
$N$ [MN]	$M_x$ [MNm]	$M_y$ [MNm]	$N$ [MN]	$M_x$ [MNm]	$M_y$ [MNm]
0.5007	-0.0048	-0.0655	0.1491	0.0373	-0.1237
0.5007	0.0331	-0.0437	0.1491	0.1045	-0.0800
0.5007	0.0629	0.0000	0.1491	0.1765	0.0000
0.5007	0.0331	0.0437	0.1491	0.1045	0.0800
0.5007	-0.0048	0.0655	0.1491	0.0373	0.1237
0.5007	-0.0426	0.0854	0.1491	-0.0341	0.1598
0.5007	-0.1054	0.1088	0.1491	-0.1414	0.1858
0.5007	-0.1228	0.0463	0.1491	-0.1875	0.0886
0.5007	-0.1235	0.0000	0.1491	-0.1950	0.0000
0.5007	-0.1228	-0.0463	0.1491	-0.1875	-0.0886
0.5007	-0.1054	-0.1088	0.1491	-0.1414	-0.1858
0.5007	-0.0426	-0.0854	0.1491	-0.0341	-0.1598
-0.2025	0.0750	-0.1742	-0.5541	0.1069	-0.2147
-0.2025	0.1654	-0.1103	-0.5541	0.2179	-0.1356
-0.2025	0.2792	0.0000	-0.5541	0.3376	0.0000
-0.2025	0.1654	0.1103	-0.5541	0.2179	0.1356
-0.2025	0.0750	0.1742	-0.5541	0.1069	0.2147
-0.2025	-0.0256	0.2152	-0.5541	-0.0170	0.2525
-0.2025	-0.1579	0.2291	-0.5541	-0.1605	0.2485
-0.2025	-0.2422	0.1251	-0.5541	-0.2817	0.1528
-0.2025	-0.2587	0.0000	-0.5541	-0.3097	0.0000
-0.2025	-0.2422	-0.1251	-0.5541	-0.2817	-0.1528
-0.2025	-0.1579	-0.2291	-0.5541	-0.1605	-0.2485
-0.2025	-0.0256	-0.2152	-0.5541	-0.0170	-0.2525
-0.9057	0.1310	-0.2417	-1.2572	0.1500	-0.2599
-0.9057	0.2577	-0.1537	-1.2572	0.2847	-0.1644
-0.9057	0.3661	0.0000	-1.2572	0.3652	0.0000
-0.9057	0.2577	0.1537	-1.2572	0.2847	0.1644
-0.9057	0.1310	0.2417	-1.2572	0.1500	0.2599
-0.9057	-0.0085	0.2757	-1.2572	0.0000	0.2822
-0.9057	-0.1547	0.2533	-1.2572	-0.1396	0.2418
-0.9057	-0.2945	0.1651	-1.2572	-0.2795	0.1614
-0.9057	-0.3472	0.0000	-1.2572	-0.3715	0.0000
-0.9057	-0.2945	-0.1651	-1.2572	-0.2795	-0.1614
-0.9057	-0.1547	-0.2533	-1.2572	-0.1396	-0.2418
-0.9057	-0.0085	-0.2757	-1.2572	0.0000	-0.2822

$N$ [MN]	$M_x$ [MNm]	$M_y$ [MNm]	$N$ [MN]	$M_x$ [MNm]	$M_y$ [MNm]
-1.6088	0.1633	-0.2681	-1.9604	0.1686	-0.2626
-1.6088	0.2985	-0.1674	-1.9604	0.2864	-0.1555
-1.6088	0.3420	0.0000	-1.9604	0.3127	0.0000
-1.6088	0.2985	0.1674	-1.9604	0.2864	0.1555
-1.6088	0.1633	0.2681	-1.9604	0.1686	0.2626
-1.6088	0.0085	0.2790	-1.9604	0.0170	0.2548
-1.6088	-0.1213	0.2249	-1.9604	-0.1000	0.2028
-1.6088	-0.2486	0.1485	-1.9604	-0.2128	0.1327
-1.6088	-0.3802	0.0000	-1.9604	-0.3720	0.0000
-1.6088	-0.2486	-0.1485	-1.9604	-0.2128	-0.1327
-1.6088	-0.1213	-0.2249	-1.9604	-0.1000	-0.2028
-1.6088	0.0085	-0.2790	-1.9604	0.0170	-0.2548
-2.3120	0.1677	-0.2462	-2.6636	0.1552	-0.2097
-2.3120	0.2563	-0.1332	-2.6636	0.2165	-0.1053
-2.3120	0.2740	0.0000	-2.6636	0.2235	0.0000
-2.3120	0.2563	0.1332	-2.6636	0.2165	0.1053
-2.3120	0.1677	0.2462	-2.6636	0.1552	0.2097
-2.3120	0.0256	0.2206	-2.6636	0.0341	0.1792
-2.3120	-0.0752	0.1745	-2.6636	-0.0462	0.1391
-2.3120	-0.1720	0.1141	-2.6636	-0.1250	0.0918
-2.3120	-0.3155	0.0000	-2.6636	-0.2420	0.0000
-2.3120	-0.1720	-0.1141	-2.6636	-0.1250	-0.0918
-2.3120	-0.0752	-0.1745	-2.6636	-0.0462	-0.1391
-2.3120	0.0256	-0.2206	-2.6636	0.0341	-0.1792
-3.0152	0.1350	-0.1601	-3.3668	0.1030	-0.0898
-3.0152	0.1668	-0.0717	-3.3668	0.1095	-0.0337
-3.0152	0.1667	0.0000	-3.3668	0.1096	0.0000
-3.0152	0.1668	0.0717	-3.3668	0.1095	0.0337
-3.0152	0.1350	0.1601	-3.3668	0.1030	0.0898
-3.0152	0.0426	0.1293	-3.3668	0.0511	0.0689
-3.0152	-0.0135	0.0972	-3.3668	0.0212	0.0519
-3.0152	-0.0706	0.0653	-3.3668	-0.0085	0.0345
-3.0152	-0.1555	0.0000	-3.3668	-0.0535	0.0000
-3.0152	-0.0706	-0.0653	-3.3668	-0.0085	-0.0345
-3.0152	-0.0135	-0.0972	-3.3668	0.0212	-0.0519
-3.0152	0.0426	-0.1293	-3.3668	0.0511	-0.0689

$$\{N, M_x, M_y\}_{\max} = \{0.8523, -0.0511, 0.0000\}$$

$$\{N, M_x, M_y\}_{\min} = \{-3.7184, 0.0511, 0.0000\}$$

Table 2.7: Failure surface points ( $12 \times 12$ ) of the T-shaped section of figure 2.16



**Concrete:**

$$R_{ck} = 40 \text{ N/mm}^2$$

$$f_{ck} = 33.2 \text{ N/mm}^2$$

**Steel: FeB44K**

$$f_{yk} = 430 \text{ N/mm}^2$$

$\phi$  16 at the corners

$\phi$  16 on the faces

Figure 2.17: Y-shaped section

$N$ [MN]	$M_x$ [MNm]	$M_y$ [MNm]	$N$ [MN]	$M_x$ [MNm]	$M_y$ [MNm]
1.0972	0.2155	-0.2525	0.4242	0.3325	-0.4792
1.0972	0.3522	-0.1631	0.4242	0.5841	-0.3050
1.0972	0.5497	0.0000	0.4242	0.9824	0.0000
1.0972	0.3522	0.1631	0.4242	0.5841	0.3050
1.0972	0.2155	0.2525	0.4242	0.3325	0.4792
1.0972	0.0697	0.3474	0.4242	0.0558	0.6491
1.0972	-0.2024	0.4714	0.4242	-0.4281	0.8381
1.0972	-0.2041	0.1581	0.4242	-0.4685	0.3027
1.0972	-0.2044	0.0000	0.4242	-0.4715	0.0000
1.0972	-0.2041	-0.1581	0.4242	-0.4685	-0.3027
1.0972	-0.2024	-0.4714	0.4242	-0.4281	-0.8381
1.0972	0.0697	-0.3474	0.4242	0.0558	-0.6491
-0.2488	0.4306	-0.6733	-0.9218	0.5052	-0.8267
-0.2488	0.7788	-0.4255	-0.9218	0.9376	-0.5252
-0.2488	1.2862	0.0000	-0.9218	1.4468	0.0000
-0.2488	0.7788	0.4255	-0.9218	0.9376	0.5252
-0.2488	0.4306	0.6733	-0.9218	0.5052	0.8267
-0.2488	0.0418	0.8649	-0.9218	0.0279	0.9808
-0.2488	-0.5170	0.9680	-0.9218	-0.5491	0.9994
-0.2488	-0.7025	0.4298	-0.9218	-0.8934	0.5319
-0.2488	-0.7237	0.0000	-0.9218	-0.9493	0.0000
-0.2488	-0.7025	-0.4298	-0.9218	-0.8934	-0.5319
-0.2488	-0.5170	-0.9680	-0.9218	-0.5491	-0.9994
-0.2488	0.0418	-0.8649	-0.9218	0.0279	-0.9808
-1.5948	0.5531	-0.9338	-2.2678	0.5767	-0.9988
-1.5948	1.0388	-0.5917	-2.2678	1.0804	-0.6238
-1.5948	1.4421	0.0000	-2.2678	1.3213	0.0000
-1.5948	1.0388	0.5917	-2.2678	1.0804	0.6238
-1.5948	0.5531	0.9338	-2.2678	0.5767	0.9988
-1.5948	0.0139	1.0435	-2.2678	0.0000	1.0575
-1.5948	-0.5524	0.9809	-2.2678	-0.5329	0.9230
-1.5948	-1.0169	0.5952	-2.2678	-1.0410	0.6010
-1.5948	-1.1557	0.0000	-2.2678	-1.3380	0.0000
-1.5948	-1.0169	-0.5952	-2.2678	-1.0410	-0.6010
-1.5948	-0.5524	-0.9809	-2.2678	-0.5329	-0.9230
-1.5948	0.0139	-1.0435	-2.2678	0.0000	-1.0575

$N$ [MN]	$M_x$ [MNm]	$M_y$ [MNm]	$N$ [MN]	$M_x$ [MNm]	$M_y$ [MNm]
-2.9408	0.5853	-1.0379	-3.6138	0.5716	-1.0383
-2.9408	1.0554	-0.6174	-3.6138	0.9508	-0.5651
-2.9408	1.1771	0.0000	-3.6138	1.0087	0.0000
-2.9408	1.0554	0.6174	-3.6138	0.9508	0.5651
-2.9408	0.5853	1.0379	-3.6138	0.5716	1.0383
-2.9408	-0.0139	1.0214	-3.6138	-0.0279	0.9359
-2.9408	-0.5015	0.8445	-3.6138	-0.4607	0.7497
-2.9408	-0.9774	0.5563	-3.6138	-0.8860	0.4954
-2.9408	-1.4713	0.0000	-3.6138	-1.5133	0.0000
-2.9408	-0.9774	-0.5563	-3.6138	-0.8860	-0.4954
-2.9408	-0.5015	-0.8445	-3.6138	-0.4607	-0.7497
-2.9408	-0.0139	-1.0214	-3.6138	-0.0279	-0.9359
-4.2868	0.5364	-1.0016	-4.9598	0.4625	-0.8978
-4.2868	0.7869	-0.4785	-4.9598	0.5995	-0.3783
-4.2868	0.8160	0.0000	-4.9598	0.6014	0.0000
-4.2868	0.7869	0.4785	-4.9598	0.5995	0.3783
-4.2868	0.5364	1.0016	-4.9598	0.4625	0.8978
-4.2868	-0.0418	0.8094	-4.9598	-0.0558	0.6599
-4.2868	-0.4096	0.6370	-4.9598	-0.3452	0.5013
-4.2868	-0.7711	0.4211	-4.9598	-0.6307	0.3319
-4.2868	-1.4278	0.0000	-4.9598	-1.1990	0.0000
-4.2868	-0.7711	-0.4211	-4.9598	-0.6307	-0.3319
-4.2868	-0.4096	-0.6370	-4.9598	-0.3452	-0.5013
-4.2868	-0.0418	-0.8094	-4.9598	-0.0558	-0.6599
-5.6328	0.3320	-0.6958	-6.3058	0.1453	-0.3966
-5.6328	0.3848	-0.2624	-6.3058	0.1533	-0.1368
-5.6328	0.3764	0.0000	-6.3058	0.1493	0.0000
-5.6328	0.3848	0.2624	-6.3058	0.1533	0.1368
-5.6328	0.3320	0.6958	-6.3058	0.1453	0.3966
-5.6328	-0.0697	0.4734	-6.3058	-0.0837	0.2388
-5.6328	-0.2644	0.3372	-6.3058	-0.1825	0.1712
-5.6328	-0.4659	0.2287	-6.3058	-0.2829	0.1150
-5.6328	-0.8918	0.0000	-6.3058	-0.4981	0.0000
-5.6328	-0.4659	-0.2287	-6.3058	-0.2829	-0.1150
-5.6328	-0.2644	-0.3372	-6.3058	-0.1825	-0.1712
-5.6328	-0.0697	-0.4734	-6.3058	-0.0837	-0.2388

$$\{N, M_x, M_y\}_{\max} = \{1.7702, 0.0837, 0.0000\}$$

$$\{N, M_x, M_y\}_{\min} = \{-6.9788, -0.0837, 0.0000\}$$

Table 2.8: Failure surface points ( $12 \times 12$ ) of the Y-shaped section of figure 2.17

## Chapter 3

# Nonlinear analysis of RC frame structures

From an historical point of view lumped plasticity models were the first ones to be introduced, mainly due to their simplicity and physical meaning. Actually, under seismic excitation the inelastic behaviour of reinforced concrete frames substantially concentrates at the ends of beams and columns. Basically, depending on each specific formulation, lumped models consist of several springs that are connected in parallel or in series.

The earliest parallel component element was introduced by Clough and Johnston [25] and allowed for a bilinear moment-rotation relation: the element consisted of two parallel elements, one elastic-perfectly plastic to represent yielding and the other perfectly elastic to represent strain-hardening. The stiffness matrix of the member was the sum of the stiffnesses of the two components. Subsequently, Takizawa [95] generalized the previous model to multilinear monotonic behaviour allowing for the effect of cracking in RC members.

The series model, first formalized by Giberson [43] although it had been used earlier, consisted of a linear elastic element with one equivalent nonlinear rotational spring attached to each end. Giberson's model proved to be more versatile than the original Clough model, since it could describe more complex hysteretic behaviour by selecting appropriate moment-rotation relations for the end springs, thus making the model more attractive for the phenomenological representation of the hysteretic behaviour of reinforced concrete members.

Several lumped plasticity constitutive models have been proposed since then by including phenomena with an increasing degree of sophistication

and complexity such as stiffness degradation in flexure and shear [24, 94, 13], pinching under reversal [5, 13] and fixed end rotations at the beam-column joint interface due to bar pull-out [74, 41]. Typically, axial-flexure coupling was neglected. Nonlinear rate constitutive representations have also been generalized from the basic endochronic theory formulation in [75] to provide continuous hysteretic relations for the nonlinear springs. However a critical issue for these models was the selection of parameters for representing the experimental hysteretic behaviour of reinforced concrete members. In spite of the simplicity of lumped models, that reduce storage requirements and computational cost, basic aspects of the hysteretic behaviour of reinforced concrete members were oversimplified.

This is associated with restrictive a-priori assumptions on the values of the spring parameters which strongly depend upon loading patterns, with special emphasis on the axial force, and levels of inelastic deformation. Because of this history dependence, damage predictions at the global, but particularly at the local level, may be grossly inaccurate. Such information can only be obtained with more refined models capable of describing the hysteretic behaviour of the section as a function of axial load. Another limitation of most lumped plasticity models is their inability to describe adequately the deformation softening behaviour of reinforced concrete members such as the reduction in lateral resistance of an axially loaded cantilever column under monotonically increasing lateral tip displacement.

Subsequently, the dependence of flexural strength on the axial load under uniaxial and biaxial bending conditions has been explicitly included in lumped plasticity models by introducing yield surfaces for stress resultants and assuming an associated flow rule [58].

The response is assumed to be linear for stress states that fall within the yield surface and the flexural and axial stiffness of the member are uncoupled. Within this framework several yield surfaces, endowed with sophisticated hardening rules, have been proposed [96]. They assume for the springs multilinear constitutive representations that include cracking and cyclic stiffness degradation.

To improve the description of the interaction between axial force and bending moments Lai et al. [57] proposed a fiber hinge model consisting of a linear elastic element extending over the entire length of the reinforced concrete member and having one inelastic element at each end.

In spite of further improvements on lumped models [38], a more accurate description of the inelastic behaviour of reinforced concrete members can be achieved only by employing models with distributed non-linearity. In contrast to lumped plasticity models, material non-linearity can take place

at any element section and the element behaviour is derived by weighted integration of the section response. In practice, since the element integrals are evaluated numerically, only the behaviour of selected sections at the integration points is monitored.

Either the element deformations or the element forces are the primary unknowns of the model and these are obtained by suitable interpolation functions from the global element displacements or forces, respectively. Discrete cracks are represented as 'smeared' over a finite length rather than treated explicitly.

The constitutive behaviour of the cross section is either formulated in accordance with classical plasticity theory in terms of stress and strain resultants or is explicitly derived from the discretization of the cross section into fibers. The first elements with distributed non linearity were formulated with the classical stiffness method using cubic Hermitian polynomials to approximate the deformations along the element [45, 63]. The formulation has been extended in [6] to include the effect of shear by means of multiaxial constitutive laws based on the endochronic theory.

However, it is well known that finite elements with a displacement based formulation are unable to describe the behaviour of frame members which exhibit inelastic behaviours. The main limitation of such formulations, which adopt cubic Hermitian interpolation functions, is that of assuming a linear distribution of curvature along the element. Although such assumption well describes the linear elastic behavior of the member, it cannot catch the highly non linear curvature distribution of elements which undergo into an inelastic range. For this reasons proposals of force and mixed formulations have become more and more popular in scientific literature [69, 91, 92], even if displacement based formulations are still object of active research.

The goal of this thesis is that of describing a method for evaluating resisting forces and stiffness matrix of a cross section of frame elements by avoiding the so-called fiber method, i.e. without the need of discretizing the section into fibers. Such integration method is used both in the force and displacement formulations as well as in mixed elements.

In this chapter two displacement based formulations are described in order to show how the section analysis method described in chapters 4 and 5 can be used in a non-linear finite element analysis of the structure. To the end of pointing out the general application of the proposed method, a force based formulation is also described in the sequel.

Finally some general definitions about the internal force vector and the tangent matrix of the element cross sections are introduced.

### 3.1 Two beam finite elements with displacement based formulations

We describe in the sequel two displacement based formulations for beam finite elements. The first one is based upon the bending behaviour of the beam while the other one accounts for the shear deformations too. The two formulations have in common the definition of the nodal parameters, i.e. nodal displacement and nodal force vectors, and the evaluation of the stiffness matrix and the residual vector.

Conversely they mainly differ for the definition of the strain and stress fields along the element since the shear strains and the shear internal forces could be neglected or not. Consequently the strain and the tangent operators need to be properly defined.

#### 3.1.1 Bending formulation

Let us consider the beam element shown in figure 3.1 and the element reference frame  $e_1, e_2, e_3$ . The values of the displacements associated with the

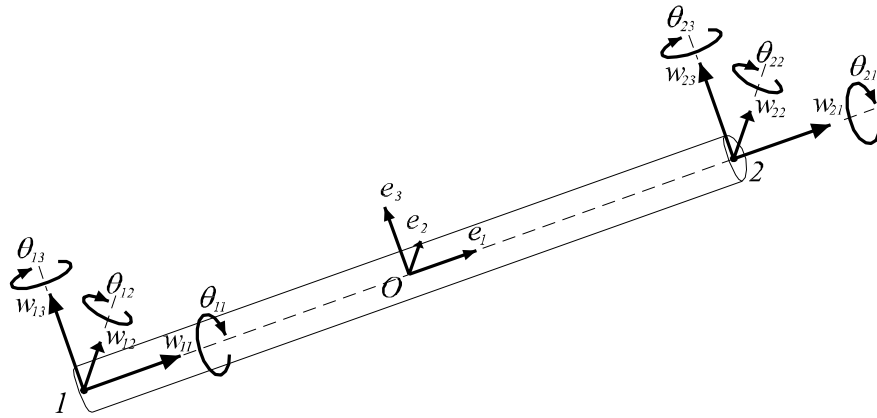


Figure 3.1: Nodal displacements of the beam element

six degrees of freedom of each node are collected in the node displacement vector:

$$\mathbf{d}_n^T = \{w_{n1}, w_{n2}, w_{n3}, \theta_{n1}, \theta_{n2}, \theta_{n3}\} \quad (3.1)$$

where the suffix  $n = 1, 2$  stands for the element node index. The components  $w_{n1}, w_{n2}$  and  $w_{n3}$  correspond to the displacements along the three axis of

the local reference frame while  $\theta_{n1}$ ,  $\theta_{n2}$  and  $\theta_{n3}$  are the rotations about the same axes.

The complete displacements vector of the element is:

$$\mathbf{d}^T = \left\{ \mathbf{d}_1^T \quad \mathbf{d}_2^T \right\} \quad (3.2)$$

The value of the displacement  $w_1(x_1)$  along the element axis  $\mathbf{e}_1$  is given as a function of the nodal displacements  $w_{11}$  and  $w_{21}$ :

$$w_1(x_1) = N_1(x_1)w_{11} + N_2(x_1)w_{21} \quad (3.3)$$

where  $N_1(x_1)$  and  $N_2(x_1)$  are linear shape functions which assume unit value at one node of the element and a null value at the other node (see figure 3.2):

$$N_1(x_1) = -\frac{1}{L}x_1 + \frac{1}{2}; \quad N_2(x_1) = \frac{1}{L}x_1 + \frac{1}{2} \quad (3.4)$$

where the co-ordinates of the two nodes of the element are  $-L/2$  for node 1 and  $L/2$  for node 2,  $L$  being the length of the element.

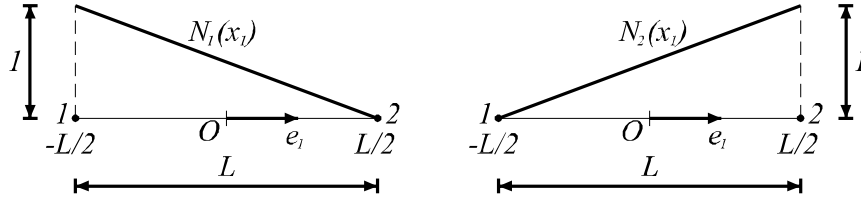


Figure 3.2: Linear shape functions

Conversely, the displacements  $w_2(x_1)$  and  $w_3(x_1)$  are evaluated as:

$$w_2(x_1) = H_{11}(x_1)w_{21} + H_{12}(x_1)\theta_{31} + H_{21}(x_1)w_{22} + H_{22}(x_1)\theta_{32} \quad (3.5)$$

and

$$w_3(x_1) = H_{11}(x_1)w_{31} - H_{12}(x_1)\theta_{21} + H_{21}(x_1)w_{32} - H_{22}(x_1)\theta_{22} \quad (3.6)$$

The shape functions  $H_{ij}$ , with  $i, j = 1, 2$ , are cubic polynomials defined on the element. They are evaluated as:

$$\begin{aligned} H_{11}(x_1) &= \frac{2}{L^3}x_1^3 - \frac{3}{2L}x_1 + \frac{1}{2}; \\ H_{12}(x_1) &= \frac{1}{L^2}x_1^3 - \frac{1}{2L}x_1^2 - \frac{1}{4}x_1 + \frac{L}{8}; \\ H_{21}(x_1) &= -\frac{2}{L^3}x_1^3 + \frac{3}{2L}x_1 + \frac{1}{2}; \\ H_{22}(x_1) &= \frac{1}{L^2}x_1^3 + \frac{1}{2L}x_1^2 - \frac{1}{4}x_1 - \frac{L}{8} \end{aligned} \quad (3.7)$$

and are plotted in figure 3.3.

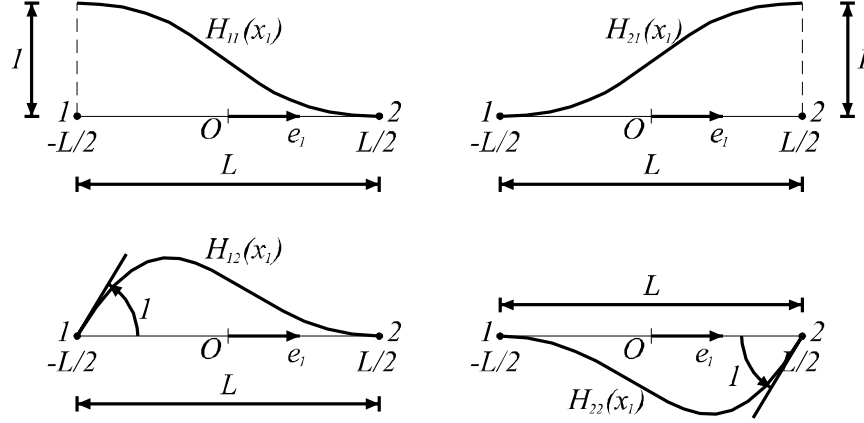


Figure 3.3: Cubic shape functions

The rotation  $\theta_1(x_1)$  about the axis  $e_1$  is evaluated as a function of the nodal rotations  $\theta_{11}$  and  $\theta_{21}$ :

$$\theta_1(x_1) = N_1(x_1)\theta_{11} + N_2(x_1)\theta_{21} \quad (3.8)$$

while the two rotations  $\theta_2(x_1)$  and  $\theta_3(x_1)$  are evaluated by differentiating  $w_3(x_1)$  and  $w_2(x_1)$  respectively:

$$\theta_2(x_1) = -w_3'(x_1); \quad \theta_3(x_1) = w_2'(x_1) \quad (3.9)$$

Derivatives of  $w_1(x_1)$ ,  $\theta_1(x_1)$ ,  $\theta_2(x_1)$  and  $\theta_3(x_1)$  furnish the axial strain  $\epsilon$ , the twist  $\psi$  and the two components of curvature  $\kappa_2$  and  $\kappa_3$ , respectively. They are collected in the following strain vector:

$$\boldsymbol{\varepsilon}^T = \{\epsilon, \kappa_2, \kappa_3, \psi\} \quad (3.10)$$

The axial strain  $\epsilon$  and the twist  $\psi$  are, thus, determined as follows:

$$\epsilon = N_1'(x_1)w_{11} + N_2'(x_1)w_{21}; \quad \psi = N_1'(x_1)\theta_{11} + N_2'(x_1)\theta_{21} \quad (3.11)$$

where  $N_1'(x_1)$  and  $N_2'(x_1)$  are the derivatives of the linear shape functions  $N_1(x_1)$  and  $N_2(x_1)$ :

$$N_1'(x_1) = -\frac{1}{L}; \quad N_2'(x_1) = \frac{1}{L} \quad (3.12)$$

Conversely the two components of curvature  $\kappa_2$  and  $\kappa_3$  are determined by means of the second order derivatives of the cubic Hermitian interpolation functions:

$$\begin{aligned}\kappa_2 &= -H''_{11}(x_1)w_{31} + H''_{12}(x_1)\theta_{21} - H''_{21}(x_1)w_{32} + H''_{22}(x_1)\theta_{22} \\ \kappa_3 &= H''_{11}(x_1)w_{21} + H''_{12}(x_1)\theta_{31} + H''_{21}(x_1)w_{22} + H''_{22}(x_1)\theta_{32}\end{aligned}\quad (3.13)$$

with:

$$\begin{aligned}H''_{11}(x_1) &= \frac{12}{L^3}x_1; & H''_{12}(x_1) &= \frac{6x_1 - L}{L^2}; \\ H''_{21}(x_1) &= -\frac{12}{L^3}x_1; & H''_{22}(x_1) &= \frac{6x_1 + L}{L^2}\end{aligned}\quad (3.14)$$

The strain operator  $\mathbf{B}$  of the element is thus defined in such a way that:

$$\boldsymbol{\varepsilon} = \mathbf{B}\mathbf{d} = \sum_{n=1}^2 \mathbf{B}_n \mathbf{d}_n \quad (3.15)$$

Making use of equations (3.11) and (3.13) into (3.15) one gets:

$$\begin{Bmatrix} \epsilon \\ \kappa_2 \\ \kappa_3 \\ \psi \end{Bmatrix} = \sum_{n=1}^2 \begin{bmatrix} N'_n & 0 & 0 & 0 & 0 & 0 \\ 0 & 0 & -H''_{n1} & 0 & H''_{n2} & 0 \\ 0 & H''_{n1} & 0 & 0 & 0 & H''_{n2} \\ 0 & 0 & 0 & N'_n & 0 & 0 \end{bmatrix} \begin{Bmatrix} w_{n1} \\ w_{n2} \\ w_{n3} \\ \theta_{n1} \\ \theta_{n2} \\ \theta_{n3} \end{Bmatrix} \quad (3.16)$$

where dependence of the shape functions upon  $x_1$  has been omitted for simplicity. Thus the strain operator relevant to node 1 is:

$$\mathbf{B}_1 = \begin{bmatrix} -\frac{1}{L} & 0 & 0 & 0 & 0 & 0 \\ 0 & 0 & -\frac{12}{L^3}x_1 & 0 & \frac{6x_1 - L}{L^2} & 0 \\ 0 & \frac{12}{L^3}x_1 & 0 & 0 & 0 & \frac{6x_1 - L}{L^2} \\ 0 & 0 & 0 & -\frac{1}{L} & 0 & 0 \end{bmatrix} \quad (3.17)$$

while the one relevant to node 2 is:

$$\mathbf{B}_2 = \begin{bmatrix} \frac{1}{L} & 0 & 0 & 0 & 0 & 0 \\ 0 & 0 & \frac{12}{L^3}x_1 & 0 & \frac{6x_1 + L}{L^2} & 0 \\ 0 & -\frac{12}{L^3}x_1 & 0 & 0 & 0 & \frac{6x_1 + L}{L^2} \\ 0 & 0 & 0 & \frac{1}{L} & 0 & 0 \end{bmatrix} \quad (3.18)$$

In figure 3.4 the nodal forces of the element are shown. They are collected

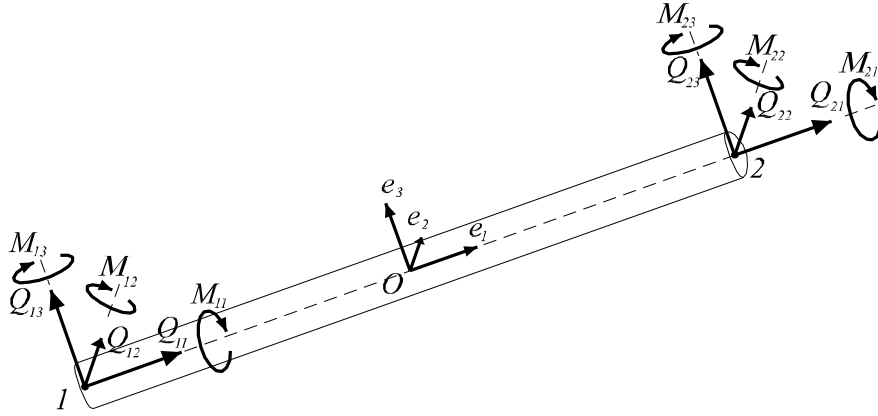


Figure 3.4: Nodal forces of the beam element

in the element force vector  $\mathbf{q}_e$  which is the composition of the vectors relevant to each node of the element:

$$\mathbf{q}^T = [\mathbf{q}_1^T \quad \mathbf{q}_2^T] \quad (3.19)$$

with:

$$\mathbf{q}_n^T = \{Q_{n1}, Q_{n2}, Q_{n3}, M_{n1}, M_{n2}, M_{n3}\} \quad (3.20)$$

where  $Q_{n1}$ ,  $Q_{n2}$  and  $Q_{n3}$  are the nodal forces along the axis of the element reference frame,  $M_{n1}$ ,  $M_{n2}$  and  $M_{n3}$  are the moments about the same axis.

The values of the internal forces are collected in the stress vector:

$$\boldsymbol{\sigma}^T = \{N, M_2, M_3, T\} \quad (3.21)$$

where  $N$  is the axial force,  $M_2$  and  $M_3$  are the bending moments about the axis  $e_2$  and  $e_3$ ,  $T$  is the twisting moment.

The relation between  $\mathbf{q}$  and  $\boldsymbol{\sigma}$  can be obtained by writing the internal virtual work of the whole structure:

$$\begin{aligned} IVW &= \int_V \delta \boldsymbol{\varepsilon}^T \boldsymbol{\sigma} dV = \sum_{e=1}^{n_{elem}} \int_{L_e} \delta \boldsymbol{\varepsilon}^T \boldsymbol{\sigma} dx_1 = \sum_{e=1}^{n_{elem}} \int_{L_e} (\mathbf{B} \delta \mathbf{d})^T \boldsymbol{\sigma} dx_1 = \\ &= \sum_{e=1}^{n_{elem}} \delta \mathbf{d}^T \int_{L_e} \mathbf{B}^T \boldsymbol{\sigma} dx_1 = \sum_{e=1}^{n_{elem}} \delta \mathbf{d}^T \mathbf{q} \end{aligned} \quad (3.22)$$

where use of (3.15) has been made in order to express the virtual strain vector  $\delta \boldsymbol{\varepsilon}$  as a function of the strain operator  $\mathbf{B}$  and the virtual displacement vector  $\delta \mathbf{d}$  of the element  $e$ .

From equation (3.22) we obtain:

$$\mathbf{q} = \int_{L_e} \mathbf{B}^T \boldsymbol{\sigma} dx_1 \quad (3.23)$$

In linear elasticity  $\boldsymbol{\sigma}$  is determined as a function of the strain vector  $\boldsymbol{\varepsilon}$ :

$$\boldsymbol{\sigma} = \mathbf{K}_s \boldsymbol{\varepsilon} = \mathbf{T} \mathbf{B} \mathbf{d} \quad (3.24)$$

where  $\mathbf{K}_s$  is the tangent matrix of the element cross section.

Substitution of (3.24) into (3.23) yields:

$$\mathbf{q} = \mathbf{K} \mathbf{d} \quad (3.25)$$

where the stiffness matrix of the element is:

$$\mathbf{K} = \int_{L_e} \mathbf{B}^T \mathbf{K}_s \mathbf{B} dx_1 \quad (3.26)$$

### 3.1.2 Bending-shear formulation

Hereafter we are going to illustrate an alternative beam finite element formulation which accounts for the effects due to shear strains and shear internal forces along the element.

The nodal displacement vector is the same defined in the previous section. The values of the displacements and rotations along the element axis  $e_1$  are given by means of the linear shape functions  $N_n(x_1)$  defined in equation (3.4) and figure 3.2:

$$w_i(\xi) = \sum_{n=1}^2 N_n(x_1) w_{ni}; \quad \theta_i(x_1) = \sum_{n=1}^2 N_n(x_1) \theta_{ni} \quad (3.27)$$

We also shall remark that there is no need to assume the same shape functions for transverse and extensional displacements or for bending and torsional rotations [47].

The values of the strain field along the element are collected in the following strain vector:

$$\boldsymbol{\varepsilon}^T = \{\epsilon, \gamma_2, \gamma_3, \psi, \kappa_2, \kappa_3\} \quad (3.28)$$

where  $\epsilon$  is the axial strain,  $\gamma_2$  and  $\gamma_3$  are the shear strains along the axis  $e_2$  and  $e_3$ ,  $\psi$  is the twist,  $\kappa_2$  and  $\kappa_3$  are the curvatures about the axis  $e_2$  and  $e_3$ .

The strain vector  $\boldsymbol{\varepsilon}$  is expressed as a function of the element displacement vector  $\boldsymbol{d}$  by means of the strain operator  $\boldsymbol{B}$  of the element:

$$\boldsymbol{\varepsilon} = \boldsymbol{B}\boldsymbol{d} = \sum_{n=1}^2 \boldsymbol{B}_n \boldsymbol{d}_n \quad (3.29)$$

where:

$$\boldsymbol{B} = [\boldsymbol{B}_1 \quad \boldsymbol{B}_2] \quad (3.30)$$

As shown in [47], the strain operator  $\boldsymbol{B}_n$ , relative to the node  $n$ , is the composition of an axial, a shear, a torsional and a bending part.

The axial strain along the element is given by:

$$\epsilon = \sum_{n=1}^2 \boldsymbol{B}_n^a \boldsymbol{d}_n \quad (3.31)$$

where:

$$\boldsymbol{B}_n^a = \begin{bmatrix} N'_n & 0 & 0 & 0 & 0 & 0 \end{bmatrix} \quad (3.32)$$

is the axial part of the strain operator  $\boldsymbol{B}_n$ .

Similarly the evaluation of the shear strains, by means of:

$$\begin{Bmatrix} \gamma_2 \\ \gamma_3 \end{Bmatrix} = \sum_{n=1}^2 \boldsymbol{B}_n^s \boldsymbol{d}_n \quad (3.33)$$

defines the shear part of the strain operator as:

$$\boldsymbol{B}_n^s = \begin{bmatrix} 0 & N'_n & 0 & 0 & 0 & -N_n \\ 0 & 0 & N'_n & 0 & N_n & 0 \end{bmatrix} \quad (3.34)$$

Analogously the twist and the curvatures are evaluated by means of the torsional and the bending parts of the strain operator:

$$\psi = \sum_{n=1}^2 \mathbf{B}_n^t \mathbf{d}_n \quad (3.35)$$

and

$$\begin{Bmatrix} \kappa_2 \\ \kappa_3 \end{Bmatrix} = \sum_{n=1}^2 \mathbf{B}_n^b \mathbf{d}_n \quad (3.36)$$

where

$$\mathbf{B}_n^t = \begin{bmatrix} 0 & 0 & 0 & N'_n & 0 & 0 \end{bmatrix} \quad (3.37)$$

and

$$\mathbf{B}_n^s = \begin{bmatrix} 0 & 0 & 0 & 0 & N'_n & 0 \\ 0 & 0 & 0 & 0 & 0 & N'_n \end{bmatrix} \quad (3.38)$$

Consequently, the strain operator at node  $n$  is:

$$\mathbf{B}_n = \begin{bmatrix} \mathbf{B}_n^a \\ \mathbf{B}_n^s \\ \mathbf{B}_n^t \\ \mathbf{B}_n^b \end{bmatrix} = \begin{bmatrix} N'_n & 0 & 0 & 0 & 0 & 0 \\ 0 & N'_n & 0 & 0 & 0 & -N_n \\ 0 & 0 & N'_n & 0 & N_n & 0 \\ 0 & 0 & 0 & N'_n & 0 & 0 \\ 0 & 0 & 0 & 0 & N'_n & 0 \\ 0 & 0 & 0 & 0 & 0 & N'_n \end{bmatrix} \quad (3.39)$$

which specifies into:

$$\mathbf{B}_1 = \begin{bmatrix} -1/L & 0 & 0 & 0 & 0 & 0 \\ 0 & -1/L & 0 & 0 & 0 & -\frac{L-2x_1}{2L} \\ 0 & 0 & -1/L & 0 & \frac{L-2x_1}{2L} & 0 \\ 0 & 0 & 0 & -1/L & 0 & 0 \\ 0 & 0 & 0 & 0 & -1/L & 0 \\ 0 & 0 & 0 & 0 & 0 & -1/L \end{bmatrix} \quad (3.40)$$

for node 1 and

$$\mathbf{B}_2 = \begin{bmatrix} 1/L & 0 & 0 & 0 & 0 & 0 \\ 0 & 1/L & 0 & 0 & 0 & -\frac{L+2x_1}{2L} \\ 0 & 0 & 1/L & 0 & \frac{L+2x_1}{2L} & 0 \\ 0 & 0 & 0 & 1/L & 0 & 0 \\ 0 & 0 & 0 & 0 & 1/L & 0 \\ 0 & 0 & 0 & 0 & 0 & 1/L \end{bmatrix} \quad (3.41)$$

for node 2.

The nodal force vector is the one defined in the previous section while the stress vector collects the shear forces along the axis  $e_2$  and  $e_3$  too:

$$\boldsymbol{\sigma}^T = \{N, S_2, S_3, T, M_2, M_3\} \quad (3.42)$$

The nodal forces of the element are thus evaluated as a function of the stress vector:

$$\mathbf{q} = \int_{L_e} \mathbf{B}^T \boldsymbol{\sigma} dx_1 \quad (3.43)$$

while the stiffness matrix of the element is evaluated as:

$$\mathbf{K} = \int_{L_e} \mathbf{B}^T \mathbf{K}_s \mathbf{B} dx_1 \quad (3.44)$$

where  $\mathbf{K}_s$  is the tangent matrix of the element cross section. Clearly the tangent matrix  $\mathbf{K}_s$  needs to account for the shear stiffness of the section too.

Adopting the shape functions described above, i.e. linear shape functions for displacements and rotations, such element tends to lock if the shear term is not handled properly. For this reason a reduced integration, in which the quadrature rule is taken to be one order lower than the normal one, is employed. It is possible to show that such reduced-integration element is equivalent to an exactly integrated one in which linear shape functions are used for axial displacements and rotations and quadratic shape functions are used for transverse displacements [47].

### 3.2 A beam finite element with force based formulation

An interesting beam finite element with a force formulation is the one presented in [97] and [91], which is briefly reported hereafter.

Even if it is based on the force method, such beam element is formulated as a mixed method where the displacement shape functions are expressed by means of the interpolation functions for the forces.

The structure is assumed to be solved by means of an iterative procedure, namely the *structure state determination*. At the  $i$ -th step of such procedure the compatibility-equilibrium equations are expressed in terms of increments of the nodal forces  $\Delta \mathbf{q}^i$  and nodal displacements  $\Delta \mathbf{d}^i$ :

$$\begin{bmatrix} -\mathbf{F}^{i-1} & \mathbf{T} \\ \mathbf{T}^T & \mathbf{0} \end{bmatrix} \begin{Bmatrix} \Delta \mathbf{q}^i \\ \Delta \mathbf{d}^i \end{Bmatrix} = \begin{Bmatrix} \mathbf{0} \\ \mathbf{p} - \mathbf{T}^T \mathbf{q}^{i-1} \end{Bmatrix} \quad (3.45)$$

where the superscripts  $i$  and  $i-1$  indicate the step of the iterative procedure at which each quantity is evaluated and  $\mathbf{p}$  is the vector of external loads.

The element flexibility matrix  $\mathbf{F}^{i-1}$ , which is evaluated at the previous iteration, is determined by integrating the section flexibility matrix  $\mathbf{F}_s^{i-1}$  as follows:

$$\mathbf{F}^{i-1} = \int_{L_e} \mathbf{D}^T \mathbf{F}_s^{i-1} \mathbf{D} dx_1 \quad (3.46)$$

where  $\mathbf{D}$  is the stress operator, i.e. the matrix that is used to evaluate the section internal forces  $\boldsymbol{\sigma}$  by interpolating the nodal forces:

$$\boldsymbol{\sigma} = \mathbf{D} \mathbf{q} \quad (3.47)$$

The matrix  $\mathbf{T}$  appearing in equation (3.45) is evaluated as:

$$\mathbf{T} = \int_{L_e} \mathbf{D}^T \mathbf{B} dx_1 \quad (3.48)$$

Some manipulations need now to be done on the two equations of formula (3.45) in order to transform such compatibility and equilibrium equations in a more simple form which makes of this one a force based formulation.

First (3.45)<sub>1</sub> is solved for  $\Delta \mathbf{q}^i$  and then it is substituted in (3.45)<sub>2</sub> yielding:

$$\mathbf{T}^T [\mathbf{F}^{i-1}]^{-1} \mathbf{T} \Delta \mathbf{d}^i = \mathbf{p} - \mathbf{T} \mathbf{q}^{i-1} \quad (3.49)$$

The strain operator is expressed as a function of the stress operator:

$$\mathbf{B} = \mathbf{F}_s^{i-1} \mathbf{D} [\mathbf{F}^{i-1}]^{-1} \quad (3.50)$$

which leads to:

$$\mathbf{T} = \mathbf{I} \quad (3.51)$$

that is the identity matrix. Substituting in (3.49) one gets the system of equation of the classical flexibility method:

$$[\mathbf{F}^{i-1}]^{-1} \Delta \mathbf{d}^i = \mathbf{p} - \mathbf{q}^{i-1} \quad (3.52)$$

In order to fix the ideas, equation (3.52) is the only one used to solve the structural problem, thus it is the starting point for the element formulation described hereafter. As for a displacement based formulation, at each iteration of the *structure state determination* procedure the nodal force vector  $\mathbf{q}$  of the element and the element stiffness matrix  $\mathbf{K}$  need to be computed. The main difference is that, in the flexibility method,  $\mathbf{K}$  is computed by inverting  $\mathbf{F}$ , which is the element flexibility matrix evaluated by assuming an equilibrate internal force distribution along the element.

At the generic iteration  $i$  of the *structure state determination* the element nodal displacements  $\mathbf{d}^i$  are given.

For the beam elements with a stiffness formulation, like the ones described in sections 3.1.1 and 3.1.2, the section deformations  $\boldsymbol{\varepsilon}^i$  need to be evaluated in order to compute the force vector and the stiffness matrix of the element. The values of  $\boldsymbol{\varepsilon}^i$  are directly determined as a function of the nodal displacements by means of the strain operator  $\mathbf{B}$ .

Similarly, in the flexibility method  $\boldsymbol{\varepsilon}^i$  is evaluated by means of the strain operator  $\mathbf{B}$  determined through equation (3.50). Since in formula (3.50), the section and element flexibility matrices are evaluated at the previous iteration, the value of  $\boldsymbol{\varepsilon}^i$  is wrong and, when integrated along the element, will produce a residual in terms of nodal displacements. Consequently, a nested iterative procedure, namely the *element state determination*, needs to be implemented within the *structure state determination*.

Only a subset  $\bar{\mathbf{d}}$  of the nodal displacements  $\mathbf{d}$  defined in equation (3.1) is considered. Actually, both the free body modes of the element and the rotation about the  $\mathbf{e}_1$  axis are kept out, thus:

$$\bar{\mathbf{d}} = \{w, \theta_{12}, \theta_{22}, \theta_{13}, \theta_{23}\} \quad (3.53)$$

Before the *element state determination* is started, the nodal displacements  $\bar{\mathbf{d}}$  need to be computed from  $\mathbf{d}$ , as:

$$\bar{\mathbf{d}} = \mathbf{M} \mathbf{d} \quad (3.54)$$

where  $\mathbf{M}$  is the following transformation matrix:

$$\mathbf{M} = \left[ \begin{array}{cccccc|cccccc} -1 & 0 & 0 & 0 & 0 & 0 & 1 & 0 & 0 & 0 & 0 & 0 \\ 0 & 0 & -1/L_e & 0 & 1 & 0 & 0 & 0 & 1/L_e & 0 & 0 & 0 \\ 0 & 0 & -1/L_e & 0 & 0 & 0 & 0 & 0 & 1/L_e & 0 & 1 & 0 \\ 0 & 1/L_e & 0 & 0 & 0 & 1 & 0 & 1/L_e & 0 & 0 & 0 & 0 \\ 0 & 1/L_e & 0 & 0 & 0 & 0 & 0 & -1/L_e & 0 & 0 & 0 & 1 \end{array} \right] \quad (3.55)$$

Similarly for the nodal force vector, only 5 of the 12 components are considered:

$$\bar{\mathbf{q}} = \{N, M_{12}, M_{22}, M_{13}, M_{23}\} \quad (3.56)$$

Due to such definition, the components of the internal force vector  $\boldsymbol{\sigma}$  are evaluated by means of formula 3.47 where  $\bar{\mathbf{q}}$  is used in place of  $\mathbf{q}$ , and the stress operator  $\mathbf{D}$  is given by:

$$\mathbf{D} = \left[ \begin{array}{ccccc} 1 & 0 & 0 & 0 & 0 \\ 0 & N_1 & N_2 & 0 & 0 \\ 0 & 0 & 0 & N_1 & N_2 \end{array} \right] \quad (3.57)$$

where  $N_1(x_1)$  and  $N_2(x_1)$  are the shape functions defined in equation (3.4).

Such internal forces are used into the *element state determination* procedure to evaluate the element force vector  $\mathbf{q}$  and the element flexibility matrix  $\mathbf{F}$  associated with the given nodal displacements  $\mathbf{d}$ . Since the displacements  $\bar{\mathbf{d}}$  are used in place of  $\mathbf{d}$ , at the end of the *element state determination* procedure, the element force vector  $\mathbf{q}$  and the element stiffness matrix  $\mathbf{K}$ , i.e. the inverse of the element flexibility matrix  $\mathbf{F}$ , need to be evaluated starting from the relevant values determined for  $\bar{\mathbf{d}}$ :

$$\mathbf{q} = \mathbf{M}^T \bar{\mathbf{q}}; \quad \mathbf{K} = \mathbf{M}^T \bar{\mathbf{K}} \mathbf{M} = \mathbf{M}^T \bar{\mathbf{F}}^{-1} \mathbf{M} \quad (3.58)$$

Let us now describe the sequence of operations executed within the *element state determination* procedure.

Once everything is set as described above, the *element state determination* is called at the  $i$ -th step of the *structure state determination*. At the generic  $j$ -th step of the *element state determination* the residual nodal displacements  $\Delta \bar{\mathbf{d}}_{j-1}^i$  are given.

Since this formulation does not mean to violate equilibrium along the element, the value of the internal forces  $\boldsymbol{\sigma}_j^i$  are evaluated by interpolating

the nodal forces  $\mathbf{q}_j^i$  which are obtained from the nodal displacements by means of the flexibility matrix of the element:

$$\bar{\mathbf{q}}_j^i = \bar{\mathbf{q}}_{j-1}^i + [\bar{\mathbf{F}}_{j-1}^i]^{-1} \Delta \bar{\mathbf{d}}_{j-1}^i \quad (3.59)$$

thus

$$\boldsymbol{\sigma}_j^i = \mathbf{D} \bar{\mathbf{q}}_j^i = \boldsymbol{\sigma}_{j-1}^i + \mathbf{D} [\bar{\mathbf{F}}_{j-1}^i]^{-1} \Delta \bar{\mathbf{d}}_{j-1}^i \quad (3.60)$$

The corresponding value of the section deformation vector  $\boldsymbol{\varepsilon}_j^i$  can be obtained from  $\boldsymbol{\sigma}_j^i$  by means of the section flexibility matrix:

$$\boldsymbol{\varepsilon}_j^i = \boldsymbol{\varepsilon}_{j-1}^i + \mathbf{F}_{sj-1}^i \mathbf{D} [\bar{\mathbf{F}}_{j-1}^i]^{-1} \Delta \bar{\mathbf{d}}_{j-1}^i \quad (3.61)$$

where  $\mathbf{F}_{sj-1}^i$  and  $\bar{\mathbf{F}}_{j-1}^i$  are the section and element tangent matrices evaluated at the previous iteration of the *element state determination*. If  $j = 1$ , i.e. the first iteration of the *element state determination* is considered, it is assumed  $\mathbf{F}_{s0}^i = \mathbf{F}_s^{i-1}$  and  $\bar{\mathbf{F}}_0^i = \bar{\mathbf{F}}^{i-1}$ .

It is worth to notice that formula (3.61) can be seen as the evaluation of  $\boldsymbol{\varepsilon}_j^i$  by means of the strain operator defined in equation (3.50).

Once  $\boldsymbol{\varepsilon}_j^i$  is determined, the section resisting forces  $\boldsymbol{\sigma}_{Rj}^i$  and tangent matrix  $\mathbf{K}_{sj}^i$  are evaluated by means of the fiber method, or alternatively by means of the fiber-free approach presented in the present thesis. The section flexibility matrix  $\mathbf{F}_{sj}^i$  is then obtained by inverting  $\mathbf{K}_{sj}^i$ :

$$\mathbf{F}_{sj}^i = [\mathbf{K}_{sj}^i]^{-1} \quad (3.62)$$

In a stiffness formulation, like the ones described in sections 3.1.1 and 3.1.2, such quantities are directly used to evaluate the force vector and tangent matrix of the element.

Conversely, in this flexibility formulation the section unbalance needs to be determined:

$$\Delta \boldsymbol{\sigma}_j^i = \boldsymbol{\sigma}_j^i - \boldsymbol{\sigma}_{Rj}^i \quad (3.63)$$

which the following section deformation residual corresponds to:

$$\Delta \boldsymbol{\varepsilon}_j^i = \mathbf{F}_{sj}^i [\boldsymbol{\sigma}_j^i - \boldsymbol{\sigma}_{Rj}^i] \quad (3.64)$$

Integrating the previous quantity along the element the new value of the nodal displacement is evaluated:

$$\Delta \bar{\mathbf{d}}_j^i = \int_{L_e} \mathbf{D}^T \Delta \boldsymbol{\varepsilon}_j^i dx_1 \quad (3.65)$$

A convergence check is now executed. If it is not satisfied, the iterative index  $j$  is incremented and the whole iterative process is repeated starting from equation (3.59) where the new value of  $\Delta\bar{\mathbf{d}}_j^i$  is used.

Otherwise, if the convergence check is satisfied, the value of element force vector  $\bar{\mathbf{q}}_j^i$  is the one evaluated in formula (3.59), while the element flexibility matrix is evaluated by means of equation (3.46), which specifies to:

$$\bar{\mathbf{F}}_j^i = \int_{L_e} \mathbf{D}^T \mathbf{F}_{s_j}^i \mathbf{D} dx_1 \quad (3.66)$$

It is then inverted in order to evaluate the element stiffness matrix to be used in equation (3.52) so that a new loop of the *structure state determination* procedure can be executed.

As a remark, it is worth to notice that in equation (3.65) the residual in terms of section strains is integrated along the element in order to obtain the residual in terms of nodal displacements. It is similar to formula (3.23) used for evaluating the nodal forces as a function of the section forces and is derived in the same way, by writing the internal virtual work of the structure:

$$\begin{aligned} IVW &= \int_V \boldsymbol{\varepsilon}^T \delta \boldsymbol{\sigma} dV = \sum_{e=1}^{n_{elem}} \int_{L_e} \boldsymbol{\varepsilon}^T \delta \boldsymbol{\sigma} dx_1 = \sum_{e=1}^{n_{elem}} \int_{L_e} \boldsymbol{\varepsilon}^T \mathbf{D} \delta \bar{\mathbf{q}} dx_1 = \\ &= \sum_{e=1}^{n_{elem}} \int_{L_e} \boldsymbol{\varepsilon}^T \mathbf{D} dx_1 \delta \bar{\mathbf{q}} = \sum_{e=1}^{n_{elem}} \bar{\mathbf{d}}^T \delta \bar{\mathbf{q}} \end{aligned} \quad (3.67)$$

where (3.47) is used in order to express the virtual stress vector  $\delta \boldsymbol{\sigma}$  as a function of the stress operator  $\mathbf{D}$  and the virtual force vector  $\delta \bar{\mathbf{q}}$  of the element. Consequently the nodal displacements are evaluated as a function of the section strain components by means of:

$$\bar{\mathbf{d}} = \int_{L_e} \mathbf{D}^T \boldsymbol{\varepsilon} dx_1 \quad (3.68)$$

hence formula (3.65).

In [72] a slight modification to the *element state determination* procedure described above is presented. Such version allows to englobe the *element state determination* into the *structure state determination*, in such a way to avoid a loop of iterations.

Actually, since the section unbalance  $\Delta\boldsymbol{\sigma}_j^i$  is given by equation (3.63) the value of section force vector used in the *element state determination* is assumed to be:

$$\boldsymbol{\sigma}^i = \boldsymbol{\sigma}^{i-1} + \mathbf{D}[\bar{\mathbf{F}}^{i-1}]^{-1} \Delta\bar{\mathbf{d}}^{i-1} - \boldsymbol{\sigma}_R^{i-1} \quad (3.69)$$

in place of the one evaluated by means of equation (3.60). Please notice that the index  $j$  is missing since, with this approach, the *element state determination* is not an iterative procedure.

The section strain components are again determined by means of the section flexibility matrix, but this time the section forces are given from the previous equation, thus:

$$\boldsymbol{\varepsilon}^i = \boldsymbol{\varepsilon}^{i-1} + \mathbf{F}_s^{i-1} \left\{ \mathbf{D}[\bar{\mathbf{F}}^{i-1}]^{-1} \Delta \bar{\mathbf{d}}^{i-1} - \boldsymbol{\sigma}_R^{i-1} \right\} \quad (3.70)$$

Either the fiber method or the fiber free approach are now used for the evaluation of the section resisting forces  $\boldsymbol{\sigma}_{Rj}^i$  and tangent matrix  $\mathbf{K}_s^i$ , which is inverted to obtain the section flexibility matrix  $\mathbf{F}_s^i = [\mathbf{K}_s^i]^{-1}$ .

Such quantities are used for evaluating the section strain residual  $\Delta \boldsymbol{\varepsilon}^i$  and the residual element displacements  $\Delta \bar{\mathbf{d}}^i$ , through equations (3.64) and (3.65), respectively.

Since further iterations for imposing compatibility want to be avoided, compatibility is restored by adding the nodal force residual  $-[\bar{\mathbf{F}}^i]^{-1} \Delta \bar{\mathbf{d}}^i$  to the element resisting forces evaluated by formula (3.59), where the index  $j$  is suppressed:

$$\bar{\mathbf{q}}^i = \bar{\mathbf{q}}^{i-1} + [\bar{\mathbf{F}}^{i-1}]^{-1} \Delta \bar{\mathbf{d}}^{i-1} - [\bar{\mathbf{F}}^i]^{-1} \Delta \bar{\mathbf{d}}^i \quad (3.71)$$

while the element flexibility matrix is still evaluated as:

$$\bar{\mathbf{F}}^i = \int_{L_e} \mathbf{D}^T \mathbf{F}_s^i \mathbf{D} dx_1 \quad (3.72)$$

### 3.3 Tangent matrix and internal forces of the element cross sections

A Cartesian coordinate system with origin  $O$  and axes  $x$  and  $y$  lying on the plane of the cross section is introduced. Axis  $z$  is orthogonal to the plane  $x$ - $y$  and lies along the length of the beam. Each point of the section is defined by its position vector  $\mathbf{r} = (x, y)^T$  while the third coordinate is constant and is omitted for simplicity. One or more polygonal domains defined by means of their vertices ordered counter-clockwise define the geometry of the section in the given reference system.

For what concerns the axial-bending behavior of the section we assume that the beam sections remain plane after deformation. Thus the axial strain of a generic point of the section is evaluated as

$$\varepsilon = \epsilon - \kappa_y x + \kappa_x y \quad (3.73)$$

$\epsilon$  being the strain in  $O$  and  $\boldsymbol{\kappa} = (\kappa_x, \kappa_y)^T$  being the curvature of the section. Such strain parameters are collected in the bending part of the section strain vector  $\boldsymbol{\epsilon}^b = (\epsilon, \kappa_x, \kappa_y)^T$ .

A time dependent parameter  $t$  is introduced and  $\boldsymbol{\epsilon}^{b t_i}$  indicates the bending strain vector that describes the deformation of the section when  $t = t_i$ .

The material associated with each polygonal domain is described by means of an inelastic stress-strain relationship that is supposed to be uniaxial in the direction of the beam axis. The normal stress at  $t = t_i$  on a generic point  $\mathbf{r}$  of the section is expressed as a function of its current strain  $\epsilon^{t_i}$  and of the maximum strain  $\epsilon_m^{t_i}$  ever reached at  $\mathbf{r}$  for  $t \leq t_i$ . Such assumption is common to most of the stress-strain relations for concrete [50, 61] and can be expressed symbolically as:

$$\sigma^{t_i}(\mathbf{r}) = \hat{\sigma}^{t_i}[\epsilon^{t_i}(\mathbf{r}), \epsilon_m^{t_i}(\mathbf{r})] \quad (3.74)$$

From now on, the dependence of the considered quantities upon the time parameter  $t_i$  is understood and the apex  $t_i$  will be canceled for simplicity. Consequently the previous equation can be rewritten as:

$$\sigma(\mathbf{r}) = \hat{\sigma}[\epsilon(\mathbf{r}), \epsilon_m(\mathbf{r})] \quad (3.75)$$

The resultants of such stress field on the section are the axial force

$$N = \int_{\Omega} \sigma(\mathbf{r}) d\Omega \quad (3.76)$$

and the two components of the bending moment, collected in the vector

$$\mathbf{M} = (M_x, M_y)^T = \int_{\Omega} \sigma(\mathbf{r}) \boldsymbol{\rho} d\Omega \quad (3.77)$$

where  $\boldsymbol{\rho} = (y, -x)^T$ . Such stress resultants are collected in the bending part of the section force vector  $\boldsymbol{\sigma}^b = (N, M_x, M_y)^T$ . The derivative of the bending force vector with respect to the current bending strain vector is

$$\mathbf{K}_s^b = \frac{\partial \boldsymbol{\sigma}^b}{\partial \boldsymbol{\epsilon}^b} = \begin{bmatrix} \frac{\partial N}{\partial \epsilon} & \frac{\partial N}{\partial \kappa_x} & \frac{\partial N}{\partial \kappa_y} \\ \frac{\partial M_x}{\partial \epsilon} & \frac{\partial M_x}{\partial \kappa_x} & \frac{\partial M_x}{\partial \kappa_y} \\ \frac{\partial M_y}{\partial \epsilon} & \frac{\partial M_y}{\partial \kappa_x} & \frac{\partial M_y}{\partial \kappa_y} \end{bmatrix} \quad (3.78)$$

that is the bending part of the tangent matrix of the section.

Also twisting and shear effects shall be determined in order to evaluate the full force vector and the full tangent matrix of the cross section

of the element. To this end we make the assumption that the section behaves elastically when subject to shear forces and twisting moments. Such assumption is clearly rough, but future developments of the fiber-free approach presented in the following chapters will be addressed to find formulas for handling tangential stresses on polygonal section.

Given the values of the twist and shear stiffnesses of the section, the following relation holds:

$$T = K_s^t \psi; \quad \begin{Bmatrix} S_2 \\ S_3 \end{Bmatrix} = \mathbf{K}_s^s \begin{Bmatrix} \gamma_2 \\ \gamma_3 \end{Bmatrix} \quad (3.79)$$

where  $K_s^t$  is the twisting part of tangent matrix of the section while  $\mathbf{K}_s^s$  is the relevant shear part.

Obviously the shear forces and tangent matrix have to be considered only in elements with shear-bending formulation.

### 3.3.1 The fiber method

The fiber method is a very simple method of integration for evaluating the integrals (3.76) and (3.83) and the items of the matrix in equation (3.84) where the bending part of the stiffness matrix of the section is reported.

The cross section is divided in a given number  $n_f$  of sub-sections called fibers. The generic  $i$ -th fiber, of area  $A_i$ , is identified by means of the position of its centroid  $(x_i, y_i)$  as shown in figure 3.5.

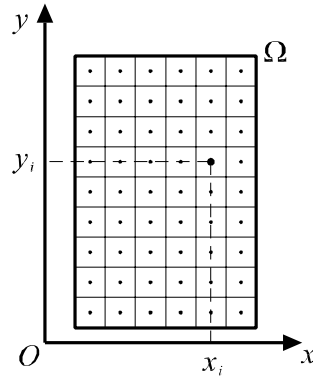


Figure 3.5: Sub-division of the section into fibers

The value of the strain at the centroid of the  $i$ -th fiber is evaluated by means of equation (3.73) as:

$$\varepsilon_i = \epsilon - \kappa_y x_i + \kappa_x y_i \quad (3.80)$$

while the value of the maximum strain  $\varepsilon_{mi}$  ever attained by  $\varepsilon_i$  is updated at each load step.

The constitutive law (3.75) furnishes the value of the stress  $\sigma_i$  and the tangent modulus  $E_i$  of each fiber as:

$$\sigma_i = \hat{\sigma}[\varepsilon_i, \varepsilon_{mi}]; \quad E_i = \left. \frac{\partial \hat{\sigma}[\varepsilon, \varepsilon_{mi}]}{\partial \varepsilon} \right|_{\varepsilon_i} \quad (3.81)$$

The integrals of equations (3.76) and (3.83) are evaluated as:

$$N = \int_{\Omega} \sigma(\mathbf{r}) d\Omega = \sum_{i=1}^{n_f} \sigma_i A_i \quad (3.82)$$

and the two components of the bending moment, collected in the vector

$$\mathbf{M} = \begin{pmatrix} M_x \\ M_y \end{pmatrix} = \int_{\Omega} \sigma(\mathbf{r}) \boldsymbol{\rho} d\Omega = \sum_{i=1}^{n_f} \sigma_i \begin{pmatrix} y_i \\ -x_i \end{pmatrix} A_i \quad (3.83)$$

Finally the stiffness matrix of the section is evaluated as:

$$\mathbf{K}_s^b = \begin{bmatrix} \sum_{i=1}^{n_f} E_i A_i & \sum_{i=1}^{n_f} E_i A_i y_i & -\sum_{i=1}^{n_f} E_i A_i x_i \\ \sum_{i=1}^{n_f} E_i A_i y_i & \sum_{i=1}^{n_f} E_i A_i y_i y_i & -\sum_{i=1}^{n_f} E_i A_i y_i x_i \\ -\sum_{i=1}^{n_f} E_i A_i x_i & -\sum_{i=1}^{n_f} E_i A_i x_i y_i & \sum_{i=1}^{n_f} E_i A_i x_i x_i \end{bmatrix} \quad (3.84)$$

As a remark, it is worth to notice that, even if this method seems to be easy to implement, it requires a procedure for evaluating the position  $(x_i, y_i)$  of the fibers. This task is very simple for rectangular sections or sections that are composition of rectangles, but a meshing procedure is required for sections of generic shape.

Also, for each fiber, its position  $(x_i, y_i)$ , its area  $A_i$  and at least one history variable  $\varepsilon_{mi}$  need to be stored. Consequently, for the application of this method, at least  $4 \times n_f$  values need to be recorded in the computer memory. As shown in the sequel, since the results obtained by means of the fiber method are quite approximate, a very large number of fibers  $n_f$  is required in order to reduce the approximations. As a consequence computer memory exhaustion might occur and/or computational time might be a problem.

### 3.3.2 Gradient of the section strain field

To the end of having a more efficient symbology we introduce the gradient  $\mathbf{g} = (g_x, g_y)^T = (-\kappa_y, \kappa_x)^T$  of the section strain. Accordingly the strain in a generic point of the section is given by:

$$\varepsilon = \epsilon + g_x x + g_y y = \epsilon + \mathbf{g} \cdot \mathbf{r} \quad (3.85)$$

The vector collecting such strain parameters is  $\mathbf{u} = (\varepsilon_o, g_x, g_y)^T$ .

Such symbology allow us to re-write the bending moment in the form:

$$[\mathbf{M}]^\perp = (-M_y, M_x)^T = \int_{\Omega} \sigma(\mathbf{r}) \mathbf{r} d\Omega \quad (3.86)$$

Accordingly the components of the resultant force vector are collected in a new vector  $\mathbf{v} = (N, -M_y, M_x)^T$ . Its derivative with respect to the strain parameters is:

$$\mathbf{Z} = \frac{\partial \mathbf{v}}{\partial \mathbf{u}} = \begin{bmatrix} \frac{\partial N}{\partial \epsilon} & \frac{\partial N}{\partial g_x} & \frac{\partial N}{\partial g_y} \\ -\frac{\partial M_y}{\partial \epsilon} & -\frac{\partial M_y}{\partial g_x} & -\frac{\partial M_y}{\partial g_y} \\ \frac{\partial M_x}{\partial \epsilon} & \frac{\partial M_x}{\partial g_x} & \frac{\partial M_x}{\partial g_y} \end{bmatrix} \quad (3.87)$$

Recalling that  $(g_x, g_y)^T = (-\kappa_y, \kappa_x)^T$  the following relation holds:

$$\mathbf{K}_s^b = \begin{bmatrix} K_{s11}^b & K_{s12}^b & K_{s13}^b \\ K_{s21}^b & K_{s22}^b & K_{s23}^b \\ K_{s31}^b & K_{s32}^b & K_{s33}^b \end{bmatrix} = \begin{bmatrix} Z_{11} & Z_{13} & -Z_{12} \\ Z_{31} & Z_{33} & -Z_{32} \\ -Z_{21} & -Z_{23} & Z_{22} \end{bmatrix} \quad (3.88)$$

between  $\mathbf{Z}$  and the bending part of the tangent matrix  $\mathbf{K}_s^b$  of the section

## Chapter 4

# Integration formulas for polygonal sections

### 4.1 Integration formulas for $f^{(k)}(\varepsilon)$

Let us consider a polygonal domain  $\Omega$  defined by means of the vertices  $\mathbf{r}_i = (x_i, y_i)$  of its boundary in a Cartesian reference system  $(x, y)$  with center in  $O$ .

Let  $\varepsilon(\mathbf{r})$  be a linear function of  $\mathbf{r}$  defined on  $\Omega$ :

$$\varepsilon(\mathbf{r}) = \epsilon + \mathbf{g} \cdot \mathbf{r} \quad (4.1)$$

where  $\epsilon$  is the value of  $\varepsilon(\mathbf{r})$  in  $O$  and  $\mathbf{g}$  is the relevant gradient.

Let  $f(\varepsilon)$  be a scalar function of  $\varepsilon$  and  $f^{(k)}(\varepsilon)$  be its primitive of order  $k$ , such that  $f^{(0)}(\varepsilon) = \partial f^{(k)} / \partial \varepsilon^k$ . The identity  $f^{(0)}(\varepsilon) = f(\varepsilon)$  clearly holds.

In the sequel we are going to evaluate the integrals:

$$N[f^{(k)}(\varepsilon)] = \int_{\Omega} f^{(k)}(\varepsilon) d\Omega \quad (4.2)$$

$$\mathbf{m}^{\perp}[f^{(k)}(\varepsilon)] = \int_{\Omega} f^{(k)}(\varepsilon) \mathbf{r} d\Omega \quad (4.3)$$

and

$$\mathbf{B}[f^{(k)}(\varepsilon)] = \int_{\Omega} f^{(k)}(\varepsilon) \mathbf{r} \otimes \mathbf{r} d\Omega \quad (4.4)$$

by means of the value that suitable functions of  $f^{(k)}(\varepsilon)$  attain at the vertices of  $\Omega$ .

#### 4.1.1 The case $\mathbf{g} = 0$

If  $\mathbf{g} = \mathbf{0}$  then  $\varepsilon(\mathbf{r}) = \epsilon$  is constant on  $\Omega$  as well as  $f^{(k)}(\varepsilon) = f^{(k)}(\epsilon)$ . The integrals (4.2), (4.3) and (4.4) are thus evaluated as:

$$N[f^{(k)}(\varepsilon)] = \int_{\Omega} f^{(k)}(\varepsilon) d\Omega = f^{(k)}(\epsilon) \int_{\Omega} d\Omega = f^{(k)}(\epsilon) \frac{1}{2} \sum_{i=1}^n \mathbf{r}_i \cdot \mathbf{r}_{i+1}^{\perp} \quad (4.5)$$

$$\begin{aligned} \mathbf{m}^{\perp}[f^{(k)}(\varepsilon)] &= \int_{\Omega} f^{(k)}(\varepsilon) \mathbf{r} d\Omega = f^{(k)}(\epsilon) \int_{\Omega} \mathbf{r} d\Omega \\ &= f^{(k)}(\epsilon) \frac{1}{6} \sum_{i=1}^n \mathbf{r}_i \cdot \mathbf{r}_{i+1}^{\perp} (\mathbf{r}_i + \mathbf{r}_{i+1}) \end{aligned} \quad (4.6)$$

and

$$\begin{aligned} \mathbf{B}[f^{(k)}(\varepsilon)] &= \int_{\Omega} f^{(k)}(\varepsilon) (\mathbf{r} \otimes \mathbf{r}) d\Omega = f^{(k)}(\epsilon) \int_{\Omega} (\mathbf{r} \otimes \mathbf{r}) d\Omega \\ &= f^{(k)}(\epsilon) \frac{1}{12} \sum_{i=1}^n \mathbf{r}_i \cdot \mathbf{r}_{i+1}^{\perp} \left[ \mathbf{r}_i \otimes \mathbf{r}_i + \mathbf{r}_{i+1} \otimes \mathbf{r}_{i+1} \right. \\ &\quad \left. + \frac{1}{2} (\mathbf{r}_i \otimes \mathbf{r}_{i+1} + \mathbf{r}_{i+1} \otimes \mathbf{r}_i) \right] \end{aligned} \quad (4.7)$$

Such formulas are similar to the ones adopted in the case of linear elastic stress-strain relations, where the behavior of a point of the section subject to normal stress is a function of the Young modulus  $E$  of the material, and  $f^{(k)}(\varepsilon) = E\varepsilon$ .

#### 4.1.2 Some useful formulas

In a more general case  $\mathbf{g} \neq \mathbf{0}$ , the integrals (4.2), (4.3) and (4.4) are not of easy evaluation. In order to transform such area integrals into line integrals we will adopt the divergence theorem which states as follows:

**Theorem 4.1.1** *Let  $\mathbf{v}$  be a vectorial field with components of class  $C^{(1)}$  in the regular domain  $\Omega$ . The following relation holds:*

$$\int_{\Omega} \operatorname{div}(\mathbf{v}) d\Omega = \int_{\partial\Omega} \mathbf{v} \cdot \mathbf{n} ds \quad (4.8)$$

where  $\partial\Omega$  is the boundary of  $\Omega$  and  $\mathbf{n}$  is the unit vector orthogonal to  $\partial\Omega$  and directed outwards.

In order to adopt such theorem we need to express the quantities  $f^{(k)}(\varepsilon)$ ,  $f^{(k)}(\varepsilon)\mathbf{r}$  and  $f^{(k)}(\varepsilon)\mathbf{r} \otimes \mathbf{r}$  as divergence functions. This task is addressed hereafter.

If  $\mathbf{g} \neq \mathbf{0}$  we define:

$$\hat{\mathbf{g}} = \frac{\mathbf{g}}{\mathbf{g} \cdot \mathbf{g}} = \left\{ \frac{g_x}{g_x^2 + g_y^2}, \frac{g_y}{g_x^2 + g_y^2} \right\}^T = \{\hat{g}_x, \hat{g}_y\}^T \quad (4.9)$$

Since both components of  $\hat{\mathbf{g}}$  do not depend upon  $x$  and  $y$ , the following divergence is evaluated:

$$\begin{aligned} \operatorname{div} [f^{(k+1)}(\varepsilon)\hat{\mathbf{g}}] &= \frac{\partial(f^{(k+1)}(\varepsilon))}{\partial x} \hat{g}_x + \frac{\partial(f^{(k+1)}(\varepsilon))}{\partial y} \hat{g}_y = \\ &= \frac{\partial(f^{(k+1)}(\varepsilon))}{\partial \varepsilon} \frac{\partial \varepsilon}{\partial x} \hat{g}_x + \frac{\partial(f^{(k+1)}(\varepsilon))}{\partial \varepsilon} \frac{\partial \varepsilon}{\partial y} \hat{g}_y \end{aligned} \quad (4.10)$$

Reminding that:

$$\frac{\partial(f^{(k+1)}(\varepsilon))}{\partial \varepsilon} = f^{(k)}(\varepsilon) \quad (4.11)$$

and that  $\varepsilon$  is a function of  $\mathbf{r}$  by means of equation (4.1) we have:

$$\frac{\partial \varepsilon}{\partial x} = g_x; \quad \frac{\partial \varepsilon}{\partial y} = g_y \quad (4.12)$$

Substitution of (4.9), (4.11) and (4.12) into (4.10) yields:

$$\begin{aligned} \operatorname{div} [f^{(k+1)}(\varepsilon)\hat{\mathbf{g}}] &= f^{(k)}(\varepsilon)(\hat{g}_x g_x + \hat{g}_y g_y) = \\ &= f^{(k)}(\varepsilon) \left( \frac{g_x}{g_x^2 + g_y^2} g_x + \frac{g_y}{g_x^2 + g_y^2} g_y \right) = f^{(k)}(\varepsilon) \frac{g_x^2 + g_y^2}{g_x^2 + g_y^2} \end{aligned} \quad (4.13)$$

thus the following relation holds:

$$f^{(k)}(\varepsilon) = \operatorname{div} [f^{(k+1)}(\varepsilon)\hat{\mathbf{g}}] \quad (4.14)$$

Let us, now, consider the following identity:

$$\mathbf{r} f^{(k)}(\varepsilon) = \mathbf{r} \operatorname{div} [f^{(k+1)}(\varepsilon)\hat{\mathbf{g}}] = \operatorname{div} [f^{(k+1)}(\varepsilon)\mathbf{r} \otimes \hat{\mathbf{g}}] - f^{(k+1)}(\varepsilon)\hat{\mathbf{g}} \quad (4.15)$$

Applying formula (4.14) to the last term we get

$$\mathbf{r} f^{(k)}(\varepsilon) = \operatorname{div} [f^{(k+1)}(\varepsilon)\mathbf{r} \otimes \hat{\mathbf{g}}] - \operatorname{div} [f^{(k+2)}(\varepsilon)\hat{\mathbf{g}} \otimes \hat{\mathbf{g}}] \quad (4.16)$$

Finally, it is straightforward to prove that the following relation holds:

$$\begin{aligned} (\mathbf{r} \otimes \mathbf{r})f^{(k)}(\varepsilon) &= (\mathbf{r} \otimes \mathbf{r})\operatorname{div}(f^{(k+1)}(\varepsilon)\hat{\mathbf{g}}) = \\ &= \operatorname{div}(f^{(k+1)}(\varepsilon)\mathbf{r} \otimes \mathbf{r} \otimes \hat{\mathbf{g}}) - [f^{(k+1)}(\varepsilon)\mathbf{r}] \otimes \hat{\mathbf{g}} - \hat{\mathbf{g}} \otimes [f^{(k+1)}(\varepsilon)\mathbf{r}] \end{aligned} \quad (4.17)$$

Equation (4.16) can be applied to the last two terms of the previous equation as:

$$\begin{aligned} [f^{(k+1)}(\varepsilon)\mathbf{r}] \otimes \hat{\mathbf{g}} + \hat{\mathbf{g}} \otimes [f^{(k+1)}(\varepsilon)\mathbf{r}] &= \operatorname{div}[f^{(k+2)}(\varepsilon)\mathbf{r} \otimes \hat{\mathbf{g}}] \otimes \hat{\mathbf{g}} + \\ &- \operatorname{div}[f^{(k+3)}(\varepsilon)\hat{\mathbf{g}} \otimes \hat{\mathbf{g}}] \otimes \hat{\mathbf{g}} + \hat{\mathbf{g}} \otimes \operatorname{div}[f^{(k+2)}(\varepsilon)\mathbf{r} \otimes \hat{\mathbf{g}}] + \\ &- \hat{\mathbf{g}} \otimes \operatorname{div}[f^{(k+3)}(\varepsilon)\hat{\mathbf{g}} \otimes \hat{\mathbf{g}}] \end{aligned} \quad (4.18)$$

thus:

$$\begin{aligned} (\mathbf{r} \otimes \mathbf{r})f^{(k)}(\varepsilon) &= \operatorname{div}[f^{(k+1)}(\varepsilon)\mathbf{r} \otimes \mathbf{r} \otimes \hat{\mathbf{g}}] + \\ &- \operatorname{div}[f^{(k+2)}(\varepsilon)\mathbf{r} \otimes \hat{\mathbf{g}}] \otimes \hat{\mathbf{g}} + \operatorname{div}[f^{(k+3)}(\varepsilon)\hat{\mathbf{g}} \otimes \hat{\mathbf{g}}] \otimes \hat{\mathbf{g}} + \\ &- \hat{\mathbf{g}} \otimes \operatorname{div}[f^{(k+2)}(\varepsilon)\mathbf{r} \otimes \hat{\mathbf{g}}] + \hat{\mathbf{g}} \otimes \operatorname{div}[f^{(k+3)}(\varepsilon)\hat{\mathbf{g}} \otimes \hat{\mathbf{g}}] \end{aligned} \quad (4.19)$$

### 4.1.3 Evaluation of the integral $N[f^{(k)}(\varepsilon)]$

Making use of (4.14) and the divergence theorem we get:

$$N[f^{(k)}(\varepsilon)] = \int_{\Omega} f^{(k)}(\varepsilon)d\Omega = \int_{\partial\Omega} f^{(k+1)}(\varepsilon)(\hat{\mathbf{g}} \cdot \mathbf{n})ds \quad (4.20)$$

where the area integrals, extended to the domain  $\Omega$  has been transformed in line integrals extended to the boundary of  $\Omega$ , namely  $\partial\Omega$ . If  $\partial\Omega$  is a polygon with  $n$  vertices, its  $i$ -th side is described by means of the following parametric expression:

$$\mathbf{r}(s_i) = \mathbf{r}_i + \frac{s_i}{l_i}(\mathbf{r}_{i+1} - \mathbf{r}_i) \quad (l_i = |\mathbf{r}_{i+1} - \mathbf{r}_i|; \quad 0 \leq s_i \leq l_i) \quad (4.21)$$

Assuming  $\varepsilon_{i+1} \neq \varepsilon_i$  the linearity of  $\varepsilon_i(\mathbf{r})$  yields the following relation:

$$\frac{s_i}{l_i} = \frac{\varepsilon - \varepsilon_i}{\varepsilon_{i+1} - \varepsilon_i}; \quad \varepsilon \in [\varepsilon_i, \varepsilon_{i+1}] \quad (4.22)$$

so that equation (4.21) can be re-written as:

$$\mathbf{r}(\varepsilon) = \mathbf{r}_i + \frac{\varepsilon - \varepsilon_i}{\varepsilon_{i+1} - \varepsilon_i}(\mathbf{r}_{i+1} - \mathbf{r}_i) \quad (4.23)$$

By adopting equation (4.22) and (4.23), a suitable change of variable in the integral appearing on the right hand side of equation (4.20) provides:

$$\begin{aligned} \int_{\partial\Omega} f^{(k+1)}(\varepsilon)(\hat{\mathbf{g}} \cdot \mathbf{n}) ds &= \sum_{i=1}^n \int_0^{l_i} f^{(k+1)}(\varepsilon)(\hat{\mathbf{g}} \cdot \mathbf{n}_i) ds_i \\ &= \sum_{i=1}^n \int_{\varepsilon_i}^{\varepsilon_{i+1}} f^{(k+1)}(\varepsilon)(\hat{\mathbf{g}} \cdot \mathbf{n}_i) \frac{\partial s_i}{\partial \varepsilon} d\varepsilon = \sum_{i=1}^n l_i(\hat{\mathbf{g}} \cdot \mathbf{n}_i) \int_{\varepsilon_i}^{\varepsilon_{i+1}} \frac{f^{(k+1)}(\varepsilon)}{\varepsilon_{i+1} - \varepsilon_i} d\varepsilon \end{aligned} \quad (4.24)$$

where:

$$\frac{\partial s_i}{\partial \varepsilon} = \frac{l_i}{\varepsilon_{i+1} - \varepsilon_i} \quad (4.25)$$

has been obtained by differentiating equation (4.22) and  $\mathbf{n}_i$  is the unit vector orthogonal to the  $i$ -th side of  $\Omega$  and directed outwards:

$$\mathbf{n}_i = \frac{1}{l_i}(\mathbf{r}_{i+1}^\perp - \mathbf{r}_i^\perp) = \frac{1}{l_i} \begin{pmatrix} -(y_{i+1} - y_i) \\ x_{i+1} - x_i \end{pmatrix} \quad (4.26)$$

In order to simplify the symbology in (4.24) the following function is defined:

$$\Phi_i^j[f^{(k)}(\varepsilon)] = \int_{\varepsilon_i}^{\varepsilon_{i+1}} \frac{f^{(k)}(\varepsilon)(\varepsilon - \varepsilon_i)^j}{(\varepsilon_{i+1} - \varepsilon_i)^{j+1}} d\varepsilon \quad (4.27)$$

so that the integral in (4.24) becomes:

$$\Phi_i^0[f^{(k)}(\varepsilon)] = \int_{\varepsilon_i}^{\varepsilon_{i+1}} \frac{f^{(k)}(\varepsilon)}{\varepsilon_i - \varepsilon_{i+1}} d\varepsilon = \frac{[f^{(k+1)}(\varepsilon)]_{\varepsilon_i}^{\varepsilon_{i+1}}}{\varepsilon_{i+1} - \varepsilon_i} \quad (4.28)$$

if  $j = 0$ .

Since  $\Phi_i^0[f^{(k)}(\varepsilon)]$  is not defined if  $\varepsilon_{i+1} = \varepsilon_i$ , we get:

$$\lim_{\varepsilon_{i+1} \rightarrow \varepsilon_i} \Phi_i^0[f^{(k)}(\varepsilon)] = f^{(k)}(\varepsilon_{i+1}) \quad (4.29)$$

by means of L'Hopital's rule.

Thus we can extend the definition of  $\Phi_i^0[f^{(k)}(\varepsilon)]$  to the cases in which  $\varepsilon_{i+1} = \varepsilon_i$  as:

$$\Phi_i^0[f^{(k)}(\varepsilon)] = \begin{cases} \frac{[f^{(k+1)}(\varepsilon)]_{\varepsilon_i}^{\varepsilon_{i+1}}}{\varepsilon_{i+1} - \varepsilon_i} & \text{if } \varepsilon_{i+1} \neq \varepsilon_i \\ f^{(k)}(\varepsilon_{i+1}) & \text{if } \varepsilon_{i+1} = \varepsilon_i \end{cases} \quad (4.30)$$

Substituting in (4.24) we get:

$$\int_{\partial\Omega} f^{(k+1)}(\varepsilon)(\hat{\mathbf{g}} \cdot \mathbf{n})ds = \sum_{i=1}^n l_i(\hat{\mathbf{g}} \cdot \mathbf{n}_i)\Phi_i^0[f^{(k+1)}(\varepsilon)] \quad (4.31)$$

Adopting equation (4.31) in (4.20) we get:

$$N[f^{(k)}(\varepsilon)] = \sum_{i=1}^n l_i \mathbf{n}_i \cdot \hat{\mathbf{g}} \Phi_i^0[f^{(k+1)}(\varepsilon)] \quad (4.32)$$

#### 4.1.4 Evaluation of the integral $\mathbf{m}^\perp[f^{(k)}(\varepsilon)]$

If  $f^{(k)}(\varepsilon)$  is a continuous function, and making use of (4.16), the divergence theorem can be applied to (4.3) yielding:

$$\begin{aligned} \mathbf{m}^\perp[f^{(k)}(\varepsilon)] &= \int_{\Omega} f^{(k)}(\varepsilon) \mathbf{r} d\Omega = \\ &= \int_{\partial\Omega} (f^{(k+1)}(\varepsilon) \mathbf{r}) (\hat{\mathbf{g}} \cdot \mathbf{n}) ds - \left( \int_{\partial\Omega} f^{(k+2)}(\varepsilon) (\hat{\mathbf{g}} \cdot \mathbf{n}) ds \right) \hat{\mathbf{g}} \end{aligned} \quad (4.33)$$

The second term in the previous formula has been evaluated in equation (4.30). For the evaluation of the other integral we can adopt the same change of variable made in (4.24). In this case it specifies in:

$$\begin{aligned} \int_{\partial\Omega} f^{(k+1)}(\varepsilon)(\hat{\mathbf{g}} \cdot \mathbf{n}) \mathbf{r} ds &= \sum_{i=1}^n \int_0^{l_i} f^{(k+1)}(\varepsilon)(\hat{\mathbf{g}} \cdot \mathbf{n}_i) \mathbf{r}(s_i) ds_i = \\ &= \sum_{i=1}^n \int_{\varepsilon_i}^{\varepsilon_{i+1}} f^{(k+1)}(\varepsilon)(\hat{\mathbf{g}} \cdot \mathbf{n}_i) \left( \mathbf{r}_i + \frac{\varepsilon - \varepsilon_i}{\varepsilon_{i+1} - \varepsilon_i} (\mathbf{r}_{i+1} - \mathbf{r}_i) \right) \frac{\partial s_i}{\partial \varepsilon} d\varepsilon = \\ &= \sum_{i=1}^n l_i \hat{\mathbf{g}} \cdot \mathbf{n}_i \int_{\varepsilon_i}^{\varepsilon_{i+1}} \frac{f^{(k+1)}(\varepsilon)}{\varepsilon_{i+1} - \varepsilon_i} \mathbf{r}_i + \frac{f^{(k+1)}(\varepsilon)(\varepsilon - \varepsilon_i)}{(\varepsilon_{i+1} - \varepsilon_i)^2} (\mathbf{r}_{i+1} - \mathbf{r}_i) d\varepsilon = \\ &= \sum_{i=1}^n l_i \hat{\mathbf{g}} \cdot \mathbf{n}_i \left[ \left( \int_{\varepsilon_i}^{\varepsilon_{i+1}} \frac{f^{(k+1)}(\varepsilon)}{\varepsilon_{i+1} - \varepsilon_i} d\varepsilon \right) \mathbf{r}_i + \right. \\ &\quad \left. + \left( \int_{\varepsilon_i}^{\varepsilon_{i+1}} \frac{f^{(k+1)}(\varepsilon)(\varepsilon - \varepsilon_i)}{(\varepsilon_{i+1} - \varepsilon_i)^2} d\varepsilon \right) (\mathbf{r}_{i+1} - \mathbf{r}_i) \right] \end{aligned} \quad (4.34)$$

where (4.22), (4.23), (4.25) and (4.26) have been adopted. Adopting the set of functions defined in (4.27) the previous integral yields:

$$\begin{aligned} \int_{\partial\Omega} f^{(k+1)}(\varepsilon)(\hat{\mathbf{g}} \cdot \mathbf{n}) \mathbf{r} ds \\ = \sum_{i=1}^n l_i \hat{\mathbf{g}} \cdot \mathbf{n}_i \left[ \Phi_i^0[f^{(k+1)}(\varepsilon)] \mathbf{r}_i + \Phi_i^1[f^{(k+1)}(\varepsilon)] (\mathbf{r}_{i+1} - \mathbf{r}_i) \right] \end{aligned} \quad (4.35)$$

where  $\Phi_i^0[f^{(k+1)}(\varepsilon)]$  is the same function evaluated in (4.30) and  $\Phi_i^1[f^{(1)}(\varepsilon)]$  is obtained from (4.27) setting  $j = 1$ .

The function (4.27) corresponding to the value  $j = 1$  is:

$$\Phi_i^1[f^{(k)}(\varepsilon)] = \int_{\varepsilon_i}^{\varepsilon_{i+1}} \frac{f^{(k)}(\varepsilon)(\varepsilon - \varepsilon_i)}{(\varepsilon_{i+1} - \varepsilon_i)^2} d\varepsilon \quad (4.36)$$

Integrating by parts it yields:

$$\Phi_i^1[f^{(k)}(\varepsilon)] = \frac{f^{(k+1)}(\varepsilon_{i+1})}{\varepsilon_{i+1} - \varepsilon_i} - \frac{[f^{(k+2)}(\varepsilon)]_{\varepsilon_i}^{\varepsilon_{i+1}}}{(\varepsilon_{i+1} - \varepsilon_i)^2} \quad (4.37)$$

The case  $\varepsilon_{i+1} = \varepsilon_i$  is handled by means of L'Hopital's rule as follows:

$$\lim_{\varepsilon_{i+1} \rightarrow \varepsilon_i} \Phi_i^1[f^{(k)}(\varepsilon)] = \frac{1}{2} f^{(k)}(\varepsilon_{i+1}) \quad (4.38)$$

thus we extend the domain of definition of  $\Phi_i^1[f^{(k)}(\varepsilon)]$  to the cases in which  $\varepsilon_{i+1} = \varepsilon_i$  as follows:

$$\Phi_i^1[f^{(k)}(\varepsilon)] = \begin{cases} \frac{f^{(k+1)}(\varepsilon_{i+1})}{\varepsilon_{i+1} - \varepsilon_i} - \frac{[f^{(k+2)}(\varepsilon)]_{\varepsilon_i}^{\varepsilon_{i+1}}}{(\varepsilon_{i+1} - \varepsilon_i)^2} & \text{if } \varepsilon_{i+1} \neq \varepsilon_i \\ \frac{1}{2} f^{(k)}(\varepsilon_{i+1}) & \text{if } \varepsilon_{i+1} = \varepsilon_i \end{cases} \quad (4.39)$$

Substituting (4.31) and (4.35) in (4.33) we finally get:

$$\begin{aligned} \mathbf{m}^\perp[f^{(k)}(\varepsilon)] &= \sum_{i=1}^n l_i \mathbf{n}_i \cdot \hat{\mathbf{g}} \left[ \Phi_i^0[f^{(k+1)}(\varepsilon)] \mathbf{r}_i \right. \\ &\quad \left. + \Phi_i^1[f^{(k+1)}(\varepsilon)] (\mathbf{r}_{i+1} - \mathbf{r}_i) - \Phi_i^0[f^{(k+2)}(\varepsilon)] \hat{\mathbf{g}} \right] \end{aligned} \quad (4.40)$$

#### 4.1.5 Evaluation of the integral $\mathbf{B}[f^{(k)}(\varepsilon)]$

If  $f^{(k)}(\varepsilon)$  is a continuous function the divergence theorem and formula (4.19) can be used as follows:

$$\begin{aligned} \mathbf{B}[f^{(k)}(\varepsilon)] &= \int_{\Omega} f^{(k)}(\varepsilon) (\mathbf{r} \otimes \mathbf{r}) d\Omega = \int_{\partial\Omega} f^{(k+1)}(\varepsilon) (\mathbf{r} \otimes \mathbf{r}) (\hat{\mathbf{g}} \cdot \mathbf{n}) ds + \\ &\quad - \int_{\partial\Omega} f^{(k+2)}(\varepsilon) (\mathbf{r} \otimes \hat{\mathbf{g}}) (\hat{\mathbf{g}} \cdot \mathbf{n}) ds - \int_{\partial\Omega} f^{(k+2)}(\varepsilon) (\hat{\mathbf{g}} \otimes \mathbf{r}) (\hat{\mathbf{g}} \cdot \mathbf{n}) ds + \\ &\quad + 2 \int_{\partial\Omega} f^{(k+3)}(\varepsilon) (\hat{\mathbf{g}} \otimes \hat{\mathbf{g}}) (\hat{\mathbf{g}} \cdot \mathbf{n}) ds = \\ &= \int_{\partial\Omega} f^{(k+1)}(\varepsilon) (\mathbf{r} \otimes \mathbf{r}) (\hat{\mathbf{g}} \cdot \mathbf{n}) ds - \left[ \int_{\partial\Omega} f^{(k+2)}(\varepsilon) \mathbf{r} (\hat{\mathbf{g}} \cdot \mathbf{n}) ds \right] \otimes \hat{\mathbf{g}} + \\ &\quad - \hat{\mathbf{g}} \otimes \left[ \int_{\partial\Omega} f^{(k+2)}(\varepsilon) \mathbf{r} (\hat{\mathbf{g}} \cdot \mathbf{n}) ds \right] + 2 \left[ \int_{\partial\Omega} f^{(k+3)}(\varepsilon) (\hat{\mathbf{g}} \cdot \mathbf{n}) ds \right] \hat{\mathbf{g}} \otimes \hat{\mathbf{g}} \end{aligned} \quad (4.41)$$

Integrals of the kind of the last three ones in the previous equation are evaluated by means of equations (4.31) and (4.35). The remaining integral will be evaluated in the sequel following the same approach.

If  $\partial\Omega$  is a polygon we can decompose the line integral in the sum of integrals extended to the sides of  $\partial\Omega$  as:

$$\begin{aligned} \int_{\partial\Omega} f^{(k)}(\varepsilon)(\mathbf{r} \otimes \mathbf{r})(\hat{\mathbf{g}} \cdot \mathbf{n}) ds &= \\ &= \sum_{i=1}^n \int_0^{l_i} f^{(k)}(\varepsilon)[\mathbf{r}(s_i) \otimes \mathbf{r}(s_i)](\hat{\mathbf{g}} \cdot \mathbf{n}_i) ds_i \end{aligned} \quad (4.42)$$

By means of a change of variable between  $s_i$  and  $\varepsilon$ , through equation (4.22), the integral extended to the  $i$ -th side of  $\Omega$  is:

$$\begin{aligned} \int_0^{l_i} f^{(k)}(\varepsilon)[\mathbf{r}(s_i) \otimes \mathbf{r}(s_i)](\hat{\mathbf{g}} \cdot \mathbf{n}_i) ds_i &= \\ &= \int_{\varepsilon_i}^{\varepsilon_{i+1}} f^{(k)}(\varepsilon)[\mathbf{r}(\varepsilon) \otimes \mathbf{r}(\varepsilon)](\hat{\mathbf{g}} \cdot \mathbf{n}_i) \frac{\partial s_i}{\partial \varepsilon} d\varepsilon \end{aligned} \quad (4.43)$$

and adopting equations (4.23) and (4.25) it yields:

$$\begin{aligned} \int_0^{l_i} f^{(k)}(\varepsilon)[\mathbf{r}(s_i) \otimes \mathbf{r}(s_i)](\hat{\mathbf{g}} \cdot \mathbf{n}_i) ds_i &= \\ &= \int_{\varepsilon_i}^{\varepsilon_{i+1}} f^{(k)}(\varepsilon) \left[ \left( \mathbf{r}_i + \frac{\varepsilon - \varepsilon_i}{\varepsilon_{i+1} - \varepsilon_i} (\mathbf{r}_{i+1} - \mathbf{r}_i) \right) \right. \\ &\quad \left. \otimes \left( \mathbf{r}_i + \frac{\varepsilon - \varepsilon_i}{\varepsilon_{i+1} - \varepsilon_i} (\mathbf{r}_{i+1} - \mathbf{r}_i) \right) \right] (\hat{\mathbf{g}} \cdot \mathbf{n}_i) \frac{l_i}{\varepsilon_{i+1} - \varepsilon_i} d\varepsilon \end{aligned} \quad (4.44)$$

Finally, adopting the set of formulas defined in equation (4.27) we get:

$$\begin{aligned}
& \int_{\partial\Omega} f^{(k)}(\varepsilon)(\mathbf{r} \otimes \mathbf{r})(\hat{\mathbf{g}} \cdot \mathbf{n}) ds = \\
& = \sum_{i=1}^n l_i \mathbf{n}_i \cdot \hat{\mathbf{g}} \left\{ \int_{\varepsilon_i}^{\varepsilon_{i+1}} \frac{f^{(k)}(\varepsilon)}{\varepsilon_{i+1} - \varepsilon_i} \mathbf{r}_i \otimes \mathbf{r}_i \right. \\
& \quad + \frac{f^{(k)}(\varepsilon)(\varepsilon - \varepsilon_i)}{(\varepsilon_{i+1} - \varepsilon_i)^2} [\mathbf{r}_i \otimes (\mathbf{r}_{i+1} - \mathbf{r}_i) + (\mathbf{r}_{i+1} - \mathbf{r}_i) \otimes \mathbf{r}_i] + \\
& \quad \left. + \frac{f^{(k)}(\varepsilon)(\varepsilon - \varepsilon_i)^2}{(\varepsilon_{i+1} - \varepsilon_i)^3} (\mathbf{r}_{i+1} - \mathbf{r}_i) \otimes (\mathbf{r}_{i+1} - \mathbf{r}_i) d\varepsilon \right\} \quad (4.45) \\
& = \sum_{i=1}^n l_i \mathbf{n}_i \cdot \hat{\mathbf{g}} \left\{ \Phi_i^0[f^{(k)}(\varepsilon)] \mathbf{r}_i \otimes \mathbf{r}_i \right. \\
& \quad + \Phi_i^1[f^{(k)}(\varepsilon)] [\mathbf{r}_i \otimes (\mathbf{r}_{i+1} - \mathbf{r}_i) + (\mathbf{r}_{i+1} - \mathbf{r}_i) \otimes \mathbf{r}_i] + \\
& \quad \left. + \Phi_i^2[f^{(k)}(\varepsilon)] (\mathbf{r}_{i+1} - \mathbf{r}_i) \otimes (\mathbf{r}_{i+1} - \mathbf{r}_i) \right\}
\end{aligned}$$

where  $\Phi_i^0[f^{(k)}(\varepsilon)]$  and  $\Phi_i^1[f^{(k)}(\varepsilon)]$  are given by equations (4.30) and (4.39). The integral  $\Phi_i^2[f^{(k)}(\varepsilon)]$  is defined by means of equation (4.27) where the value  $j = 2$  is set:

$$\Phi_i^2[f^{(k)}(\varepsilon)] = \int_{\varepsilon_i}^{\varepsilon_{i+1}} \frac{f^{(k)}(\varepsilon)(\varepsilon - \varepsilon_i)^2}{(\varepsilon_{i+1} - \varepsilon_i)^3} d\varepsilon \quad (4.46)$$

Integrating twice by parts we get:

$$\Phi_i^2[f^{(k)}(\varepsilon)] = \frac{f^{(k+1)}(\varepsilon_{i+1})}{\varepsilon_{i+1} - \varepsilon_i} - 2 \frac{f^{(k+2)}(\varepsilon_{i+1})}{(\varepsilon_{i+1} - \varepsilon_i)^2} + 2 \frac{[f^{(k+3)}(\varepsilon)]_{\varepsilon_i}^{\varepsilon_{i+1}}}{(\varepsilon_{i+1} - \varepsilon_i)^3} \quad (4.47)$$

Again, the case  $\varepsilon_{i+1} = \varepsilon_i$  is handled evaluating the limit of  $\Phi_i^2[f^{(k)}(\varepsilon)]$  for  $\varepsilon_{i+1} \rightarrow \varepsilon_i$ . Adopting L'Hopital's rule it yields:

$$\begin{aligned}
\lim_{\varepsilon_{i+1} \rightarrow \varepsilon_i} \Phi_i^2[f^{(k)}(\varepsilon)] & = \lim_{\varepsilon_{i+1} \rightarrow \varepsilon_i} \left\{ f^{(k+1)}(\varepsilon_{i+1})(\varepsilon_{i+1} - \varepsilon_i)^2 \right. \\
& \quad \left. - 2f^{(k+2)}(\varepsilon_{i+1})(\varepsilon_{i+1} - \varepsilon_i) + 2 [f^{(k+3)}(\varepsilon)]_{\varepsilon_i}^{\varepsilon_{i+1}} \right\} \frac{1}{(\varepsilon_{i+1} - \varepsilon_i)^3} = (4.48) \\
& = \frac{1}{3} f^{(k)}(\varepsilon_{i+1})
\end{aligned}$$

and  $\Phi_i^2[f^{(k)}(\varepsilon)]$  is extended to the cases in which  $\varepsilon_{i+1} = \varepsilon_i$  as:

$$\Phi_i^2[f^{(k)}(\varepsilon)] = \begin{cases} \frac{f^{(k+1)}(\varepsilon_{i+1})}{\varepsilon_{i+1} - \varepsilon_i} - 2 \frac{f^{(k+2)}(\varepsilon_{i+1})}{(\varepsilon_{i+1} - \varepsilon_i)^2} & \text{if } \varepsilon_{i+1} \neq \varepsilon_i \\ + 2 \frac{[f^{(k+3)}(\varepsilon)]_{\varepsilon_i}^{\varepsilon_{i+1}}}{(\varepsilon_{i+1} - \varepsilon_i)^3} & \\ \frac{1}{3} f^{(k)}(\varepsilon_{i+1}) & \text{if } \varepsilon_{i+1} = \varepsilon_i \end{cases} \quad (4.49)$$

Now all the quantities appearing in (4.45) are known. Thus we can substitute (4.31), (4.35) and (4.45) in (4.41) and get:

$$\begin{aligned} \mathbf{B}[f^{(k)}(\varepsilon)] &= \sum_{i=1}^n (l_i \mathbf{n}_i \cdot \hat{\mathbf{g}}) \left\{ \Phi_i^0[f^{(k+1)}(\varepsilon)](\mathbf{r}_i \otimes \mathbf{r}_i) + \right. \\ &+ \Phi_i^1[f^{(k+1)}(\varepsilon)][\mathbf{r}_i \otimes (\mathbf{r}_{i+1} - \mathbf{r}_i) + (\mathbf{r}_{i+1} - \mathbf{r}_i) \otimes \mathbf{r}_i] + \\ &+ \Phi_i^2[f^{(k+1)}(\varepsilon)][(\mathbf{r}_{i+1} - \mathbf{r}_i) \otimes (\mathbf{r}_{i+1} - \mathbf{r}_i)] + \\ &- \Phi_i^0[f^{(k+2)}(\varepsilon)][\mathbf{r}_i \otimes \hat{\mathbf{g}} + \hat{\mathbf{g}} \otimes \mathbf{r}_i] + \\ &- \Phi_i^1[f^{(k+2)}(\varepsilon)][(\mathbf{r}_{i+1} - \mathbf{r}_i) \otimes \hat{\mathbf{g}} + \hat{\mathbf{g}} \otimes (\mathbf{r}_{i+1} - \mathbf{r}_i)] + \\ &\left. + 2\Phi_i^0[f^{(k+3)}(\varepsilon)](\hat{\mathbf{g}} \otimes \hat{\mathbf{g}}) \right\} \end{aligned} \quad (4.50)$$

## 4.2 Derivatives of $N[f^{(k)}(\varepsilon)]$ , $\mathbf{m}^\perp[f^{(k)}(\varepsilon)]$ and $\mathbf{B}[f^{(k)}(\varepsilon)]$ with respect to $\varepsilon$ and $\mathbf{g}$

The goal of this section is the evaluation of the derivatives of the integrals  $N[f^{(k)}(\varepsilon)]$ ,  $\mathbf{m}^\perp[f^{(k)}(\varepsilon)]$  and  $\mathbf{B}[f^{(k)}(\varepsilon)]$  with respect to the quantities  $\varepsilon$  and  $\mathbf{g}$  appearing in equation (4.1). Such derivatives will be evaluated as function of the values attained by suitable quantities defined at the vertices of  $\Omega$ .

To this end it is worth noting that if the domain  $\Omega$  has vertices  $\mathbf{r}_i$  whose coordinates depend upon  $\varepsilon$  and  $\mathbf{g}$  then the quantities  $\mathbf{r}_{i,\varepsilon}$  and  $\mathbf{r}_{i,\mathbf{g}}$ , i.e. the derivatives of  $\mathbf{r}_i$ , are not null as it is described in section 5.1.

Accordingly the derivatives of the vector  $l_i \mathbf{n}_i$ , that is orthogonal to the  $i$ -th side of  $\Omega$  and directed outward, are obtained multiplying equation (4.26) by  $l_i$  and differentiating with respect to  $\varepsilon$  and  $\mathbf{g}$  as follows:

$$[l_i \mathbf{n}_i]_{,\varepsilon} = \mathbf{r}_{i+1,\varepsilon}^\perp - \mathbf{r}_{i,\varepsilon}^\perp; \quad [l_i \mathbf{n}_i]_{,\mathbf{g}} = \mathbf{r}_{i+1,\mathbf{g}}^\perp - \mathbf{r}_{i,\mathbf{g}}^\perp \quad (4.51)$$

The vector  $\hat{\mathbf{g}}$  does not depend on  $\varepsilon$  while the derivative of  $\hat{\mathbf{g}}$  with respect to  $\mathbf{g}$  is evaluated as:

$$\hat{\mathbf{g}}_{,\mathbf{g}} = \frac{\mathbf{I}}{\mathbf{g} \cdot \mathbf{g}} - 2 \frac{\mathbf{g} \otimes \mathbf{g}}{(\mathbf{g} \cdot \mathbf{g})^2} \quad (4.52)$$

where  $\mathbf{I}$  is the 2D identity tensor.

Applying the chain rule we can evaluate the derivatives of  $f^{(k)}(\varepsilon_i)$  with respect to  $\varepsilon$  and  $\mathbf{g}$  as:

$$f_{,\varepsilon}^{(k)}(\varepsilon_i) = f^{(k-1)}(\varepsilon_i) \varepsilon_{i,\varepsilon}; \quad f_{,\mathbf{g}}^{(k)}(\varepsilon_i) = f^{(k-1)}(\varepsilon_i) \varepsilon_{i,\mathbf{g}} \quad (4.53)$$

$\varepsilon_{i,\varepsilon}$  and  $\varepsilon_{i,\mathbf{g}}$  being the derivatives of  $\varepsilon_i$ , i.e. the value of  $\varepsilon(\mathbf{r})$  in the vertex  $\mathbf{r}_i$ . The derivatives of  $\varepsilon_i$  with respect to  $\varepsilon$  and  $\mathbf{g}$  are determined by differentiating equation (4.1) where  $\mathbf{r}_i$  is used in place of  $\mathbf{r}$ :

$$\varepsilon_{i,\varepsilon} = 1 + \mathbf{g} \cdot \mathbf{r}_{i,\varepsilon}; \quad \varepsilon_{i,\mathbf{g}} = \mathbf{r}_i + [\mathbf{r}_{i,\mathbf{g}}]^T \mathbf{g} \quad (4.54)$$

Similarly the derivatives of  $\varepsilon_{i+1}$  are computed by means of the same formulas wherein  $\mathbf{r}_{i+1}$ ,  $\mathbf{r}_{i+1,\varepsilon}$  and  $\mathbf{r}_{i+1,\mathbf{g}}$  are used in place of  $\mathbf{r}_i$ ,  $\mathbf{r}_{i,\varepsilon}$  and  $\mathbf{r}_{i,\mathbf{g}}$  respectively.

We also consider the special case in which one needs to evaluate the derivatives of  $N[f^{(k)}(\varepsilon_m)]$ ,  $\mathbf{m}^\perp[f^{(k)}(\varepsilon_m)]$  and  $\mathbf{B}[f^{(k)}(\varepsilon_m)]$ , i.e. when a quantity  $\varepsilon_m(\mathbf{r}) = \varepsilon_m + \mathbf{g}_m \cdot \mathbf{r}$  is assumed to be the argument of  $f^{(k)}$ , being  $\varepsilon_m$  and  $\mathbf{g}_m$  unrelated to  $\varepsilon$  and  $\mathbf{g}$ . In such a case the integration formulas that we are going to illustrate still hold with the exception that the derivatives:

$$\hat{\mathbf{g}}_{m,\mathbf{g}} = \mathbf{0}; \quad \varepsilon_{mi,\varepsilon} = \mathbf{g}_m \cdot \mathbf{r}_{i,\varepsilon}; \quad \varepsilon_{mi,\hat{\mathbf{g}}} = [\mathbf{r}_{i,\mathbf{g}}]^T \mathbf{g}_m \quad (4.55)$$

have to be used in place of the corresponding ones evaluated in equations (4.52) and (4.54).

### 4.2.1 The case $\mathbf{g} = \mathbf{0}$

If  $\mathbf{g} = \mathbf{0}$  the formulas for the determination of  $N[f^{(k)}(\varepsilon)]$ ,  $\mathbf{m}^\perp[f^{(k)}(\varepsilon)]$  and  $\mathbf{B}[f^{(k)}(\varepsilon)]$  are (4.5), (4.6) and (4.7) respectively. In such cases, since  $\varepsilon$  is constant on  $\Omega$ , the position vectors of the vertices of the domain have zero derivatives as it is described in section 5.1, thus  $\Omega$  does not depend on  $\varepsilon$  and  $\mathbf{g}$  and from equation (4.54) and (4.53) one gets:

$$f_{,\varepsilon}^{(k)}(\varepsilon) = f^{(k-1)}(\varepsilon); \quad f_{,\mathbf{g}}^{(k)}(\varepsilon) = f^{(k-1)}(\varepsilon) \mathbf{r}_i \quad (4.56)$$

Differentiating equation (4.5) and recalling that  $\Omega$  does not depend on  $\varepsilon$  and  $\mathbf{g}$  the derivatives of  $N[f^{(k)}(\varepsilon)]$  are:

$$\begin{aligned} N_{,\varepsilon}[f^{(k)}(\varepsilon)] &= \frac{\partial}{\partial \varepsilon} \int_{\Omega} f^{(k)}(\varepsilon) d\Omega = \int_{\Omega} f_{,\varepsilon}^{(k)}(\varepsilon) d\Omega = \\ &= f^{(k-1)}(\varepsilon) \int_{\Omega} d\Omega = f^{(k-1)}(\varepsilon) \frac{1}{2} \sum_{i=1}^n \mathbf{r}_i \cdot \mathbf{r}_{i+1}^\perp \end{aligned} \quad (4.57)$$

and:

$$\begin{aligned}
N_{,\mathbf{g}}[f^{(k)}(\epsilon)] &= \frac{\partial}{\partial \mathbf{g}} \int_{\Omega} f^{(k)}(\epsilon) d\Omega = \int_{\Omega} f^{(k)}_{,\mathbf{g}}(\epsilon) d\Omega = \\
&= f^{(k-1)}(\epsilon) \int_{\Omega} \mathbf{r} d\Omega = \\
&= f^{(k-1)}(\epsilon) \frac{1}{6} \sum_{i=1}^n \mathbf{r}_i \cdot \mathbf{r}_{i+1}^{\perp} (\mathbf{r}_i + \mathbf{r}_{i+1})
\end{aligned} \tag{4.58}$$

Similarly differentiating equation (4.6) we obtain:

$$\begin{aligned}
\mathbf{m}_{,\epsilon}^{\perp}[f^{(k)}(\epsilon)] &= \frac{\partial}{\partial \epsilon} \int_{\Omega} f^{(k)}(\epsilon) \mathbf{r} d\Omega = \int_{\Omega} f^{(k)}_{,\epsilon}(\epsilon) \mathbf{r} d\Omega = \\
&= f^{(k-1)}(\epsilon) \int_{\Omega} \mathbf{r} d\Omega = \\
&= f^{(k-1)}(\epsilon) \frac{1}{6} \sum_{i=1}^n \mathbf{r}_i \cdot \mathbf{r}_{i+1}^{\perp} (\mathbf{r}_i + \mathbf{r}_{i+1})
\end{aligned} \tag{4.59}$$

and:

$$\begin{aligned}
\mathbf{m}_{,\mathbf{g}}^{\perp}[f^{(k)}(\epsilon)] &= \frac{\partial}{\partial \mathbf{g}} \int_{\Omega} f^{(k)}(\epsilon) \mathbf{r} d\Omega = \int_{\Omega} \mathbf{r} \otimes f^{(k)}_{,\mathbf{g}}(\epsilon) d\Omega = \\
&= f^{(k-1)}(\epsilon) \int_{\Omega} \mathbf{r} \otimes \mathbf{r} d\Omega = \\
&= f^{(k-1)}(\epsilon) \frac{1}{12} \sum_{i=1}^n \mathbf{r}_i \cdot \mathbf{r}_{i+1}^{\perp} \left[ \mathbf{r}_i \otimes \mathbf{r}_i + \frac{1}{2} (\mathbf{r}_i \otimes \mathbf{r}_{i+1} + \right. \\
&\quad \left. - \mathbf{r}_{i+1} \otimes \mathbf{r}_i) + \mathbf{r}_{i+1} \otimes \mathbf{r}_{i+1} \right]
\end{aligned} \tag{4.60}$$

Finally the derivatives of equation (4.7) yield:

$$\begin{aligned}
\mathbf{B}_{,\epsilon}[f^{(k)}(\epsilon)] &= \frac{\partial}{\partial \epsilon} \int_{\Omega} f^{(k)}(\epsilon) (\mathbf{r} \otimes \mathbf{r}) d\Omega = \int_{\Omega} f^{(k)}_{,\epsilon}(\epsilon) (\mathbf{r} \otimes \mathbf{r}) = \\
&= f^{(k-1)}(\epsilon) \int_{\Omega} \mathbf{r} \otimes \mathbf{r} d\Omega = \\
&= f^{(k-1)}(\epsilon) \frac{1}{12} \sum_{i=1}^n \mathbf{r}_i \cdot \mathbf{r}_{i+1}^{\perp} \left[ \mathbf{r}_i \otimes \mathbf{r}_i + \frac{1}{2} (\mathbf{r}_i \otimes \mathbf{r}_{i+1} + \right. \\
&\quad \left. - \mathbf{r}_{i+1} \otimes \mathbf{r}_i) + \mathbf{r}_{i+1} \otimes \mathbf{r}_{i+1} \right]
\end{aligned} \tag{4.61}$$

and:

$$\begin{aligned}
 \mathbf{B}_{,\mathbf{g}}[f^{(k)}(\epsilon)] &= \frac{\partial}{\partial \mathbf{g}} \int_{\Omega} f^{(k)}(\epsilon) (\mathbf{r} \otimes \mathbf{r}) d\Omega = \int \mathbf{r} \otimes \mathbf{r} \otimes f_{,\mathbf{g}}^{(k)}(\epsilon) = \\
 &= f^{(k-1)}(\epsilon) \int_{\Omega} \mathbf{r} \otimes \mathbf{r} \otimes \mathbf{r} d\Omega = \\
 &= f^{(k-1)}(\epsilon) \frac{1}{20} \sum_{i=1}^n \mathbf{r}_i \cdot \mathbf{r}_{i+1}^\perp \left[ \mathbf{r}_i \otimes \mathbf{r}_i \otimes \mathbf{r}_i + \mathbf{r}_{i+1} \otimes \mathbf{r}_{i+1} \otimes \mathbf{r}_{i+1} + \right. \\
 &\quad \left. + \frac{1}{3} \left( \mathbf{r}_{i+1} \otimes \mathbf{r}_i \otimes \mathbf{r}_i + \mathbf{r}_i \otimes \mathbf{r}_{i+1} \otimes \mathbf{r}_i + \right. \right. \\
 &\quad \left. \left. + \mathbf{r}_i \otimes \mathbf{r}_i \otimes \mathbf{r}_{i+1} + \mathbf{r}_i \otimes \mathbf{r}_{i+1} \otimes \mathbf{r}_{i+1} + \right. \right. \\
 &\quad \left. \left. + \mathbf{r}_{i+1} \otimes \mathbf{r}_i \otimes \mathbf{r}_{i+1} + \mathbf{r}_{i+1} \otimes \mathbf{r}_{i+1} \otimes \mathbf{r}_i \right) \right] \quad (4.62)
 \end{aligned}$$

### 4.2.2 Derivatives of $N[f^{(k)}(\epsilon)]$

The derivative of  $N[f^{(k)}(\epsilon)]$  with respect to  $\epsilon$  is obtained by differentiating equation (4.32):

$$N_{,\epsilon}[f^{(k)}(\epsilon)] = \sum_{i=1}^n \left[ [l_i \mathbf{n}_i]_{,\epsilon} \cdot \hat{\mathbf{g}} \Phi_i^0[f^{(k+1)}(\epsilon)] + l_i \mathbf{n}_i \cdot \hat{\mathbf{g}} \Phi_{i,\epsilon}^0[f^{(k+1)}(\epsilon)] \right] \quad (4.63)$$

where  $\Phi_i^0[f^{(k+1)}(\epsilon)]$  is given by equation (4.30) with  $k = 1$  and  $\Phi_{i,\epsilon}^0[f^{(1)}(\epsilon)]$  denotes its derivative with respect to  $\epsilon$ . Similarly, the derivative of  $N[f^{(k)}(\epsilon)]$  with respect to  $\mathbf{g}$  is given by:

$$\begin{aligned}
 N_{,\mathbf{g}}[f^{(k)}(\epsilon)] &= \sum_{i=1}^n \left[ [l_i \mathbf{n}_i]_{,\mathbf{g}}^T \hat{\mathbf{g}} \Phi_i^0[f^{(k+1)}(\epsilon)] \right. \\
 &\quad \left. + [\hat{\mathbf{g}}, \mathbf{g}]^T \mathbf{n}_i l_i \Phi_i^0[f^{(k+1)}(\epsilon)] \right. \\
 &\quad \left. + l_i \mathbf{n}_i \cdot \hat{\mathbf{g}} \Phi_{i,\mathbf{g}}^0[f^{(k+1)}(\epsilon)] \right] \quad (4.64)
 \end{aligned}$$

where  $\Phi_{i,\mathbf{g}}^0[f^{(k+1)}(\epsilon)]$  is the derivative of  $\Phi_i^0[f^{(k+1)}(\epsilon)]$  with respect to  $\mathbf{g}$ .

The derivatives of the functions  $\Phi_i^0[f^{(k)}(\epsilon)]$  are obtained from equation (4.30)<sub>1</sub>. Differentiating with respect to  $\epsilon$  it turns out to be:

$$\Phi_{i,\epsilon}^0[f^{(k)}(\epsilon)] = \frac{[f^{(k+1)}(\epsilon)]_{\epsilon_i}^{\epsilon_{i+1}}}{\epsilon_{i+1} - \epsilon_i} - \frac{[f^{(k+1)}(\epsilon)]_{\epsilon_i}^{\epsilon_{i+1}} (\epsilon_{i+1,\epsilon} - \epsilon_{i,\epsilon})}{(\epsilon_{i+1} - \epsilon_i)^2} \quad (4.65)$$

that is not defined when  $\varepsilon_{i+1} = \varepsilon_i$ . In order to extend  $\Phi_{i,\varepsilon}^0[f^{(k)}(\varepsilon)]$  to such cases we re-write the previous equation as:

$$\Phi_{i,\varepsilon}^0[f^{(k)}(\varepsilon)] = \frac{1}{(\varepsilon_{i+1} - \varepsilon_i)^2} \left\{ \left[ f_{,\varepsilon}^{(k+1)}(\varepsilon) \right]_{\varepsilon_i}^{\varepsilon_{i+1}} (\varepsilon_{i+1} - \varepsilon_i) + \right. \\ \left. - \left[ f^{(k+1)}(\varepsilon) \right]_{\varepsilon_i}^{\varepsilon_{i+1,\varepsilon}} (\varepsilon_{i+1,\varepsilon} - \varepsilon_{i,\varepsilon}) \right\} \quad (4.66)$$

The limit for  $\varepsilon_{i+1} \rightarrow \varepsilon_i$  is in the form 0/0 thus use of L'Hopital rule can be done, yielding:

$$\lim_{\varepsilon_{i+1} \rightarrow \varepsilon_i} \Phi_{i,\varepsilon}^0[f^{(k)}(\varepsilon)] = \lim_{\varepsilon_{i+1} \rightarrow \varepsilon_i} \frac{1}{2(\varepsilon_{i+1} - \varepsilon_i)} \left\{ f_{,\varepsilon}^{(k)}(\varepsilon_{i+1})(\varepsilon_{i+1} - \varepsilon_i) + \right. \\ \left. + \left[ f_{,\varepsilon}^{(k+1)}(\varepsilon) \right]_{\varepsilon_i}^{\varepsilon_{i+1}} - f^{(k)}(\varepsilon_{i+1})(\varepsilon_{i+1,\varepsilon} - \varepsilon_{i,\varepsilon}) \right\} \quad (4.67)$$

where

$$\left[ f_{,\varepsilon}^{(k+1)}(\varepsilon) \right]_{\varepsilon_i}^{\varepsilon_{i+1}} - f^{(k)}(\varepsilon_{i+1})(\varepsilon_{i+1,\varepsilon} - \varepsilon_{i,\varepsilon}) = \\ = f^{(k)}(\varepsilon_{i+1})\varepsilon_{i+1,\varepsilon} - f^{(k)}(\varepsilon_i)\varepsilon_{i,\varepsilon} + \\ - f^{(k)}(\varepsilon_{i+1})\varepsilon_{i+1,\varepsilon} + f^{(k)}(\varepsilon_{i+1})\varepsilon_{i,\varepsilon} \quad (4.68)$$

which is zero for  $\varepsilon_{i+1} \rightarrow \varepsilon_i$ , thus the limit in (4.67) is again in the form 0/0. Applying L'Hopital rule we get:

$$\lim_{\varepsilon_{i+1} \rightarrow \varepsilon_i} \Phi_{i,\varepsilon}^0[f^{(k)}(\varepsilon)] = \frac{1}{2} \left\{ f_{,\varepsilon}^{(k-1)}(\varepsilon_{i+1})(\varepsilon_{i+1} - \varepsilon_i) + f_{,\varepsilon}^{(k)}(\varepsilon_{i+1}) + \right. \\ \left. + f_{,\varepsilon}^{(k)}(\varepsilon_{i+1}) - f^{(k-1)}(\varepsilon_{i+1})(\varepsilon_{i+1,\varepsilon} - \varepsilon_{i,\varepsilon}) \right\} = \\ = \frac{1}{2} f^{(k-1)}(\varepsilon_{i+1})(\varepsilon_{i+1,\varepsilon} + \varepsilon_{i,\varepsilon}) \quad (4.69)$$

Thus we assume:

$$\Phi_{i,\varepsilon}^0[f^{(k)}(\varepsilon)] = \begin{cases} \frac{\left[ f_{,\varepsilon}^{(k+1)}(\varepsilon) \right]_{\varepsilon_i}^{\varepsilon_{i+1}}}{\varepsilon_{i+1} - \varepsilon_i} + & \text{if } \varepsilon_{i+1} \neq \varepsilon_i \\ - \frac{\left[ f^{(k+1)}(\varepsilon) \right]_{\varepsilon_i}^{\varepsilon_{i+1,\varepsilon}} (\varepsilon_{i+1,\varepsilon} - \varepsilon_{i,\varepsilon})}{(\varepsilon_{i+1} - \varepsilon_i)^2} & \\ \frac{1}{2} f^{(k-1)}(\varepsilon_{i+1})(\varepsilon_{i+1,\varepsilon} + \varepsilon_{i,\varepsilon}) & \text{if } \varepsilon_{i+1} = \varepsilon_i \end{cases} \quad (4.70)$$

## 4.2 Derivatives of $N[f^{(k)}(\varepsilon)]$ , $\mathbf{m}^\perp[f^{(k)}(\varepsilon)]$ and $\mathbf{B}[f^{(k)}(\varepsilon)]$ with respect to $\varepsilon$ and $\mathbf{g}$ 109

In the same way one can evaluate the derivative of  $\Phi_i^0[f^{(k)}(\varepsilon)]$  with respect to  $\mathbf{g}$  that is:

$$\Phi_{i,\mathbf{g}}^0[f^{(k)}(\varepsilon)] = \begin{cases} \frac{[f_{\mathbf{g}}^{(k+1)}(\varepsilon)]_{\varepsilon_i}^{\varepsilon_{i+1}}}{\varepsilon_{i+1} - \varepsilon_i} & \text{if } \varepsilon_{i+1} \neq \varepsilon_i \\ -\frac{[f^{(k+1)}(\varepsilon)]_{\varepsilon_i}^{\varepsilon_{i+1}} (\varepsilon_{i+1,\mathbf{g}} - \varepsilon_{i,\mathbf{g}})}{(\varepsilon_{i+1} - \varepsilon_i)^2} & \\ \frac{1}{2}f^{(k-1)}(\varepsilon_{i+1})(\varepsilon_{i+1,\mathbf{g}} + \varepsilon_{i,\mathbf{g}}) & \text{if } \varepsilon_{i+1} = \varepsilon_i \end{cases} \quad (4.71)$$

### 4.2.3 Derivatives of $\mathbf{m}^\perp[f^{(k)}(\varepsilon)]$

As we have done for  $N[f^{(k)}(\varepsilon)]$ , the derivatives of  $\mathbf{m}^\perp[f^{(k)}(\varepsilon)]$  with respect to  $\varepsilon$  and  $\mathbf{g}$  are evaluated from equation (4.40) as:

$$\begin{aligned} \mathbf{m}_{,\varepsilon}^\perp[f^{(k)}(\varepsilon)] &= \sum_{i=1}^n [l_i \mathbf{n}_i]_{,\varepsilon} \cdot \hat{\mathbf{g}} \left[ \Phi_i^0[f^{(k+1)}(\varepsilon)] \mathbf{r}_i + \right. \\ &\quad \left. + \Phi_i^1[f^{(k+1)}(\varepsilon)] (\mathbf{r}_{i+1} - \mathbf{r}_i) - \Phi_i^0[f^{(k+2)}(\varepsilon)] \hat{\mathbf{g}} \right] + \\ &\quad + l_i \mathbf{n}_i \cdot \hat{\mathbf{g}} \left[ \Phi_{i,\varepsilon}^0[f^{(k+1)}(\varepsilon)] \mathbf{r}_i + \Phi_{i,\varepsilon}^1[f^{(k+1)}(\varepsilon)] (\mathbf{r}_{i+1} - \mathbf{r}_i) + \right. \\ &\quad \left. - \Phi_{i,\varepsilon}^0[f^{(k+2)}(\varepsilon)] \hat{\mathbf{g}} + \Phi_i^0[f^{(k+1)}(\varepsilon)] \mathbf{r}_{i,\varepsilon} + \right. \\ &\quad \left. + \Phi_i^1[f^{(k+1)}(\varepsilon)] (\mathbf{r}_{i+1,\varepsilon} - \mathbf{r}_{i,\varepsilon}) \right] \end{aligned} \quad (4.72)$$

where  $\Phi_{i,\varepsilon}^1[f^{(k+1)}(\varepsilon)]$  is the derivative of  $\Phi_i^1[f^{(k+1)}(\varepsilon)]$  with respect to  $\varepsilon$  and:

$$\begin{aligned} \mathbf{m}_{,\mathbf{g}}^\perp[f^{(k)}(\varepsilon)] &= \sum_{i=1}^n \left[ \Phi_i^0[f^{(k+1)}(\varepsilon)] \mathbf{r}_i + \Phi_i^1[f^{(k+1)}(\varepsilon)] (\mathbf{r}_{i+1} - \mathbf{r}_i) + \right. \\ &\quad \left. - \Phi_i^0[f^{(k+2)}(\varepsilon)] \hat{\mathbf{g}} \right] \otimes \left( [l_i \mathbf{n}_i]_{,\mathbf{g}}^T \hat{\mathbf{g}} + [\hat{\mathbf{g}}_{,\mathbf{g}}]^T \mathbf{n}_i l_i \right) + \\ &\quad + l_i \mathbf{n}_i \cdot \hat{\mathbf{g}} \left[ \mathbf{r}_i \otimes \Phi_{i,\mathbf{g}}^0[f^{(k+1)}(\varepsilon)] + (\mathbf{r}_{i+1} - \mathbf{r}_i) \otimes \Phi_{i,\mathbf{g}}^1[f^{(k+1)}(\varepsilon)] + \right. \\ &\quad \left. - \hat{\mathbf{g}} \otimes \Phi_{i,\mathbf{g}}^0[f^{(k+2)}(\varepsilon)] + \Phi_i^0[f^{(k+1)}(\varepsilon)] \mathbf{r}_{i,\mathbf{g}} + \right. \\ &\quad \left. + \Phi_i^1[f^{(k+1)}(\varepsilon)] (\mathbf{r}_{i+1,\mathbf{g}} - \mathbf{r}_{i,\mathbf{g}}) - \Phi_i^0[f^{(k+2)}(\varepsilon)] \hat{\mathbf{g}}_{,\mathbf{g}} \right] \end{aligned} \quad (4.73)$$

where  $\Phi_{i,\mathbf{g}}^1[f^{(k+1)}(\varepsilon)]$  is the derivative of  $\Phi_i^1[f^{(k+1)}(\varepsilon)]$  with respect to  $\mathbf{g}$ .

The derivative of the functions  $\Phi_i^1[f^{(k)}(\varepsilon)]$  with respect to  $\varepsilon$  is obtained differentiating equation (4.39) as follows:

$$\begin{aligned} \Phi_{i,\varepsilon}^1[f^{(k)}(\varepsilon)] &= \frac{f_{,\varepsilon}^{(k+1)}(\varepsilon_{i+1})}{\varepsilon_{i+1} - \varepsilon_i} - \frac{[f_{,\varepsilon}^{(k+2)}(\varepsilon)]_{\varepsilon_i}^{\varepsilon_{i+1}}}{(\varepsilon_{i+1} - \varepsilon_i)^2} + \\ &\quad - \frac{f^{(k+1)}(\varepsilon_{i+1})(\varepsilon_{i+1,\varepsilon} - \varepsilon_{i,\varepsilon})}{(\varepsilon_{i+1} - \varepsilon_i)^2} + \\ &\quad + 2 \frac{[f^{(k+2)}(\varepsilon)]_{\varepsilon_i}^{\varepsilon_{i+1}} (\varepsilon_{i+1,\varepsilon} - \varepsilon_{i,\varepsilon})}{(\varepsilon_{i+1} - \varepsilon_i)^3} \end{aligned} \quad (4.74)$$

In the cases in which  $\varepsilon_{i+1} = \varepsilon_i$  the same strategy adopted for the evaluation of  $\Phi_{i,\varepsilon}^0[f^{(k)}(\varepsilon)]$  is used after re-writing  $\Phi_{i,\varepsilon}^1[f^{(k)}(\varepsilon)]$  in the form:

$$\begin{aligned} \Phi_{i,\varepsilon}^1[f^{(k)}(\varepsilon)] &= \frac{1}{(\varepsilon_{i+1} - \varepsilon_i)^3} \left\{ f_{,\varepsilon}^{(k+1)}(\varepsilon_{i+1})(\varepsilon_{i+1} - \varepsilon_i)^2 + \right. \\ &\quad - [f_{,\varepsilon}^{(k+2)}(\varepsilon)]_{\varepsilon_i}^{\varepsilon_{i+1}} (\varepsilon_{i+1} - \varepsilon_i) + \\ &\quad - f^{(k+1)}(\varepsilon_{i+1})(\varepsilon_{i+1,\varepsilon} - \varepsilon_{i,\varepsilon})(\varepsilon_{i+1} - \varepsilon_i) + \\ &\quad \left. + 2 [f^{(k+2)}(\varepsilon)]_{\varepsilon_i}^{\varepsilon_{i+1}} (\varepsilon_{i+1,\varepsilon} - \varepsilon_{i,\varepsilon}) \right\} \end{aligned} \quad (4.75)$$

The relevant limit for  $\varepsilon_{i+1} \rightarrow \varepsilon_i$  is in the form 0/0. L'Hopital's rule is, thus, applied as follows:

$$\begin{aligned} &\lim_{\varepsilon_{i+1} \rightarrow \varepsilon_i} \Phi_{i,\varepsilon}^1[f^{(k)}(\varepsilon)] = \\ &= \lim_{\varepsilon_{i+1} \rightarrow \varepsilon_i} \frac{1}{3(\varepsilon_{i+1} - \varepsilon_i)^2} \left\{ f_{,\varepsilon}^{(k+1)}(\varepsilon_{i+1})(\varepsilon_{i+1} - \varepsilon_i) + \right. \\ &\quad + f_{,\varepsilon}^{(k)}(\varepsilon_{i+1})(\varepsilon_{i+1} - \varepsilon_i)^2 - [f_{,\varepsilon}^{(k+2)}(\varepsilon)]_{\varepsilon_i}^{\varepsilon_{i+1}} + \\ &\quad - f^{(k)}(\varepsilon_{i+1})(\varepsilon_{i+1,\varepsilon} - \varepsilon_{i,\varepsilon})(\varepsilon_{i+1} - \varepsilon_i) + \\ &\quad \left. + f^{(k+1)}(\varepsilon_{i+1})(\varepsilon_{i+1,\varepsilon} - \varepsilon_{i,\varepsilon}) \right\} \end{aligned} \quad (4.76)$$

**4.2 Derivatives of  $N[f^{(k)}(\varepsilon)$ ,  $\mathbf{m}^\perp[f^{(k)}(\varepsilon)]$  and  $\mathbf{B}[f^{(k)}(\varepsilon)]$  with respect to  $\varepsilon$  and  $\mathbf{g}$**  **111**

which is still in the form 0/0. L'Hopital's rule is applied again yielding:

$$\begin{aligned}
 & \lim_{\varepsilon_{i+1} \rightarrow \varepsilon_i} \Phi_{i,\varepsilon}^1[f^{(k)}(\varepsilon)] = \\
 & = \lim_{\varepsilon_{i+1} \rightarrow \varepsilon_i} \frac{1}{6(\varepsilon_{i+1} - \varepsilon_i)} \left\{ 3f_{,\varepsilon}^{(k)}(\varepsilon_{i+1})(\varepsilon_{i+1} - \varepsilon_i) + \right. \\
 & \quad \left. + f_{,\varepsilon}^{(k-1)}(\varepsilon_{i+1})(\varepsilon_{i+1} - \varepsilon_i)^2 + \right. \\
 & \quad \left. - f^{(k-1)}(\varepsilon_{i+1})(\varepsilon_{i+1,\varepsilon} - \varepsilon_{i,\varepsilon})(\varepsilon_{i+1} - \varepsilon_i) \right\} = \\
 & = \frac{1}{6} f^{(k-1)}(\varepsilon_{i+1}) (2\varepsilon_{i+1,\varepsilon} + \varepsilon_{i,\varepsilon})
 \end{aligned} \tag{4.77}$$

where use of (4.53) has been made.

Thus we extend the function  $\Phi_{i,\varepsilon}^1[f^{(k)}(\varepsilon)]$  to the cases where  $\varepsilon_{i+1} = \varepsilon_i$  as:

$$\Phi_{i,\varepsilon}^1[f^{(k)}(\varepsilon)] = \begin{cases} \frac{f_{,\varepsilon}^{(k+1)}(\varepsilon_{i+1})}{\varepsilon_{i+1} - \varepsilon_i} - \frac{[f_{,\varepsilon}^{(k+2)}(\varepsilon)]_{\varepsilon_i}^{\varepsilon_{i+1}}}{(\varepsilon_{i+1} - \varepsilon_i)^2} + \\ - \frac{f^{(k+1)}(\varepsilon_{i+1})(\varepsilon_{i+1,\varepsilon} - \varepsilon_{i,\varepsilon})}{(\varepsilon_{i+1} - \varepsilon_i)^2} + & \text{if } \varepsilon_{i+1} \neq \varepsilon_i \\ + 2 \frac{[f^{(k+2)}(\varepsilon)]_{\varepsilon_i}^{\varepsilon_{i+1}} (\varepsilon_{i+1,\varepsilon} - \varepsilon_{i,\varepsilon})}{(\varepsilon_{i+1} - \varepsilon_i)^3} \\ \frac{1}{6} f^{(k-1)}(\varepsilon_{i+1}) (2\varepsilon_{i+1,\varepsilon} + \varepsilon_{i,\varepsilon}) & \text{if } \varepsilon_{i+1} = \varepsilon_i \end{cases} \tag{4.78}$$

Similarly the derivative of  $\Phi_i^1[f^{(k)}(\varepsilon)]$  with respect to  $\mathbf{g}$  is equal to:

$$\Phi_{i,\mathbf{g}}^1[f^{(k)}(\varepsilon)] = \begin{cases} \frac{f_{,\mathbf{g}}^{(k+1)}(\varepsilon_{i+1})}{\varepsilon_{i+1} - \varepsilon_i} - \frac{[f_{,\mathbf{g}}^{(k+2)}(\varepsilon)]_{\varepsilon_i}^{\varepsilon_{i+1}}}{(\varepsilon_{i+1} - \varepsilon_i)^2} + \\ - \frac{f^{(k+1)}(\varepsilon_{i+1})(\varepsilon_{i+1,\mathbf{g}} - \varepsilon_{i,\mathbf{g}})}{(\varepsilon_{i+1} - \varepsilon_i)^2} + & \text{if } \varepsilon_{i+1} \neq \varepsilon_i \\ + 2 \frac{[f^{(k+2)}(\varepsilon)]_{\varepsilon_i}^{\varepsilon_{i+1}} (\varepsilon_{i+1,\mathbf{g}} - \varepsilon_{i,\mathbf{g}})}{(\varepsilon_{i+1} - \varepsilon_i)^3} \\ \frac{1}{6} f^{(k-1)}(\varepsilon_{i+1}) (2\varepsilon_{i+1,\mathbf{g}} + \varepsilon_{i,\mathbf{g}}) & \text{if } \varepsilon_{i+1} = \varepsilon_i \end{cases} \tag{4.79}$$

#### 4.2.4 Derivatives of $\mathbf{B}[f^{(k)}(\varepsilon)]$

The derivative of  $\mathbf{B}[f^{(k)}(\varepsilon)]$  with respect to  $\varepsilon$  is evaluated differentiating equation (4.50):

$$\mathbf{B}_{,\varepsilon}[f^{(k)}(\varepsilon)] = \sum_{i=1}^n ([l_i \mathbf{n}_i]_{,\varepsilon} \cdot \hat{\mathbf{g}}) \mathbf{A}_i + (l_i \mathbf{n}_i \cdot \hat{\mathbf{g}}) \mathbf{A}_{i,\varepsilon} \quad (4.80)$$

where the tensor:

$$\begin{aligned} \mathbf{A}_i = & \Phi_i^0[f^{(k+1)}(\varepsilon)](\mathbf{r}_i \otimes \mathbf{r}_i) + \\ & + \Phi_i^1[f^{(k+1)}(\varepsilon)][\mathbf{r}_i \otimes (\mathbf{r}_{i+1} - \mathbf{r}_i) + (\mathbf{r}_{i+1} - \mathbf{r}_i) \otimes \mathbf{r}_i] + \\ & + \Phi_i^2[f^{(k+1)}(\varepsilon)][(\mathbf{r}_{i+1} - \mathbf{r}_i) \otimes (\mathbf{r}_{i+1} - \mathbf{r}_i)] + \\ & - \Phi_i^0[f^{(k+2)}(\varepsilon)][\mathbf{r}_i \otimes \hat{\mathbf{g}} + \hat{\mathbf{g}} \otimes \mathbf{r}_i] + \\ & - \Phi_i^1[f^{(k+2)}(\varepsilon)][(\mathbf{r}_{i+1} - \mathbf{r}_i) \otimes \hat{\mathbf{g}} + \hat{\mathbf{g}} \otimes (\mathbf{r}_{i+1} - \mathbf{r}_i)] + \\ & + 2\Phi_i^0[f^{(k+3)}(\varepsilon)](\hat{\mathbf{g}} \otimes \hat{\mathbf{g}}) \end{aligned} \quad (4.81)$$

has been introduced. Differentiating the previous formula one gets:

$$\begin{aligned} \mathbf{A}_{i,\varepsilon} = & \Phi_{i,\varepsilon}^0[f^{(k+1)}(\varepsilon)](\mathbf{r}_i \otimes \mathbf{r}_i) + \\ & + \Phi_{i,\varepsilon}^0[f^{(k+1)}(\varepsilon)](\mathbf{r}_{i,\varepsilon} \otimes \mathbf{r}_i + \mathbf{r}_i \otimes \mathbf{r}_{i,\varepsilon}) + \\ & + \Phi_{i,\varepsilon}^1[f^{(k+1)}(\varepsilon)][\mathbf{r}_i \otimes (\mathbf{r}_{i+1} - \mathbf{r}_i) + (\mathbf{r}_{i+1} - \mathbf{r}_i) \otimes \mathbf{r}_i] + \\ & + \Phi_{i,\varepsilon}^1[f^{(k+1)}(\varepsilon)][\mathbf{r}_{i,\varepsilon} \otimes (\mathbf{r}_{i+1} - \mathbf{r}_i) + \mathbf{r}_i \otimes (\mathbf{r}_{i+1,\varepsilon} - \mathbf{r}_{i,\varepsilon}) + \\ & \quad + (\mathbf{r}_{i+1,\varepsilon} - \mathbf{r}_{i,\varepsilon}) \otimes \mathbf{r}_i + (\mathbf{r}_{i+1} - \mathbf{r}_i) \otimes \mathbf{r}_{i,\varepsilon}] + \\ & + \Phi_{i,\varepsilon}^2[f^{(k+1)}(\varepsilon)][(\mathbf{r}_{i+1} - \mathbf{r}_i) \otimes (\mathbf{r}_{i+1} - \mathbf{r}_i)] + \\ & + \Phi_{i,\varepsilon}^2[f^{(k+1)}(\varepsilon)][(\mathbf{r}_{i+1,\varepsilon} - \mathbf{r}_{i,\varepsilon}) \otimes (\mathbf{r}_{i+1} - \mathbf{r}_i) + \\ & \quad + (\mathbf{r}_{i+1} - \mathbf{r}_i) \otimes (\mathbf{r}_{i+1,\varepsilon} - \mathbf{r}_{i,\varepsilon})] + \\ & - \Phi_{i,\varepsilon}^0[f^{(k+2)}(\varepsilon)][\mathbf{r}_i \otimes \hat{\mathbf{g}} + \hat{\mathbf{g}} \otimes \mathbf{r}_i] + \\ & - \Phi_{i,\varepsilon}^0[f^{(k+2)}(\varepsilon)][\mathbf{r}_{i,\varepsilon} \otimes \hat{\mathbf{g}} + \hat{\mathbf{g}} \otimes \mathbf{r}_{i,\varepsilon}] + \\ & - \Phi_{i,\varepsilon}^1[f^{(k+2)}(\varepsilon)][(\mathbf{r}_{i+1} - \mathbf{r}_i) \otimes \hat{\mathbf{g}} + \hat{\mathbf{g}} \otimes (\mathbf{r}_{i+1} - \mathbf{r}_i)] + \\ & - \Phi_{i,\varepsilon}^1[f^{(k+2)}(\varepsilon)][(\mathbf{r}_{i+1,\varepsilon} - \mathbf{r}_{i,\varepsilon}) \otimes \hat{\mathbf{g}} + \hat{\mathbf{g}} \otimes (\mathbf{r}_{i+1,\varepsilon} - \mathbf{r}_{i,\varepsilon})] + \\ & + 2\Phi_{i,\varepsilon}^0[f^{(k+3)}(\varepsilon)](\hat{\mathbf{g}} \otimes \hat{\mathbf{g}}) \end{aligned} \quad (4.82)$$

The derivatives of  $\Phi_i^0[f^{(k)}(\varepsilon)]$  and  $\Phi_i^1[f^{(k)}(\varepsilon)]$  with respect to  $\varepsilon$  are given by equations (4.70) and (4.78), respectively. In the same way  $\Phi_{i,\varepsilon}^2[f^{(k)}(\varepsilon)]$  is

obtained differentiating equation (4.49):

$$\begin{aligned}
 \Phi_{i,\varepsilon}^2[f^{(k)}(\varepsilon)] &= \frac{f_{,\varepsilon}^{(k+1)}(\varepsilon_{i+1})}{\varepsilon_{i+1} - \varepsilon_i} - \frac{f^{(k+1)}(\varepsilon_{i+1})(\varepsilon_{i+1,\varepsilon} - \varepsilon_{i,\varepsilon})}{(\varepsilon_{i+1} - \varepsilon_i)^2} + \\
 &- 2 \frac{f_{,\varepsilon}^{(k+2)}(\varepsilon_{i+1})}{(\varepsilon_{i+1} - \varepsilon_i)^2} + 4 \frac{f^{(k+2)}(\varepsilon_{i+1})(\varepsilon_{i+1,\varepsilon} - \varepsilon_{i,\varepsilon})}{(\varepsilon_{i+1} - \varepsilon_i)^3} + \\
 &+ 2 \frac{\left[ f_{,\varepsilon}^{(k+3)}(\varepsilon) \right]_{\varepsilon_i}^{\varepsilon_{i+1}}}{(\varepsilon_{i+1} - \varepsilon_i)^3} - 6 \frac{\left[ f^{(k+3)}(\varepsilon) \right]_{\varepsilon_i}^{\varepsilon_{i+1}} (\varepsilon_{i+1,\varepsilon} - \varepsilon_{i,\varepsilon})}{(\varepsilon_{i+1} - \varepsilon_i)^4}
 \end{aligned} \tag{4.83}$$

The same strategy adopted for evaluating  $\Phi_{i,\varepsilon}^0[f^{(k)}(\varepsilon)]$  and  $\Phi_{i,\varepsilon}^1[f^{(k)}(\varepsilon)]$  in the cases in which  $\varepsilon_{i+1} = \varepsilon_i$  is used here. To this end we re-write the previous formula as:

$$\begin{aligned}
 \Phi_{i,\varepsilon}^2[f^{(k)}(\varepsilon)] &= \frac{1}{(\varepsilon_{i+1} - \varepsilon_i)^4} \left\{ f_{,\varepsilon}^{(k+1)}(\varepsilon_{i+1})(\varepsilon_{i+1} - \varepsilon_i)^3 + \right. \\
 &- f^{(k+1)}(\varepsilon_{i+1})(\varepsilon_{i+1,\varepsilon} - \varepsilon_{i,\varepsilon})(\varepsilon_{i+1} - \varepsilon_i)^2 + \\
 &- 2f_{,\varepsilon}^{(k+2)}(\varepsilon_{i+1})(\varepsilon_{i+1} - \varepsilon_i)^2 \\
 &+ 4f^{(k+2)}(\varepsilon_{i+1})(\varepsilon_{i+1,\varepsilon} - \varepsilon_{i,\varepsilon})(\varepsilon_{i+1} - \varepsilon_i) + \\
 &+ 2 \left[ f_{,\varepsilon}^{(k+3)}(\varepsilon) \right]_{\varepsilon_i}^{\varepsilon_{i+1}} (\varepsilon_{i+1} - \varepsilon_i) + \\
 &\left. - 6 \left[ f^{(k+3)}(\varepsilon) \right]_{\varepsilon_i}^{\varepsilon_{i+1}} (\varepsilon_{i+1,\varepsilon} - \varepsilon_{i,\varepsilon}) \right\}
 \end{aligned} \tag{4.84}$$

whose limit for  $\varepsilon_{i+1} \rightarrow \varepsilon_i$  is in the form 0/0. Application of L'Hopital's rule yields:

$$\begin{aligned}
 \lim_{\varepsilon_{i+1} \rightarrow \varepsilon_i} \Phi_{i,\varepsilon}^2[f^{(k)}(\varepsilon)] &= \lim_{\varepsilon_{i+1} \rightarrow \varepsilon_i} \frac{1}{4(\varepsilon_{i+1} - \varepsilon_i)^3} \left\{ \right. \\
 &f_{,\varepsilon}^{(k)}(\varepsilon_{i+1})(\varepsilon_{i+1} - \varepsilon_i)^3 + f_{,\varepsilon}^{(k+1)}(\varepsilon_{i+1})(\varepsilon_{i+1} - \varepsilon_i)^2 + \\
 &- f^{(k)}(\varepsilon_{i+1})(\varepsilon_{i+1,\varepsilon} - \varepsilon_{i,\varepsilon})(\varepsilon_{i+1} - \varepsilon_i)^2 + \\
 &- 2f_{,\varepsilon}^{(k+2)}(\varepsilon_{i+1})(\varepsilon_{i+1} - \varepsilon_i) + \\
 &+ 2f^{(k+1)}(\varepsilon_{i+1})(\varepsilon_{i+1,\varepsilon} - \varepsilon_{i,\varepsilon})(\varepsilon_{i+1} - \varepsilon_i) + \\
 &\left. + 2 \left[ f_{,\varepsilon}^{(k+3)}(\varepsilon) \right]_{\varepsilon_i}^{\varepsilon_{i+1}} - 2f^{(k+2)}(\varepsilon_{i+1})(\varepsilon_{i+1,\varepsilon} - \varepsilon_{i,\varepsilon}) \right\}
 \end{aligned} \tag{4.85}$$

L'Hopital's rule is applied again since the previous limit is again in the form 0/0:

$$\begin{aligned} \lim_{\varepsilon_{i+1} \rightarrow \varepsilon_i} \Phi_{i,\epsilon}^2[f^{(k)}(\varepsilon)] &= \lim_{\varepsilon_{i+1} \rightarrow \varepsilon_i} \frac{1}{12(\varepsilon_{i+1} - \varepsilon_i)^2} \left\{ \right. \\ & f_{,\epsilon}^{(k-1)}(\varepsilon_{i+1})(\varepsilon_{i+1} - \varepsilon_i)^3 + 4f_{,\epsilon}^{(k)}(\varepsilon_{i+1})(\varepsilon_{i+1} - \varepsilon_i)^2 + \\ & \left. - f^{(k-1)}(\varepsilon_{i+1})(\varepsilon_{i+1,\epsilon} - \varepsilon_{i,\epsilon})(\varepsilon_{i+1} - \varepsilon_i)^2 \right\} \end{aligned} \quad (4.86)$$

Finally we extend the domain of the function  $\Phi_{i,\epsilon}^2[f^{(k)}(\varepsilon)]$  of equation (4.83) assuming the value

$$\Phi_{i,\epsilon}^2[f^{(k)}(\varepsilon)] = \frac{1}{12} f^{(k-1)}(\varepsilon_{i+1})(3\varepsilon_{i+1,\epsilon} + \varepsilon_{i,\epsilon}) \quad (4.87)$$

for the cases in which  $\varepsilon_{i+1} = \varepsilon_i$ .

Differentiating equation (4.50) with respect to  $\mathbf{g}$  we get:

$$\mathbf{B}_{,\epsilon}[f^{(k)}(\varepsilon)] = \sum_{i=1}^n \mathbf{A}_i \otimes \left( [l_i \mathbf{n}_i]_{,\mathbf{g}}^T \hat{\mathbf{g}} + [\hat{\mathbf{g}}, \mathbf{g}]^T \mathbf{n}_i l_i \right) + (l_i \mathbf{n}_i \cdot \hat{\mathbf{g}}) \mathbf{A}_{i,\mathbf{g}} \quad (4.88)$$

where the derivative of  $\mathbf{A}_i$  with respect to  $\mathbf{g}$  is obtained from equation (4.81):

$$\begin{aligned}
\mathbf{A}_{i,\mathbf{g}} = & (\mathbf{r}_i \otimes \mathbf{r}_i) \otimes \Phi_{i,\mathbf{g}}^0[f^{(k+1)}(\varepsilon)] + \\
& + \Phi_{i,\mathbf{g}}^0[f^{(k+1)}(\varepsilon)] \left[ (\mathbf{r}_{i,\mathbf{g}} \otimes \mathbf{r}_i)^T + \mathbf{r}_i \otimes \mathbf{r}_{i,\mathbf{g}} \right] + \\
& + [\mathbf{r}_i \otimes (\mathbf{r}_{i+1} - \mathbf{r}_i) + (\mathbf{r}_{i+1} - \mathbf{r}_i) \otimes \mathbf{r}_i] \otimes \Phi_{i,\mathbf{g}}^1[f^{(k+1)}(\varepsilon)] + \\
& + \Phi_{i,\mathbf{g}}^1[f^{(k+1)}(\varepsilon)] \left\{ [\mathbf{r}_{i,\mathbf{g}} \otimes (\mathbf{r}_{i+1} - \mathbf{r}_i)]^T + \mathbf{r}_i \otimes (\mathbf{r}_{i+1,\mathbf{g}} - \mathbf{r}_{i,\mathbf{g}}) + \right. \\
& \quad \left. + [(\mathbf{r}_{i+1,\mathbf{g}} - \mathbf{r}_{i,\mathbf{g}}) \otimes \mathbf{r}_i]^T + (\mathbf{r}_{i+1} - \mathbf{r}_i) \otimes \mathbf{r}_{i,\mathbf{g}} \right\} + \\
& + [(\mathbf{r}_{i+1} - \mathbf{r}_i) \otimes (\mathbf{r}_{i+1} - \mathbf{r}_i)] \otimes \Phi_{i,\mathbf{g}}^2[f^{(k+1)}(\varepsilon)] + \\
& + \Phi_{i,\mathbf{g}}^2[f^{(k+1)}(\varepsilon)] \left\{ [(\mathbf{r}_{i+1,\mathbf{g}} - \mathbf{r}_{i,\mathbf{g}}) \otimes (\mathbf{r}_{i+1} - \mathbf{r}_i)]^T + \right. \\
& \quad \left. + (\mathbf{r}_{i+1} - \mathbf{r}_i) \otimes (\mathbf{r}_{i+1,\mathbf{g}} - \mathbf{r}_{i,\mathbf{g}}) \right\} + \\
& - [\mathbf{r}_i \otimes \hat{\mathbf{g}} + \hat{\mathbf{g}} \otimes \mathbf{r}_i] \otimes \Phi_{i,\mathbf{g}}^0[f^{(k+2)}(\varepsilon)] + \\
& - \Phi_{i,\mathbf{g}}^0[f^{(k+2)}(\varepsilon)] \left[ (\mathbf{r}_{i,\mathbf{g}} \otimes \hat{\mathbf{g}})^T + \mathbf{r}_i \otimes \hat{\mathbf{g}}_{,\mathbf{g}} + \right. \\
& \quad \left. + (\hat{\mathbf{g}}_{,\mathbf{g}} \otimes \mathbf{r}_i)^T + \hat{\mathbf{g}} \otimes \mathbf{r}_{i,\varepsilon} \right] + \\
& - [(\mathbf{r}_{i+1} - \mathbf{r}_i) \otimes \hat{\mathbf{g}} + \hat{\mathbf{g}} \otimes (\mathbf{r}_{i+1} - \mathbf{r}_i)] \otimes \Phi_{i,\mathbf{g}}^1[f^{(k+2)}(\varepsilon)] + \\
& - \Phi_{i,\mathbf{g}}^1[f^{(k+2)}(\varepsilon)] \left\{ [(\mathbf{r}_{i+1,\mathbf{g}} - \mathbf{r}_{i,\mathbf{g}}) \otimes \hat{\mathbf{g}}]^T + (\mathbf{r}_{i+1} - \mathbf{r}_i) \otimes \hat{\mathbf{g}}_{,\mathbf{g}} + \right. \\
& \quad \left. + [\hat{\mathbf{g}}_{,\mathbf{g}} \otimes (\mathbf{r}_{i+1} - \mathbf{r}_i)]^T + \hat{\mathbf{g}} \otimes (\mathbf{r}_{i+1,\mathbf{g}} - \mathbf{r}_{i,\mathbf{g}}) \right\} + \\
& + 2(\hat{\mathbf{g}} \otimes \hat{\mathbf{g}}) \otimes \Phi_{i,\mathbf{g}}^0[f^{(k+3)}(\varepsilon)] + \\
& + 2\Phi_{i,\mathbf{g}}^0[f^{(k+3)}(\varepsilon)] \left[ (\hat{\mathbf{g}}_{,\mathbf{g}} \otimes \hat{\mathbf{g}})^T + \hat{\mathbf{g}} \otimes \hat{\mathbf{g}}_{,\mathbf{g}} \right]
\end{aligned} \tag{4.89}$$

where the third order tensors of the kind  $(\mathbf{a}_{,\mathbf{g}} \otimes \mathbf{b})^T$  are expressed in index notation as:

$$\left[ (\mathbf{a}_{,\mathbf{g}} \otimes \mathbf{b})^T \right]_{jkl} = (\mathbf{a}_{,\mathbf{g}} \otimes \mathbf{b})_{jlk} = a_{j,l} b_k \tag{4.90}$$

The quantities  $\Phi_{i,\mathbf{g}}^0[f^{(k)}(\varepsilon)]$  and  $\Phi_{i,\mathbf{g}}^1[f^{(k)}(\varepsilon)]$  are given from the relevant equations in the previous two subsections. For what concerns the derivative of  $\Phi_{i,\mathbf{g}}^2[f^{(k)}(\varepsilon)]$  with respect to  $\mathbf{g}$  the same strategy adopted for  $\Phi_{i,\varepsilon}^2[f^{(k)}(\varepsilon)]$

yields:

$$\begin{aligned}
\Phi_{i,\mathbf{g}}^2[f^{(k)}(\varepsilon)] &= \frac{f_{,\mathbf{g}}^{(k+1)}(\varepsilon_{i+1})}{\varepsilon_{i+1} - \varepsilon_i} - \frac{f^{(k+1)}(\varepsilon_{i+1})(\varepsilon_{i+1,\mathbf{g}} - \varepsilon_{i,\mathbf{g}})}{(\varepsilon_{i+1} - \varepsilon_i)^2} + \\
&- 2 \frac{f_{,\mathbf{g}}^{(k+2)}(\varepsilon_{i+1})}{(\varepsilon_{i+1} - \varepsilon_i)^2} + 4 \frac{f^{(k+2)}(\varepsilon_{i+1})(\varepsilon_{i+1,\mathbf{g}} - \varepsilon_{i,\mathbf{g}})}{(\varepsilon_{i+1} - \varepsilon_i)^3} + \\
&+ 2 \frac{[f_{,\mathbf{g}}^{(k+3)}(\varepsilon)]_{\varepsilon_i}^{\varepsilon_{i+1}}}{(\varepsilon_{i+1} - \varepsilon_i)^3} - 6 \frac{[f^{(k+3)}(\varepsilon)]_{\varepsilon_i}^{\varepsilon_{i+1}} (\varepsilon_{i+1,\mathbf{g}} - \varepsilon_{i,\mathbf{g}})}{(\varepsilon_{i+1} - \varepsilon_i)^4}
\end{aligned} \tag{4.91}$$

if  $\varepsilon_{i+1} \neq \varepsilon_i$  and:

$$\Phi_{i,\mathbf{g}}^2[f^{(k)}(\varepsilon)] = \frac{1}{12} f^{(k-1)}(\varepsilon_{i+1})(3\varepsilon_{i+1,\mathbf{g}} + \varepsilon_{i,\mathbf{g}}) \tag{4.92}$$

otherwise.

## Chapter 5

# Inelastic stress-strain laws

The integration formulas developed in chapter 4 can be used for non-linear elastic stress-strain relations, i.e. when the plastic strain distribution on the section is neglected. In this chapter we will show how to adapt such formulas to the case of more complex material models which account for the deformation history of each point of the section.

Stress-strain relations commonly used for the points P of a non-linear RC section is similar to the one shown in figure 5.1.

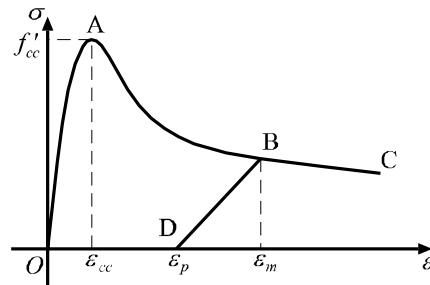


Figure 5.1: Plastic non-linear stress-strain relation

It is characterized by a non-linear envelope curve (OABC) which corresponds to an uniaxial monotonic loading of P. Unloading-reloading paths (BDO) are given as a function of the strain  $\varepsilon_m$  which is the maximum compressive value that the axial strain has ever reached at P. In general the complete unloading strain  $\varepsilon_p$ , corresponding to the residual or plastic strain in P, has a value which is given as a non-linear function of  $\varepsilon_m$ :

$$\varepsilon_p = \varepsilon_p(\varepsilon_m) \quad (5.1)$$

Clearly, once the value of  $\varepsilon_m$  is assigned, the behavior of P is univocally determined as a function of the current strain  $\varepsilon$ :

$$\sigma(\mathbf{r}) = \sigma[\varepsilon_m(\mathbf{r}), \varepsilon(\mathbf{r})] \quad (5.2)$$

where  $\mathbf{r}$  is the position vector of the generic point P.

Since  $\varepsilon_m$  is responsible for the behavior of the points of the section, a partition of the section can be executed by grouping the points where one of the previous states of the section produces maximum values of the strain.

Let us consider, for instance, the case shown in figure 5.2, and imagine that a sequence of three strain parameter vectors  $\mathbf{d}_1$ ,  $\mathbf{d}_2$  and  $\mathbf{d}_3$ , which correspond to strain states of the section previous then the current one, are given. By comparing the values of such vectors the partitions  $P_1$  and  $P_3$ , shown in figure 5.2, are determined.

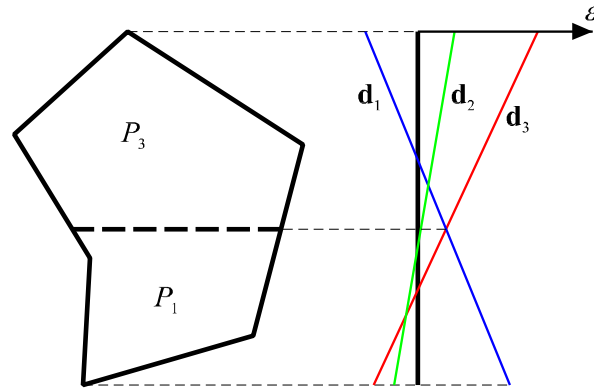


Figure 5.2: Partition of the section according to the previously attained maximum strain

In particular,  $P_1$  is the portion of the section where the maximum strain is attained when  $\mathbf{d}_1$  acts on the section. The maximum strain on  $P_1$  is, thus, given by:

$$\varepsilon_{m1} = \varepsilon_1 + \mathbf{g}_1 \cdot \mathbf{r} \quad \text{with} \quad \mathbf{d}_1^T = \{\varepsilon_1, g_{x1}, g_{y1}\} \quad (5.3)$$

Similarly  $P_3$  is the partition where  $\mathbf{d}_3$  maximizes the strain:

$$\varepsilon_{m3} = \varepsilon_3 + \mathbf{g}_3 \cdot \mathbf{r} \quad \text{with} \quad \mathbf{d}_3^T = \{\varepsilon_3, g_{x3}, g_{y3}\} \quad (5.4)$$

Conversely,  $\mathbf{d}_2$  does not maximize the strain at any point of the section, thus there is no partition related to it.

Since the values of the maximum strain are given for each partition, the stress-strain law is determined with a unique non-linear expression which is a function of the current strain  $\varepsilon$ , as shown in figure 5.3, where the case of the partition  $P_3$  is considered.

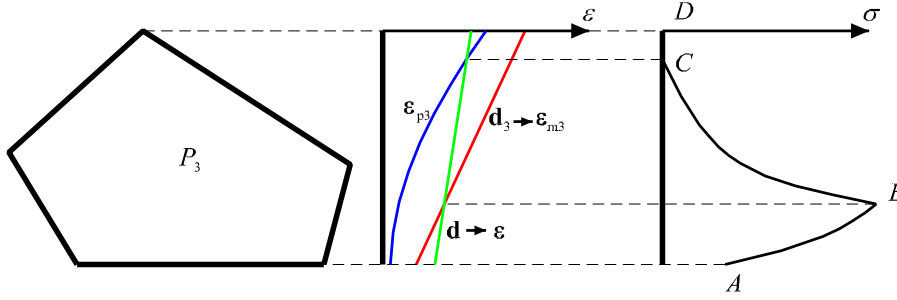


Figure 5.3: Stresses on partition  $P_3$

The maximum strain  $\varepsilon_{m3}$  is given, thus the value of the plastic strain  $\varepsilon_{p3}$  is evaluated by means of the relation  $\varepsilon_p = \varepsilon_p(\varepsilon_m)$ . If, at the generic point P, the current strain  $\varepsilon$  attains values greater than the ones given by  $\varepsilon_{m3}$  the stress at P will follow the envelope curve of the material stress-strain law. Such behaviour is shown by the curve AB in figure 5.3.

Similarly, the strain is decreasing at the points of the section where  $\varepsilon_{p3} < \varepsilon < \varepsilon_{m3}$  thus the stress is evaluated according to the unloading-reloading behaviour of the material. The curve BC in figure 5.3 shows such behaviour.

Finally, the points where  $\varepsilon < \varepsilon_{p3}$  are completely unloaded and the stress is null as shown in figure 5.3 between the points C and D.

Since each of the paths AB, BC and CD is determined by means of a unique expression containing the value attained by  $\varepsilon_{m3}$ ,  $\varepsilon_{p3}$  and  $\varepsilon$ , the integration formulas described in chapter 4 can be applied for the evaluation of the force vector and the stiffness matrix of a section in which the material model of figure 5.1 is considered.

To fix the ideas the application of the procedure above will be illustrated in the following sections for a general class of non-linear stress-strain laws which can be set in the form:

$$\sigma(\varepsilon, \varepsilon_m) = \varepsilon h(\varepsilon_m) + k(\varepsilon_m) + l(\varepsilon) \quad (5.5)$$

Significant examples belonging to this class are a bilinear stress-strain law with no-tensile strength, see section 5.3, and the Mander's envelope curve discussed in section 5.4.

The case of a single partition will be considered, thus the maximum strain  $\varepsilon_m$  is given by:

$$\varepsilon_m(\mathbf{r}) = \epsilon_m + \mathbf{g}_m \cdot \mathbf{r} \quad (5.6)$$

the plastic strain is evaluated as a function of  $\varepsilon_m$ :

$$\varepsilon_p(\mathbf{r}) = \varepsilon_p[\varepsilon_m(\mathbf{r})] \quad (5.7)$$

and the current strain is evaluated as:

$$\varepsilon(\mathbf{r}) = \epsilon + \mathbf{g} \cdot \mathbf{r} \quad (5.8)$$

## 5.1 Partition of the section

The partition of the section is a procedure which we refer to in order to divide polygonal sections. Hereafter we are going to illustrate how the coordinates of the vertices of the partitions are determined and how their derivatives with respect to the strain parameters  $\epsilon$  and  $\mathbf{g}$  are evaluated.

We remind that a Cartesian co-ordinate system with origin  $O$  and axes  $x$  and  $y$  lying on the plane of the cross section is introduced. The points of the plane  $x - y$  are identified by means of the relevant position vector  $\mathbf{r} = (x, y)^T$ . One or more polygonal domains  $\Omega$  are defined by means of their vertices  $\mathbf{r}_i$  ordered counter-clockwise as shown in figure 5.4.

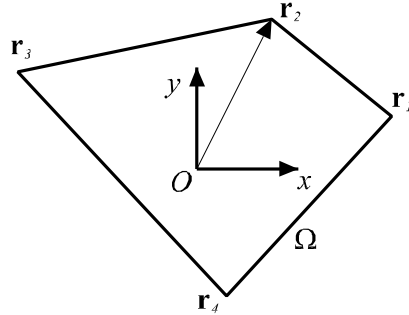


Figure 5.4: Polygonal section

A strain field  $\varepsilon(\mathbf{r})$  is defined on the polygonal domain such that:

$$\varepsilon(\mathbf{r}) = \epsilon + \mathbf{g} \cdot \mathbf{r} \quad (5.9)$$

Also one or two auxiliary strain fields  $\varepsilon_a(\mathbf{r})$  with  $a = 1, 2$  are defined on the polygons and are evaluated as:

$$\varepsilon_a(\mathbf{r}) = \epsilon_a + \mathbf{g}_a \cdot \mathbf{r} \quad (5.10)$$

The problem we want solve here is that of evaluating the vertices of a sub-domain  $\Omega_p$  of the polygon  $\Omega$  according to definitions of the kind:

$$\Omega_{p1} = \{\mathbf{r} \in \Omega : \varepsilon_1(\mathbf{r}) \leq \varepsilon(\mathbf{r})\} \quad (5.11)$$

$$\Omega_{p2} = \{\mathbf{r} \in \Omega : \varepsilon(\mathbf{r}) \leq \varepsilon_2(\mathbf{r})\} \quad (5.12)$$

or:

$$\Omega_{p3} = \{\mathbf{r} \in \Omega : \varepsilon_1(\mathbf{r}) \leq \varepsilon(\mathbf{r}) \leq \varepsilon_2(\mathbf{r})\} \quad (5.13)$$

Three possible partitions  $\Omega_{p1}$ ,  $\Omega_{p2}$  and  $\Omega_{p3}$  are shown in figure 5.5.

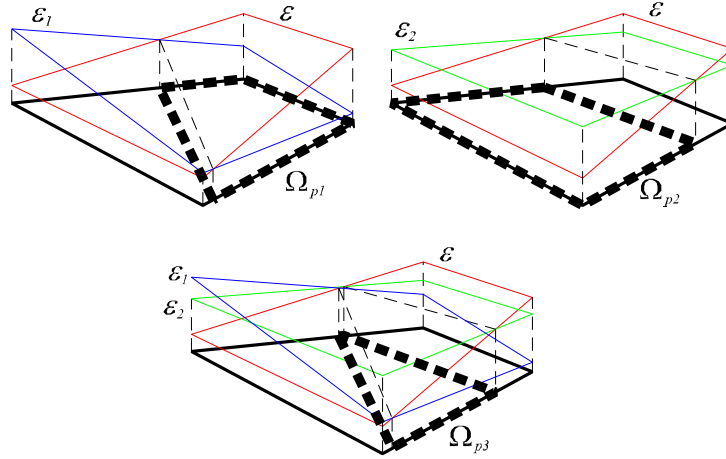


Figure 5.5: Example of three partitions

Let us consider, for instance, the case of equation (5.11), so that the vertices of the partition  $\Omega_{p1}$  need to be determined. As it can be seen in the figure, the vertices of each partition always pertain to the sides of the original section  $\Omega$ ; thus a loop over each side of the section is executed.

At the generic loop the  $i$ -th side, i.e. the one with endpoints  $\mathbf{r}_i$  and  $\mathbf{r}_{i+1}$ , is considered. Clearly, the vertex  $\mathbf{r}_i$  of  $\Omega$  is also a vertex of the partition  $\Omega_{p1}$  if  $\varepsilon_1(\mathbf{r}_i) \leq \varepsilon(\mathbf{r}_i)$ .

Since the components of  $\mathbf{r}_i$  do not depend upon  $\epsilon$  and  $\mathbf{g}$  the following relations hold:

$$\frac{\partial \mathbf{r}_i}{\partial \epsilon} = 0; \quad \frac{\partial \mathbf{r}_i}{\partial \mathbf{g}} = \mathbf{0} \quad (5.14)$$

At the successive loop step the  $i + 1$ -st side, i.e. the one with endpoints  $\mathbf{r}_{i+1}$  and  $\mathbf{r}_{i+2}$ , is considered. Consequently, in the procedure described above, the vertices  $\mathbf{r}_{i+1}$  and  $\mathbf{r}_{i+2}$  will take the place of the vertices  $\mathbf{r}_i$  and  $\mathbf{r}_{i+1}$ , respectively. The inequality  $\epsilon_1(\mathbf{r}_{i+1}) \leq \epsilon(\mathbf{r}_{i+1})$ , which has to be checked in order to include  $\mathbf{r}_{i+1}$  between the vertices of  $\Omega_{p1}$ , will be taken into account only at the loop step relevant to the  $i + 1$ -st side.

Also another vertex of  $\Omega_{p1}$  might lie on the side  $\mathbf{r}_i - \mathbf{r}_{i+1}$ , as shown in figure 5.6. Such a new vertex, namely  $\mathbf{r}_c$ , is associated with the intersection

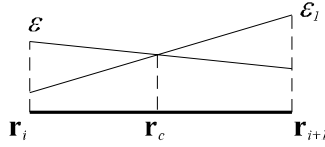


Figure 5.6: Vertex  $\mathbf{r}_c$  on the  $i$ -th side.

between  $\epsilon(\mathbf{r})$  and  $\epsilon_1(\mathbf{r})$ . Its co-ordinates are evaluated by means of the procedure described hereafter.

The segment which connects the points  $\mathbf{r}_i$  and  $\mathbf{r}_{i+1}$ , i.e. the  $i$ -th side of the section, is described by means of a parametric function:

$$\mathbf{r}(\vartheta) = \mathbf{r}_i + \vartheta(\mathbf{r}_{i+1} - \mathbf{r}_i) \quad (5.15)$$

with  $0 \leq \vartheta \leq 1$ .

The composition of  $\epsilon(\mathbf{r})$  and  $\epsilon_1(\mathbf{r})$  with  $\mathbf{r}(\vartheta)$  yields:

$$\epsilon[\mathbf{r}(\vartheta)] = \epsilon(\mathbf{r}_i) + \vartheta[\epsilon(\mathbf{r}_{i+1}) - \epsilon(\mathbf{r}_i)] \quad (5.16)$$

and

$$\epsilon_1[\mathbf{r}(\vartheta)] = \epsilon_1(\mathbf{r}_i) + \vartheta[\epsilon_1(\mathbf{r}_{i+1}) - \epsilon_1(\mathbf{r}_i)] \quad (5.17)$$

The value of  $\vartheta$  corresponding to the position of  $\mathbf{r}_c$  is evaluated by setting  $\epsilon[\mathbf{r}(\vartheta)] = \epsilon_1[\mathbf{r}(\vartheta)]$  which yields:

$$\vartheta_c = \frac{\epsilon_1(\mathbf{r}_i) - \epsilon(\mathbf{r}_i)}{\epsilon_1(\mathbf{r}_i) - \epsilon_1(\mathbf{r}_{i+1}) + \epsilon(\mathbf{r}_{i+1}) - \epsilon(\mathbf{r}_i)} \quad (5.18)$$

thus,  $\mathbf{r}_c$  is a vertex of the partition only if  $0 < \vartheta_c < 1$ . It is worth being noticed that if the denominator of formula (5.18) tends to zero,  $\vartheta_c$  goes to infinity and  $\mathbf{r}_c$  is not a vertex of the partition.

Conversely, in the case  $0 < \vartheta_c < 1$  is satisfied, the components of  $\mathbf{r}_c$  are evaluated by means of formula (5.15):

$$\mathbf{r}_c = \mathbf{r}_i + \vartheta_c(\mathbf{r}_{i+1} - \mathbf{r}_i) \quad (5.19)$$

The derivatives of  $\mathbf{r}_c$  with respect to  $\epsilon$  and  $\mathbf{g}$  are evaluated by differentiating equation (5.19):

$$\frac{\partial \mathbf{r}_c}{\partial \epsilon} = (\mathbf{r}_{i+1} - \mathbf{r}_i) \frac{\partial \vartheta_c}{\partial \epsilon}; \quad \frac{\partial \mathbf{r}_c}{\partial \mathbf{g}} = (\mathbf{r}_{i+1} - \mathbf{r}_i) \frac{\partial \vartheta_c}{\partial \mathbf{g}} \quad (5.20)$$

where  $\partial \vartheta_c / \partial \epsilon$  and  $\partial \vartheta_c / \partial \mathbf{g}$  are evaluated by differentiating equation (5.18).

Since the strain field  $\varepsilon_1(\mathbf{r})$  does not depend upon the strain parameters of  $\varepsilon(\mathbf{r})$  it turns out to be:

$$\frac{\partial \varepsilon_1(\mathbf{r}_i)}{\partial \epsilon} = \frac{\partial \varepsilon_1(\mathbf{r}_{i+1})}{\partial \epsilon} = 0 \quad (5.21)$$

and

$$\frac{\partial \varepsilon_1(\mathbf{r}_i)}{\partial \mathbf{g}} = \frac{\partial \varepsilon_1(\mathbf{r}_{i+1})}{\partial \mathbf{g}} = \mathbf{0} \quad (5.22)$$

Conversely, as we have shown in section 4.2 and making use of formulas (5.14):

$$\frac{\partial \varepsilon(\mathbf{r}_i)}{\partial \epsilon} = \frac{\partial \varepsilon(\mathbf{r}_{i+1})}{\partial \epsilon} = 1 \quad (5.23)$$

and

$$\frac{\partial \varepsilon(\mathbf{r}_i)}{\partial \mathbf{g}} = \mathbf{r}_i; \quad \frac{\partial \varepsilon(\mathbf{r}_{i+1})}{\partial \mathbf{g}} = \mathbf{r}_{i+1} \quad (5.24)$$

Thus, differentiating equation (5.18) we get:

$$\frac{\partial \vartheta_c}{\partial \epsilon} = - \frac{1}{\varepsilon_1(\mathbf{r}_i) - \varepsilon_1(\mathbf{r}_{i+1}) + \varepsilon(\mathbf{r}_{i+1}) - \varepsilon(\mathbf{r}_i)} \quad (5.25)$$

and

$$\frac{\partial \vartheta_c}{\partial \mathbf{g}} = \frac{[\varepsilon_1(\mathbf{r}_{i+1}) - \varepsilon(\mathbf{r}_{i+1})]\mathbf{r}_i - [\varepsilon_1(\mathbf{r}_i) - \varepsilon(\mathbf{r}_i)]\mathbf{r}_{i+1}}{\varepsilon_1(\mathbf{r}_i) - \varepsilon_1(\mathbf{r}_{i+1}) + \varepsilon(\mathbf{r}_{i+1}) - \varepsilon(\mathbf{r}_i)} \quad (5.26)$$

After the components of  $\mathbf{r}_c$  and its derivatives have been determined the next side of  $\Omega$  is analyzed. Such new side is the one between  $\mathbf{r}_{i+1}$  and  $\mathbf{r}_{i+2}$ .

These two endpoints will take the place of  $\mathbf{r}_i$  and  $\mathbf{r}_{i+1}$ , respectively, in the procedure described above.

Finally we remark that for the determination of a partition of the kind of  $\Omega_{p2}$ , i.e. when the inequality  $\varepsilon(\mathbf{r}) \leq \varepsilon_2(\mathbf{r})$  is considered, we adopt the same procedure described above. The only difference is that, in order to include  $\mathbf{r}_i$  between the vertices of the partition, one has to check  $\varepsilon_2(\mathbf{r}_i) \geq \varepsilon(\mathbf{r}_i)$  in place of  $\varepsilon_1(\mathbf{r}_i) \leq \varepsilon(\mathbf{r}_i)$ .

Finally, partitions of the kind of  $\Omega_{p3}$  can be obtained by means of an intersection between the partitions  $\Omega_{p1}$  and  $\Omega_{p2}$ , since the following relations hold:

$$\begin{aligned}\Omega_{p3} &= \{\mathbf{r} \in \Omega : \varepsilon_1(\mathbf{r}) \leq \varepsilon(\mathbf{r}) \leq \varepsilon_2(\mathbf{r})\} = \\ &= \{\mathbf{r} \in \Omega_{p1} : \varepsilon(\mathbf{r}) \leq \varepsilon_2(\mathbf{r})\} = \\ &= \{\mathbf{r} \in \Omega_{p2} : \varepsilon_1(\mathbf{r}) \leq \varepsilon(\mathbf{r})\}\end{aligned}\quad (5.27)$$

Consequently,  $\Omega_{p3}$  can be obtained applying twice the procedure described above.

## 5.2 Integration of inelastic stress-strain laws and relevant derivatives

Let us consider stress-strain relations which are expressed in the form:

$$\sigma(\varepsilon, \varepsilon_m) = \varepsilon h(\varepsilon_m) + k(\varepsilon_m) + l(\varepsilon) \quad (5.28)$$

where the functions  $h(\varepsilon_m)$ ,  $k(\varepsilon_m)$  and  $l(\varepsilon)$  are determined according to the considered material model.

The strains  $\varepsilon$  and  $\varepsilon_m$  are expressed by means of the following linear functions:

$$\varepsilon(\mathbf{r}) = \varepsilon + \mathbf{g} \cdot \mathbf{r}; \quad \varepsilon_m(\mathbf{r}) = \varepsilon_m + \mathbf{g}_m \cdot \mathbf{r} \quad (5.29)$$

where  $\mathbf{r}$  is the vector containing the coordinates of the points of the section  $\Omega$  in the considered reference system.

Substitution of  $\varepsilon(\mathbf{r})$  in (5.28) yields:

$$\sigma(\varepsilon, \varepsilon_m) = \varepsilon h(\varepsilon_m) + h(\varepsilon_m) \mathbf{g} \cdot \mathbf{r} + k(\varepsilon_m) + l(\varepsilon) \quad (5.30)$$

With reference to the function  $\sigma(\varepsilon, \varepsilon_m)$  of the last equation, the following integrals need to be evaluated:

$$N[\sigma(\varepsilon, \varepsilon_m)] = \int_{\Omega} \sigma(\varepsilon, \varepsilon_m) d\Omega; \quad \mathbf{m}^{\perp}[\sigma(\varepsilon, \varepsilon_m)] = \int_{\Omega} \sigma(\varepsilon, \varepsilon_m) \mathbf{r} d\Omega \quad (5.31)$$

Substituting (5.30) in the first integral above one gets:

$$\begin{aligned}
 N[\sigma(\varepsilon, \varepsilon_m)] &= \epsilon \int_{\Omega} h(\varepsilon_m) d\Omega + \mathbf{g} \cdot \left[ \int_{\Omega} h(\varepsilon_m) \mathbf{r} d\Omega \right] + \int_{\Omega} k(\varepsilon_m) d\Omega + \\
 &+ \int_{\Omega} l(\varepsilon) d\Omega = \\
 &= \epsilon N[h(\varepsilon_m)] + \mathbf{g} \cdot \mathbf{m}^{\perp}[h(\varepsilon_m)] + N[k(\varepsilon_m)] + N[l(\varepsilon)]
 \end{aligned} \tag{5.32}$$

where the relevant formulas of section 4.1 are used.

Differentiation of equation (5.32) with respect to  $\epsilon$  yields:

$$\begin{aligned}
 N_{,\epsilon}[\sigma(\varepsilon, \varepsilon_m)] &= N[h(\varepsilon_m)] + \epsilon N_{,\epsilon}[h(\varepsilon_m)] + \mathbf{g} \cdot \mathbf{m}_{,\epsilon}^{\perp}[h(\varepsilon_m)] + \\
 &+ N_{,\epsilon}[k(\varepsilon_m)] + N_{,\epsilon}[l(\varepsilon)]
 \end{aligned} \tag{5.33}$$

where the derivatives  $N_{,\epsilon}[h(\varepsilon_m)]$ ,  $\mathbf{m}_{,\epsilon}^{\perp}[h(\varepsilon_m)]$  and  $N_{,\epsilon}[k(\varepsilon_m)]$  are evaluated by means of the same formulas used for  $N_{,\epsilon}[l(\varepsilon)]$ , reported in section 4.2, in which one has to account for the fact that  $\varepsilon_m$  is independent of  $\epsilon$ .

Similarly the derivative of  $N[\sigma(\varepsilon, \varepsilon_m)]$  with respect to  $\mathbf{g}$  is:

$$\begin{aligned}
 N_{,\mathbf{g}}[\sigma(\varepsilon, \varepsilon_m)] &= \epsilon N_{,\mathbf{g}}[h(\varepsilon_m)] + \mathbf{m}^{\perp}[h(\varepsilon_m)] + \{\mathbf{m}_{,\mathbf{g}}^{\perp}[h(\varepsilon_m)]\}^T \mathbf{g} + \\
 &+ N_{,\mathbf{g}}[k(\varepsilon_m)] + N_{,\mathbf{g}}[l(\varepsilon)]
 \end{aligned} \tag{5.34}$$

in which the formulas reported in sections 4.1 and 4.2 are again used with the proviso that  $\varepsilon_m$  is not related to  $\mathbf{g}$ .

Substitution of (5.30) in (5.31)<sub>2</sub> yields:

$$\begin{aligned}
 \mathbf{m}^{\perp}[\sigma(\varepsilon, \varepsilon_m)] &= \epsilon \int_{\Omega} h(\varepsilon_m) \mathbf{r} d\Omega + \left[ \int_{\Omega} h(\varepsilon_m) (\mathbf{r} \otimes \mathbf{r}) d\Omega \right] \mathbf{g} + \\
 &+ \int_{\Omega} k(\varepsilon_m) \mathbf{r} d\Omega + \int_{\Omega} l(\varepsilon) \mathbf{r} d\Omega = \\
 &= \epsilon \mathbf{m}^{\perp}[h(\varepsilon_m)] + \mathbf{B}[h(\varepsilon_m)] \mathbf{g} + \mathbf{m}^{\perp}[k(\varepsilon_m)] + \mathbf{m}^{\perp}[l(\varepsilon)]
 \end{aligned} \tag{5.35}$$

The derivative of  $\mathbf{m}^{\perp}[\sigma(\varepsilon, \varepsilon_m)]$  with respect to  $\epsilon$  yields:

$$\begin{aligned}
 \mathbf{m}_{,\epsilon}^{\perp}[\sigma(\varepsilon, \varepsilon_m)] &= \mathbf{m}^{\perp}[h(\varepsilon_m)] + \epsilon \mathbf{m}_{,\epsilon}^{\perp}[h(\varepsilon_m)] + \mathbf{B}_{,\epsilon}[h(\varepsilon_m)] \mathbf{g} + \\
 &+ \mathbf{m}_{,\epsilon}^{\perp}[k(\varepsilon_m)] + \mathbf{m}_{,\epsilon}^{\perp}[l(\varepsilon)]
 \end{aligned} \tag{5.36}$$

Finally differentiating equation (5.35) with respect to  $\mathbf{g}$  one gets:

$$\begin{aligned}
 \mathbf{m}_{,\mathbf{g}}^{\perp}[\sigma(\varepsilon, \varepsilon_m)] &= \epsilon \mathbf{m}_{,\mathbf{g}}^{\perp}[h(\varepsilon_m)] + \mathbf{B}[h(\varepsilon_m)] + \{\mathbf{B}_{,\mathbf{g}}[h(\varepsilon_m)]\}^T \mathbf{g} + \\
 &+ \mathbf{m}_{,\mathbf{g}}^{\perp}[k(\varepsilon_m)] + \mathbf{m}_{,\mathbf{g}}^{\perp}[l(\varepsilon)]
 \end{aligned} \tag{5.37}$$

where the third order tensor  $(\mathbf{B}, \mathbf{g})^T$  is expressed in index notation as:

$$\left[ (\mathbf{B}, \mathbf{g})^T \right]_{jlk} = (\mathbf{B}, \mathbf{g})_{jkl} = B_{jk,l} \quad (5.38)$$

Again, in equations (5.35), (5.36) and (5.37) the relevant formulas in sections 4.1 and 4.2 are used and, when appropriate, the independence between  $\varepsilon_m$  and the two parameters  $\varepsilon$  and  $\mathbf{g}$  has to be taken into account.

### 5.3 Inelastic bilinear stress-strain law with no tensile strength

Let us consider the case of the material model described in Figure 5.7 with the assumption that compressive stresses and strains are positive. The envelope curve OABC is bilinear. Once the strain reaches its maximum compressive value, i.e. point B, an unloading will follow the path BD. Further unloading will not produce any stress increment since the material does not have any tensile strength. Finally successive reloading is assumed to take place along the curve ODBC.

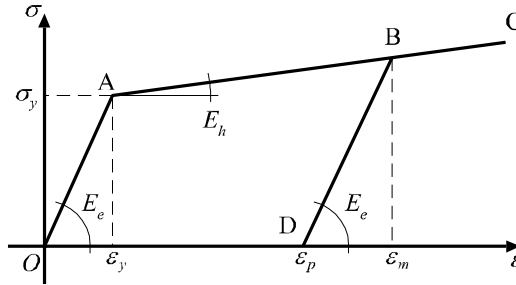


Figure 5.7: bilinear material model with no tension strength

The envelope curve (OABC) has the following analytical expression:

$$e(\varepsilon) = \begin{cases} 0 & \text{if } \varepsilon \leq 0 \\ E_e \varepsilon & \text{if } 0 \leq \varepsilon \leq \varepsilon_y \\ (E_e - E_h)\varepsilon_y + E_h \varepsilon & \text{if } \varepsilon_y \leq \varepsilon \end{cases} \quad (5.39)$$

where  $\varepsilon_y$  is the yielding strain. The elastic stiffness is  $E_e$  and the hardening is  $E_h$ .

When the strain  $\varepsilon$  reaches values beyond the yielding strain  $\varepsilon_y$ , up to the maximum compressive strain  $\varepsilon_m$ , a plastic strain  $\varepsilon_p$  is produced. Accordingly, there will be a part of the section, namely  $\Omega_1$ , where the maximum

### 5.3 Inelastic bilinear stress-strain law with no tensile strength 127

compressive strain has never reached values beyond the yielding strain in compression, and where no plastic strain has been ever produced. Conversely, on the remaining part of the section, i.e.  $\Omega_2$ , the maximum compressive strain is  $\varepsilon_m \geq \varepsilon_y$ , hence the value of  $\varepsilon_p$  is not null on  $\Omega_2$  as prompts from the next formula:

$$\varepsilon_p[\varepsilon_m(\mathbf{r})] = \begin{cases} 0 & \text{on } \Omega_1 \\ [\varepsilon_m(\mathbf{r}) - \varepsilon_y] \left(1 - \frac{E_h}{E_e}\right) & \text{on } \Omega_2 \end{cases} \quad (5.40)$$

The two sub domains  $\Omega_1$  and  $\Omega_2$  are determined by means of the procedure described in the section 5.1 with the strain limits reported in the following equation:

$$\Omega = \begin{cases} \Omega_1 = \{\mathbf{r} \in \Omega : \varepsilon_m(\mathbf{r}) \leq \varepsilon_y\} \\ \Omega_2 = \{\mathbf{r} \in \Omega : \varepsilon_y \leq \varepsilon_m(\mathbf{r})\} \end{cases} \quad (5.41)$$

Notice that the vertices of such partitions do not depend upon the current strain  $\varepsilon$ , so that their derivatives with respect to  $\varepsilon$  and  $\mathbf{g}$  are zero.

While  $\varepsilon_p$  is null on  $\Omega_1$ , the plastic strain  $\varepsilon_p$  is a linear function of  $\mathbf{r}$  when  $\mathbf{r} \in \Omega_2$ :

$$\varepsilon_p = \varepsilon_p + \mathbf{g}_p \cdot \mathbf{r} \quad (5.42)$$

the strain parameters  $\varepsilon_p$  and  $\mathbf{g}_p$  are determined from (5.40)<sub>2</sub> as:

$$\varepsilon_p = (\varepsilon_m - \varepsilon_y) \left(1 - \frac{E_h}{E_e}\right) \quad \mathbf{g}_p = \mathbf{g}_m \left(1 - \frac{E_h}{E_e}\right) \quad (5.43)$$

Clearly, since the plastic strain is null on  $\Omega_1$ , the points of such partition have a behavior that follows the envelope curve  $e(\varepsilon)$ :

$$\sigma_1(\varepsilon, \varepsilon_m) = e(\varepsilon) \quad (5.44)$$

Conversely, the stress at a point of the partition  $\Omega_2$  is a function of the values attained by  $\varepsilon$ ,  $\varepsilon_m$  and  $\varepsilon_p$ :

$$\sigma(\varepsilon, \varepsilon_m) = \begin{cases} 0 & \text{on } \Omega_{2a} \\ \frac{e(\varepsilon_m)}{\varepsilon_m - \varepsilon_p(\varepsilon_m)} [\varepsilon - \varepsilon_p(\varepsilon_m)] & \text{on } \Omega_{2b} \\ e(\varepsilon) & \text{on } \Omega_{2c} \end{cases} \quad (5.45)$$

where  $e(\varepsilon_m)$  is given by equation (5.39) with  $\varepsilon_m$  used in place of  $\varepsilon$ . A further partition of the domain  $\Omega_2$  has been introduced as follows:

$$\Omega_2 = \begin{cases} \Omega_{2a} = \{\mathbf{r} \in \Omega_2 : \varepsilon(\mathbf{r}) \leq \varepsilon_p[\varepsilon_m(\mathbf{r})]\} \\ \Omega_{2b} = \{\mathbf{r} \in \Omega_2 : \varepsilon_p[\varepsilon_m(\mathbf{r})] \leq \varepsilon(\mathbf{r}) \leq \varepsilon_m(\mathbf{r})\} \\ \Omega_{2c} = \{\mathbf{r} \in \Omega_2 : \varepsilon_m(\mathbf{r}) \leq \varepsilon(\mathbf{r})\} \end{cases} \quad (5.46)$$

### 5.3.1 Determination of the functions $h(\varepsilon_m)$ , $k(\varepsilon_m)$ and $l(\varepsilon)$

The goal of this section is that of re-writing the stress-strain law described above by means of a unique expression of the kind of equation (5.28) so as to make it integrable by means of the formulas of section 5.2.

On the partition  $\Omega_1$  the stress-strain relation is coincident with the envelope curve, so that the functions  $h(\varepsilon_m)$  and  $k(\varepsilon_m)$  of equation (5.28) have to assume a null value while  $l(\varepsilon) = e(\varepsilon)$ .

The stress-strain law is identically null on  $\Omega_{2a}$ ; thus, on such domain, the functions  $h(\varepsilon_m)$ ,  $k(\varepsilon_m)$  and  $l(\varepsilon)$  are null too.

Substitution of (5.40)<sub>2</sub> in (5.86)<sub>2</sub> yields the stress-strain relation on  $\Omega_{2b}$ , that is:

$$\begin{aligned} \sigma_{2b}(\varepsilon, \varepsilon_m) &= \frac{e(\varepsilon_m)}{\varepsilon_m - (\varepsilon_m - \varepsilon_y) \left(1 - \frac{E_h}{E_e}\right)} \left[ \varepsilon - (\varepsilon_m - \varepsilon_y) \left(1 - \frac{E_h}{E_e}\right) \right] = \\ &= \frac{E_e e(\varepsilon_m) \varepsilon}{E_h(\varepsilon_m - \varepsilon_y) + E_e \varepsilon_y} + \frac{(E_h - E_e)(\varepsilon_m - \varepsilon_y) e(\varepsilon_m)}{E_h(\varepsilon_m - \varepsilon_y) + E_e \varepsilon_y} = \\ &= \varepsilon h_{2b}(\varepsilon_m) + k_{2b}(\varepsilon_m) \end{aligned} \quad (5.47)$$

Finally the stress-strain law on  $\Omega_{2c}$  does not depend upon  $\varepsilon_p$  and  $\varepsilon_m$ ; hence, the functions  $h(\varepsilon_m)$  and  $k(\varepsilon_m)$  assume null values on such domains. Conversely the function  $l(\varepsilon)$  is equal to the envelope curve on  $\Omega_{2c}$  and is null everywhere else.

As a result we can write the stress strain relation on  $\Omega$  as:

$$\sigma(\varepsilon, \varepsilon_m) = \varepsilon h(\varepsilon_m) + k(\varepsilon_m) + l(\varepsilon) \quad (5.48)$$

where:

$$h(\varepsilon_m) = \begin{cases} 0 & \text{on } \Omega_1, \Omega_{2a} \text{ and } \Omega_{2c} \\ \frac{E_e e(\varepsilon_m)}{E_h(\varepsilon_m - \varepsilon_y) + E_e \varepsilon_y} & \text{on } \Omega_{2b} \end{cases} \quad (5.49)$$

### 5.3 Inelastic bilinear stress-strain law with no tensile strength 129

$$k(\varepsilon_m) = \begin{cases} 0 & \text{on } \Omega_1, \Omega_{2a} \text{ and } \Omega_{2c} \\ \frac{(E_h - E_e)(\varepsilon_m - \varepsilon_y)e(\varepsilon_m)}{E_h(\varepsilon_m - \varepsilon_y) + E_e\varepsilon_y} & \text{on } \Omega_{2b} \end{cases} \quad (5.50)$$

and:

$$l(\varepsilon) = \begin{cases} 0 & \text{on } \Omega_{2a} \text{ and } \Omega_{2b} \\ e(\varepsilon) & \text{on } \Omega_1 \text{ and } \Omega_{2c} \end{cases} \quad (5.51)$$

#### Primitives of $h(\varepsilon_m)$ and its derivative

The primitives of the function  $h(\varepsilon_m)$ , up to the fourth order, and its first derivative are used in chapter 4 and in section 5.2 in order to evaluate the stress resultants and their derivatives. Hereafter we are going to furnish an expression of such functions over each of the partitions considered in the section 5.3.

As shown in section 5.3.1 the function  $h(\varepsilon_m)$  assumes a null value on the domains  $\Omega_1$ ,  $\Omega_{2a}$  and  $\Omega_{2c}$ ; hence the primitives of  $h(\varepsilon_m)$  and its derivative are identically null in such domains.

The expression of  $h(\varepsilon_m)$  on  $\Omega_{2b}$  is obtained from equation (5.88). Substitution of (5.39) in (5.88) yields:

$$h_{2b}(\varepsilon_m) = \frac{E_e e(\varepsilon_m)}{E_h(\varepsilon_m - \varepsilon_y) + E_e \varepsilon_y} = \begin{cases} 0 & \text{if } \varepsilon_m \leq 0 \\ \frac{E_e^2 \varepsilon_m}{E_h(\varepsilon_m - \varepsilon_y) + E_e \varepsilon_y} & \text{if } 0 \leq \varepsilon_m \leq \varepsilon_y \\ E_e & \text{if } \varepsilon_y \leq \varepsilon_m \end{cases} \quad (5.52)$$

For  $0 \leq \varepsilon_m \leq \varepsilon_y$  the first order primitives of  $h_{2b}(\varepsilon_m)$  up to the fourth order are:

$$h_{2b_1}^{(1)}(\varepsilon_m) = -\frac{E_e^2 \left[ (E_e - E_h) \varepsilon_y \log(E_h \varepsilon_m + E_e \varepsilon_y - E_h \varepsilon_y) - E_h \varepsilon_m \right]}{E_h^2} \quad (5.53)$$

$$h_{2b_1}^{(2)}(\varepsilon_m) = \frac{-E_e^2}{2E_h^3} \left\{ -\{E_h \varepsilon_m [E_h(\varepsilon_m - 2\varepsilon_y) + 2E_e \varepsilon_y]\} + 2(E_e - E_h) \varepsilon_y [E_h(\varepsilon_m - \varepsilon_y) + E_e \varepsilon_y] \log(E_h \varepsilon_m + E_e \varepsilon_y - E_h \varepsilon_y) \right\} \quad (5.54)$$

$$\begin{aligned}
h_{2b_1}^{(3)}(\varepsilon_m) = & \frac{-E_e^2}{12E_h^4} \left\{ - \{ E_h \varepsilon_m [ 3E_e E_h (3\varepsilon_m - 4\varepsilon_y) \varepsilon_y + 6E_e^2 \varepsilon_y^2 + \right. \\
& + E_h^2 (2\varepsilon_m^2 - 9\varepsilon_m \varepsilon_y + 6\varepsilon_y^2) \} + 6(E_e - E_h) \varepsilon_y [ E_h (\varepsilon_m - \varepsilon_y) + \\
& \left. + E_e \varepsilon_y ]^2 \log(E_h \varepsilon_m + E_e \varepsilon_y - E_h \varepsilon_y) \right\} \quad (5.55)
\end{aligned}$$

$$\begin{aligned}
h_{2b_1}^{(4)}(\varepsilon_m) = & \frac{E_e^2}{72E_h^5} \{ 3E_h^4 \varepsilon_m^4 - 22E_h^3 (E_h - E_e) \varepsilon_m^3 \varepsilon_y + \\
& + 30(E_e - E_h)^2 E_h^2 \varepsilon_m^2 \varepsilon_y^2 - 12E_h (E_h - E_e)^3 \varepsilon_m \varepsilon_y^3 + \\
& - 12(E_e - E_h)^4 \varepsilon_y^4 \log(E_h \varepsilon_m + E_e \varepsilon_y - E_h \varepsilon_y) + \\
& + 12E_h (E_h - E_e) \varepsilon_m \varepsilon_y [ 3E_e E_h (\varepsilon_m - 2\varepsilon_y) \varepsilon_y + 3E_e^2 \varepsilon_y^2 + \\
& + E_h^2 (\varepsilon_m^2 - 3\varepsilon_m \varepsilon_y + 3\varepsilon_y^2) ] \log(E_h \varepsilon_m + E_e \varepsilon_y - E_h \varepsilon_y) \} \quad (5.56)
\end{aligned}$$

The primitives of  $h_{2b}(\varepsilon_m)$  for  $\varepsilon_y \leq \varepsilon_m$  are reported hereafter:

$$\begin{aligned}
h_{2b_2}^{(1)}(\varepsilon_m) = & \frac{E_e}{E_h^2} \{ E_h [ E_h (\varepsilon_m - \varepsilon_y) + E_e \varepsilon_y ] + \\
& + E_e (E_h - E_e) \varepsilon_y \log(E_e \varepsilon_y) \} \quad (5.57)
\end{aligned}$$

$$\begin{aligned}
h_{2b_2}^{(2)}(\varepsilon_m) = & \frac{E_e}{2E_h^3} E_e \{ E_h [ E_h^2 (\varepsilon_m - \varepsilon_y)^2 + E_e E_h (2\varepsilon_m - 3\varepsilon_y) \varepsilon_y + \\
& + 2E_e^2 \varepsilon_y^2 ] - 2E_e (E_e - E_h) \varepsilon_y [ E_h (\varepsilon_m - \varepsilon_y) + E_e \varepsilon_y ] \log(E_e \varepsilon_y) \} \quad (5.58)
\end{aligned}$$

$$\begin{aligned}
h_{2b_2}^{(3)}(\varepsilon_m) = & \frac{E_e}{12E_h^4} \{ E_h [ 2E_h^3 (\varepsilon_m - \varepsilon_y)^3 + 3E_e^2 E_h (4\varepsilon_m - 5\varepsilon_y) \varepsilon_y^2 + \\
& + 6E_e^3 \varepsilon_y^3 + E_e E_h^2 \varepsilon_y (6\varepsilon_m^2 - 18\varepsilon_m \varepsilon_y + 11\varepsilon_y^2) ] + \\
& - 6E_e (E_e - E_h) \varepsilon_y [ E_h (\varepsilon_m - \varepsilon_y) + E_e \varepsilon_y ]^2 \log(E_e \varepsilon_y) \} \quad (5.59)
\end{aligned}$$

$$\begin{aligned}
h_{2b_2}^{(4)}(\varepsilon_m) = & \frac{E_e}{72E_h^5} \{ E_h [ 3E_h^4 (\varepsilon_m - \varepsilon_y)^4 + 6E_e^3 E_h (6\varepsilon_m - 7\varepsilon_y) \varepsilon_y^3 + \\
& + 12E_e^4 \varepsilon_y^4 + 2E_e^2 E_h^2 \varepsilon_y^2 (18\varepsilon_m^2 - 45\varepsilon_m \varepsilon_y + 26\varepsilon_y^2) + \\
& + E_e E_h^3 \varepsilon_y (12\varepsilon_m^3 - 54\varepsilon_m^2 \varepsilon_y + 66\varepsilon_m \varepsilon_y^2 - 25\varepsilon_y^3) ] + \\
& - 12E_e (E_e - E_h) \varepsilon_y [ E_h (\varepsilon_m - \varepsilon_y) + E_e \varepsilon_y ]^3 \log(E_e \varepsilon_y) \} \quad (5.60)
\end{aligned}$$

The constants of integration of the primitives of  $h_{2b_2}(\varepsilon_m)$  have been evaluated by solving the equations  $h_{2b_2}^{(j)}(\varepsilon_y) = h_{2b_1}^{(j)}(\varepsilon_y)$  for  $j = 1, \dots, 4$ .

Also the derivative of  $h(\varepsilon_m)$  will be used in the integration formulas described in the following sections. Notice that such derivative is used just

### 5.3 Inelastic bilinear stress-strain law with no tensile strength 131

in the cases in which the strain field  $\varepsilon_m$  is constant thus  $h'(\varepsilon_m) = h^{(-1)}(\varepsilon_m)$  is not needed to be continuous.

For  $0 \leq \varepsilon_m \leq \varepsilon_y$  the derivative of  $h_{2b_1}(\varepsilon_m)$  is:

$$h_{2b_1}^{(-1)}(\varepsilon_m) = \frac{E_e^2(E_e - E_h)\varepsilon_y}{[E_h(\varepsilon_m - \varepsilon_y) + E_e\varepsilon_y]^2} \quad (5.61)$$

and, for  $\varepsilon_y \leq \varepsilon_m$ , it is  $h_{2b_2}^{(-1)}(\varepsilon_m) = 0$ .

#### Primitives of $k(\varepsilon_m)$ and its derivative

In the same way as it has been done for  $h(\varepsilon_m)$  we will evaluate the primitives of  $k(\varepsilon_m)$  and its derivative only where  $k(\varepsilon_m) \neq 0$ , i.e. on  $\Omega_{2b}$  for  $0 \leq \varepsilon_m$ . In the other cases  $k(\varepsilon_m)$  is identically null, the constants of integration are null too what makes its derivative and primitives vanish.

The expression of  $k(\varepsilon_m)$  on  $\Omega_{2b}$  is obtained from equation (5.88). Substitution of (5.39) in (5.88) yields:

$$k_{2b}(\varepsilon_m) = \frac{(E_h - E_e)(\varepsilon_m - \varepsilon_y)e(\varepsilon_m)}{E_h(\varepsilon_m - \varepsilon_y) + E_e\varepsilon_y} = \begin{cases} 0 & \text{if } \varepsilon_m \leq 0 \\ \frac{E_e(E_h - E_e)(\varepsilon_m - \varepsilon_y)\varepsilon_m}{E_h(\varepsilon_m - \varepsilon_y) + E_e\varepsilon_y} & \text{if } 0 \leq \varepsilon_m \leq \varepsilon_y \\ (E_h - E_e)(\varepsilon_m - \varepsilon_y) & \text{if } \varepsilon_y \leq \varepsilon_m \end{cases} \quad (5.62)$$

For  $0 \leq \varepsilon_m \leq \varepsilon_y$  the primitives of  $k(\varepsilon_m)$  are:

$$k_{2b_1}^{(1)}(\varepsilon_m) = \frac{-E_e(E_e - E_h)}{2E_h^3} [E_h\varepsilon_m(E_h\varepsilon_m - 2E_e\varepsilon_y) + 2E_e(E_e - E_h)\varepsilon_y^2 \log(E_h\varepsilon_m + E_e\varepsilon_y - E_h\varepsilon_y)] \quad (5.63)$$

$$k_{2b_1}^{(2)}(\varepsilon_m) = \frac{-E_e(E_e - E_h)}{6E_h^4} \{E_h\varepsilon_m[E_h^2\varepsilon_m^2 - 6E_e^2\varepsilon_y^2 + 3E_eE_h\varepsilon_y(-\varepsilon_m + 2\varepsilon_y)] + 6E_e(E_e - E_h)\varepsilon_y^2[E_h(\varepsilon_m - \varepsilon_y) + E_e\varepsilon_y] \log(E_h\varepsilon_m + E_e\varepsilon_y - E_h\varepsilon_y)\} \quad (5.64)$$

$$k_{2b_1}^{(3)}(\varepsilon_m) = \frac{-E_e(E_e - E_h)}{24E_h^5} \{E_h\varepsilon_m[E_h^3\varepsilon_m^3 - 6E_e^2E_h(3\varepsilon_m - 4\varepsilon_y)\varepsilon_y^2 + 12E_e^3\varepsilon_y^3 - 2E_eE_h^2\varepsilon_y(2\varepsilon_m^2 - 9\varepsilon_m\varepsilon_y + 6\varepsilon_y^2)] + 12E_e(E_e - E_h)\varepsilon_y^2[E_h(\varepsilon_m - \varepsilon_y) + E_e\varepsilon_y]^2 \log(E_h\varepsilon_m + E_e\varepsilon_y - E_h\varepsilon_y)\} \quad (5.65)$$

while for  $\varepsilon_y \leq \varepsilon_m$  the primitives of  $k(\varepsilon_m)$  are:

$$k_{2b_2}^{(1)}(\varepsilon_m) = \frac{-(E_e - E_h)}{2E_h^3} \{E_h[E_h^2(\varepsilon_m - \varepsilon_y)^2 - 2E_e^2\varepsilon_y^2 + E_eE_h\varepsilon_y^2] + 2E_e^2(E_e - E_h)\varepsilon_y^2 \log(E_e\varepsilon_y)\} \quad (5.66)$$

$$k_{2b_2}^{(2)}(\varepsilon_m) = \frac{-(E_e - E_h)}{6E_h^4} \{E_h[E_h^3(\varepsilon_m - \varepsilon_y)^3 + E_eE_h^2(3\varepsilon_m - 2\varepsilon_y)\varepsilon_y^2 - 6E_e^3\varepsilon_y^3 + 3E_e^2E_h\varepsilon_y^2(-2\varepsilon_m + 3\varepsilon_y)] + 6E_e^2(E_e - E_h)\varepsilon_y^2[E_h(\varepsilon_m - \varepsilon_y) + E_e\varepsilon_y] \log(E_e\varepsilon_y)\} \quad (5.67)$$

$$k_{2b_2}^{(3)}(\varepsilon_m) = \frac{-(E_e - E_h)}{24E_h^5} \{E_h[E_h^4(\varepsilon_m - \varepsilon_y)^4 - 6E_e^3E_h(4\varepsilon_m - 5\varepsilon_y)\varepsilon_y^3 - 12E_e^4\varepsilon_y^4 + E_eE_h^3\varepsilon_y^2(6\varepsilon_m^2 - 8\varepsilon_m\varepsilon_y + 3\varepsilon_y^2) - 2E_e^2E_h^2\varepsilon_y^2(6\varepsilon_m^2 - 18\varepsilon_m\varepsilon_y + 11\varepsilon_y^2)] + 12E_e^2(E_e - E_h)\varepsilon_y^2[E_h(\varepsilon_m - \varepsilon_y) + E_e\varepsilon_y]^2 \log(E_e\varepsilon_y)\} \quad (5.68)$$

in which the integration constants have been evaluated by adopting the same strategy adopted for  $h(\varepsilon_m)$ .

Finally, for  $0 \leq \varepsilon_m \leq \varepsilon_y$  the derivative of  $k(\varepsilon_m)$  is:

$$k_{2b_1}^{(-1)}(\varepsilon_m) = \frac{E_e}{[E_h(\varepsilon_m - \varepsilon_y) + E_e\varepsilon_y]^2} [E_h^2(\varepsilon_m - \varepsilon_y)^2 + E_e^2\varepsilon_y(-2\varepsilon_m + \varepsilon_y) - E_eE_h(\varepsilon_m^2 - 4\varepsilon_m\varepsilon_y + 2\varepsilon_y^2)] \quad (5.69)$$

while for  $\varepsilon_y \leq \varepsilon_m$  it is  $k_{2b_2}^{(-1)}(\varepsilon_m) = E_h - E_e$ .

### Primitives of $l(\varepsilon)$ and its derivative

In the same way as it has been done for  $h(\varepsilon_m)$  and  $k(\varepsilon_m)$  we will evaluate the primitives of  $l(\varepsilon)$  and its derivatives only on  $\Omega_1$  and  $\Omega_{2c}$ , for  $0 \leq \varepsilon$ , where  $l(\varepsilon) = e(\varepsilon)$ . In the other cases  $l(\varepsilon)$  is identically null, the constants of integration are null too so that its derivative and its primitives are zero.

For  $0 \leq \varepsilon \leq \varepsilon_y$  the primitives of  $l(\varepsilon)$  are:

$$l_{1_1}^{(1)}(\varepsilon) = l_{2c_1}^{(1)}(\varepsilon) = \frac{E_e\varepsilon^2}{2} \quad (5.70)$$

$$l_{1_1}^{(2)}(\varepsilon) = l_{2c_1}^{(2)}(\varepsilon) = \frac{E_e\varepsilon^3}{6} \quad (5.71)$$

$$l_{1_1}^{(3)}(\varepsilon) = l_{2_{c_1}}^{(2)}(\varepsilon) = \frac{E_e \varepsilon^4}{24} \quad (5.72)$$

while for  $\varepsilon_y \leq \varepsilon$  the primitives of  $l(\varepsilon)$  are:

$$l_{1_2}^{(1)}(\varepsilon) = l_{2_{c_2}}^{(1)}(\varepsilon) = \frac{E_h(\varepsilon - \varepsilon_y)^2 + E_e(2\varepsilon - \varepsilon_y)\varepsilon_y}{2} \quad (5.73)$$

$$l_{1_2}^{(2)}(\varepsilon) = l_{2_{c_2}}^{(2)}(\varepsilon) = \frac{E_h(\varepsilon - \varepsilon_y)^3 + E_e \varepsilon_y (3\varepsilon^2 - 3\varepsilon\varepsilon_y + \varepsilon_y^2)}{6} \quad (5.74)$$

$$l_{1_2}^{(3)}(\varepsilon) = l_{2_{c_2}}^{(2)}(\varepsilon) = \frac{E_h(\varepsilon - \varepsilon_y)^4 - E_e \varepsilon_y (-4\varepsilon^3 + 6\varepsilon^2 \varepsilon_y - 4\varepsilon \varepsilon_y^2 + \varepsilon_y^3)}{24} \quad (5.75)$$

in which the integration constants have been evaluated in the same way as it has been done for  $h(\varepsilon_m)$  and  $k(\varepsilon_m)$ .

Finally, for  $0 \leq \varepsilon \leq \varepsilon_y$  the derivative of  $l(\varepsilon)$  is  $l_{1_1}^{(-1)}(\varepsilon) = l_{2_{c_1}}^{(-1)}(\varepsilon) = E_e$ , while for  $\varepsilon_y \leq \varepsilon$  it is  $l_{1_2}^{(-1)}(\varepsilon) = l_{2_{c_2}}^{(-1)}(\varepsilon) = E_h$ .

## 5.4 Inelastic stress strain law with Mander's envelope curve

The material model shown in figure 5.8 is described in this section. Still the assumption of positive stresses and strains in compression has been done. The envelope curve OABC is the one described in [61] while for the plastic behavior of the material simpler assumptions have been considered. The maximum compressive strain is determined once the material reaches the point B and starts unloading. The unloading path will take place along the segment BD. From the point D a further unloading will not produce any stress increment since the material has not any tensile strength. Finally successive reloading is assumed to take place along the curve ODBC.

The envelope curve [61] is determined by means of the following formula:

$$e(\varepsilon) = \begin{cases} 0 & \text{if } \varepsilon \leq 0 \\ \frac{r f'_{cc} \frac{\varepsilon}{\varepsilon_{cc}}}{r - 1 + \left(\frac{\varepsilon}{\varepsilon_{cc}}\right)^r} & \text{if } 0 \leq \varepsilon \leq \varepsilon_{cu} \end{cases} \quad (5.76)$$

where  $f'_{cc}$  and  $\varepsilon_{cc}$  are the confined concrete strength and the relevant strain. They are determined as function of the unconfined concrete strength  $f'_{co}$  and the relevant strain  $\varepsilon_{co}$  as:

$$f'_{cc} = f'_{co} + k_1 f_l; \quad \varepsilon_{cc} = \varepsilon_{co} \left(1 + k_2 \frac{f_l}{f'_{co}}\right) \quad (5.77)$$

where  $k_1$  and  $k_2$  are two numerical coefficients determined as a function of the concrete mix and the lateral pressure  $f_l$  due to the confinement. For a description of how to determine the parameters  $k_1$  and  $k_2$  and the lateral pressure  $f_l$  see [61].

The parameter  $r$  in (5.76) is also a function of the confinement and its value is determined as:

$$r = \frac{E_c}{E_c - E_{sec}} \quad (5.78)$$

where  $E_c$  is the tangent stiffness of concrete:

$$E_c = 5000\sqrt{f'_{co}} \text{ MPa} \quad (5.79)$$

and  $E_{sec}$  is the secant stiffness corresponding to the point of the envelope curve where the material strength is reached:

$$E_{sec} = \frac{f'_{cc}}{\varepsilon_{cc}} \quad (5.80)$$

Finally  $\varepsilon_u$  is the ultimate concrete compression strain [61]. It is defined as the longitudinal strain at which the first fracture of the hoop occurs [86], since such strain can be regarded as the end of the region of the stress-strain law in which the confinement parameters are effective. Several approaches for the determination of the value of  $\varepsilon_u$  are presented in literature. Here, we adopt a simple formula obtained by means of a simple manipulation of the formulas reported in [86] which well approximates the values obtained with more sophisticated methods:

$$\varepsilon_u = 0.004 + 0.9 \frac{f'_{cc} - f'_{co}}{300} \quad (5.81)$$

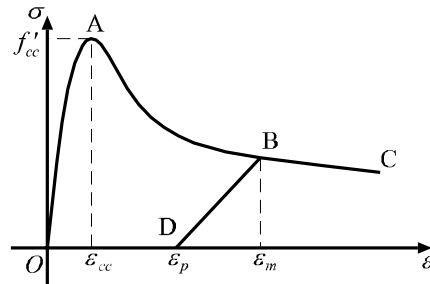


Figure 5.8: Inelastic material with Mander's envelope curve

#### 5.4 Inelastic stress strain law with Mander's envelope curve 135

where  $f'_{cc}$  and  $f'_{co}$  are expressed in MPa.

Since only positive values of  $\varepsilon_m$  will produce plastic strains we divide the section in a part  $\Omega_1$ , where  $\varepsilon_m \leq 0$  and no plastic strain is produced, and a part  $\Omega_2$ , where  $\varepsilon_m \geq 0$  and  $\varepsilon_p$  is given by means of the following formula:

$$\varepsilon_p[\varepsilon_m(\mathbf{r})] = \begin{cases} 0 & \text{on } \Omega_1 \\ \varepsilon_m - \frac{(\varepsilon_m + \varepsilon_a)e(\varepsilon_m)}{e(\varepsilon_m) + E_c \varepsilon_a} & \text{on } \Omega_2 \end{cases} \quad (5.82)$$

where

$$\varepsilon_a = a\sqrt{\varepsilon_m \varepsilon_{cc}}; \quad a = \frac{\varepsilon_{cc}}{\varepsilon_{cc} + \varepsilon_m} \quad (5.83)$$

It is worth to notice that the value  $a = 0.09\varepsilon_m/\varepsilon_{cc}$  reported in [61] is not considered here since, for big values of  $\varepsilon_m$ , it gives an increasing stiffness of the unloading path. Such circumstance is in contrast with the assumption of an increasing damage of the material.

The two sub domains  $\Omega_1$  and  $\Omega_2$  are determined by means of the procedure described in the section 5.1 with the strain limits reported hereafter:

$$\Omega = \begin{cases} \Omega_1 = \{\mathbf{r} \in \Omega : \varepsilon_m(\mathbf{r}) \leq 0\} \\ \Omega_2 = \{\mathbf{r} \in \Omega : 0 \leq \varepsilon_m(\mathbf{r}) \leq \varepsilon_{cu}\} \end{cases} \quad (5.84)$$

Notice that the vertices of such partitions do not depend upon the current strain  $\varepsilon$ , thus their derivatives with respect to  $\varepsilon$  and  $\mathbf{g}$  are null.

Since on  $\Omega_1$  the plastic strain is null, the points of such partition have a behavior that follows the envelope curve  $e(\varepsilon)$ :

$$\sigma_1(\varepsilon, \varepsilon_m) = e(\varepsilon) \quad (5.85)$$

Conversely, the stress in a point of the partition  $\Omega_2$  is a function of the values attained by  $\varepsilon$ ,  $\varepsilon_m$  and  $\varepsilon_p$ :

$$\sigma(\varepsilon, \varepsilon_m) = \begin{cases} 0 & \text{on } \Omega_{2a} \\ \frac{e(\varepsilon_m)}{\varepsilon_m - \varepsilon_p(\varepsilon_m)}[\varepsilon - \varepsilon_p(\varepsilon_m)] & \text{on } \Omega_{2b} \\ e(\varepsilon) & \text{on } \Omega_{2c} \end{cases} \quad (5.86)$$

where  $e(\varepsilon_m)$  is given by equation (5.76) with  $\varepsilon_m$  used in place of  $\varepsilon$ . A further partition of the domain  $\Omega_2$  has been introduced as follows:

$$\Omega_2 = \begin{cases} \Omega_{2a} = \{\mathbf{r} \in \Omega_2 : \varepsilon(\mathbf{r}) \leq \varepsilon_p[\varepsilon_m(\mathbf{r})]\} \\ \Omega_{2b} = \{\mathbf{r} \in \Omega_2 : \varepsilon_p[\varepsilon_m(\mathbf{r})] \leq \varepsilon(\mathbf{r}) \leq \varepsilon_m(\mathbf{r})\} \\ \Omega_{2c} = \{\mathbf{r} \in \Omega_2 : \varepsilon_m(\mathbf{r}) \leq \varepsilon(\mathbf{r})\} \end{cases} \quad (5.87)$$

#### 5.4.1 Determination of the functions $h(\varepsilon_m)$ , $k(\varepsilon_m)$ and $l(\varepsilon)$

The goal of this section is that of re-writing the stress-strain law described above by means of a unique expression of the kind of equation (5.28) which can be integrated by means of the formulas of section 5.2.

On the partition  $\Omega_1$  the stress-strain relation is coincident with the envelope curve, thus  $h(\varepsilon_m) = 0$  and  $k(\varepsilon_m) = 0$   $l(\varepsilon) = e(\varepsilon)$ .

The stress-strain law is identically null on  $\Omega_{2a}$ , thus the functions  $h(\varepsilon_m)$ ,  $k(\varepsilon_m)$  and  $l(\varepsilon)$  assume a null value on such domain.

The stress-strain relation on  $\Omega_{2b}$  is given by equation (5.86)<sub>2</sub>, which yields:

$$\begin{aligned}\sigma_{2ib}(\varepsilon, \varepsilon_m) &= \frac{e(\varepsilon_m)}{\varepsilon_m - \varepsilon_p(\varepsilon_m)} \left[ \varepsilon - \varepsilon_p(\varepsilon_m) \right] = \\ &= \frac{e(\varepsilon_m)}{\varepsilon_m - \varepsilon_p(\varepsilon_m)} \varepsilon - \frac{e(\varepsilon_m)}{\varepsilon_m - \varepsilon_p(\varepsilon_m)} \varepsilon_p(\varepsilon_m) = \\ &= \varepsilon h_{2ib}(\varepsilon_m) + k_{2ib}(\varepsilon_m)\end{aligned}\tag{5.88}$$

Finally the stress-strain law on  $\Omega_{2c}$  does not depend upon  $\varepsilon_p$  and  $\varepsilon_m$ , thus the functions  $h(\varepsilon_m)$  and  $k(\varepsilon_m)$  are identically null on such domains. Conversely the function  $l(\varepsilon)$  is equal to the envelope curve.

As a result we can write the stress strain relation on  $\Omega$  as:

$$\sigma(\varepsilon, \varepsilon_m) = \varepsilon h(\varepsilon_m) + k(\varepsilon_m) + l(\varepsilon)\tag{5.89}$$

with:

$$h(\varepsilon_m) = \begin{cases} 0 & \text{on } \Omega_1, \Omega_{2a} \text{ and } \Omega_{2c} \\ \frac{e(\varepsilon_m)}{\varepsilon_m - \varepsilon_p(\varepsilon_m)} & \text{on } \Omega_{2b} \end{cases}\tag{5.90}$$

$$k(\varepsilon_m) = \begin{cases} 0 & \text{on } \Omega_1, \Omega_{2a} \text{ and } \Omega_{2c} \\ -\frac{e(\varepsilon_m)}{\varepsilon_m - \varepsilon_p(\varepsilon_m)} \varepsilon_p(\varepsilon_m) & \text{on } \Omega_{2b} \end{cases}\tag{5.91}$$

and:

$$l(\varepsilon) = \begin{cases} 0 & \text{on } \Omega_{2a} \text{ and } \Omega_{2b} \\ e(\varepsilon) & \text{on } \Omega_1 \text{ and } \Omega_{2c} \end{cases}\tag{5.92}$$

### 5.4.2 Considerations upon the partition of the section

A partition of the section involving a comparison between  $\varepsilon$  and  $\varepsilon_p$  is used in equation (5.87) in order to distinguish between parts of the section which are unloading and parts of the section where the stress is null.

Since  $\varepsilon_m$  corresponds to one of the previous states of the section it is a linear function of the position vector  $\mathbf{r}$ . Conversely,  $\varepsilon_p$  is a non-linear function of  $\varepsilon_m$ , thus it is a non-linear function of  $\mathbf{r}$  too. The partitions  $\Omega_{2a}$  and  $\Omega_{2b}$  are determined by means of such non-linear relation which leads to obtain non-polygonal partitions, as shown in figure 5.9. Notwithstanding, we need all the partitions to be polygonal in order to adopt the formulas for evaluating the integrals over concrete sections.

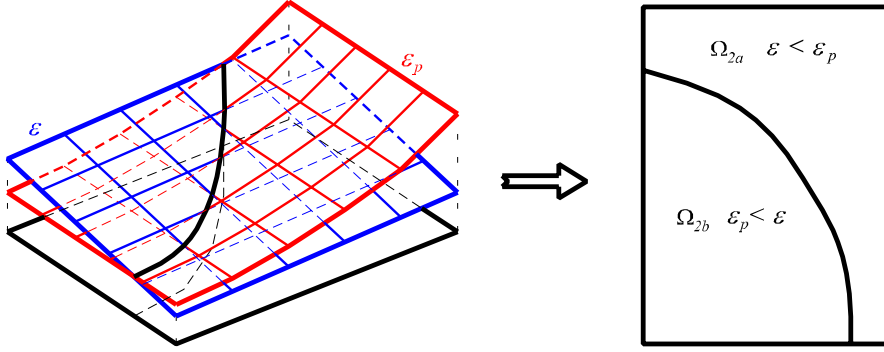


Figure 5.9:  $\Omega_{2a}$  and  $\Omega_{2b}$  are non polygonal partitions

Polygonal approximations of the actual partitions are obtained by adopting a fictitious strain  $\tilde{\varepsilon}_p = \tilde{\varepsilon}_p + \tilde{\mathbf{g}}_p \cdot \mathbf{r}$  which is determined by linearizing the relation  $\varepsilon_p(\varepsilon_m)$  for values of  $\varepsilon_m$  between  $\varepsilon_{ma}$  and  $\varepsilon_{mb}$ :

$$\tilde{\varepsilon}_p(\varepsilon_m) = \varepsilon_p(\varepsilon_{ma}) + \frac{\varepsilon_p(\varepsilon_{mb}) - \varepsilon_p(\varepsilon_{ma})}{\varepsilon_{mb} - \varepsilon_{ma}}(\varepsilon_m - \varepsilon_{ma}) \quad (5.93)$$

The strain parameters of  $\tilde{\varepsilon}_p$  are determined as:

$$\begin{aligned} \tilde{\varepsilon}_p &= \varepsilon_p(\varepsilon_{ma}) + \frac{\varepsilon_p(\varepsilon_{mb}) - \varepsilon_p(\varepsilon_{ma})}{\varepsilon_{mb} - \varepsilon_{ma}}(\varepsilon_m - \varepsilon_{ma}) \\ \tilde{\mathbf{g}}_p &= \frac{\varepsilon_p(\varepsilon_{mb}) - \varepsilon_p(\varepsilon_{ma})}{\varepsilon_{mb} - \varepsilon_{ma}} \mathbf{g}_m \end{aligned} \quad (5.94)$$

It is worth to notice that for  $\varepsilon_m < 0$  we have  $\varepsilon_p = 0$ . Also for  $\varepsilon_m > \varepsilon_{cu}$  the constitutive model is not defined. Consequently we need to approximate the function  $\varepsilon_p(\varepsilon_m)$  only in the interval  $[0, \varepsilon_{cu}]$ .

Clearly any interpolation with a unique linear function will end up in a very rough approximation of  $\varepsilon_p(\varepsilon_m)$ . Thus several intervals  $[\varepsilon_{ma_i}, \varepsilon_{mb_i}]$ , matching the whole interval  $[0, \varepsilon_{cu}]$ , are considered. In this way a piecewise linear interpolation of  $\varepsilon_p(\varepsilon_m)$  is produced. Each of the intervals  $[\varepsilon_{ma_i}, \varepsilon_{mb_i}]$  corresponds to a partition of  $\Omega_2$  defined as:

$$\Omega_{2_i} = \{\mathbf{r} \in \Omega_2 : \varepsilon_{ma_i} \leq \varepsilon_m \leq \varepsilon_{mb_i}\} \quad (5.95)$$

in which the relevant linear function  $\tilde{\varepsilon}_{p_i}(\varepsilon_m)$  is defined.

Each of the partitions  $\Omega_{2_i}$  is further divided into two sub-partitions:

$$\begin{cases} \Omega_{2_{i,a}} = \{\mathbf{r} \in \Omega_{2_i} : \varepsilon \leq \tilde{\varepsilon}_{p_i} \leq \varepsilon\} \\ \Omega_{2_{i,b}} = \{\mathbf{r} \in \Omega_{2_i} : \tilde{\varepsilon}_{p_i} \leq \varepsilon \leq \varepsilon_m\} \end{cases} \quad (5.96)$$

Since  $\tilde{\varepsilon}_{p_i}(\varepsilon_m)$  is a linear approximation of  $\varepsilon_p(\varepsilon_m)$ , on  $\Omega_{2_i}$ , the sub-partitions  $\Omega_{2_{i,a}}$  and  $\Omega_{2_{i,b}}$  approximate the non-polygonal partitions  $\Omega_{2a}$  and  $\Omega_{2b}$ , respectively, as shown in figure 5.10.

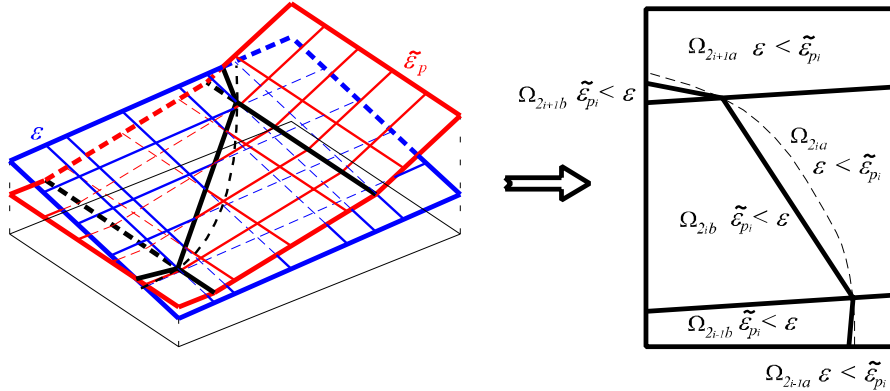


Figure 5.10: The sub-partitions  $\Omega_{2_{i,a}}$  and  $\Omega_{2_{i,b}}$  approximate the non-polygonal partitions  $\Omega_{2a}$  and  $\Omega_{2b}$

Remind that  $\Omega_{2c}$ , obtained by means of (5.87)<sub>3</sub>, is still polygonal. Thus it does not need any special care.

### 5.4.3 Spline interpolation of $h(\varepsilon_m)$ , $k(\varepsilon_m)$ and $l(\varepsilon)$

The very special form of the envelope curve  $e(\varepsilon)$  in (5.76) and the non-linear relation between  $\varepsilon_m$  and  $\varepsilon_p$  in (5.82) cause great difficulties in the determination of the primitives of the functions  $h(\varepsilon_m)$ ,  $k(\varepsilon_m)$  and  $l(\varepsilon)$  in

(5.90), (5.91) and (5.92), respectively. Here we furnish a spline interpolation of such functions so that they can be easily integrated over each partition.

Let us consider a continuous function  $f(x)$ . We want to approximate  $f(x)$  by means of a third order polynomial:

$$p(x) = p_0 + p_1x + p_2x^2 + p_3x^3 \quad (5.97)$$

for values of  $x$  between  $x_a$  and  $x_b$ . The four parameters  $p_0, \dots, p_3$  are thus determined by solving the following system of equations:

$$\begin{cases} p(x_a) = f(x_a) \\ p^{(-1)}(x_a) = f^{(-1)}(x_a) \\ p(x_b) = f(x_b) \\ p^{(-1)}(x_b) = f^{(-1)}(x_b) \end{cases} \quad (5.98)$$

which is obtained by setting the value that  $f(x)$  and its derivative  $f^{(-1)}(x)$  attain at the endpoints of the interval  $[x_a, x_b]$  equal to the value that  $p(x)$  and its derivative  $p^{(-1)}(x)$  attain at the same points.

The system (5.98) is solved for the values of the four parameters  $p_0, p_1, p_2$  and  $p_3$  obtaining:

$$p_0 = \frac{1}{(x_a - x_b)^3} [f(x_b)x_a^3 + x_b(x_b - x_a)f^{(-1)}(x_b)x_a^2 - 3x_bf(x_b)x_a^2 + x_b^2(x_b - x_a)f^{(-1)}(x_a)x_a + 3x_b^2f(x_a)x_a - x_b^3f(x_a)] \quad (5.99)$$

$$p_1 = \frac{1}{(x_a - x_b)^3} \{x_a\{(x_a^2 + x_bx_a - 2x_b^2)f^{(-1)}(x_b) + 6x_b[f(x_b) - f(x_a)]\} - x_b(x_bx_a - 2x_a^2 + x_b^2)f^{(-1)}(x_a)\} \quad (5.100)$$

$$p_2 = \frac{1}{(x_a - x_b)^3} \{(x_bx_a - 2x_a^2 + x_b^2)f^{(-1)}(x_b) - (x_a^2 + x_bx_a - 2x_b^2)f^{(-1)}(x_a) + 3(x_a + x_b)[f(x_a) - f(x_b)]\} \quad (5.101)$$

$$p_3 = \frac{(x_a - x_b)f^{(-1)}(x_a) + (x_a - x_b)f^{(-1)}(x_b) - 2f(x_a) + 2f(x_b)}{(x_a - x_b)^3} \quad (5.102)$$

It is worth to notice that we need to approximate  $h(\varepsilon_m)$ ,  $k(\varepsilon_m)$  and  $l(\varepsilon)$  in the interval  $[0, \varepsilon_{cu}]$  since they assume a null value elsewhere. Clearly repeating the previous steps for the three functions  $h(\varepsilon_m)$ ,  $k(\varepsilon_m)$  and  $l(\varepsilon)$  by assuming  $[x_a, x_b] = [0, \varepsilon_{cu}]$  will end up in a very rough approximation.

For this reason we subdivide the whole interval  $[0, \varepsilon_{cu}]$  in several subintervals  $[x_{a_i}, x_{b_i}]$  wherein the function is approximated with the relevant polynomials  $p_i(x)$ . They will form a piecewise polynomial, i.e. a spline interpolation of the actual function. Smaller the amplitude of the adjacent intervals  $[x_{a_i}, x_{b_i}]$ , finest the approximation of the actual function. Since the several intervals relevant to each polynomial segment of the spline function are adjacent, the following property holds:

$$x_{a_i} = x_{b_{i-1}} \quad (5.103)$$

meaning that the final endpoint of any interval is equal to the initial endpoint of the successive one.

### Primitives of $h(\varepsilon_m)$ , $k(\varepsilon_m)$ and $l(\varepsilon)$ and their derivatives

The functions  $h(\varepsilon_m)$ ,  $k(\varepsilon_m)$  and  $l(\varepsilon)$  are interpolated by means of splines defined in the interval  $[0, \varepsilon_{cu}]$ . Any single polynomial which compose the whole spline function is a third order polynomial:

$$p_i(x) = p_{0_i} + p_{1_i}x + p_{2_i}x^2 + p_{3_i}x^3 \quad (5.104)$$

defined in the interval  $[x_{a_i}, x_{b_i}] \subset [0, \varepsilon_{cu}]$ . The variable  $x$  stands for  $\varepsilon_m$  if the spline refers to  $h(\varepsilon_m)$  or  $k(\varepsilon_m)$  and  $\varepsilon$  if it refers to  $l(\varepsilon)$ .

The first order derivative of the generic polynomial  $p_i(x)$  is:

$$p_i^{(-1)}(x) = p_{1_i} + 2p_{2_i}x + 3p_{3_i}x^2 \quad (5.105)$$

The first order primitive of the generic polynomial segment of the interpolating spline is:

$$p_i^{(1)}(x) = p_{0_i}x + p_{1_i}\frac{x^2}{2} + p_{2_i}\frac{x^3}{3} + p_{3_i}\frac{x^4}{4} + P_{1_i} \quad (5.106)$$

Since the primitive of the whole spline has to be continuous, the constant of integration  $P_{1_i}$  is determined by setting:

$$p_i^{(1)}(x_{a_i}) = p_{i-1}^{(1)}(x_{b_{i-1}}) \quad \Rightarrow \quad p_i^{(1)}(x_{a_i}) = p_{i-1}^{(1)}(x_{a_i}) \quad (5.107)$$

where the property (5.103) has been used.

Similarly the second, third and fourth order primitives of  $p_i(x)$  are:

$$p_i^{(2)}(x) = p_{0_i}\frac{x^2}{2} + p_{1_i}\frac{x^3}{6} + p_{2_i}\frac{x^4}{12} + p_{3_i}\frac{x^5}{20} + P_{1_i}x + P_{2_i} \quad (5.108)$$

$$p_i^{(3)}(x) = p_{0_i}\frac{x^3}{6} + p_{1_i}\frac{x^4}{24} + p_{2_i}\frac{x^5}{60} + p_{3_i}\frac{x^6}{120} + P_{1_i}\frac{x^2}{2} + P_{2_i}x + P_{3_i} \quad (5.109)$$

and

$$p_i^{(4)}(x) = p_{0_i} \frac{x^4}{20} + p_{1_i} \frac{x^5}{120} + p_{2_i} \frac{x^6}{360} + p_{3_i} \frac{x^7}{840} + P_{1_i} \frac{x^3}{6} + P_{2_i} \frac{x^2}{2} + P_{3_i} x + P_{4_i} \quad (5.110)$$

where  $P_{2_i}$ ,  $P_{3_i}$  and  $P_{4_i}$  are determined by setting:

$$p_i^{(2)}(x_{a_i}) = p_{i-1}^{(2)}(x_{a_i}) \quad (5.111)$$

$$p_i^{(3)}(x_{a_i}) = p_{i-1}^{(3)}(x_{a_i}) \quad (5.112)$$

and

$$p_i^{(4)}(x_{a_i}) = p_{i-1}^{(4)}(x_{a_i}) \quad (5.113)$$

Let us consider the case of the polynomial defined in the interval with initial endpoint  $x_{a_i} = 0$ , which is equal to the initial endpoint of the interval  $[0, \varepsilon_{cu}]$  where the spline function is defined. This is the case in which the first polynomial segment of the spline function is considered. Thus the polynomial  $p_{i-1}(x)$  is not defined hence the constants of integration cannot be determined by means of the procedure explained previously. Actually, recalling equations (5.90), (5.91) and (5.92), we have that the three functions  $h(\varepsilon_m)$ ,  $k(\varepsilon_m)$  and  $l(\varepsilon)$  assume a null value outside the interval  $[0, \varepsilon_{cu}]$ . Thus we define  $p_{i-1}(x) = 0$  and we set equal to zero its primitives too. Consequently, all the constants of integration, relevant to the first polynomial segment of the spline function, are null.



## Chapter 6

# Numerical results

In order to show the effectiveness of the integration formulas presented in this thesis, several numerical tests have been carried out by comparing the results entailed by the proposed approach with those associated with the use of fibers.

Specifically, two separate kind of tests have been conceived, one for the bilinear stress-strain law presented in section 5.3 and the other one for the Mander's constitutive law which, in a sense, is representative of complex stress-strain laws which either do not possess primitives amenable to an exact analytical form or are directly assigned as collection of experimentally determined pairs of stress-strain values.

In the former case, the fiber-free approach provides exact values both for the stress resultants, see e.g. integrals (5.32) and (5.35), and for its derivatives, provided by formulas (5.33), (5.34), (5.36) and (5.37).

In the latter case, the constitutive law has to be somehow interpolated so that the exact value of the stress resultants and of its derivatives permitted by the fiber-free approach pertains to the interpolated constitutive law rather than to the original one.

In both cases aim of this section is to investigate on the degree of approximation introduced by the adoption of the traditional fiber approach, to date the only existing method for integrating elastic-plastic normal stress fields.

### 6.1 Integration of bilinear stress-strain laws

It has been pointed out before that, in the case of bilinear stress-strain laws the fiber-free approach provides exact results both for the stress resultants

and its derivatives.

However, in order to check the correctness of the formulas derived in the previous sections and the relevant implementation, it has been decided to compare the results obtained by the fiber-free approach with those associated with the use of the traditional fiber approach. Due to the inherent approximation of this last method an increasing number of fibers has been considered up to a maximum allowed by the computer memory, on one side, and by the machine precision on the other.

As a representative example of the several numerical tests which have been carried out we discuss the results obtained for a rectangular section of size  $0.3 \times 0.4$  made of the material described in section 5.3 with  $E_e = 10$ ,  $E_h = 0.1$  and  $\varepsilon_y = -1$ .

To provide this example, and the additional ones presented in the sequel, with a deeper engineering sense, we specify that, although unnecessary to make the numerical tests consistent, the adopted units are meters for lengths and Newton for forces.

The section has been analyzed by keeping constant  $\epsilon = 0$  and  $g_y = 0$ . A loading-unloading analysis has been executed by increasing the  $g_x$  component of the strain gradient from  $-0.5$  to  $-10$  and then decreasing back to  $-0.5$  with steps of  $0.5$ . The relevant  $M_y - g_x$  curves obtained by the fiber-free approach and the fiber method is plotted in figure 6.1.

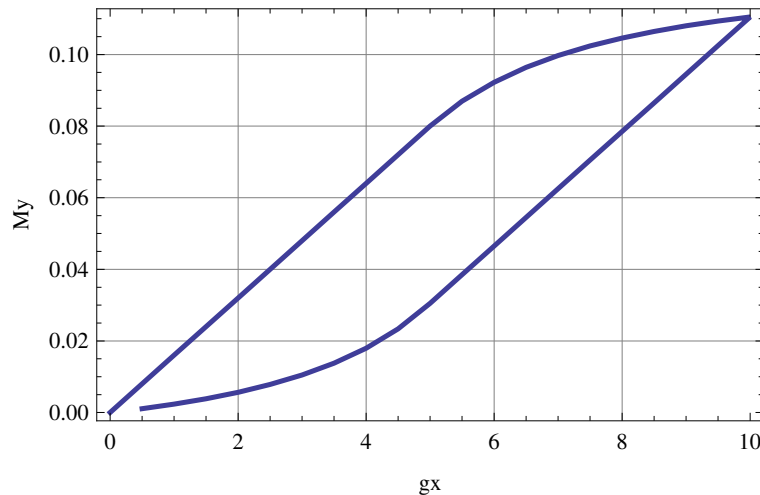


Figure 6.1:  $M_y - g_x$  relation

The force vector and the tangent matrix of the section relevant to the

last step of the analysis carried out by the fiber-free approach are:

$$\begin{pmatrix} N \\ M_x \\ M_y \end{pmatrix} = \begin{pmatrix} -1.57978723404256E - 02 \\ -1.08120190131281E - 03 \\ -1.55366171317172E - 18 \end{pmatrix} \quad (6.1)$$

and

$$\begin{pmatrix} N_{,\epsilon} & N_{,g_x} & N_{,g_y} \\ M_{x,\epsilon} & M_{x,g_x} & M_{x,g_y} \\ M_{y,\epsilon} & M_{y,g_x} & M_{y,g_y} \end{pmatrix} = \begin{pmatrix} 6.31914893617021E - 01 \\ 3.32763693979175E - 02 \\ 1.19939865331208E - 18 \\ 3.32763693979176E - 02 & -3.10461292091224E - 18 \\ 2.33642593644953E - 03 & -1.25422987137241E - 18 \\ -7.76446868316442E - 20 & 1.89574468085106E - 02 \end{pmatrix} \quad (6.2)$$

Notice that for computers with machine precision of  $10^{-16}$ , the values of  $M_y$ ,  $N_{,g_y}$ ,  $M_{x,g_y}$ ,  $M_{y,\epsilon}$  and  $M_{y,g_x}$  are numerically zero.

In this respect we remind that for a FORTRAN variable declared as real\*8 the machine precision, defined as:

$$e_x = \frac{|x_m - x|}{|x|} \sim 10^{-16} \quad (6.3)$$

is of order  $10^{-16}$  where  $x$  is the exact value and  $x_m$  is the machine value.

The same analysis has been carried out with the fiber method adopting an increasing number of fibers. The section was first discretized into  $50 \times 50$  fibers, then  $100 \times 100$  and so on, up to  $5'000 \times 5'000$ . When a bigger number of fibers was used, i.e.  $10'000 \times 10'000$ , a crash down occurred due to exhaustion of the whole computer memory since  $10^8$  history variables needed to be stored.

The relevant values of the force vector and of the stiffness matrix are reported here only for the last step of the analysis referred to the use of  $5'000 \times 5'000 = 25 \times 10^6$  fibers:

$$\begin{pmatrix} N^f \\ M_x^f \\ M_y^f \end{pmatrix} = \begin{pmatrix} -1.57978291200150E - 02 \\ -1.08119734932519E - 03 \\ 1.60060750692240E - 19 \end{pmatrix} \quad (6.4)$$

and

$$\left\{ \begin{array}{ccc} N_{,\epsilon}^f & N_{,g_x}^f & N_{,g_y}^f \\ M_{x,\epsilon}^f & M_{x,g_x}^f & M_{x,g_y}^f \\ M_{y,\epsilon}^f & M_{y,g_x}^f & M_{y,g_y}^f \end{array} \right\} = \left\{ \begin{array}{l} 6.31679999952975E - 01 \\ 3.32516352000149E - 02 \\ -8.91825770040781E - 18 \\ 3.32516352000149E - 02 \quad -8.91837681441602E - 18 \\ 2.33382109901700E - 03 \quad -3.48495327971653E - 19 \\ -3.50321742764170E - 19 \quad 1.89503992419888E - 02 \end{array} \right\} \quad (6.5)$$

This clearly shows the exactness of the fiber-free approach and the correctness of its implementation. According to formula (6.3) the approximations obtained by using  $25 \times 10^6$  fibers at the last step of the analysis concerning the construction of the  $M_y - g_x$  curves in figure 6.1 are:

$$\left\{ \begin{array}{c} e_N \\ e_{M_x} \\ e_{M_y} \end{array} \right\} = \left\{ \begin{array}{c} 2.7E - 06 \\ 4.2E - 06 \\ \mathbf{1.1E + 00} \end{array} \right\} \quad (6.6)$$

and

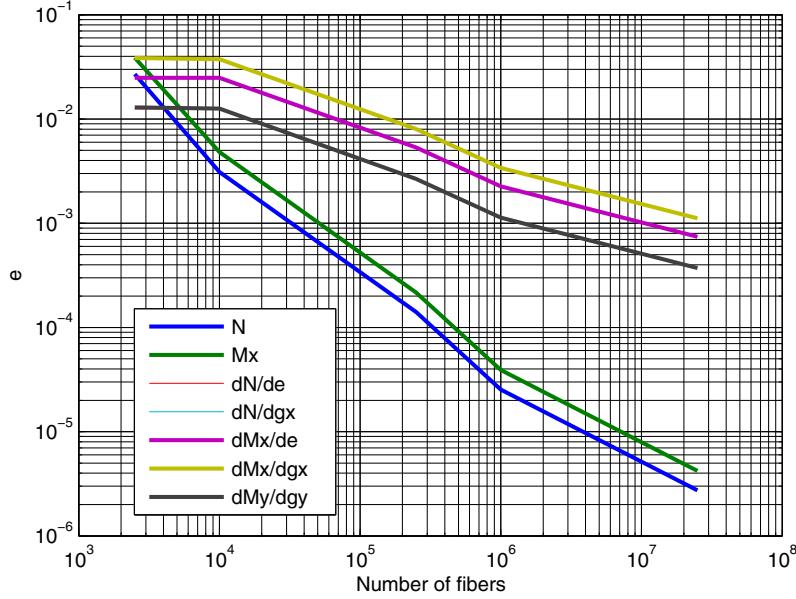
$$\left\{ \begin{array}{ccc} e_{N,\epsilon} & e_{N,g_x} & e_{N,g_y} \\ e_{M_{x,\epsilon}} & e_{M_{x,g_x}} & e_{M_{x,g_y}} \\ e_{M_{y,\epsilon}} & e_{M_{y,g_x}} & e_{M_{y,g_y}} \end{array} \right\} = \left\{ \begin{array}{ccc} 3.7E - 04 & 7.4E - 04 & \mathbf{1.9E + 00} \\ 7.4E - 04 & 1.1E - 03 & \mathbf{7.2E - 01} \\ \mathbf{8.4E + 00} & \mathbf{3.5E + 00} & 3.7E - 04 \end{array} \right\} \quad (6.7)$$

Notice that the values of  $e_{M_y}$ ,  $e_{N,g_y}$ ,  $e_{M_{x,g_y}}$ ,  $e_{M_{y,\epsilon}}$  and  $e_{M_{y,g_x}}$  do not make particular sense since they refer to an error evaluated for variables which are numerically zero, thus they shall be neglected. In any case the discretization of the section into  $25 \times 10^6$  fibers is not enough to obtain numerically exact results.

The remaining values of the error, which are relevant to each discretization of the section, are reported in the bi-logarithmic plot of figure 6.2 as a function of the adopted number of fibers. It is apparent that the relevant errors tend to zero when the number of fibers is increased.

Since the convergence of the fiber method seems to be linear in the bi-logarithmic scale (see figures 6.2), the slope of the plots can be defined as the ratio:

$$r_n = \frac{|\text{Log}(e_n) - \text{Log}(e_1)|}{|\text{Log}(N_{f,n}) - \text{Log}(N_{f,1})|} \quad (6.8)$$

Figure 6.2:  $e_x$  vs. number of fibers

where  $e_n$  and  $e_1$  are the error relevant to a number of fibers equal to  $N_{f,n}$  and  $N_{f,1}$  respectively. Consequently such ratio is used as a measure of how fast the fiber method converges.

The value of  $r_n$  is the same for the three components of the force vector and is  $r_n \simeq 0.99$ , while for the components of the tangent matrix it turns out to be  $r_n \simeq 0.38$ . Consequently the fiber method results to be less accurate and less performing when it is used for the evaluation of the tangent matrix of the section.

Apart from the fact that the fiber-free approach provides exact values both for the stress resultants and its derivatives, the crucial remark which strongly recommends its use in practical inelastic analysis of RC structures is represented by the appealing feature that it is much less memory consuming with respect to the traditional fiber approach. During the whole  $M_y - g_x$  analysis only 6 history variables have been used, i.e. the three components of the strain vector relative to the maximization of the strain on 2 partitions of the section (see chapter 5).

Actually the test described above shows the effectiveness of the fiber-free approach at the section level. In order to investigate on the behavior of the

proposed method of integration at the structural level, the beam elements described in chapter 3 have been implemented in the finite element program FEAP developed by Professor R. L. Taylor at the University of California, Berkeley. The fiber-free approach and the fiber method have been used for the section analysis of the elements so that structural analyses with both the integration methods can be carried out.

Many tests have been executed adopting such elements. The one reported here refers to the problem of figure 6.3, where the same rectangular section and material of the test described above is used.

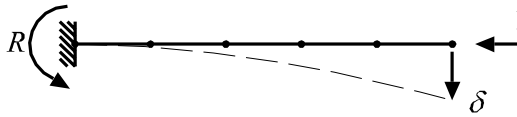


Figure 6.3: Cantilever

The cantilever has been modeled by means of 5 elements. A unit compressive force is applied at the free node in order to pre-stress the structure. A vertical displacement  $\delta$  is assigned to the same node. Its value is changed so that a full load-unload-reload cycle is completed and the relevant value of the reaction  $R$  at the left hand side node is recorded. The cyclic behavior of such model is shown in figure 6.4 where the  $R - \delta$  relationship is plotted.

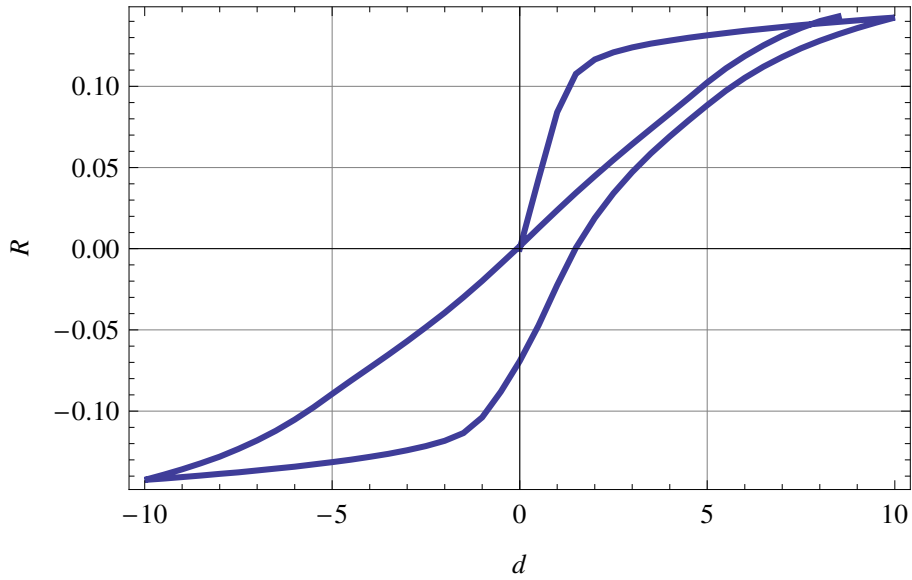
As it has been done at the section level, the result of the analysis carried out adopting the fiber-free approach is compared with the ones obtained by means of the fiber method, where several numbers of fibers have been used to divide the sections.

In particular, the values of the reactions  $R$  recorded at the end of the analysis are reported in table 6.1 where only five digits are kept.

Method	$R$
fiber-free	0.14307
fiber: $10 \times 10$	0.14207
fiber: $20 \times 20$	0.14293
fiber: $40 \times 40$	0.14311
fiber: $80 \times 80$	0.14305

Table 6.1: Values of the reaction at the end of the analysis

The relative error is evaluated using formula (6.3) with the data of table 6.1 and adopting the value of  $R$  obtained by the fiber-free approach as a

Figure 6.4:  $R - \delta$  relationship

reference. The error is plotted against the number of fibers in figure 6.5 and the relevant values are reported in table 6.2.

Method	$e_R$
fiber-free	0
fiber: $10 \times 10$	7.0E-03
fiber: $20 \times 20$	9.8E-04
fiber: $40 \times 40$	2.8E-04
fiber: $80 \times 80$	1.4E-04

Table 6.2:  $p_x$  vs. number of fibers

Both the values of table 6.2 and the plot of figure 6.5 show how the results of the fiber method, with an increasing number of fibers, tends to the one obtained from the fiber-free approach .

The value of  $r_n$  relevant to such analysis is  $r_n \simeq 0.94$  which is close to the one evaluated for the determination of the resultant forces in the previous test.

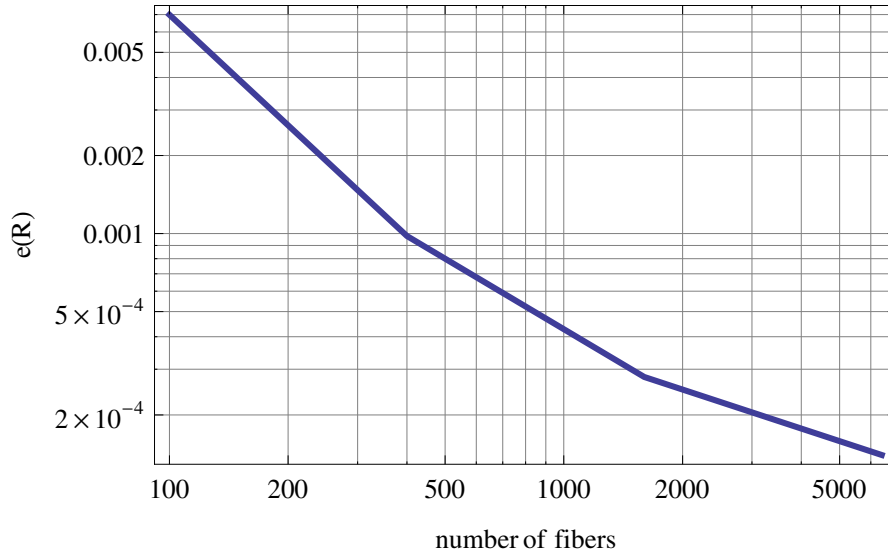


Figure 6.5:  $e_R$  vs. number of fibers

## 6.2 Integration of the stress-strain law with Mander's envelope curve

The bilinear constitutive law described in section 5.3 has been used to engender the results of the tests described in the previous section. In this section the stress-strain relationship of section 5.4 will be used for carrying out now numerical results with the aim of checking the effectiveness of the fiber-free approach with more complex materials.

As it is explained in sections 5.4.2 and 5.4.3 the constitutive functions need to be interpolated. The interpolation procedure, which is numerically detailed in the following section, produces slight approximations in the results of the integration method proposed in this thesis. In order to understand the magnitude of such approximations, in the sections that follow, the results of the fiber-free approach are compared with those of the fiber method.

### 6.2.1 Interpolation of $l(\varepsilon)$ , $h(\varepsilon_m)$ , $k(\varepsilon_m)$ and $\varepsilon_p(\varepsilon_m)$

As it is explained in section 5.4.3, spline interpolations of the functions  $l(\varepsilon)$ ,  $h(\varepsilon_m)$  and  $k(\varepsilon_m)$ , respectively defined in equations (5.92), (5.90) and (5.91),

needs to be done before applying the fiber-free approach.

Adopting 4 segments of spline for the function  $l(\varepsilon)$ , corresponding to 4 intervals  $[x_a, x_b]$  in which each polynomial is defined by means of formula (5.98), the interpolation of figure 6.6 is produced, where the thick solid line is  $l(\varepsilon)$  and the dashed line is the relevant spline interpolation. It refers to

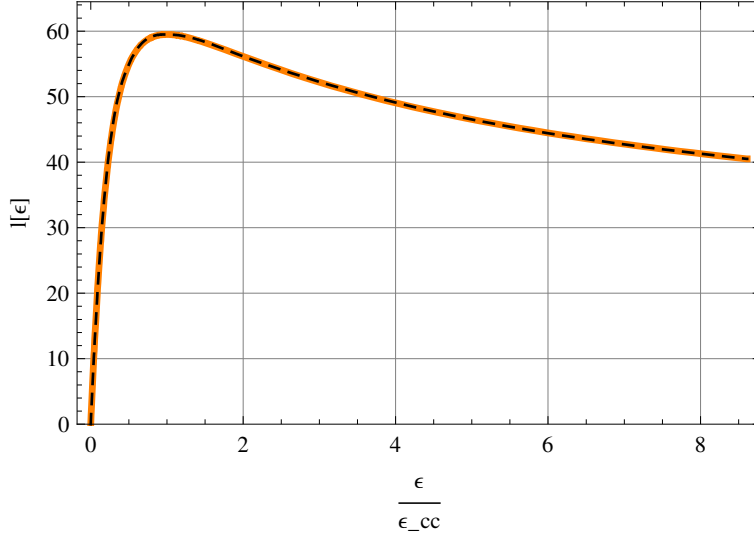


Figure 6.6: Spline interpolation for  $l(\varepsilon)$

the use of the following interpolation points:

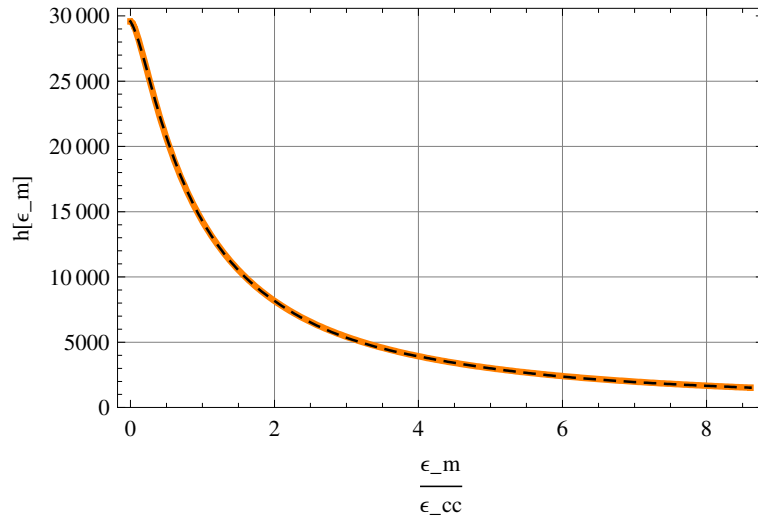
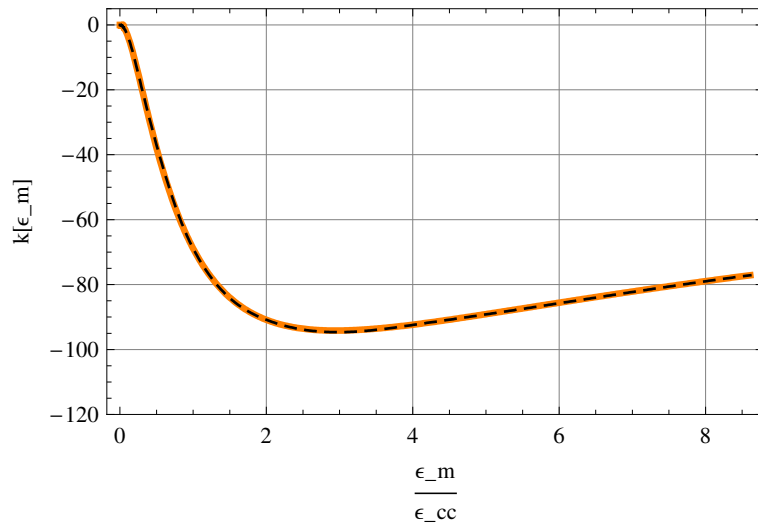
$$\varepsilon_1 = 0; \quad \varepsilon_2 = \frac{\varepsilon_{cc}}{2}; \quad \varepsilon_3 = \varepsilon_{cc}; \quad \varepsilon_4 = 2\varepsilon_{cc}; \quad \varepsilon_5 = \varepsilon_u \quad (6.9)$$

which are used as endpoints of the 4 intervals  $[x_a, x_b]$ .

Please notice that, since the interpolation is derived in a general case, it applies to a vast range of material properties and the plots reported in this section are just an example of how accurate the interpolation is. The plot of figure 6.6, together with the plots below, refers to a material with the following machanic properties:

$$\begin{aligned} f'_{cc} = 59.50[\text{MPa}]; \quad E_c = 29580[\text{MPa}]; \quad \varepsilon_{cc} = 0.0090; \\ E_{sec} = 6611[\text{MPa}]; \quad \varepsilon_u = 0.07750 \end{aligned} \quad (6.10)$$

In figures 6.7 and 6.8 the interpolations of  $h(\varepsilon_m)$  and  $k(\varepsilon_m)$  are plotted. The splines are obtained by means of the interpolation of the value attained

Figure 6.7: Spline interpolation for  $h(\varepsilon_m)$ Figure 6.8: Spline interpolation for  $k(\varepsilon_m)$ 

by the two functions and the relevant derivatives at the following points:

$$\begin{aligned}
 \varepsilon_{m1} &= 0; & \varepsilon_{m2} &= \frac{\varepsilon_{cc}}{4}; & \varepsilon_{m3} &= \varepsilon_{cc}; \\
 \varepsilon_{m4} &= 2\varepsilon_{cc}; & \varepsilon_{m5} &= \frac{\varepsilon_u}{2}; & \varepsilon_{m6} &= \varepsilon_u
 \end{aligned}
 \tag{6.11}$$

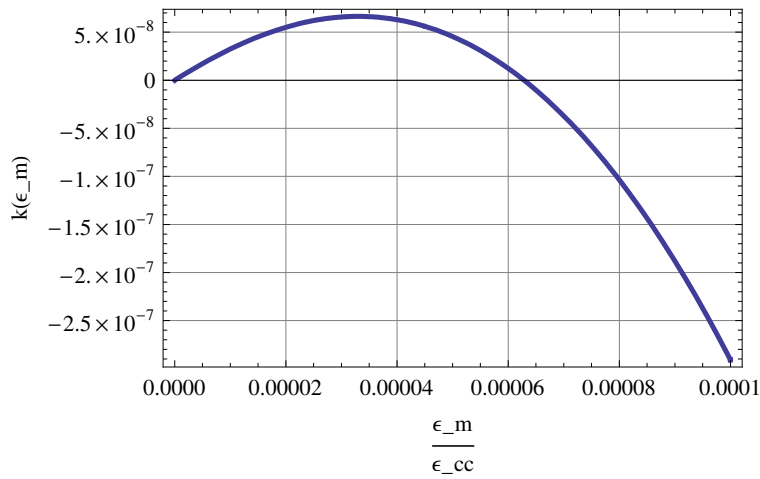


Figure 6.9: Plot of  $k(\varepsilon_m)$  near zero

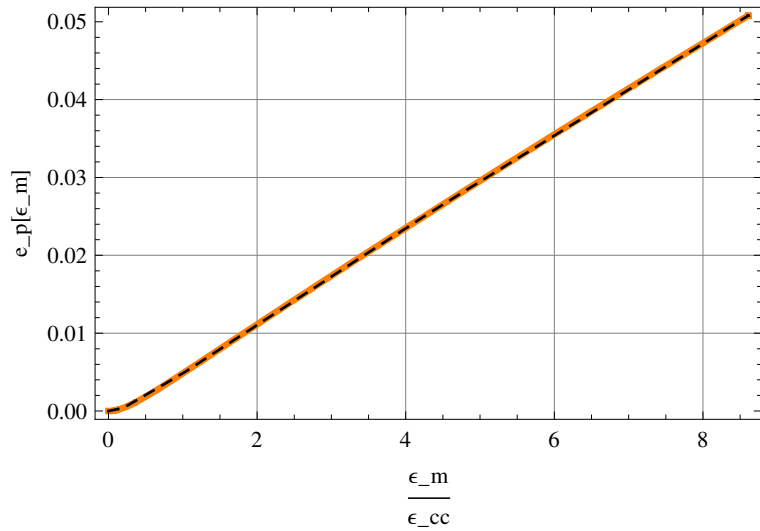


Figure 6.10: Piecewise linear interpolation of  $\varepsilon_p(\varepsilon_m)$

Special care shall be taken when the interpolation point  $\varepsilon_{m1} = 0$  is considered in the system of equations (5.98) since the value that  $h(\varepsilon_m)$ ,  $k(\varepsilon_m)$  and their derivatives attain at  $\varepsilon_m = 0$  are not of easy evaluation. For the interpolations of figures 6.7 and 6.8 the following values have been assumed:

$$h(0) = E_c; \quad h'(0) = 0; \quad k(0) = 0; \quad k'(0) = 0; \quad (6.12)$$

The assumptions (6.13)<sub>1</sub>, (6.13)<sub>2</sub>, and (6.13)<sub>3</sub> correspond to the evaluation of the limits:

$$\lim_{\varepsilon_m \rightarrow 0} h(\varepsilon_m) = E_c; \quad \lim_{\varepsilon_m \rightarrow 0} h'(\varepsilon_m) = 0; \quad \lim_{\varepsilon_m \rightarrow 0} k(\varepsilon_m) = 0 \quad (6.13)$$

which are quite difficult to determine.

Conversely the value of the limit of  $k'(\varepsilon_m)$  when  $\varepsilon_m$  tends to 0 is far from being 0, as it can be also seen in figure 6.9. Notwithstanding, since the value of  $k'(\varepsilon_m)$  has a sudden change of sign around zero, the value  $k'(0) = 0$  has been chosen for the interpolation.

Finally, as it is described in section 5.4.2 also the function  $\varepsilon_p(\varepsilon_m)$ , given by equation (5.82), needs to be approximated with a piecewise linear function. In figure 6.10 the function  $\varepsilon_p(\varepsilon_m)$  and its interpolation are plotted with a thick solid line and a dashed line respectively.

Such interpolation has been obtained considering the values that  $\varepsilon_p(\varepsilon_m)$  attains at the following values of  $\varepsilon_m$ :

$$\varepsilon_{m1} = 0; \quad \varepsilon_{m2} = \frac{\varepsilon_{cc}}{5}; \quad \varepsilon_{m3} = \varepsilon_{cc}; \quad \varepsilon_{m4} = \frac{\varepsilon_u}{2}; \quad \varepsilon_{m5} = \varepsilon_u \quad (6.14)$$

### 6.2.2 Section analysis

Once the constitutive functions have been interpolated as it is shown in section 6.2.1, the fiber-free approach can be applied to the analysis of any polygonal section.

As it has been done for the bi-linear constitutive model, the results of the application of the fiber-free approach are compared with the ones engendered by the fiber method where several discretizations of the section have been considered. In the case of the material model of section 5.4 both the fiber method and the fiber free approach do not yield numerically exact results. Consequently, the reference for evaluating the errors due to the approximations connected to the use of both the methods of integration needs to be found somewhere else. To this end, for the numerical examples that follow, we refer to the results obtained by means of the program Wolfram Mathematica, a well known software for symbolic and numerical evaluations.

As a remark, due to the complexity of the integrals to evaluate and since Mathematica is a scientific software of general purpose, it has been possible to analyze only rectangular sections in which only one history stain vector is considered. Further when biaxial bending has been considered many warnings and errors of convergence have been experienced. Conversely these problems do not occur when the fiber free and the fiber methods are used to evaluate the same integrals.

The first results reported hereafter refer to the evaluation of the resisting forces on a section  $0.20\text{m} \times 0.40\text{m}$  where the material with the stress-strain laws interpolated in section 6.2.1 is considered. The current strain state is determined by the following strain parameters:

$$\epsilon = 0.0025; \quad \mathbf{g} = \{0.1, 0\}^T \tag{6.15}$$

while the strain parameters which maximize the strain over the whole section are:

$$\epsilon_m = 0.0002; \quad \mathbf{g}_m = \{0.2, 0\}^T \tag{6.16}$$

In figure 6.11 the strain fields  $\epsilon$ ,  $\epsilon_m$  and  $\epsilon_p$  are plotted in red, green and blue, respectively.

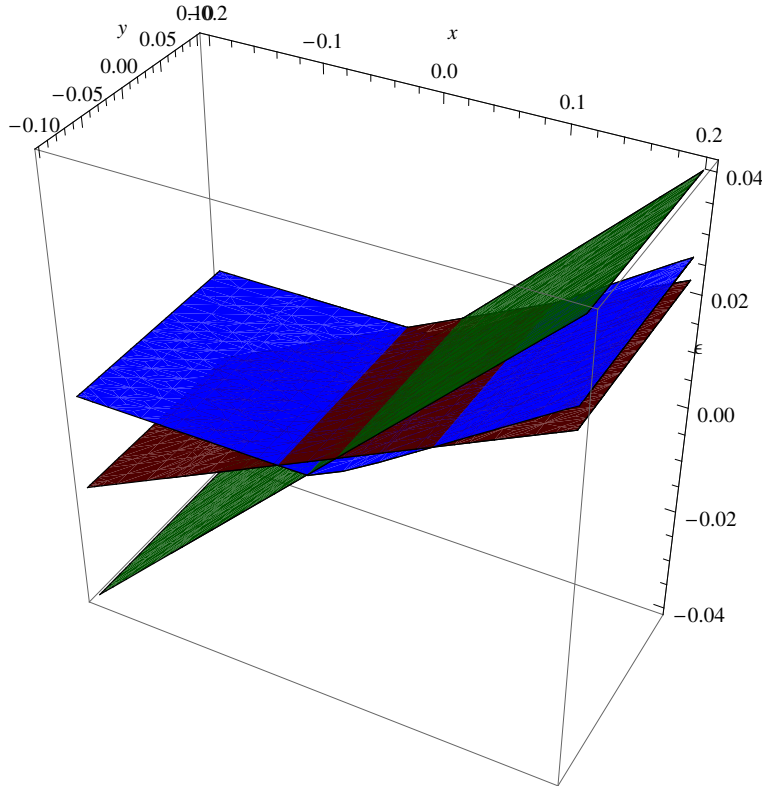


Figure 6.11: Strain fields  $\epsilon$  in red,  $\epsilon_m$  in green and  $\epsilon_p$  in blue

The relevant stress field on the section is plotted in figure 6.12 where the loading and unloading areas of the section are apparent.

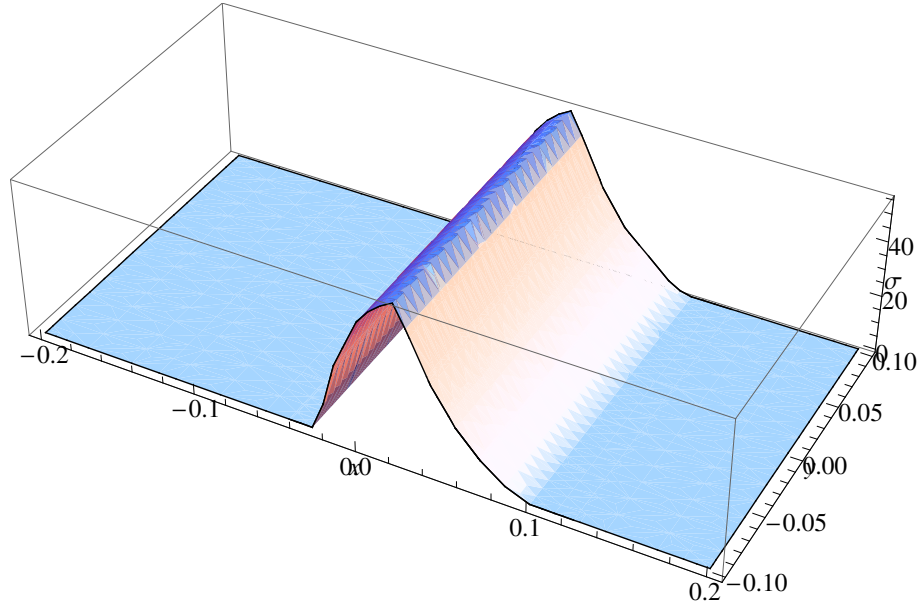


Figure 6.12: The stress field in the section

The resultant axial force and bending moment have been evaluated with the fiber free approach, the fiber method and Mathematica's `NIntegrate` function. In particular, for the fiber method, a number of fibers which goes from  $10 \times 10$  up to  $100 \times 100$  is used.

The results engendered by Mathematica are assumed to be exact, while formula (6.3) is used for evaluating the errors  $e_{ff}$  and  $e_f$  connected to the use of the fiber free approach and the fiber method, respectively.

In order to properly compare the results of the fiber free approach with those of the fiber method, we also define the relative error  $e_r$  as follows. For the fiber method, the relative error  $e_r^f$  is defined as the ratio between the error  $e_f$ , relevant to the considered number of fibers, and the error  $e_{ff}$ :

$$e_r^f = \frac{e_f}{e_{ff}} \quad (6.17)$$

A similar definition for the fiber free approach yields:

$$e_r^{ff} = \frac{e_{ff}}{e_{ff}} = 1 \quad (6.18)$$

Figures 6.13 and 6.14 are relative to the evaluation of the axial force and the bending moment, respectively.

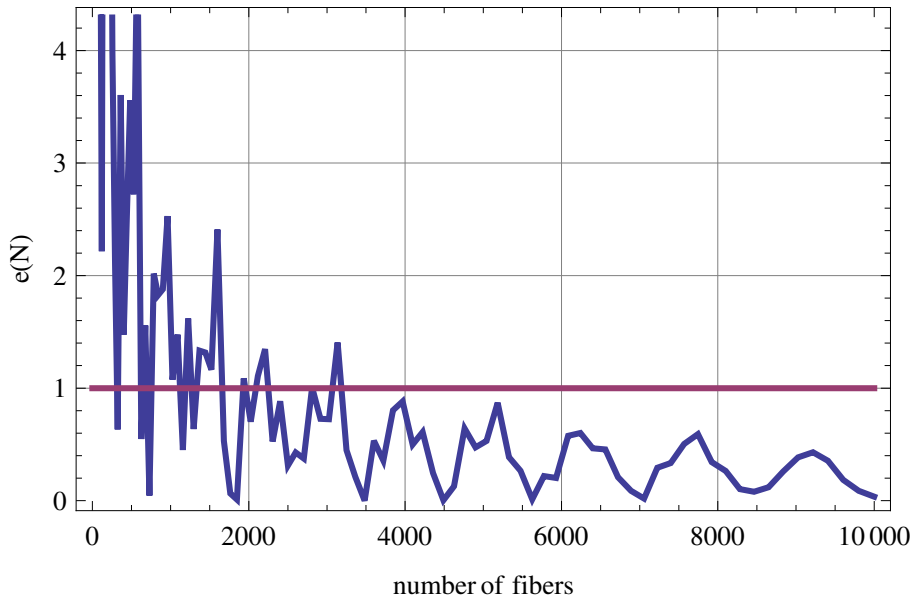


Figure 6.13: Plot of  $e_r^f$  vs. the number of fibers for the axial force

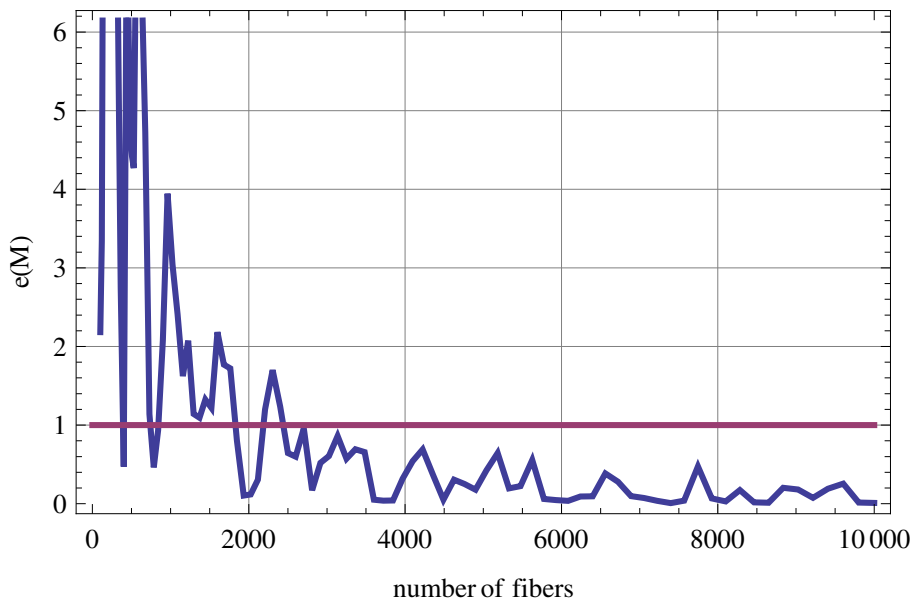
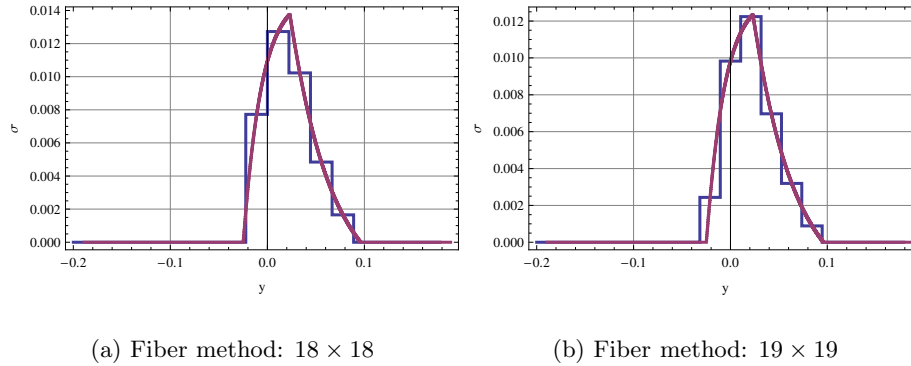


Figure 6.14: Plot of  $e_r^f$  vs. the number of fibers for the bending moment

Figure 6.15: Stress fields *read* by the fibers

In such plots the values of the relative errors  $e_r^f$ , i.e. the ones connected to the use of the fiber method, are reported as a function of the number of fibers used in the section analysis.

Also the value of the relative error  $e_r^{ff}$  is reported for convenience. Obviously, since  $e_r^{ff} = 1$  does not depend upon the number of fibers, the data relevant to the fiber free approach are represented by a horizontal line at  $e_r = 1$ .

The very irregular convergence behaviour of the fiber method is apparent in figures 6.13 and 6.14. In order to explain such behaviour, let us consider, for example, the case in which two discretizations of the section are assumed, namely  $18 \times 18$  and  $19 \times 19$ . The relevant stress fields *read* by the fibers which lie on the  $y$  axis are plotted with the step functions of figures 6.15(a) and 6.15(b).

It is apparent that both the discretizations of the section very roughly approximate the actual stress field. Notwithstanding, while the value of the relative error connected to the use of  $18 \times 18$  fibres is  $e_r^{18 \times 18} = 0.633$ , the value of  $e_r^{19 \times 19}$  is equal to 3.605.

Such behaviour is imputable to the fact that the results obtained with the fiber method strongly depend upon the position of the fibers. Actually, the fortuitous fiber distribution of figure 6.15(a) produces a *lucky* compensation of the approximations which results in a much better result. As it is easily intuible, a slight modification of the number of fibers or the strain parameters makes *unlucky* such fiber distribution.

In order to better clarify how the position of the fiber affects the approximation of the results another tipology of tests has been carried out. Several

strain states have been assumed to act on the section in such a way that the stress field is only translated. This task is accomplished by assuming the following strain fields:

$$\epsilon = 0.005 + 0.0001 k; \quad \mathbf{g} = \{0.1, 0\}^T \tag{6.19}$$

$$\epsilon_m = 0.005 + 0.0002 k; \quad \mathbf{g}_m = \{0.2, 0\}^T \tag{6.20}$$

with  $k$  assuming values between 0 and 20 with a step of 0.25. The value of the axial force  $N$  has been evaluated both with the fiber free approach and with the fiber method. For the latter a constant number of fibers has been used to divide the section and, in this particular case, it has been set equal to  $45 \times 45$ . The relevant errors  $e^f(N)$  and  $e^{ff}(N)$  have been recorded for each value of  $k$  and plotted in figure 6.16.

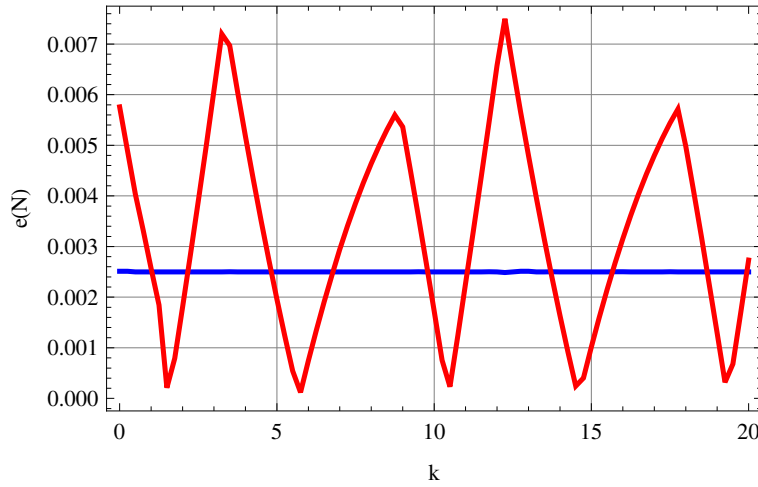


Figure 6.16: Plot of  $e^f(N)$  vs. the number of fibers for the axial force

Obviously, since the stress field is only translated, the value of the axial force does not depend upon  $k$  and is constant. Also, please recall that the approximations of the fiber free approach are connected to the interpolation of the constitutive law, thus the relative position of the stress field with respect to the section geometry does not afflict the results. Consequently,  $e^f(N)$  is constant and equal to  $e^f(N) \sim 0.0025$ .

Conversely, the plot of figure 6.16 shows the strong relation between the value of the approximations of the fiber method and the relative position between the fibers and the stress field.

For these reasons the first test presented in this section, i.e. the one which produced the plots 6.13 and 6.14, is not much indicative of the general behaviour of the fiber method; thus new analyses that assume different values of strain parameters need do be carried out.

In figures 6.17 and 6.18 the values of  $e_r^f$  are reported for the axial force and the bending moment on the same section of the previous test, but assuming several values of the strain parameters:

$$\epsilon = 0.0005 \div 0.0035; \quad \mathbf{g} = \{0.1, 0\}^T \quad (6.21)$$

$$\epsilon_m = 0.0005 \div 0.0035; \quad \mathbf{g}_m = \{0.2, 0\}^T \quad (6.22)$$

The envelope of the values of  $e_r^f$  is reported with a solid line in order to highlight the relation between the approximations of the fiber method and those of the fiber free approach, which are represented by the blue horizontal line at  $e_r^{ff} = 1$ .

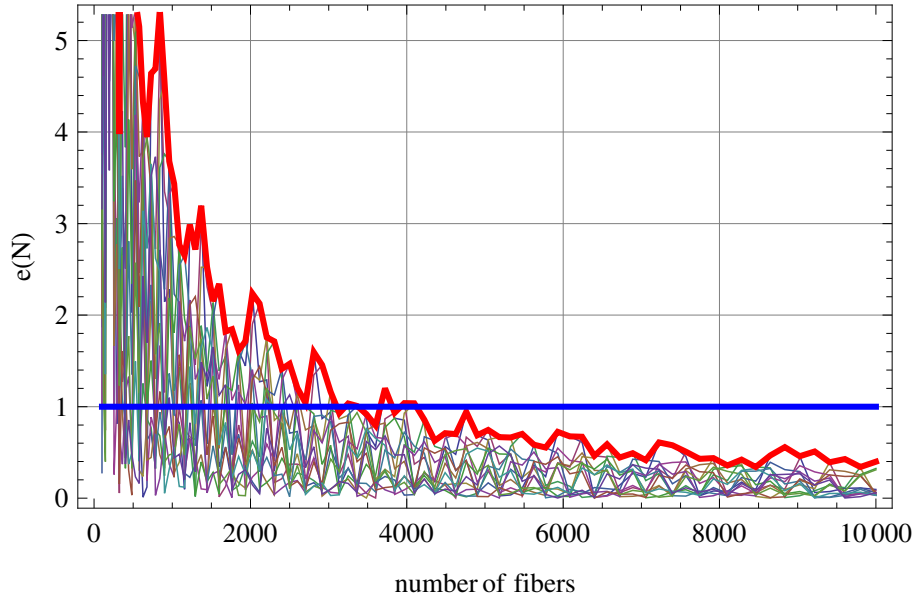


Figure 6.17: Plot of  $e_r^f$  vs. the number of fibers for the axial force

The same test has also been done for the case of biaxial bending. The plots of figures 6.19 and 6.20 refers to values of  $e_r^f$  determined from the evaluation of the axial force  $N$  and bending moment  $M_x$  when the following strain parameters are considered:

$$\epsilon = 0.01; \quad \mathbf{g} = \{0.3 \div 0.45, 0.1\}^T \quad (6.23)$$

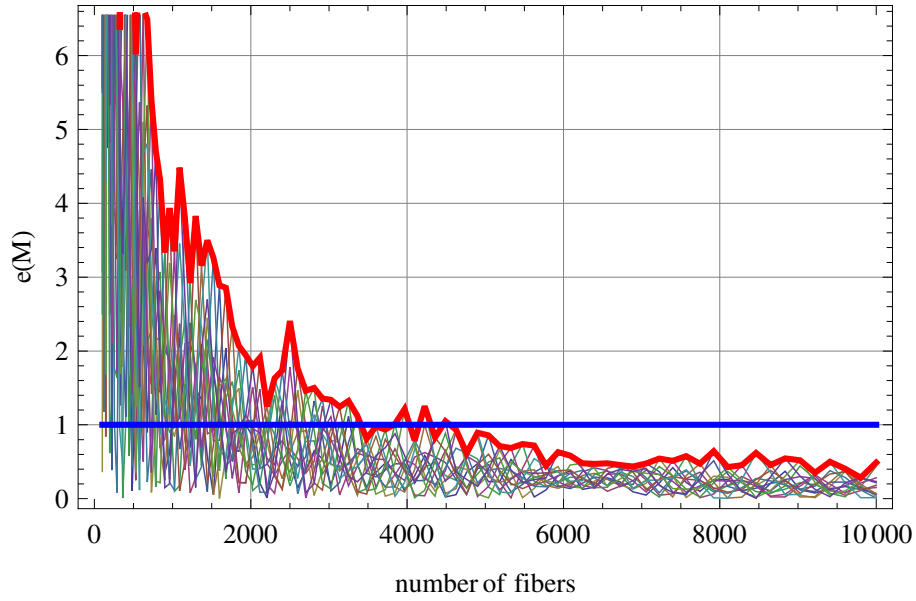


Figure 6.18: Plot of  $e_r^f$  vs. the number of fibers for the bending moment

$$\epsilon_m = 0.01; \quad \mathbf{g}_m = \{0.2, 0.2\}^T \quad (6.24)$$

Finally, plots 6.21 and 6.22 refers to the evaluation of the axial force  $N$  and bending moment  $M_x$  when one assumes:

$$\epsilon = -0.004 \div 0.01; \quad \mathbf{g} = \{0.45, 0.1\}^T \quad (6.25)$$

$$\epsilon_m = 0.01; \quad \mathbf{g}_m = \{0.2, 0.2\}^T \quad (6.26)$$

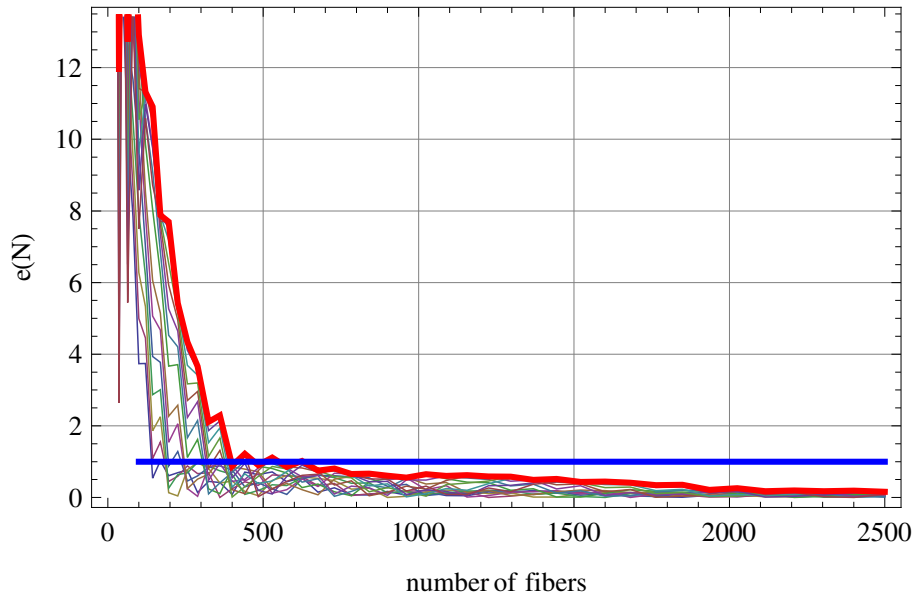


Figure 6.19: Plot of  $e_r^f(N)$  vs. the number of fibers for the axial force

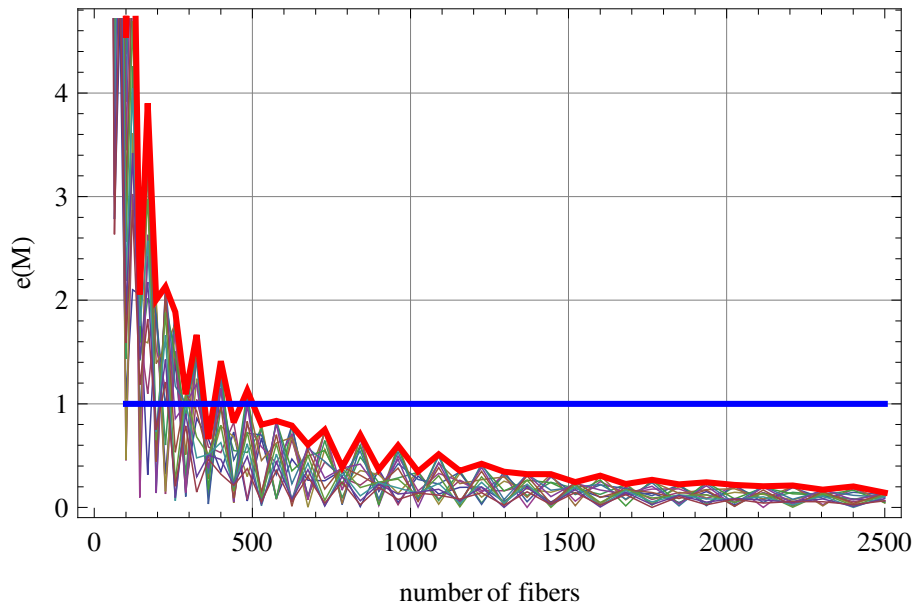


Figure 6.20: Plot of  $e_r^f(M_x)$  vs. the number of fibers for the bending moment

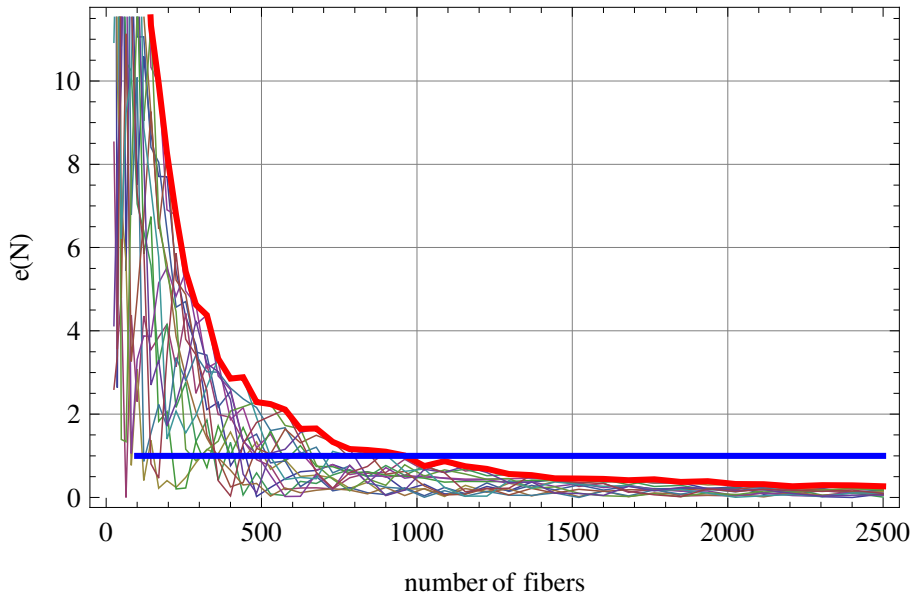


Figure 6.21: Plot of  $e_r^f(N)$  vs. the number of fibers for the axial force

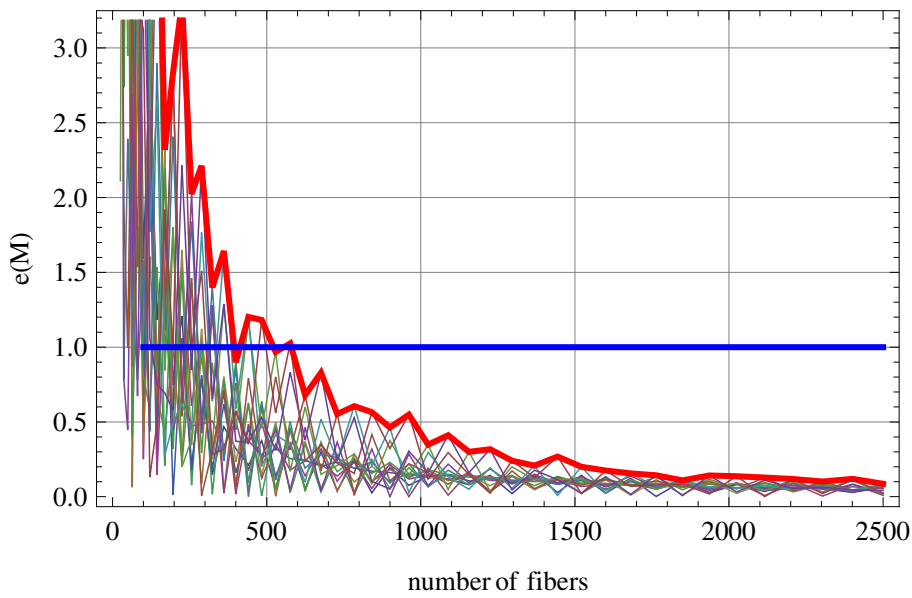


Figure 6.22: Plot of  $e_r^f(M_x)$  vs. the number of fibers for the bending moment



# Bibliography

- [1] G. Alfano, F. Marmo, L. Rosati, An unconditionally convergent algorithm for the evaluation of the ultimate limit state of RC sections subject to axial force and biaxial bending. *Int. J. Numer. Meth. Engng.*, **72**, 924-963, (2007).
- [2] J.M. Bairan, A nonlinear coupled model for the analysis of reinforced concrete sections under bending, shear and torsion and axial forces. PhD thesis, Technical University of Catalonia, Barcelona, Spain, (2005).
- [3] J.M. Bairan, A.R. Mari, Coupled model for the non-linear analysis of anisotropic sections subjected to general 3D loading. Part 1: Theoretical formulation. *Computers & Structures*, **84**, 2254-2263, (2006).
- [4] J.M. Bairan, A.R. Mari, Coupled model for the non-linear analysis of anisotropic sections subjected to general 3D loading. Part 2: Implementation and validation. *Computers & Structures*, **84**, 2264-2276, (2006).
- [5] H. Banon, J. Biggs, M. Irvine, Seismic damage in reinforced concrete frames. *ASCE Journal of Structural Engineering*, **107**(ST9), 1713-1729, (1981).
- [6] S. Bazant, P. Bhat, Prediction of Hysteresis in Reinforced Concrete Members. *ASCE Journal of Structural Engineering*, **103**(ST1), 151-167, (1977).
- [7] Z.P. Bazant, B.H. Oh, Microplane model for progressive fracture of concrete and rock. *ASCE Journal of Engineering Mechanics*, **111**(4), 559-582, (1985).

- 
- [8] Z.P. Bazant, P.C. Prat, Microplane model for brittle-plastic material. Parts I and II. *ASCE Journal of Engineering Mechanics*, **114**(10), 1672-1702, (1988).
- [9] Z.P. Bazant, J. Ozbolt, Nonlocal microplane model for fracture, damage and size effect in concrete structures. *ASCE Journal of Engineering Mechanics*, **116**(11), 2484-2504, (1990).
- [10] E.C. Bentz, Sectional analysis of reinforced concrete members. PhD thesis, University of Toronto, Toronto, Canada, (2000).
- [11] J.L. Bonet, M.L. Romero, P. F. Miguel, M.A. Fernandez, A fast stress section integration algorithm for reinforced concrete sections with axial loads and biaxial bending. *Computers & Structures*, **82**, 213-225, (2004).
- [12] S.N. Bousias, T.B. Panagiotakos, M.N. Fardis, Modelling of RC members under cyclic biaxial flexure and axial force. *Journal of Earthquake Engineering*, **6**(2), 213-238, (2002).
- [13] F. Brancaleoni, V. Ciampi, R. Di Antonio, Rate-Type models for non-linear hysteretic structural behavior. *EUROMECH Colloquium*, Palermo, Italy, (1983).
- [14] B. Brelser, Design criteria for reinforced concrete columns under axial load and biaxial bending. *ACI Journal*, **57**, 481-490, (1960).
- [15] T. Brondum, Ultimate limit states of cracked arbitrary cross sections under axial loads and biaxial bending. *ACI Concrete International*, **4**(11), 51-55, (1982).
- [16] T. Brondum, Ultimate flexural capacity of cracked polygonal concrete sections under axial loads and biaxial bending. *ACI Concrete International*, **84**(3), 212-215, (1987).
- [17] P. Ceresa, L. Petrini, R. Pinho, Flexure-shear fiber beam-column elements for modeling frame structures under seismic loading - State of the art. *Journal of Earthquake Engineering*, **11**, 46-88, (2007).
- [18] A.E. Charalampakis, V.K. Koumoussis, Ultimate strength analysis of arbitrary cross sections under biaxial bending and axial load by fiber model and curvilinear polygons. *5<sup>th</sup> GRACM International Congress on Computational Mechanics*, (2005).

- 
- [19] S.F. Chen, J.G. Teng, S.L. Chan, Design of biaxially loaded short composite columns of arbitrary section. *ASCE Journal of Structural Engineering*, **127**(6), 678-686, (2001).
- [20] C.G. Chiorean, A fast incremental-iterative procedure for inelastic analysis of RC sections of arbitrary shape. *Acta Technica Napocensis*, **47**, 85-98, (2005).
- [21] P.H. Chuang, X. Li, Noniterative flexibility method for non-linear analysis of frames. *Journal of Structural Engineering*, **125**(11), 1338-1346, (1999).
- [22] V. Ciampi, L. Carlesimo, A non-linear beam element for seismic analysis of structures. *8<sup>th</sup> European Conference on Earthquake Engineering*, Lisbon, (1986)
- [23] A. Cladera, Shear design of reinforced high-strength concrete beams, PhD thesis, Technical University of Catalonia, Barcelona, Spain, (2002).
- [24] R. Clough, L. Benuska, Non-linear earthquake behavior of tall buildings. *ASCE Journal of mechanical engineering*, **93**(EM3), 129-146, (1967).
- [25] R. Clough, S. Johnston, Effect of stiffness degradation on earthquake ductility requirements. Transactions of Japan Earthquake Engineering Symposium, Tokyo, 195-198, (1966).
- [26] M. Contaldo and G. Faella, Un procedimento per il calcolo automatico per la verifica allo stato limite ultimo per tensioni normali. *Giornale del Genio Civile*, **10**, 23-37, (1987).
- [27] Comité Euro-internacional du beton. New developments in non-linear analysis methods. *CEB Bull No 229*, Paris, France, 1995.
- [28] E. Cosenza, G. Manfredi, G.M. Verderame, A fibre model for push-over analysis of underdesigned reinforced concrete frames. *Computers and Structures*, **84**, 904-916, (2006).
- [29] M.A. Crisfield *Finite elements and solution procedures for structural analysis, Vol. 1: linear analysis*, Pineridge Press, Swansea, U.K., (1986).

- [30] M.A. Crisfield *Non-linear finite element analysis of solids and structures*, John Wiley & Sons, 1991.
- [31] L. Davenne, F. Ragueneau, J. Mazars, A. Ibrahimbegovic, Efficient approaches to finite element analysis in earthquake engineering. *Computer and Structures*, **81**, 1223-1239, (2003).
- [32] M.D. Davidster, Analysis of reinforced concrete columns of arbitrary geometry subjected to axial load and biaxial bending: A computer program for exact analysis. *ACI Concrete International: Design and Construction*, **8**, 56-61, (1986).
- [33] Decreto Ministeriale del Ministero dei Lavori Pubblici del 01.09.1996, Norme tecniche per il calcolo, l'esecuzione ed il collaudo delle strutture in cemento armato, normale e precompresso e delle strutture metalliche.
- [34] J.C. De la Llera, J. Vasquez, A.K. Chopra, J.L. Almazan, A macro element model for inelastic building analysis. *Earthquake Engineering and Structural Dynamics*, **29**, 1725-1757, (2000).
- [35] L. De Vivo, L. Rosati, Ultimate strength analysis of reinforced concrete sections subject to axial force and biaxial bending. *Comp. Meth. Appl. Mech. Engrg.*, **166**, pag.261-287, (1998).
- [36] M.A. Dides, J.C. De la Llera, A comparative study of concentrated plasticity models in dynamics analysis of building structures. *Earthquake Engineering and Structural Dynamics*, **34**, 1005-1026, (2005).
- [37] M.G. D'Urso, Generalized moments of polygonal domains. Submitted to *Int. J. Num. Meth. Engrg.*, (2007).
- [38] S. El-Tawil, G.G. Deierlein, Analysis Models for Mixed Steel-Concrete Space Frames Part I - Beam-Column Element Formulation, Part II - Implementation and Verification, *Journal of Structural Engineering*, ASCE, **127**(6), (2001).
- [39] UNI ENV Eurocode 2: Design of Concrete Structures, European Pre-standard, UNI ENV 1992-1-3: 1992. Brussels, September (1995).
- [40] A. Fafitis, Interaction surfaces of reinforced-concrete sections in biaxial bending. *ASCE Journal of structural engineering*, **127**(7), 840-846, (2001).

- 
- [41] F.C. Filippou, A. Issa, Non-linear analysis of reinforced concrete frames under cyclic load reversals. *EERC Report 88-12*, Earthquake Engineering, Research Center, Berkeley, (1988).
- [42] R. Fletcher *Practical methods of optimization*. J. Wiley & Sons, Chichester, 1980.
- [43] M. Giberson, The response of non-linear multi-story structures subjected to earthquake excitations. *Earthquake Engineering Research Laboratory*, Pasadena, (1967).
- [44] J. Guedes, P. Pegon, A.V. Pinto, A fibre/Timoshenko beam element in CASTEM 2000, *Special Publication Nr. I.94.31* Applied Mechanics Unit, Safety Technology Institute, Commission of the European Communities, Joint Research Centre, Ispra Establishment, Italy, (1994).
- [45] J. Hellesland, A. Scordelis, Analysis of RC Bridge Columns Under Imposed Deformations. *IABSE Colloquium*, Delfts, Netherlands, 545-559, (1981).
- [46] K.D. Hjelmstad, E. Taciroglu, Mixed variational methods for finite element analysis of geometrically non-linear, inelastic Bernoulli-Euler beams. *Commun. Numer. Meth. Engng*, **19**, 809-832, (2003).
- [47] T.J.R. Hughes, *Finite Element Method - Linear Static and Dynamic Finite Element Analysis*. Dover publications, inc. Mineola, New York, (2000).
- [48] B.A. Izzudin, D. Lloyd Smith, Efficient non-linear analysis of elastoplastic 3D R/C frames using adaptive techniques. *Computers & Structures*, **78**, 549-573, (2000).
- [49] B.A. Izzudin, A.A.F.M. Siyam, D. Lloyd Smith, An efficient beam-column formulation for 3D reinforced concrete frames. *Computers & Structures*, **80**, 659-676, (2002).
- [50] I.D. Karsan and J.O. Jirsa, Behavior of concrete under compressive loading. *Journal of Structural Division ASCE*, **95ST12** (1969)
- [51] H. Kaufmann, On existence and uniqueness of a vector minimizing a convex function. *ZOR - Methods and Models of Operations Research* 1988, **32**:357-373.

- [52] M.T. Kawakami, M. Kagayaù, M. Hirata, Limit states of cracking and ultimates strength of arbitrary cross sections under biaxial loading. *ACI J*, **82**(1), 203-212, (1985).
- [53] P. Kotronis, Cisaillement dynamique de murs en béton armé. Modèles simplifiés 2D et 3D. PhD thesis, Ecole Normale Supérieure de Cachan, (2000).
- [54] P. Kotronis, J. Mazars, Simplified modelling strategies to simulate the dynamic behaviour of R/C walls. *Journal of Earthquake Engineering*, **9**(2), 285-306, (2005).
- [55] E. Kreyszig, *Advanced Engineering Mathematics* (8th edn). John Wiley, (1998).
- [56] K.H. Kwan and C.T. Liauw, Computerized ultimate strength analysis of reinforced concrete sections subjected to axial compression and biaxial bending. *Computers & Structures*, **21**(6), 1119-1127, (1985).
- [57] S. Lai, G. Will, S. Otani, Model for Inelastic Biaxial Bending of Concrete Members. *Journal of Structural Engineering*, ASCE, **110**(ST11), 2563-2584,(1984).
- [58] J. Lubliner, *Plasticity theory*, MacMillan Publishing Company, (1998).
- [59] Luenberger DG. *Linear and Nonlinear Programming* (2nd edn). Addison-Wesley, (1989).
- [60] M. Malena, A.S. Petrolo, R. Casciaro, Caratterizzazione di domini di interazione e suo uso nell'analisi non lineare di telai 3D in C.A.. Report n°9 Lab. Mec., Università della Calabria, <http://www.labmec.unical.it> (2003).
- [61] J.B. Mander, M.J.N. Priestley and R. Park , Theoretical stress-strain model for confined concrete. *Journal of Structural Engineering ASCE*, **114**(8), 1804-1825, (1988).
- [62] G. Manfredi, M. Pecce, A refined RC beam element including bond-slip relationship for the analysis of continuous beams. *Computers and Structures* **69**, 53-62, (1998).
- [63] A. Mari, A. Scordelis, Nonlinear Geometric Material and Time Dependent Analysis of Three Dimensional Reinforced and Prestressed Concrete Frames. *SESM Report 82-12*, Department fo Civil Engineering, University of California, Berkeley, (1984).

- [64] J. Marin, Design aids for L-shaped reinforced concrete columns. *ACI Journal*, **76**(11), 1197-1216, (1979).
- [65] A. Marini, E. Spacone, Analysis of reinforced concrete elements including shear effects. *ACI Structural Journal*, **103**(5), 645-655, (2006).
- [66] L. Martinelli, Numerical simulation of cyclic tests of R/C shear walls. *Proceedings of the Twelfth European Conference on Earthquake Engineering*, London, United Kingdom, (2002).
- [67] J. Mazars, P. Kotronis, F. Ragueneau, G. Casaux, Using multifibre beams to account for shear and torsion, applications to concrete structural elements. *Computers Methods in Applied Mechanics and Engineering*, **195**(52), 7264-7281, (2006).
- [68] M. Menegotto, P.E. Pinto, Method of analysis for cyclically loaded reinforced concrete plane frames including changes in geometry and nonelastic behaviour of elements under combined normal force and bending. *IABSE Symposium on Resistance and Ultimate Deformability of Structures Acted on by Well-Defined Repeated Loads*, Final Report, Lisbon, Portugal, (1973).
- [69] M. Menegotto, P.E. Pinto, Slender RC Compressed Members in Biaxial Bending. *Journal of Structural Engineering*, ASCE **103**(ST3), 587-605, (1977).
- [70] Ministero delle Infrastrutture e dei Trasporti, Testo Unico, Norme Tecniche per le Costruzioni.
- [71] G. Monti, C. Nuti, Nonlinear cyclic behaviour of reinforcing bars including buckling. *ASCE Journal of Structural Engineering*, **118**(12), 3268-3284, (1992).
- [72] A. Neuenhofer, F.C. Filippou, Evaluation of non-linear frame finite-element models. *Journal of Structural Engineering*, **123**(7), 958-966, (1997).
- [73] Ordinanza della Presidenza del Consiglio dei Ministri n. 3274 del 20.03.2003, Primi elementi in materia di criteri generali per la classificazione sismica del territorio nazionale e di normative tecniche per le costruzioni in zone sismiche.
- [74] S. Otani, Inelastic analysis of RC frame structures. *Journal of Structural Division ASCE*, **100**ST7 (1974).

- [75] H. Ozdemir, Non-linear transient dynamic analysis of yielding structures. Ph. D. Thesis, Department of Civil Engineering, University of California, Berkeley, (1981).
- [76] D. Palermo, F.J. Vecchio, Behaviour and analysis of reinforced concrete walls subjected to reversed cyclic loading. Publication No 2002-01, Department of Civil Engineering, University of Toronto, Canada, (2002).
- [77] M. Petrangeli, V. Ciampi, Equilibrium based iterative solutions for the non-linear beam problem. *International Journal for numerical methods in Engineering*, **40**, 423-437, (1997).
- [78] M. Petrangeli, P.E. Pinto, V. Ciampi, Fibre element for cyclic bending and shear of RC structures. I: theory. *Journal of Engineering Mechanics*, **125**(9), 994-1001, (1999).
- [79] M. Petrangeli, Fibre element for cyclic bending and shear of RC structures. II: verification. *Journal of Engineering Mechanics*, **125**(9), 1002-1009, (1999).
- [80] P. Pinto, G.G. Penelis, A.J. Kappos, *Earthquake resistant concrete structures*, Spon Press, (1996)
- [81] G. Ranzo, M. Petrangeli, A fibre finite beam element with section shear modelling for seismic analysis of RC structures. *Journal of Earthquake Engineering*, **2**, 443-473, (1998).
- [82] M. Remino, Shear modelling of reinforced concrete structures. PhD Thesis, Dipartimento di Ingegneria Civile, Università degli Studi di Brescia, Italy, (2004).
- [83] Rockafellar RT. *Convex Analysis*. Princeton University Press, (1970).
- [84] J.A. Rodriguez-Gutierrez, D.J. Aristizabal-Ochoa, Biaxial interaction diagrams for short RC columns of any cross section. *ASCE Journal of Structural Engineering*, **125**(6), 672-683, (1999).
- [85] L. Rosati, F. Marmo, R. Serpieri, Enhanced solution strategies for the ultimate strength analysis of composite steel-concrete sections subject to axial force and biaxial bending. *Comp. Meth. Appl. Mech. Engrg.*, in press, (2007).

- [86] B.D. Scott, R. Park, M.J.N. Priestley, Stress-strain behavior of concrete confined by overlapping hoops at low and high strain rates. *Am. Concr. Inst. J.*, **79**(1), 13-27, (1982).
- [87] M.G. Sfakianakis, Biaxial bending with axial force of reinforced, composite and repaired concrete sections of arbitrary shape by fiber model and computer graphics. *Adv. in Engrg. Software*, **33**, 227-242, (2002).
- [88] Sherif El-Tawil, G.G. Deirlein, Stress-resultant plasticity for frame structures. *Journal of Engineering Mechanics*, **124**(12), 1360-1370, (1998).
- [89] E. Spacone, V. Ciampi, F.C. Filippou, A beam element for seismic damage analysis. University of California at Berkeley, Earthquake Engineering Research Centre report 92/08, (1992).
- [90] E. Spacone, V. Ciampi, F.C. Filippou, Mixed formulation of nonlinear beam finite element. *Computers & Structures*, **25**, 711-725, (1996).
- [91] E. Spacone, F.C. Filippou, F. Taucer, Fibre beam-column model for non-linear analysis of RC frames: Part I Formulation. *Earthquake Engineering and Structural Dynamics*, **25**, 711-725, (1996).
- [92] E. Spacone, F.C. Filippou, F. Taucer, Fibre beam-column model for non-linear analysis of RC frames: Part II Applications. *Earthquake Engineering and Structural Dynamics*, **25**, 727-742, (1996).
- [93] E. Spacone, S. Limkatanyu, Response of RC members including bond-slip effects. *ACI Structural Journal*, **6**, 831-839, (2000).
- [94] T. Takeda, M.A. Sozen, N. Nielsen, Reinforced concrete response to simulated earthquakes. *Journal of Structural Engineering ASCE*, **96**(ST12), 2557-2573, (1970).
- [95] H. Takizawa, Notes on some basic problems in inelastic analysis of planar RC structures. *Trans. of Arch. Inst. of Japan*, 240, Part I in Feb. 1976, 51-62, Part II in March 1976, 65-77, (1976).
- [96] T. Takayanagi, W. Shnobrich, Nonlinear Analysis of Coupled Wall Systems. *Earthquake Engineering and Structural Dynamics*, **7**, 1-22, (1979).

- [97] F.F. Taucer, E. Spacone and F.C. Filippou, A Fiber Beam-Column Element for Seismic Response Analysis of Reinforced Concrete Structures. *UCB/EERC 91/17*, Earthquake Engineering Research Center, University of California, Berkeley, (1991).
- [98] R.L. Taylor, F.C. Filippou, A. Saritas, F. Auricchio, A mixed finite element method for beam and frame problems. *Computational Mechanics*, **31**, 192-203, (2003).
- [99] W.A. Thanoon, A.M.M. Hamed, J. Noorzai, M.S. Jaafar, B.J. Al-Silayvani, Inelastic analysis of composite sections. *Computers & Structures*, **82**, 1649-1656, (2004).
- [100] F.J. Vecchio, M.P. Collins, The modified compression field theory for reinforced concrete elements subjected to shear. *Journal of the American Concrete Institute*, **83**(2), 219-231, (1986).
- [101] F.J. Vecchio, R.G. Selby, Towards compression-field analysis of reinforced concrete solids. *ASCE Journal of Structural Engineering*, **117**(6), 1740-1758, (1991).
- [102] F.J. Vecchio, Towards cyclic load modelling of reinforced concrete. *ACI Structural Journal*, **96**(2), 193-202, (1999).
- [103] D.C. Weber, Ultimate strength design charts for columns with biaxial bending. *ACI Journal*, **63**(11), 1205-1230, (1966).
- [104] C.Y. Yan, S.L. Chan and A.K.W. So, Biaxial bending design of arbitrarily shaped reinforced concrete columns. *ACI Structural Journal*, **90**(3), 269-278, (1993).
- [105] J.R. Yen, Quasi-Newton method for reinforced concrete column analysis and design. *ASCE Journal of Structural Engineering*, **117**(3), 657-666, (1991).
- [106] C.A. Zerin, S.A. Mahin, Analysis of reinforced concrete beam-columns under uniaxial excitation. *ASCE Journal of Structural Engineering*, **114**(ST4), 804-820, (1988).
- [107] C.A. Zerin, S.A. Mahin, Behavior of reinforced concrete structures subjected to biaxial excitation. *ASCE Journal of Structural Engineering*, **117**(ST9), 2657-2673, (1991).

- [108] O.C. Zienkiewicz, R.L. Taylor, J.Z. Zhu, *The Finite Element Method: Its basis and Fundamentals* (6th edn). Elsevier, (2005).
- [109] O.C. Zienkiewicz, R.L. Taylor, *The Finite Element Method for Solid and Structural Mechanics* (6th edn). Elsevier, (2005).